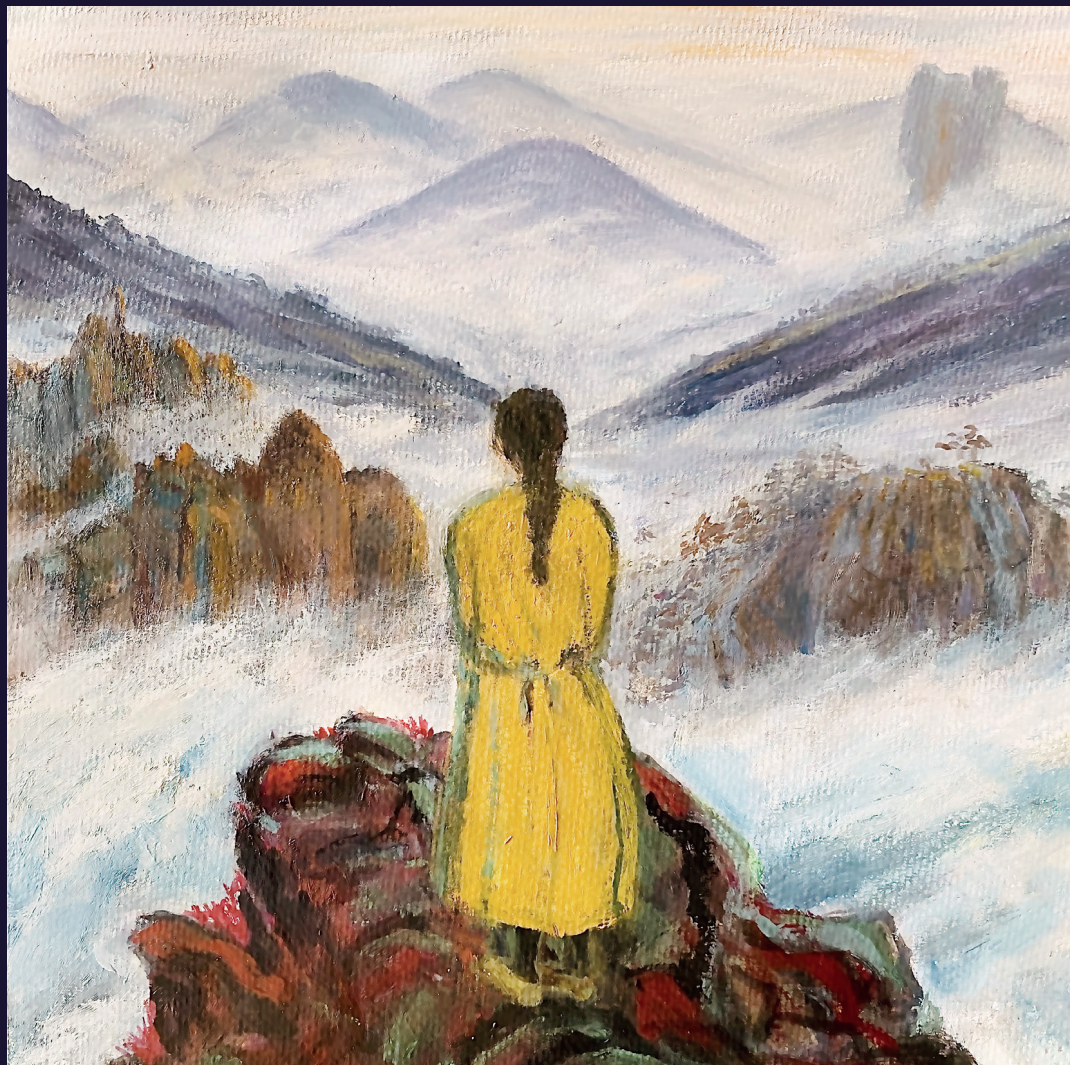


Targeting Angiotensinogen and the (Pro)renin Receptor with Small Interfering RNA or Antisense Oligonucleotides



Liwei Ren
任丽伟

Targeting Angiotensinogen and the
(Pro)renin Receptor with Small Interfering RNA
or Antisense Oligonucleotides

Liwei Ren
任丽伟

Targeting Angiotensinogen and the (Pro)renin Receptor with Small Interfering RNA or Antisense Oligonucleotides

Thesis, Erasmus University, Rotterdam. With summary in Dutch and English

The printing of this thesis was kindly supported by Erasmus University Rotterdam.

ISBN: 978-94-6416-656-9

Cover design: Qi He

Layout design: Liwei

Printing: Ridderprint, the Netherlands

Copyright: ©Liwei Ren 2021

All rights reserved. No part of this thesis maybe reproduced, store in a retrieval system of any nature, or transmitted in any form or means, without written permission of the author, or when appropriate, of the publishers of the publications.

Targeting Angiotensinogen and the (Pro)renin Receptor with Small Interfering RNA or Antisense Oligonucleotides

Aangrijpen op angiotensinogeen en de (pro)renine receptor
met small interfering RNA of antisense oligonucleotiden

Thesis

to obtain the degree of Doctor from the
Erasmus University Rotterdam
by command of the
rector magnificus

Prof.dr. F.A. van der Duijn Schouten

and in accordance with the decision of the Doctorate Board.
The public defence shall be held on

friday 9 july 2021 at 10.30hrs
by

Liwei Ren
born in Shandong, China

Doctoral Committee

Promoter: prof.dr. A.H.J. Danser

Other members: dr. D. Merkus
 dr. J. Deinum
 prof.dr. J.G.R. de Mey

Copromotor: associate professor. X. Lu

Make time the gift it is, by giving it to what really matters to you.

---S.C. Lourie

Table of contents

Chapter 1	Introduction and Aims	9
	Targeting angiotensinogen with RNA-based therapeutics.	11
	(Pro)renin Receptor Functions in Blood Pressure and Energy metabolism.	33
	Aim of this thesis	39
Chapter 2	Revisiting the Brain Renin-Angiotensin System – Focus on Novel Therapies	41
Chapter 3	No Evidence for Brain Renin-angiotensin System Activation during DOCA-salt Hypertension	57
Chapter 4	Renoprotective Effects of Small Interfering RNA Targeting Liver Angiotensinogen in Experimental Chronic Kidney Disease	89
Chapter 5	(Pro)renin Receptor Inhibition Reprograms Hepatic Metabolism and Attenuates Diet-induced Obesity and Liver Steatosis	121
Chapter 6	(Pro)renin Receptor Inhibition Reduces Plasma Cholesterol and Triglycerides but Does Not Attenuate Atherosclerosis in Atherosclerotic Mice	163
Chapter 7	Summary and Perspectives	212
	Abbreviations and Acronyms	222
	Achnowledgement	223
	Curriculum Vitae	227
	PhD portfolio	228
	Publication list	229

Chapter I

Introduction and Aims

Part 1

Targeting angiotensinogen with RNA-based therapeutics.

Liwei Ren, Katrina M. Mirabito Colafella,
Dominique M. Bovée, Estrellita Uijl, and A.H. Jan Danser

Curr Opin Nephrol Hypertens. 2020;29:180-189.

Abstract

Purpose of review: To summarize all available data on targeting angiotensinogen with RNA-based therapeutics as a new tool to combat cardiovascular diseases.

Recent findings: Liver-targeted, stable antisense oligonucleotides and small interfering RNA targeting angiotensinogen are now available, and may allow treatment with at most a few injections per year, thereby improving adherence. Promising results have been obtained in hypertensive animal models, as well as in rodent models of atherosclerosis, polycystic kidney disease and pulmonary fibrosis. The next step will be to evaluate the optimal degree of suppression, synergy with existing renin-angiotensin-aldosterone system blockers, and to determine harmful effects of suppressing angiotensinogen in the context of common comorbidities such as heart failure and chronic kidney disease.

Summary: Targeting angiotensinogen with RNA-based therapeutics is a promising new tool to treat hypertension and diseases beyond. Their long-lasting effects are particularly exciting, and if translated to a clinical application of at most a few administrations per year, may help to eliminate non-adherence.

Keywords: antisense oligonucleotides, RNA interference, angiotensinogen, renin, angiotensin, drug adherence

Introduction

Although more than 100 commercial drugs and drug combinations are available for the treatment of hypertension, a substantial proportion of the hypertensive population remains uncontrolled or sub-optimally controlled. This could relate to non-adherence and/or drug ineffectiveness. The latter might be due to counterregulatory mechanisms (like a rise in renin [1]) that eliminate or diminish the initial blood pressure-lowering effect. Hence, given the deleterious consequences of uncontrolled blood pressure, there still is a need for novel treatment options that preferably are not counterbalanced by the upregulation of contractile mechanisms and circumvent non-adherence. An attractive option is targeting angiotensinogen (AGT) with RNA-based therapeutics. Since all angiotensins stem from AGT, deleting AGT will suppress angiotensin (Ang) formation, even when renin levels rise. Furthermore, the dosing frequency with this approach might go down to a few times per year, thereby potentially reducing the clinical and economic burden of non-adherence.

RNA therapeutic approaches

RNA-based therapies bind to RNA and change the expression of any protein, even those not amenable to traditional approaches involving small-molecule drugs. A number of RNA therapeutic approaches have been developed [2,3], with antisense oligonucleotides (ASO) that inhibit RNA translation and oligonucleotides that function via the RNA interference (RNAi) pathway being the most clinically relevant. ASO-based therapies utilize Watson-Crick's base-pairing rules and single-stranded DNA containing 15 to 30 nucleotides, which are designed in antisense orientation to the pre-mRNA and mRNA of interest. Mature mRNA is formed in the nucleus by splicing the introns of pre-mRNA. ASOs are able to modulate alternative splicing by binding to the pre-mRNA producing different protein variants and changing the prevalence of one variant. When ASOs bind to their target mRNA, RNase H1 cleaves the RNA in an RNA-DNA duplex in both the cytoplasm and nucleus [4] destroying the mRNA and inhibiting the translation of the target protein (Figure 1A). Chemically modified ASOs with phosphorothioate linkages can trigger RNA cleavage even in the absence of transfection reagent [5,6]. In contrast to the ASO approach, RNAi-based therapies utilize double-stranded RNA and exploit the RNAi process, an evolutionary conserved mechanism for the regulation of gene expression. At present, the majority of

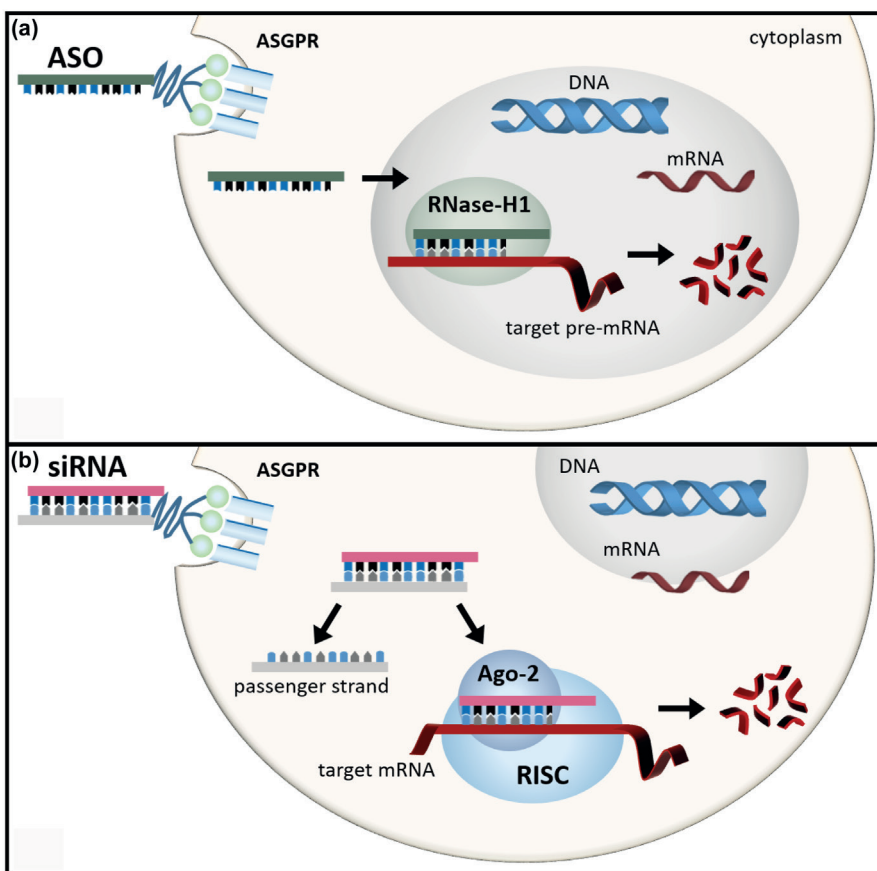


Figure 1. Inhibition of RNA translation by A) antisense oligonucleotide (ASO) or B) RNA interference. See text for further explanation. Abbreviations: ASGPR, asialoglycoprotein receptor; Ago-2, argonaute-2; RISC, RNA-induced silencing complex.

RNAi-based therapies employ non-coding small interfering RNA (siRNA) that are 21 to 23 bases in length and work naturally in the cell as a part of the RNA-Induced Silencing Complex (RISC). Unlike ASOs, when siRNA enters the cell it stays inactive until loaded by transactivation responsive RNA-binding protein into Argonaute where the passenger strand is removed and the remaining antisense strand binds complementary mRNA targets, leaving Argonaute endoribonuclease to cleave the mRNA, thus preventing protein translation [7] (Figure 1B). In mammals, Argonaute contains an RNase H domain, but cleaves RNA in an RNA-RNA duplex [8]. The majority of RNA-based therapies in clinical pipeline utilize the RNAi approach (Table 1). This is unsurprising given that a major advantage of RNAi over ASO for therapeutic applications

Introduction and Aims

is that RNAi is much more potent and has a longer inhibitory effect [9].

The clinical translation of RNAi-based therapies has faced a number of challenges including off-target effects, siRNA delivery, immune reactions and toxicity [2]. The biggest hurdle has been delivery since siRNAs do not readily cross the cell membrane. Various approaches have been proposed to solve the problem of siRNA delivery in vivo e.g., viruses, cationic lipids, polymers, nanoparticles [10,11]. One of the most promising approaches to improve the delivery and safety of siRNA is bioconjugation, the covalent connection of siRNAs with biogenic molecules such as lipophilic molecules, antibodies, aptamers, ligands, peptides, or polymers which also cause less immunoreaction [12,13]. The development of trivalent N-acetylgalactosamine (GalNAc)-siRNA conjugates for targeted delivery of siRNA to the liver is the most successful. GalNAc binds to the asialoglycoprotein receptor that is highly expressed on hepatocytes resulting in rapid endocytosis [14]. The GalNAc approach has also been employed to enhance ASO delivery to hepatocytes by ~10-fold versus free ASOs in preclinical models, resulting in a significant dose reduction [15]. In a phase 2 clinical trial, hepatocyte-directed GalNAc-siRNA molecules have been shown to yield incredible results with stable suppression of proprotein convertase subtilisin/kexin type 9 (PCSK9) achieved for at least 6 months [16]. RNA-based therapies will not only fundamentally change the way we treat diseases, but may also provide treatments for diseases with unmet clinical need. This has led to RNA-based therapeutics becoming one of the most rapidly advancing fields in drug discovery.

Current application of RNA-based therapies

To date, four ASOs and one siRNA-based therapy have been approved for clinical use. Fomivirsen, an intravitreally injected inhibition ASO indicated for the treatment of ocular cytomegalovirus retinitis (CMV) in acquired immunodeficiency syndrome (AIDS) individuals, was the first ever RNA-based therapy to be approved by the U.S. Food and Drug Administration (FDA) in 1998 and by the European Medical Association (EMA) in 1999 [17]. However, in the early 2000's, fomivirsen was withdrawn from the market as the introduction of highly active antiretroviral therapy (HAART) dramatically reduced the number of cases of CMV. A second inhibition ASO, mipomersen, which is injected subcutaneously and targets mRNA encoding apolipoprotein B for the treatment of homozygous familial hypercholesterolemia, was approved for

Chapter 1

clinical use in 2014 [18]. Two splice modulating ASOs, nusinersen for the treatment of spinal muscular atrophy (2017) [19,20] and eteplirsen for the treatment of Duchenne muscular dystrophy (2016) [21], are also approved for clinical use. In 2018, patisiran, an siRNA encapsulated in a lipid nanoparticle for delivery to hepatocytes, became the first globally (FDA and EMA) approved RNAi therapeutic. Patisiran is indicated for the treatment of hereditary transthyretin-mediated amyloidosis (hATTR) in adults [22]. In addition, >50 RNA-based therapies for diseases as varied as cancer, neurodegenerative disease and cardiovascular disease are currently in clinical development with several investigational new drug and clinical trial applications expected to be filed within the next 2 years (Table 1). Interestingly, a number of ASO and RNAi therapies are being developed for the same disease targets (Table 1), including hepatic AGT for the treatment of hypertension which are in phase 2 and phase 1 respectively.

AGT RNA-based therapy in hypertension

Since AGT is the sole precursor of the potent vasoconstrictor Ang II, it is a promising target for gene silencing. At present, inhibition of the renin-Ang-aldosterone system (RAAS) is the mainstay for the treatment of hypertension, heart failure and chronic kidney disease [23,24]. Yet, the long-term management of these conditions remains complicated by RAAS escape phenomena, during which a counterregulatory rise in plasma renin often restores Ang II to its original pre-treatment values [25-27]. As a consequence, blood pressure control commonly requires multiple antihypertensive drugs, but is impeded by a decline in therapy adherence with every drug added to the treatment regimen [28,29].

The clinical need for an antihypertensive therapeutic which prevents Ang reactivation has long been recognized and may be achieved by blocking the RAAS at the AGT level. As opposed to classical RAAS inhibitors, a compensatory rise in renin could even potentiate blood pressure lowering as it would facilitate depletion of the remaining AGT (Figure 2A). This can be explained as follows. Normally, AGT is present at levels that exceed Ang levels by many orders of magnitude. Under such conditions, blocking renin, Ang I-converting enzyme (ACE) or the Ang receptor results in a renin rise which either (partially) restores Ang II, or increases Ang II above its original level (in order to overcome blockade of its receptor). This is easily achievable, simply because there is ample AGT

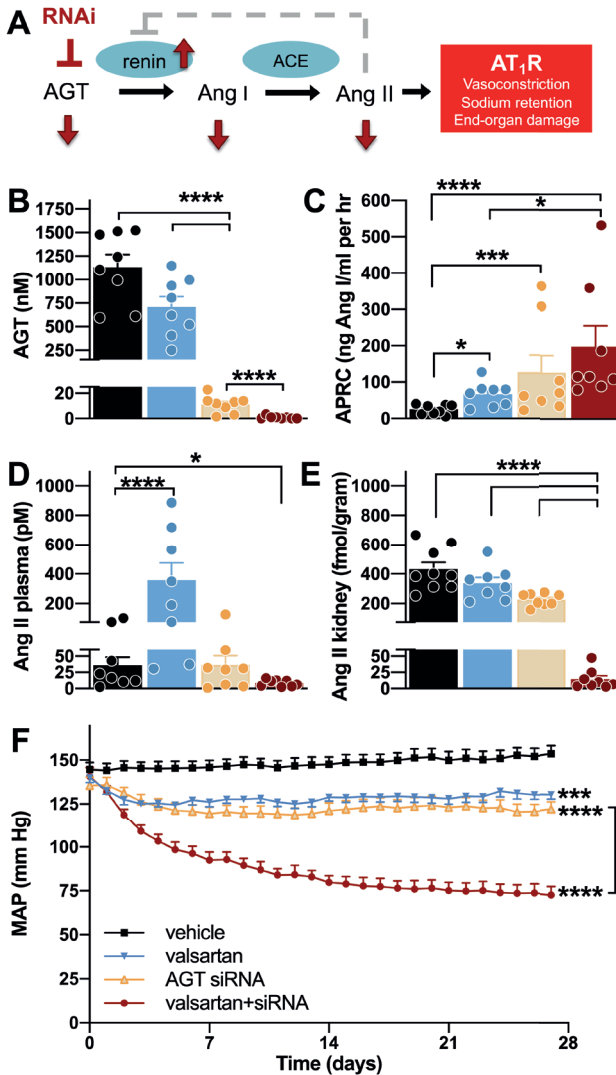


Figure 2. Near elimination of AGT is required for lowering of Ang II. A) Inhibition of the renin-angiotensin-aldosterone-system (RAAS) at the angiotensinogen (AGT) level may prevent RAAS reactivation, because a rise in plasma renin levels, due to a lack of negative feedback exerted by angiotensin (Ang) II on renin production, could now facilitate depletion of remaining AGT. B) Plasma AGT, C) active plasma renin concentration (APRC), D) plasma Ang II, E) renal Ang II and F) mean arterial pressure (MAP) of spontaneously hypertensive rats after four weeks of vehicle, valsartan, AGT siRNA or valsartan+siRNA treatment (all groups n=8). Data, modified from Uijl et al. [38], are represented as means \pm SEM and analyzed using two-way ANOVA and post-hoc Bonferroni (MAP) or transformed to natural logarithms before analysis by one-way ANOVA and post-hoc Bonferroni (RAS parameters). * $P < 0.05$, *** $P \leq 0.001$, **** $P \leq 0.0001$ vs. vehicle or otherwise indicated; # $P \leq 0.0001$.

Chapter 1

around to allow this. Even a 100-fold rise in Ang I generation (sufficient to overcome 99% renin inhibition!) is feasible. Yet, if the renin rises are substantial, it is possible that at a certain moment AGT levels start to decrease. During AGT suppression by RNA-based therapy, AGT levels are down already, and now a rise in renin might be sufficient to result in complete AGT depletion, particularly when simultaneously introducing other types of RAAS blockade, which induce further rises in renin. Restoration of Ang II levels is then no longer possible.

While initial ASO constructs targeting *Agt* lowered circulating AGT, Ang II and blood pressure in parallel in spontaneously hypertensive rats, these methods lacked potency and specificity: AGT levels were halved at most, and the effects were short-lived (<1 week) [30-32]. Similar problems also impeded the use of *Agt*-directed siRNA. The introduction of lipid nanoparticle delivery enhanced AGT downregulation, although stable suppression still necessitated weekly intravenous dosing [33]. Additionally, treatment with lipid delivery vehicles causes an inflammatory response and must therefore be given with histamine receptor antagonists, non-steroidal anti-inflammatory drugs and relatively high doses of glucocorticoids [34].

Conjugating GalNAc to ASO and RNAi molecules enabled general therapeutic application. Subsequent selective accumulation in the liver permitted minimal invasive delivery via subcutaneous injection and optimization of AGT downregulation, since circulating AGT levels are determined by hepatic synthesis [35,36]. Indeed, by improving liver activity 8-fold, GalNAc-conjugation potentiated AGT inhibition of ASOs to maximally 88% in a dose-dependent manner [37]. Interestingly, a reduction of at least 75% was required to simultaneously lower blood pressure, which then remained low for a period of 7-10 days after a single dose. This relates to the above-mentioned upregulation of renin. In fact, in a study employing GalNAc-siRNA to target *Agt* [38], even when AGT was decreased by 97.9%, circulating Ang II remained intact due to renin upregulation. Only a 99.8% reduction, achieved by combining siRNA with valsartan (which further upregulates renin, thereby additionally lowering AGT), was required to deplete both systemic and renal Ang II (Figure 2B-E). The latter observation implies that renal Ang generation relies on AGT of hepatic origin. Consequently, AGT siRNA monotherapy provided similar antihypertensive and cardioprotective efficacy as

Introduction and Aims

conventional RAAS inhibition, whereas near elimination of AGT by addition of valsartan yielded a synergistic reduction in blood pressure and cardiac hypertrophy, without adversely affecting renal function (Figure 2F). Unique to GalNAc-siRNA is its long-lasting effectiveness [22], as opposed to an ASO liver half-life of 2 to 4 weeks [37]. These findings suggest that, in clinical practice, AGT inhibition mediated by RNAi may not only prevent RAAS reactivation but also improve cardiovascular outcome and therapy adherence due to a sustained and stable single-dose efficacy lasting weeks to months [38].

AGT RNA-based therapy in other diseases

While the potential for clinical translation is currently being investigated in patients, preclinical studies now focus on safety and efficacy in models of chronic kidney disease and heart failure. However, the application of AGT inhibition is not limited to hypertension and related end-organ damage. Polycystic kidney disease (PKD) appears an especially promising target, with multiple recent studies showing beneficial effects in animal models of this disease [39-41]. PKD is caused by mutations in the *Pkd1* and *Pkd2* gene. In affected patients, these mutations lead to early onset hypertension, the progressive growth of renal cysts and kidney failure. Conventional treatment with ACE inhibitors or Ang receptor blockers (ARBs) effectively lowers blood pressure in PKD, but whether this treatment also reduces the decline in kidney function is unclear [42,43]. Experimentally, PKD may be studied in mice with targeted knockout of the *Pkd1* or *Pkd2* gene, with both models developing progressive intrarenal cysts and kidney failure [44,45]. In *Pkd2* knockout mice, treatment with AGT ASO resulted in a reduction in kidney size, lower total cyst volume and improved kidney function compared to control treatment (scrambled ASO) [39]. *Pkd1* knockout mice displayed similar reductions in kidney size and cyst volume after treatment with AGT ASO [40,41]. Interestingly, in the latter model, the effects of AGT ASO on cyst growth were independent of changes in systolic blood pressure. In contrast, ACE inhibition with lisinopril significantly lowered systolic blood pressure, but did not reduce kidney size to a similar degree as AGT ASO and had no effect on cyst volume [40].

Experimental evidence indicates that AGT ASO may also be effective in the treatment of atherosclerosis. Increased activity of the RAAS promotes atherosclerosis through activation of AT_{1A} receptors [46-48].

Table 1. RNA-based therapies currently in clinical development

Disease target	Pharmaceutical company	Drug (alternate name)	Therapeutic approach	Stage of development
CANCER				
Blood cancers				
miR-155	miRagen	Cobomarsen (MRG-106)	RNAi (miRNA)	Phase 1/2
Clear cell renal cell carcinoma				
HIF-2 α	Arrowhead	ARO-HIF2	RNAi (siRNA)	Pre-IND
Cholangiocarcinoma				
TGF- β 1 and COX2	Sirnaomics	STP705L	RNAi (siRNA)	Phase 1
Non-melanoma skin cancer				
TGF- β 1 and COX2	Sirnaomics	STP705	RNAi (siRNA)	Phase 2
Pancreatic cancer				
KRAS G12D	Silenseed	KRAS-LODER	RNAi (siRNA)	Phase 2 [60]
Prostate cancer				
Androgen receptors	Ionis	ARRx (IONIS-AR-2.5Rx)	ASO	Phase 1/2
Various cancers				
STAT3	Ionis-AstraZeneca	Danvatirsen (ISIS481464)	ASO	Phase 1/2
CARDIO-METABOLIC				
Clotting disorders				
Hepatic Factor XI	Ionis-Bayer	IONIS-FXIRx	ASO	Phase 2 [61]
	Ionis-Bayer	IONIS-FXI-LRx	ASO	Phase 1
Dyslipidemias				
Hepatic PCSK9	Alnylam- The Medicines Company	Inclisiran (ALN-PCSSC)	RNAi (siRNA)	Phase 3 [16,62-65]

Hepatic Apo C-III	Arrowhead	ARO-APOC3	RNAi (siRNA)	Phase 1
	Ionis-Akcea/Novartis	AKCEA-APOCIII-LRx	ASO	Phase 2
	Ionis-Akcea	Waylivra (Volanesorsen)	ASO	Phase 3 [66-72]
Hepatic ANGPTL3	Arrowhead	ARO-ANG3	RNAi (siRNA)	Phase 1
	Ionis-Akcea	AKCEA-ANGPTL3-LRx	ASO	Phase 2
Hepatic Apo A	Arrowhead-Amgen	AMG 890	RNAi (siRNA)	Phase 1
	Ionis-Akcea/Novartis	AKCEA-APO(a)-LRx	ASO	Phase [73]
	Silence Therapeutics	SLN360		IND/CTA due in 2020
Undisclosed target	Ionis-AstraZeneca	AZD8233 (IONIS-AZ4-2.5LRx)	ASO	Phase 1
Hypertension				
Hepatic AGT	Alnylam	ALN-AGT	RNAi (siRNA)	Phase 1
	Ionis	IONIS-AGT-LRx	ASO	Phase 2
Ischemia				
miR-92a	miRagen-Servier	MRG-110	RNAi (miRNA)	Phase 1
Type 2 diabetes				
Hepatic glucagon receptors	Ionis	IONIS-GCGR(Rx)	ASO	Phase 2 [74]
ENDOCRINE DISORDERS				
Acromegaly				
Growth hormone receptor	Ionis	IONIS-GHR-LRx	ASO	Phase 2
FIBROSIS				
Hypertrophic scar reduction				
TGF-b1 and COX2	Sirnaomics	STP705L	RNAi (siRNA)	Phase 2
Cutaneous fibrosis				
miR-29	miRagen	Remlarsen (MRG-201)	RNAi (miRNA)	Phase 2

Disease target	Pharmaceutical company	Drug (alternate name)	Therapeutic approach	Stage of development
GENETIC				
b-Thalassemia				
Hepatic TMPRSS6	Ionis	IONIS-TMPRSS6-LRx	ASO	Phase 2
	Silence Therapeutics	SLN124	RNAi (siRNA)	CTA approved
Complement-mediated diseases				
Hepatic C5	Alnylam	Cemdisiran (ALN-CC5)	RNAi (siRNA)	Phase 2
	Alnylam-Regeneron	Cemdisiran/Pozelimab Combo	RNAi (siRNA)	Phase 1/2
Hepatic complement factor B	Ionis-Roche	IONIS-FB-LRx	ASO	Phase 2
Cystic Fibrosis				
Pulmonary aENaC	Arrowhead	ARO-ENaC	RNAi (siRNA)	Pre-IND
	Ionis	IONIS-ENAC-2.5Rx	ASO	Phase 2
Hemophilia and are bleeding disorders				
Hepatic antithrombin	Alnylam- Sanofi Genzyme	Fitusiran (ALN-AT3)	RNAi (siRNA)	Phase 3
Hereditary angioedema				
Prekallikrein	Ionis	IONIS-PKK-LRx	ASO	Phase 2
Primary hyperoxaluria				
Hepatic glycolate oxidase type 1	Alnylam	Lumasiran (ALN-GO1)	RNAi (siRNA)	Phase 3
	Dicerna	DCR-PHXC	RNAi (siRNA)	Phase 1
Transthyretin-mediated (ATTR) amyloidosis				
Hepatic transthyretin	Alnylam	Vutrisiran (ALN-TTRsc02)	RNAi (siRNA)	Phase 3
	Ionis-Akcea	AKCEA-TTR-LRx	ASO	Phase 1
KIDNEY DISEASES				

Delayed graft function					
Pro-apoptotic gene p53	Quark	QRK306 (QPI-1002)	RNAi (siRNA)		Phase 3
AKI following cardiac surgery					
Pro-apoptotic gene p53	Quark	QRK209 (QPI-1002)	RNAi (siRNA)		Phase 2
LIVER DISORDERS					
AATD-associated liver disease					
Hepatic mutant AAT	Arrowhead	ARO-AAT	RNAi (siRNA)		Phase 2
	Alnylam	ALN-AAT02	RNAi (siRNA)		Phase 1/2
	Dicerna	DCR-AIAT	RNAi (siRNA)		Pre-IND
Acute hepatic porphyria					
Hepatic ALAS1	Alnylam	Givosiran (ALN-AS1)	RNAi (siRNA)		Phase 3 [75]
ARLD/NAFLD					
HSD17B13	Arrowhead	ARO-HSD	RNAi (siRNA)		Pre-IND
HBV					
HBV gene products	Arrowhead- Janssen	JNJ-3989 (ARO-HBV)	RNAi (siRNA)		Phase 2
	Arbutus	AB-729	RNAi (siRNA)		Phase 1
	Alnylam	VIR-2218 (ALN- HBV02)	RNAi (siRNA)		Phase 1/2
	Ionis-GSK	IONIS-HBV-LRx	ASO		Phase 2
	Ionis-GSK	IONIS-HBVRx	ASO		Phase 2
	Dicerna	DCR-HBVS	RNAi (siRNA)		Phase 1
NEUROLOGICAL DISORDERS					
Huntington's disease					
Huntingtin protein	Ionis-Roche	IONIS-HTTRx	ASO		Phase 3 [76]
Amyotrophic Lateral Sclerosis					
SOD1	Ionis-Biogen	Tofersen (BIIB067)	ASO		Phase 3 [77]

Disease target	Pharmaceutical company	Drug (alternate name)	Therapeutic approach	Stage of development
Mutated CORF72 gene	Ionis-Biogen	IONIS-C9Rx (BIB078)	ASO	Phase 2
Alzheimer's disease & frontotemporal degeneration				
MAPT	Ionis-Biogen	IONIS-MAPT Rx ASO (BIB080)		Phase 2
Centronuclear Myopathy				
Dynamin 2 protein	Ionis-Dynacure	IONIS-DNM2-2.5Rx	ASO	Phase 1
OCULAR DISORDERS				
Dry eye syndrome				
TRPV1	Sylentis	Tivanisiran (SYL1001)	RNAi (siRNA)	Phase 3
Glaucoma				
b-adrenergic receptor 2	Sylentis	Bamosiran (SLY040012)	RNAi (siRNA)	Phase 2 [78,79]

Introduction and Aims

Treatment of spontaneous hypertensive rats on a diet enriched with high fat and vitamin D3 (i.e., to induce atherosclerosis) with Gal-PEG-Et (GPE) nanoparticles carrying short hairpin RNA (shRNA) that specifically targets Agt in the liver decreased systolic blood pressure and attenuated the development of atherosclerotic lesions compared with control animals [49]. Similar effects were observed in another animal model for atherosclerosis and obesity, i.e., LDL receptor knockout mice fed with a saturated fat-enriched diet [50]. In these mice, treatment with AGT ASO resulted in decreased blood pressure, less atherosclerosis, and diminished body weight gain. Correspondingly, previous clinical studies also showed beneficial effects of ACE inhibitors and ARBs on the progression of atherosclerotic plaques [51,52]. However, whether AGT ASO is effective in the treatment of atherosclerosis in patients has yet to be investigated.

Finally, AGT ASO treatment has been used as a therapeutic strategy against experimental pulmonary fibrosis. Currently, treatment options for idiopathic pulmonary fibrosis are limited, leaving most patients with a poor prognosis – the median survival rate is 2–5 years. Several studies in animals (i.e., mice and rats) with bleomycin-induced lung injury showed that Ang II contributes to pulmonary fibrosis, whereas treatment with renin inhibitors, ACE inhibitors and ARBs attenuates disease progression [53-57]. In this same animal model, intratracheal administration of AGT ASO was found to decrease pulmonary AGT concentrations and lung fibrosis [58], but no comparison was made to conventional RAAS inhibitors.

Conclusion

Targeting AGT with RNA-based therapeutics is a promising new tool to treat hypertension and diseases beyond, including heart failure, atherosclerosis, diabetic nephropathy, polycystic kidney disease and pulmonary fibrosis. The long-lasting effects of RNA-based therapeutics are particularly exciting, and if translated to a clinical application of at most a few administrations per year, may help to eliminate non-adherence. To what degree the effects of such therapeutics are fully identical to those of other RAAS blockers (given the fact that they eliminate all Ang metabolites) remains to be determined. It will also be important to determine to what level AGT should be suppressed to induce meaningful effects, and whether there is a role for AGT synthesized outside the liver [59]. Syn-

Chapter 1

ergy in combination with other RAAS blockers needs to be evaluated, as well as the potential harmful effects of suppressing AGT in the context of common comorbidities such as heart failure and chronic kidney disease, where AGT might already be suppressed.

Key points

- Liver-targeted, stable antisense oligonucleotides and small interfering RNA targeting angiotensinogen, capable of suppressing angiotensinogen in a dose-dependent manner, are now available.
- Suppressing angiotensinogen exerts similar effects as classical blockers of the renin-angiotensin-aldosterone system (RAAS) in hypertensive animal models, as well as in rodent models for atherosclerosis, polycystic kidney disease and pulmonary fibrosis.
- Future studies should evaluate their safety, e.g. in the context of common comorbidities such as heart failure and chronic kidney disease, and synergy with existing RAAS blockers.
- The long-lasting effects of this approach are particularly exciting, and if translated to a clinical application of at most a few administrations per year, may help to eliminate non-adherence.

Acknowledgements

None.

Financial support and sponsorship

K.M.MC. was supported by a National Health and Medical Research Council of Australia CJ Martin Fellowship (1112125). L.R. was supported by a National Natural Science Foundation of China grant (no. 81900668).

Conflict of interest

A.H.J.D. received a grant from Alnylam Pharmaceuticals.

References

1. Balcarek J, Sevá Pessôa B, Bryson C, et al.: Multiple ascending dose study with the new renin inhibitor VTP-27999: nephrocentric consequences of too much renin inhibition. *Hypertension* 2014, 63:942-950.
2. Setten RL, Rossi JJ, Han SP: The current state and future directions of RNAi-based therapeutics. *Nat Rev Drug Discov* 2019, 18:421-446.

3. Levin AA: Treating Disease at the RNA Level with Oligonucleotides. *N Engl J Med* 2019, 380:57-70.
4. Liang XH, Sun H, Nichols JG, et al.: RNase H1-Dependent Antisense Oligonucleotides Are Robustly Active in Directing RNA Cleavage in Both the Cytoplasm and the Nucleus. *Mol Ther* 2017, 25:2075-2092.
5. Wang S, Allen N, Vickers TA, et al.: Cellular uptake mediated by epidermal growth factor receptor facilitates the intracellular activity of phosphorothioate-modified antisense oligonucleotides. *Nucleic Acids Res* 2018, 46:3579-3594.
6. Wang S, Allen N, Liang XH, et al.: Membrane Destabilization Induced by Lipid Species Increases Activity of Phosphorothioate-Antisense Oligonucleotides. *Mol Ther Nucleic Acids* 2018, 13:686-698.
7. Li C, Zamore PD: RNA Interference and Small RNA Analysis. *Cold Spring Harb Protoc* 2019, 2019:pdb top097436.
8. Daugaard I, Hansen TB: Biogenesis and Function of Ago-Associated RNAs. *Trends Genet* 2017, 33:208-219.
9. Bertrand JR, Pottier M, Vekris A, et al.: Comparison of antisense oligonucleotides and siRNAs in cell culture and in vivo. *Biochem Biophys Res Commun* 2002, 296:1000-1004.
10. Osborn MF, Khvorova A: Improving siRNA Delivery In Vivo Through Lipid Conjugation. *Nucleic Acid Ther* 2018, 28:128-136.
11. Yalcin E, Kara G, Celik E, et al.: Preparation and characterization of novel albumin-sericin nanoparticles as siRNA delivery vehicle for laryngeal cancer treatment. *Prep Biochem Biotechnol* 2019:1-12.
12. Chernikov IV, Vlassov VV, Chernolovskaya EL: Current Development of siRNA Bioconjugates: From Research to the Clinic. *Front Pharmacol* 2019, 10:444.
13. Qu X, Hu Y, Wang H, et al.: Biomimetic Dextran–Peptide Vectors for Efficient and Safe siRNA Delivery. *ACS Applied Bio Materials* 2019, 2:1456-1463.
14. Springer AD, Dowdy SF: GalNAc-siRNA Conjugates: Leading the Way for Delivery of RNAi Therapeutics. *Nucleic Acid Ther* 2018, 28:109-118.
15. Prakash TP, Graham MJ, Yu J, et al.: Targeted delivery of antisense oligonucleotides to hepatocytes using triantennary N-acetyl galactosamine improves potency 10-fold in mice. *Nucleic Acids Res* 2014, 42:8796-8807.
16. Ray KK, Landmesser U, Leiter LA, et al.: Inclisiran in Patients at High Cardiovascular Risk with Elevated LDL Cholesterol. *N Engl J Med* 2017, 376:1430-1440.
17. Roehr B: Fomivirsen approved for CMV retinitis. *J Int Assoc Physicians AIDS Care* 1998, 4:14-16.
18. Wong E, Goldberg T: Mipomersen (kynamro): a novel antisense oligonucleotide inhibitor for the management of homozygous familial hypercholesterolemia. *P t* 2014, 39:119-122.
19. Stein CA, Castanotto D: FDA-Approved Oligonucleotide Therapies in 2017. *Mol Ther* 2017, 25:1069-1075.
20. Aartsma-Rus A: FDA Approval of Nusinersen for Spinal Muscular Atrophy Makes 2016 the Year of Splice Modulating Oligonucleotides. *Nucleic Acid Ther* 2017, 27:67-69.
21. Aartsma-Rus A, Krieg AM: FDA Approves Eteplirsen for Duchenne Muscular Dystrophy: The Next Chapter in the Eteplirsen Saga. *Nucleic Acid Ther* 2017,

Chapter 1

- 27:1-3.
22. Hoy SM: Patisiran: First Global Approval. *Drugs* 2018, 78:1625-1631.
 23. Williams B, Mancia G, Spiering W, et al.: 2018 ESC/ESH Guidelines for the management of arterial hypertension. *Eur Heart J* 2018, 39:3021-3104.
 24. Arendse LB, Danser AHJ, Poglitsch M, et al.: Novel Therapeutic Approaches Targeting the Renin-Angiotensin System and Associated Peptides in Hypertension and Heart Failure. *Pharmacol Rev* 2019, 71:539-570.
 25. van den Meiracker AH, Admiraal PJ, Janssen JA, et al.: Hemodynamic and biochemical effects of the AT1 receptor antagonist irbesartan in hypertension. *Hypertension* 1995, 25:22-29.
 26. Mooser V, Nussberger J, Juillerat L, et al.: Reactive hyperreninemia is a major determinant of plasma angiotensin II during ACE inhibition. *J Cardiovasc Pharmacol* 1990, 15:276-282.
 27. Sealey JE, Laragh JH: Aliskiren, the first renin inhibitor for treating hypertension: reactive renin secretion may limit its effectiveness. *Am J Hypertens* 2007, 20:587-597.
 28. Gupta P, Patel P, Strauch B, et al.: Risk Factors for Nonadherence to Antihypertensive Treatment. *Hypertension* 2017, 69:1113-1120.
 29. Cushman WC, Ford CE, Cutler JA, et al.: Success and predictors of blood pressure control in diverse North American settings: the antihypertensive and lipid-lowering treatment to prevent heart attack trial (ALLHAT). *J Clin Hypertens (Greenwich)* 2002, 4:393-404.
 30. Tomita N, Morishita R, Higaki J, et al.: Transient decrease in high blood pressure by in vivo transfer of antisense oligodeoxynucleotides against rat angiotensinogen. *Hypertension* 1995, 26:131-136.
 31. Wielbo D, Simon A, Phillips MI, et al.: Inhibition of hypertension by peripheral administration of antisense oligodeoxynucleotides. *Hypertension* 1996, 28:147-151.
 32. Makino N, Sugano M, Ohtsuka S, et al.: Intravenous injection with antisense oligodeoxynucleotides against angiotensinogen decreases blood pressure in spontaneously hypertensive rats. *Hypertension* 1998, 31:1166-1170.
 33. Olearczyk J, Gao S, Eybye M, et al.: Targeting of hepatic angiotensinogen using chemically modified siRNAs results in significant and sustained blood pressure lowering in a rat model of hypertension. *Hypertens Res* 2014, 37:405-412.
 34. Crooke ST, Witztum JL, Bennett CF, et al.: RNA-Targeted Therapeutics. *Cell Metab* 2018, 27:714-739.
 35. Matsusaka T, Niimura F, Shimizu A, et al.: Liver angiotensinogen is the primary source of renal angiotensin II. *J Am Soc Nephrol* 2012, 23:1181-1189.
 36. Ye F, Wang Y, Wu C, et al.: Angiotensinogen and Megalin Interactions Contribute to Atherosclerosis-Brief Report. *Arterioscler Thromb Vasc Biol* 2019, 39:150-155.
 37. Mullick AE, Yeh ST, Graham MJ, et al.: Blood Pressure Lowering and Safety Improvements With Liver Angiotensinogen Inhibition in Models of Hypertension and Kidney Injury. *Hypertension* 2017, 70:566-576.
 38. Uijl E, Mirabito Colafella KM, Sun Y, et al.: Strong and Sustained Antihypertensive Effect of Small Interfering RNA Targeting Liver Angiotensinogen. *Hypertension* 2019, 73:1249-1257.

39. Ravichandran K, Ozkok A, Wang Q, et al.: Antisense-mediated angiotensinogen inhibition slows polycystic kidney disease in mice with a targeted mutation in Pkd2. *Am J Physiol Renal Physiol* 2015, 308:F349-357.
40. Saigusa T, Dang Y, Mullick AE, et al.: Suppressing angiotensinogen synthesis attenuates kidney cyst formation in a Pkd1 mouse model. *FASEB J* 2016, 30:370-379.
41. Fitzgibbon WR, Dang Y, Bunni MA, et al.: Attenuation of accelerated renal cystogenesis in Pkd1 mice by renin-angiotensin system blockade. *Am J Physiol Renal Physiol* 2018, 314:F210-F218.
42. Jafar TH, Stark PC, Schmid CH, et al.: The effect of angiotensin-converting-enzyme inhibitors on progression of advanced polycystic kidney disease. *Kidney Int* 2005, 67:265-271.
43. Irazabal MV, Abebe KZ, Bae KT, et al.: Prognostic enrichment design in clinical trials for autosomal dominant polycystic kidney disease: the HALT-PKD clinical trial. *Nephrol Dial Transplant* 2017, 32:1857-1865.
44. Piontek KB, Huso DL, Grinberg A, et al.: A functional floxed allele of Pkd1 that can be conditionally inactivated in vivo. *J Am Soc Nephrol* 2004, 15:3035-3043.
45. Wu G, D'Agati V, Cai Y, et al.: Somatic inactivation of Pkd2 results in polycystic kidney disease. *Cell* 1998, 93:177-188.
46. Cassis LA, Rateri DL, Lu H, et al.: Bone marrow transplantation reveals that recipient AT1a receptors are required to initiate angiotensin II-induced atherosclerosis and aneurysms. *Arterioscler Thromb Vasc Biol* 2007, 27:380-386.
47. Daugherty A, Rateri DL, Lu H, et al.: Hypercholesterolemia stimulates angiotensin peptide synthesis and contributes to atherosclerosis through the AT1A receptor. *Circulation* 2004, 110:3849-3857.
48. Eto H, Miyata M, Shirasawa T, et al.: The long-term effect of angiotensin II type 1a receptor deficiency on hypercholesterolemia-induced atherosclerosis. *Hypertens Res* 2008, 31:1631-1642.
49. Lu P, Yuan L, Wang Y, et al.: Effect of GPE-AGT nanoparticle shRNA transfection system mediated RNAi on early atherosclerotic lesion. *Int J Clin Exp Pathol* 2012, 5:698-706.
50. Lu H, Wu C, Howatt DA, et al.: Angiotensinogen Exerts Effects Independent of Angiotensin II. *Arterioscler Thromb Vasc Biol* 2016, 36:256-265.
51. Lonn E, Yusuf S, Dzavik V, et al.: Effects of ramipril and vitamin E on atherosclerosis: the study to evaluate carotid ultrasound changes in patients treated with ramipril and vitamin E (SECURE). *Circulation* 2001, 103:919-925.
52. Shinoda E, Yui Y, Kodama K, et al.: Quantitative coronary angiogram analysis: nifedipine retard versus angiotensin-converting enzyme inhibitors (JMIC-B side arm study). *Hypertension* 2005, 45:1153-1158.
53. Marshall RP, Gohlke P, Chambers RC, et al.: Angiotensin II and the fibroproliferative response to acute lung injury. *Am J Physiol Lung Cell Mol Physiol* 2004, 286:L156-164.
54. Otsuka M, Takahashi H, Shiratori M, et al.: Reduction of bleomycin induced lung fibrosis by candesartan cilexetil, an angiotensin II type 1 receptor antagonist. *Thorax* 2004, 59:31-38.
55. Li X, Rayford H, Uhal BD: Essential roles for angiotensin receptor AT1a in bleomycin-induced apoptosis and lung fibrosis in mice. *Am J Pathol* 2003, 163:2523-

Chapter 1

- 2530.
56. Wang R, Ibarra-Sunga O, Verlinski L, et al.: Abrogation of bleomycin-induced epithelial apoptosis and lung fibrosis by captopril or by a caspase inhibitor. *Am J Physiol Lung Cell Mol Physiol* 2000, 279:L143-151.
 57. Asker SA, Mazroa SA, Boshra V, et al.: Biochemical and histological impact of direct renin inhibition by aliskiren on myofibroblasts activation and differentiation in bleomycin induced pulmonary fibrosis in adult mice. *Tissue Cell* 2015, 47:373-381.
 58. Li X, Zhuang J, Rayford H, et al.: Attenuation of bleomycin-induced pulmonary fibrosis by intratracheal administration of antisense oligonucleotides against angiotensinogen mRNA. *Curr Pharm Des* 2007, 13:1257-1268.
 59. Ren L, Lu X, Danser AHJ: Revisiting the Brain Renin-Angiotensin System-Focus on Novel Therapies. *Curr Hypertens Rep* 2019, 21:28.
 60. Golan T, Khvalevsky EZ, Hubert A, et al.: RNAi therapy targeting KRAS in combination with chemotherapy for locally advanced pancreatic cancer patients. *Oncotarget* 2015, 6:24560-24570.
 61. Buller HR, Bethune C, Bhanot S, et al.: Factor XI antisense oligonucleotide for prevention of venous thrombosis. *N Engl J Med* 2015, 372:232-240.
 62. Fitzgerald K, White S, Borodovsky A, et al.: A Highly Durable RNAi Therapeutic Inhibitor of PCSK9. *N Engl J Med* 2017, 376:41-51.
 63. Ray KK, Stoekenbroek RM, Kallend D, et al.: Effect of 1 or 2 Doses of Inclisiran on Low-Density Lipoprotein Cholesterol Levels: One-Year Follow-up of the ORI-ON-1 Randomized Clinical Trial. *JAMA Cardiol* 2019.
 64. Leiter LA, Teoh H, Kallend D, et al.: Inclisiran Lowers LDL-C and PCSK9 Irrespective of Diabetes Status: The ORION-1 Randomized Clinical Trial. *Diabetes Care* 2019, 42:173-176.
 65. Ray KK, Stoekenbroek RM, Kallend D, et al.: Effect of an siRNA Therapeutic Targeting PCSK9 on Atherogenic Lipoproteins. *Circulation* 2018, 138:1304-1316.
 66. Witztum JL, Gaudet D, Freedman SD, et al.: Volanesorsen and Triglyceride Levels in Familial Chylomicronemia Syndrome. *N Engl J Med* 2019, 381:531-542.
 67. Hegele RA, Berberich AJ, Ban MR, et al.: Clinical and biochemical features of different molecular etiologies of familial chylomicronemia. *J Clin Lipidol* 2018, 12:920-927 e924.
 68. Digenio A, Dunbar RL, Alexander VJ, et al.: Antisense-Mediated Lowering of Plasma Apolipoprotein C-III by Volanesorsen Improves Dyslipidemia and Insulin Sensitivity in Type 2 Diabetes. *Diabetes Care* 2016, 39:1408-1415.
 69. Jorgensen AB, Frikke-Schmidt R, Nordestgaard BG, et al.: Loss-of-function mutations in APOC3 and risk of ischemic vascular disease. *N Engl J Med* 2014, 371:32-41.
 70. Graham MJ, Lee RG, Bell TA, 3rd, et al.: Antisense oligonucleotide inhibition of apolipoprotein C-III reduces plasma triglycerides in rodents, nonhuman primates, and humans. *Circ Res* 2013, 112:1479-1490.
 71. Gaudet D, Alexander VJ, Baker BF, et al.: Antisense Inhibition of Apolipoprotein C-III in Patients with Hypertriglyceridemia. *N Engl J Med* 2015, 373:438-447.
 72. Gaudet D, Brisson D, Tremblay K, et al.: Targeting APOC3 in the familial chylomicronemia syndrome. *N Engl J Med* 2014, 371:2200-2206.
 73. Viney NJ, van Capelleveen JC, Geary RS, et al.: Antisense oligonucleotides tar-

Introduction and Aims

- getting apolipoprotein(a) in people with raised lipoprotein(a): two randomised, double-blind, placebo-controlled, dose-ranging trials. *Lancet* 2016, 388:2239-2253.
74. Morgan ES, Tai LJ, Pham NC, et al.: Antisense Inhibition of Glucagon Receptor by IONIS-GCGRRx Improves Type 2 Diabetes Without Increase in Hepatic Glycogen Content in Patients With Type 2 Diabetes on Stable Metformin Therapy. *Diabetes Care* 2019, 42:585-593.
 75. Sardh E, Harper P, Balwani M, et al.: Phase 1 Trial of an RNA Interference Therapy for Acute Intermittent Porphyria. *N Engl J Med* 2019, 380:549-558.
 76. Tabrizi SJ, Leavitt BR, Landwehrmeyer GB, et al.: Targeting Huntingtin Expression in Patients with Huntington's Disease. *N Engl J Med* 2019, 380:2307-2316.
 77. Miller TM, Pestronk A, David W, et al.: An antisense oligonucleotide against SOD1 delivered intrathecally for patients with SOD1 familial amyotrophic lateral sclerosis: a phase 1, randomised, first-in-man study. *Lancet Neurol* 2013, 12:435-442.
 78. Martinez T, Gonzalez MV, Roehl I, et al.: In vitro and in vivo efficacy of SYL040012, a novel siRNA compound for treatment of glaucoma. *Mol Ther* 2014, 22:81-91.
 79. Moreno-Montanes J, Sadaba B, Ruz V, et al.: Phase I clinical trial of SYL040012, a small interfering RNA targeting beta-adrenergic receptor 2, for lowering intraocular pressure. *Mol Ther* 2014, 22:226-232.

Bulleted References (12-18 month old)

- Ref 2 (2019) ** Excellent review on the design and development of RNAi drugs
- Ref 3 (2019) ** Overview of therapeutic oligonucleotides at this moment
- Ref 36 (2019) * First evaluation of angiotensinogen antisense oligonucleotide in atherosclerosis
- Ref 38 (2019) ** Extensive biochemical evaluation of angiotensinogen siRNA in hypertensive rats
- Ref 41 (2018) * Evaluation of angiotensinogen antisense oligonucleotide in a polycystic kidney disease mouse model

Part 2

**(Pro)renin Receptor Functions in Blood Pressure and
Energy metabolism.**

The (Pro)Renin Receptor

Renin, the rate-limiting enzyme of renin-angiotensin-aldosterone system, has an inactive form called prorenin. Renin is synthesized as a pre-pro-renin protein. After cleavage of the pre-fragment, prorenin is transferred to the Golgi. From there prorenin is either directly secreted via the constitutive pathway, or sorted to the dense-core secretory granules for regulated exocytosis following its conversion to renin¹. Unlike renin, which is exclusively kidney-derived, prorenin is also synthesized by other organs, like the reproductive tract, eye, adrenal and submandibular gland². Prorenin occurs in blood in excess to renin, sometimes at concentrations that are a 100 times higher³. The (pro)renin receptor [(P)RR] was identified as a receptor for both renin and prorenin. It bound prorenin with greater affinity⁴. Combined with the much higher levels of prorenin, this made an interaction between prorenin and the (P)RR a reasonable expectation⁵. Unexpectedly, total ablation of (*P*)RR turned out to be lethal, while ablation of (pro)renin is not. This implies that the (P)RR must have important RAS-independent function(s). Remarkably, after 2 decades of research on the (P)RR, it is still not entirely clear how and to what degree the (P)RR is related to the RAS. Yet, novel and RAS-independent functions of the (P)RR have been identified. Indeed, it turned out to be an accessory protein of vacuolar H⁺-ATPase (V-ATPase), with important roles in Wnt/ β -catenin signaling, lipid metabolism, and glucose metabolism.

Characteristics of the (P)RR

The (*P*)RR is expressed in a wide range of organs, including brain, heart, kidney, liver, adipose tissue, eye, and placenta⁴. The gene ATP6AP2 (ATPase H⁺ transporting accessory protein 2), encoding for the (P)RR, is located on the X chromosome at locus p11.4. The protein consists of 350 amino acids, and is membrane-located, with a structure that encompasses 3 parts^{6,7}: a large extracellular domain that can be cleaved to form the soluble (P)RR [s(P)RR], a small transmembrane domain, and a cytoplasmic domain. The extracellular domain binds renin and prorenin, promoting their catalytic efficiency of angiotensin I generation⁴. The cytoplasmic domain is involved in intracellular signaling, and, as a subunit V-ATPase⁸ is essential to maintain an acidic pH in intracellular vesicles like lysosomes, endosomes, and synaptosomes.

Role(s) of the (P)RR in regulating blood pressure

Polymorphisms of (*P*)RR gene have been associated with blood pressure^{9,10} and hypertension¹¹. Yet, mechanistically it is hard to imagine how the receptor exerts hypertensive effects in a RAS-dependent manner, given that the affinity of the (P)RR for both renin and prorenin is many orders of magnitude above their levels in blood. One idea might be that its interaction with (pro)renin occurs at tissue sites, where higher levels are likely to be present.

In the kidney, the (P)RR has been localized to mesangial cells, podocytes, proximal tubule, distal convoluted tubule, the luminal membrane of intercalated cells, and principal cells^{7, 12-14}. In the collecting duct, the (P)RR regulates the activity and expression of the epithelial Na channel in a RAS-independent manner¹⁵, while in the medulla, (*P*)RR expression is upregulated by angiotensin II¹⁵. Overexpression of the (*P*)RR in vascular smooth muscle cells caused systolic hypertension, possibly by enhancing aldosterone synthesis¹⁶. Whether this involved angiotensin II is unknown.

In the brain, the (*P*)RR is expressed in cardiovascular regulatory nuclei, like the subfornical organ, paraventricular nucleus, rostral ventral lateral medulla, nucleus tractus of solitarii and area postrema¹⁷. (P)RR knockdown in these brain areas resulted in blood pressure lowering, supporting the concept that the brain (P)RR is involved in blood pressure regulation^{18,19}. Its blood pressure effect may relate to interference with the sympathetic nervous system. A link with (pro)renin seems highly unlikely, given the virtual absence of (pro)renin in the brain.

The (P)RR has also been linked to obesity^{20, 21}. Interestingly, adipocyte-(P)RR deficiency increased blood pressure^{22, 23}. Possibly, this involved an upregulation of s(P)RR (secreted by the liver) and angiotensin II formation, since it could be mimicked by s(P)RR infusion and blocked by losartan²².

Taken together, a wide range of (P)RR effects in multiple organs have been observed, potentially contributing to hypertension, and involving both RAS-dependent and -independent effects.

Role(s) of the (P)RR in lipid and glucose metabolism

(P)RR expression in adipose tissue doubled after a high-fat diet²⁴. Adipose tissue-specific (P)RR knockout mice displayed increased insulin sensitivity, and a reduced body weight and fat mass after exposure to a high-fat diet²⁵. Genome-wide association studies have linked sortilin-1 (SORT1) to the plasma levels of low-density lipoprotein (LDL) cholesterol²⁶. Studies applying SORT1 knockout or overexpression in rodents *in vivo* confirm this view^{26,27}. Lu et al. identified SORT1 as a high-confidence (P)RR-interacting protein via a proteomics-based approach²⁸. Importantly, (P)RR silencing in hepatocytes decreased SORT1 and low-density lipoprotein receptor (LDLR) protein abundance in hepatocytes, thus attenuating LDL uptake²⁸.

Kanda et al. observed molecular binding between *ATP6AP2* and the pyruvate dehydrogenase (PDH) E1 β subunit (PDHB). Consequently, *ATP6AP2* knockdown reduced PDH activity, resulting in a predilection to anaerobic glycolysis²⁹.

In summary, most likely due its role as a subunit of V-ATPase, the (P)RR regulates the metabolism of both lipids and glucose.

References

1. Sparks MA, Crowley SD, Gurley SB, Mirosou M and Coffman TM. Classical Renin-Angiotensin system in kidney physiology. *Compr Physiol*. 2014;4:1201-28.
2. Sihn G, Rousselle A, Vilianovitch L, Burckle C and Bader M. Physiology of the (pro)renin receptor: Wnt of change? *Kidney International*. 2010;78:246-256.
3. Danser AH and Deinum J. Renin, prorenin and the putative (pro)renin receptor. *Hypertension*. 2005;46:1069-76.
4. Nguyen G, Delarue F, Burckle C, Bouzahir L, Giller T and Sraer J-D. Pivotal role of the renin/prorenin receptor in angiotensin II production and cellular responses to renin. *Journal of Clinical Investigation*. 2002;109:1417-1427.
5. Nguyen G and Danser AHJ. Prorenin and (pro)renin receptor: a review of available data from in vitro studies and experimental models in rodents. *Experimental Physiology*. 2008;93:557-563.
6. Nguyen G and Contrepas A. Physiology and pharmacology of the (pro)renin receptor. *Curr Opin Pharmacol*. 2008;8:127-32.
7. Ramkumar N and Kohan DE. The (pro)renin receptor: an emerging player in hy-

- pertension and metabolic syndrome. *Kidney Int.* 2019;95:1041-1052.
8. Ludwig J, Kerscher S, Brandt U, Pfeiffer K, Getlawi F, Apps DK and Schägger H. Identification and characterization of a novel 9.2-kDa membrane sector-associated protein of vacuolar proton-ATPase from chromaffin granules. *J Biol Chem.* 1998;273:10939-47.
9. Hirose T, Hashimoto M, Totsune K, Metoki H, Asayama K, Kikuya M, Sugimoto K, Katsuya T, Ohkubo T, Hashimoto J, Rakugi H, Takahashi K and Imai Y. Association of (pro)renin receptor gene polymorphism with blood pressure in Japanese men: the Ohasama study. *Am J Hypertens.* 2009;22:294-9.
10. Ott C, Schneider MP, Delles C, Schlaich MP, Hilgers KF and Schmieder RE. Association of (pro)renin receptor gene polymorphism with blood pressure in Caucasian men. *Pharmacogenet Genomics.* 2011;21:347-9.
11. Brugts JJ, Isaacs A, de Maat MP, Boersma E, van Duijn CM, Akkerhuis KM, Uitterlinden AG, Witteman JC, Cambien F, Ceconi C, Remme W, Bertrand M, Ninomiya T, Harrap S, Chalmers J, MacMahon S, Fox K, Ferrari R, Simoons ML and Danser AJ. A pharmacogenetic analysis of determinants of hypertension and blood pressure response to angiotensin-converting enzyme inhibitor therapy in patients with vascular disease and healthy individuals. *Journal of Hypertension.* 2011;29:509-519.
12. Riediger F, Quack I, Qadri F, Hartleben B, Park JK, Potthoff SA, Sohn D, Sihn G, Rousselle A, Fokuhl V, Maschke U, Purfurst B, Schneider W, Rump LC, Luft FC, Dechend R, Bader M, Huber TB, Nguyen G and Muller DN. Prorenin receptor is essential for podocyte autophagy and survival. *J Am Soc Nephrol.* 2011;22:2193-202.
13. Siragy HM and Huang J. Renal (pro)renin receptor upregulation in diabetic rats through enhanced angiotensin AT1 receptor and NADPH oxidase activity. *Exp Physiol.* 2008;93:709-14.
14. Advani A, Kelly DJ, Cox AJ, White KE, Advani SL, Thai K, Connelly KA, Yuen D, Trogadis J, Herzenberg AM, Kuliszewski MA, Leong-Poi H and Gilbert RE. The (Pro)Renin Receptor. *Hypertension.* 2009;54:261-269.
15. Ichihara A and Yatabe MS. The (pro)renin receptor in health and disease. *Nat Rev Nephrol.* 2019;15:693-712.
16. Burckle CA, Jan Danser AH, Muller DN, Garrelds IM, Gasc JM, Popova E, Plehm R, Peters J, Bader M and Nguyen G. Elevated blood pressure and heart rate in human renin receptor transgenic rats. *Hypertension.* 2006;47:552-6.
17. Li W, Peng H, Cao T, Sato R, McDaniels SJ, Kobori H, Navar LG and Feng Y. Brain-targeted (pro)renin receptor knockdown attenuates angiotensin II-dependent hypertension. *Hypertension.* 2012;59:1188-94.
18. Shan Z, Shi P, Cuadra AE, Dong Y, Lamont GJ, Li Q, Seth DM, Navar LG, Katovich MJ, Sumners C and Raizada MK. Involvement of the brain (pro)renin receptor in cardiovascular homeostasis. *Circ Res.* 2010;107:934-8.
19. Li W, Peng H, Mehaffey EP, Kimball CD, Grobe JL, van Gool JM, Sullivan MN, Earley S, Danser AH, Ichihara A and Feng Y. Neuron-specific (pro)renin receptor knockout prevents the development of salt-sensitive hypertension. *Hypertension.* 2014;63:316-23.
20. Achard V, Tassistro V, Boullu-Ciocca S and Grino M. Expression and nutritional regulation of the (pro)renin receptor in rat visceral adipose tissue. *J Endocrinol In-*

Chapter 1

- vest. 2011;34:840-6.
21. Achard V, Boullu-Ciocca S, Desbriere R, Nguyen G and Grino M. Renin receptor expression in human adipose tissue. *Am J Physiol Regul Integr Comp Physiol*. 2007;292:R274-82.
 22. Gatineau E, Cohn DM, Poglitsch M, Loria AS, Gong M and Yiannikouris F. Losartan prevents the elevation of blood pressure in adipose-PPR deficient female mice while elevated circulating sPPR activates the renin-angiotensin system. *Am J Physiol Heart Circ Physiol*. 2019;316:H506-H515.
 23. Wu CH, Mohammadmoradi S, Thompson J, Su W, Gong M, Nguyen G and Yiannikouris F. Adipocyte (Pro)Renin-Receptor Deficiency Induces Lipodystrophy, Liver Steatosis and Increases Blood Pressure in Male Mice. *Hypertension*. 2016;68:213-9.
 24. Tan P, Shamansurova Z, Bisotto S, Michel C, Gauthier M-S, Rabasa-Lhoret R, Nguyen TMD, Schiller PW, Gutkowska J and Lavoie JL. Impact of the prorenin/renin receptor on the development of obesity and associated cardiometabolic risk factors. *Obesity*. 2014;22:2201-2209.
 25. Shamansurova Z, Tan P, Ahmed B, Pepin E, Seda O and Lavoie JL. Adipose tissue (P)RR regulates insulin sensitivity, fat mass and body weight. *Mol Metab*. 2016;5:959-969.
 26. Musunuru K, Strong A, Frank-Kamenetsky M, Lee NE, Ahfeldt T, Sachs KV, Li X, Li H, Kuperwasser N, Ruda VM, Pirruccello JP, Muchmore B, Prokuni-na-Olsson L, Hall JL, Schadt EE, Morales CR, Lund-Katz S, Phillips MC, Wong J, Cantley W, Racie T, Ejebe KG, Orho-Melandar M, Melander O, Koteliarsky V, Fitzgerald K, Krauss RM, Cowan CA, Kathiresan S and Rader DJ. From noncoding variant to phenotype via SORT1 at the 1p13 cholesterol locus. *Nature*. 2010;466:714-719.
 27. Kjolby M, Andersen OM, Breiderhoff T, Fjorback AW, Pedersen KM, Madsen P, Jansen P, Heeren J, Willnow TE and Nykjaer A. Sort1, encoded by the cardiovascular risk locus 1p13.3, is a regulator of hepatic lipoprotein export. *Cell Metab*. 2010;12:213-23.
 28. Lu X, Meima ME, Nelson JK, Sorrentino V, Loregger A, Scheij S, Dekkers DH, Mulder MT, Demmers JA, G MD-T, Zelcer N and Danser AH. Identification of the (Pro)renin Receptor as a Novel Regulator of Low-Density Lipoprotein Metabolism. *Circ Res*. 2016;118:222-9.
 29. Kanda A, Noda K and Ishida S. ATP6AP2/(pro)renin receptor contributes to glucose metabolism via stabilizing the pyruvate dehydrogenase E1 beta subunit. *J Biol Chem*. 2015;290:9690-700.

Aim of this thesis

Blockade of the renin-angiotensin-system (RAS) is accompanied by counterbalancing mechanisms which diminish the effectiveness of these drugs. This particularly concerns renin upregulation. Angiotensinogen siRNA is a new tool to suppress the RAS, and since it removes the substrate from which all angiotensins stem, it may prevent the angiotensin-upregulating consequences of renin stimulation. Making use of a liver-targeted angiotensinogen small interfering (si)RNA variant, it would additionally be possible to distinguish the contribution of hepatic and non-hepatic angiotensinogen.

It is widely accepted that angiotensin synthesis occurs locally in multiple organs, but whether this involves liver-derived angiotensinogen or locally synthesized angiotensinogen is still uncertain. Two sites where local angiotensinogen synthesis has been claimed to occur are the brain and the kidney. Yet, given the virtual absence of renin in the brain, local angiotensin synthesis in this organ seems impossible, raising the question why the brain synthesizes angiotensinogen at all. **Chapter 2** summarizes our knowledge with regard to angiotensin generation in the brain, and explains how centrally acting RAS blockers/agonists might work. Subsequently, in **Chapter 3** we have studied the brain RAS in full detail making use of the deoxycorticosterone acetate (DOCA)-salt rat model. It is believed that this model is representative for primary aldosteronism, and displays selective brain RAS upregulation. To obtain a better understanding of the origin of brain angiotensin, we applied liver-targeted angiotensinogen siRNA to DOCA-salt hypertensive rats. Its effects were compared with those of the aldosterone receptor antagonist spironolactone and the angiotensin II type 1 receptor blocker valsartan.

Next, in **Chapter 4**, we evaluated the effects of liver-targeted angiotensinogen siRNA in a model representing chronic kidney disease, the 5/6th nephrectomy rat. The model is characterized by hypertension, cardiac hypertrophy, proteinuria, reduced glomerular filtration rate, glomerulosclerosis, and tubulointerstitial fibrosis. Again a comparison was made versus other RAS blockers, i.e., the ACE inhibitor captopril and the angiotensin II type 1 receptor blocker losartan.

The (pro)renin receptor [(P)RR] has been proposed to facilitate angio-

Chapter 1

tensin generation at tissue sites. Yet, it only binds renin and prorenin at nanomolar levels, which do not normally occur in humans. Hence, its in-vivo functions may be entirely independent of the RAS. In **Chapters 5 and 6** we studied the role of the hepatic (P)RR in lipid metabolism in mice fed a high-fat diet, making use of liver-targeted (P)RR antisense oligonucleotides. We focused on obesity, hepatosteatosiis and atherosclerosis.

Finally, **Chapter 7** provides a general summary and discusses future perspectives.

Chapter 2

Revisiting the Brain Renin-Angiotensin System – Focus on Novel Therapies

Liwei Ren, Xifeng Lu, and A.H. Jan Danser

Curr Hypertens Rep. 2019;21:28.

Abstract

Although an independent brain renin-angiotensin system is often assumed to exist, evidence for this concept is weak. Most importantly, renin is lacking in the brain, and both brain angiotensinogen and angiotensin (Ang) II levels are exceptionally low. In fact, brain Ang II levels may well represent uptake of circulating Ang II via Ang II type 1 (AT₁) receptors. Nevertheless, novel drugs are now aimed at the brain RAS, i.e., aminopeptidase A inhibitors should block Ang III formation from Ang II, and hence diminish AT₁ receptor stimulation by Ang III, while AT₂ and Mas receptor agonists are reported to induce neuroprotection after stroke. The endogenous agonists of these receptors and their origin remain unknown. This review addresses the questions whether independent angiotensin generation truly occurs in the brain, what its relationship with the kidney is, and how centrally acting RAS blockers/agonists might work.

Keywords: brain renin-angiotensin system; aminopeptidase A inhibitor; AT₂ receptor; angiotensinogen; kidney; sympathetic nervous system; stroke

Introduction

Angiotensinogen is the precursor of all angiotensin (Ang) metabolites. Although its major source is the liver, additional sites of angiotensinogen synthesis have been reported, the most important of which are the brain, kidney, and adipose tissue [1-7]. Renin, in contrast, is derived from one source, the kidney. Its precursor, prorenin, like angiotensinogen, remarkably has several sources, including the kidney, ovaries, testis and adrenal [8]. Yet, given the fact that prorenin is inactive, it would require a (local?) activation mechanism to be of importance. Here the (pro)renin receptor, which binds and activates prorenin *in vitro*, has been proposed as a major player [9]. Unfortunately however, its affinity for prorenin is too low to allow this phenomenon to play any role *in vivo* [10], and the concept of (pro)renin receptor-prorenin interaction as a unit allowing local Ang I-generating activity is now being abandoned [11]. This does not mean that the (pro)renin receptor has no role at all – in contrast, given its ubiquitous abundance, its link with vacuolar H^+ -ATPase, and the lethal consequences of its deletion, it turns out to be of vital importance [12-15], yet apparently independently of the renin-angiotensin system (RAS). Taken together, the various sites of renin, prorenin and angiotensinogen synthesis allow multiple possibilities for angiotensin generation, e.g., in circulating blood from renal renin and hepatic angiotensinogen, or at tissue sites, from either locally synthesized angiotensinogen and prorenin, or renin, prorenin and angiotensinogen taken up from blood. Yet, regarding prorenin, we still lack a detailed insight into how it might display activity. This review focuses on the brain RAS, critically addressing the questions whether independent angiotensin generation occurs in the brain, what its relationship with the kidney is, and how centrally acting RAS blockers (in particular the recently introduced aminopeptidase A inhibitors) and activators (Ang II type 2 (AT_2) and Mas receptor agonists) might work.

Independent angiotensin generation in the brain?

Given the presence of the blood-brain barrier, diffusion of circulating renin, prorenin or angiotensinogen into the brain is impossible (Figure 1). Although early studies were able to demonstrate renin-like activity in the brain [16], its origin remained uncertain. Here one has to consider that brain tissue, when homogenized, of course contains minute amounts of trapped blood, and thus brain renin measurements have to be corrected

Chapter 2

for such admixture. Recently, making use of different mouse brain nuclei, we performed such correction, and in parallel experiments perfused the brain with buffer to remove as much blood as possible prior to brain tissue homogenization [1]. Data revealed that, although renin was easily detectable in brain nuclei, it could be entirely explained based on the presence of trapped blood in brain tissue – indeed, it disappeared after buffer perfusion. Moreover, we found no evidence for the synthesis of prorenin in the brain, not even under circumstances where activation of the brain RAS has been proposed, i.e., the deoxycorticosterone acetate (DOCA)-salt model [17, 18]. Around the same time, it was concluded that ‘intracellular renin’, a renin isoform derived from an alternative transcript of the renin gene, lacking the signal peptide and part of the prosegment (and hence being unable to leave the cell) also does not contribute to brain angiotensin generation [19]. In fact, if anything, it suppressed brain RAS activity, although the underlying mechanism remains unknown. Taken together, these data, in combination with the

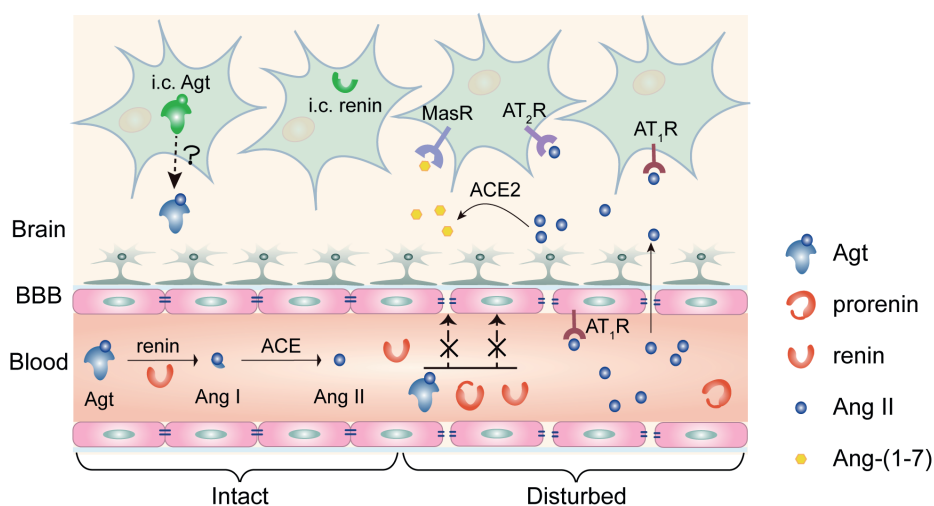


Figure 1. Current understanding of the origin of brain renin-angiotensin system (RAS) components. Circulating renin, prorenin and angiotensinogen (Agt) are unlikely to pass the blood-brain barrier (BBB). Intracellular (i.c.) renin does not contribute to brain RAS activity. Agt has been shown in brain cells and cerebrospinal fluid, yet whether actual release from cells into cerebrospinal fluid occurs remains unclear, nor do we know how brain cell-derived Agt contributes to local angiotensin (Ang) generation in the absence of renin. Ang II may bind to brain Ang II type 1 or 2 (AT₁, AT₂) receptors (R) outside the BBB, or could diffuse into the brain under conditions where the BBB is disturbed (right part of the Figure), like in hypertension. Possibly, such diffusion results in local formation of Ang-(1-7) and subsequent Mas receptor stimulation.

Brain RAS and novel therapies

exceptionally low (and often impossible to detect at all) renin mRNA expression the brain [20, 1], rule out a role for renin or prorenin in local angiotensin generation at brain tissue sites.

Data on the presence of angiotensinogen in the brain are more convincing. Multiple studies report detectable brain angiotensinogen levels that do not run in parallel with circulating angiotensinogen levels [6, 4]. Yet, generally, brain angiotensinogen levels still at most correspond with a few percent of plasma angiotensinogen levels, in a wide range of species, and thus admixture from blood cannot be entirely ruled out. Importantly, brain angiotensinogen mRNA levels, albeit being several orders of magnitude below those in the liver, are not as excessively low as those of renin [1]. At this stage, the ultimate proof for local synthesis (showing the presence of angiotensinogen in the brain of animals lacking hepatic *angiotensinogen* expression) is still awaited. When applying this approach to other organs claimed to synthesize angiotensinogen (kidney and adipose tissue) it turned out that their angiotensin generation depended entirely on hepatic angiotensinogen, implying that local angiotensinogen synthesis in these organs, if occurring at all, has no functional consequence [2, 3, 7]. If angiotensinogen synthesis truly occurs in the brain, a complicating factor remains the absence of renin. This would require non-renin enzymes to cleave angiotensinogen. There is currently no in-vivo evidence for this concept.

Angiotensins have been reported in brain tissue in widely varying levels. In some cases levels (expressed per gram tissue) were even higher than those in the kidney [18, 17]. This is hard to believe given the low angiotensinogen levels, and the absence of renin in the brain. Issues that need to be considered here are the use of very small tissue pieces for angiotensin measurements (often representing selected brain nuclei), the detection limit problems that arise from this approach (inherent to brain research), and the absence of rigorous separation techniques to distinguish true angiotensin from background noise. As an example, measuring an angiotensin (Ang) II level at the detection limit of the assay (often around 2 fmol/sample) in 10 mg brain tissue results in a theoretical tissue level of 200 fmol/g. At the same time, measuring 50 fmol Ang II in 0.5 gram renal tissue (i.e., well above the detection limit), would translate to 100 fmol/g. On this basis, it seems that brain Ang II levels are higher than in the kidney, although in reality they may be zero.

When employing liquid chromatography-tandem mass spectrometry (LC-MS/MS) to quantify the individual angiotensin metabolites, a highly sensitive method with little or no background noise, we were unable to detect Ang I in brain tissue of spontaneously hypertensive rats (SHR) [1]. Brain Ang II occurred at levels that were $\approx 25\%$ of the levels in plasma, i.e., they were several orders of magnitude below those in the kidney [21, 22]. Since Ang II type 1 (AT_1) receptor blockade reduced the brain/plasma Ang II ratio by $>80\%$, and in view of the absence of Ang I, the most likely origin of brain Ang II is accumulation of circulating Ang II via binding to AT_1 receptors [23, 21]. Additionally, considering its much smaller size versus renin and angiotensinogen, Ang II may gain access to the brain under conditions where the blood-brain barrier is (partially) disrupted, e.g., in hypertension. In fact, Ang II itself is capable of disrupting this barrier [24, 25]. Once in the brain, Ang II might be converted to metabolites, like Ang III and Ang-(1-7). However, at least in SHR, we were unable to demonstrate these metabolites [1], and thus whether angiotensin metabolites other than Ang II truly reach meaningful levels in the brain is still uncertain.

The ‘reno-cerebral reflex’

Salt intake promotes progression of chronic kidney disease. Cao et al. have suggested that renal inflammation, as occurring in the 5/6 nephrectomy rat model following exposure to high salt, results in oxidative stress and subsequent activation of the sympathetic nervous system [26]. Under these conditions, AT_1 receptors and Ang II (determined semiquantitatively by double-staining immunofluorescence), tyrosine hydroxylase (the rate-limiting enzyme for norepinephrine synthesis) and oxidative stress markers (Nox2 and Nox4) were upregulated in the brain. Remarkably, intracerebroventricular application of losartan or tempol (a reactive oxygen species scavenger) prevented this, as did renal denervation. Moreover, these procedures also prevented the paradoxical upregulation of the renal RAS (reflected by elevated angiotensinogen, ACE and AT_1 receptor levels) following high salt in this rat model. This eventually led to reduced renal inflammation and fibrosis. Based on these findings, the authors proposed that there is a ‘reno-cerebral reflex’ resulting in a positive feedback mode, further worsening kidney function (Figure 2). Similar observations were made in a mouse renal ischemia-reperfusion model under normal salt conditions [27]. Importantly, in both models

Brain RAS and novel therapies

the renal RAS upregulation occurred independently of renin, since renin was either unchanged (mouse ischemia-reperfusion model) or severely downregulated (rat 5/6 nephrectomy model during high salt). This is highly unusual, since it is normally renin that allows the up- or downregulation of angiotensin levels [28, 29]. The authors attributed this renal RAS upregulation to the increased renal *angiotensinogen* expression. Yet, it has already been shown that renal angiotensinogen does not contribute to renal angiotensin generation, neither under normal nor pathological conditions [2, 3]. Furthermore, as an indication of the brain RAS, Cao et al. identified angiotensinogen- and Ang II-‘positive’ cells in the brain, making use of anti-angiotensinogen and anti-Ang II antibodies. Given the exceptional low Ang II levels in the brain, Ang II ‘quantification’ by double-staining immunofluorescence should be interpreted with the utmost care, particularly given the inconsistencies obtained with antibodies against RAS components [30]. Why angiotensinogen, a protein which is normally secreted and not stored intracellularly, was observed in brain cells remained unexplained, nor did the authors investigate brain renin. Taken together, although of course the sympathetic connection between brain and kidney is well-established (and known to play a vital

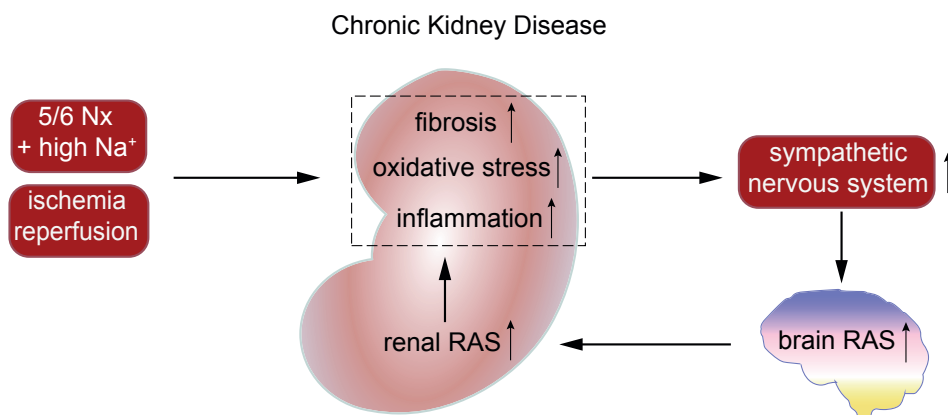


Figure 2. The reno-cerebral reflex. Renal inflammation, fibrosis and oxidative stress, as occurring in chronic kidney disease models like the 5/6 nephrectomy (Nx) model (in the presence of a high-salt diet) or after renal ischemia + reperfusion, result in sympathetic nervous system activation, which via activation of the brain renin-angiotensin system (RAS) is believed to subsequently upregulate renal angiotensinogen, thereby inducing renal RAS stimulation. A simpler explanation might be that sympathetic activation directly upregulates renal renin synthesis, since this is a well-known consequence of β -adrenergic receptor stimulation, not requiring brain RAS activation.

Chapter 2

role in blood pressure regulation and the pathogenesis of hypertension), whether sympathetic activation truly results in significant angiotensin generation at brain tissue sites cannot be concluded from these data. An alternative explanation might be that systemic Ang II, particularly in combination with high salt, via binding to brain AT₁ receptors outside the blood-brain barrier (e.g., in the subfornical organ or the organum vasculosum laminae terminalis) results in the activation of angiotensinergic projections into brain nuclei within the blood-brain barrier (like the paraventricular nucleus and the rostroventrolateral medulla) [31]. Indeed in rats, subcutaneous infusion of low-dose Ang II alone marginally affected blood pressure, while in combination with high salt it massively increased blood pressure and upregulated aldosterone [32]. Central application of either losartan or a mineralocorticoid receptor blocker prevented this. Clearly, these latter data show that protective effects of intracerebroventricular application of an AT₁ receptor blocker can also be due to interference with systemic Ang II acting in the brain. Similarly, the protective effect of centrally applied mineralocorticoid receptor blockers might relate to blockade of effects of circulating aldosterone in brain nuclei outside the blood-brain barrier, particularly because brain and plasma aldosterone levels were found to correlate closely. In conclusion, before concluding that elevated brain Ang II ‘positivity’ truly reflects activation of the brain RAS based on a reno-cerebral reflex we need to exclude that this is due to uptake of circulating Ang II, either into nuclei outside the blood-brain barrier, or, following disruption of this barrier (as occurring during pathological conditions, including a high-salt diet), into nuclei within this barrier, like the brain stem and hypothalamus [33, 25]. Here it is important to realize, as stated above, that Ang II itself is capable of disrupting this barrier. Moreover, central application of an AT₁ receptor antagonist prevented the central effects of systemic Ang II, and thus effects of centrally applied drugs cannot be taken as evidence for selective interference with brain-derived Ang II. Finally, the sympathetic nervous system is a well-known stimulator of renin release, and thus elevating renal sympathetic nervous activity is likely to activate the renal RAS, yet not necessarily via brain RAS activation.

Central aminopeptidase A inhibition

Apart from Ang II, its metabolite Ang III, generated by aminopeptidase A (APA), is an alternative activator of AT receptors. It displays similar affinity for the AT₁ receptor, and might even be the preferred agonist

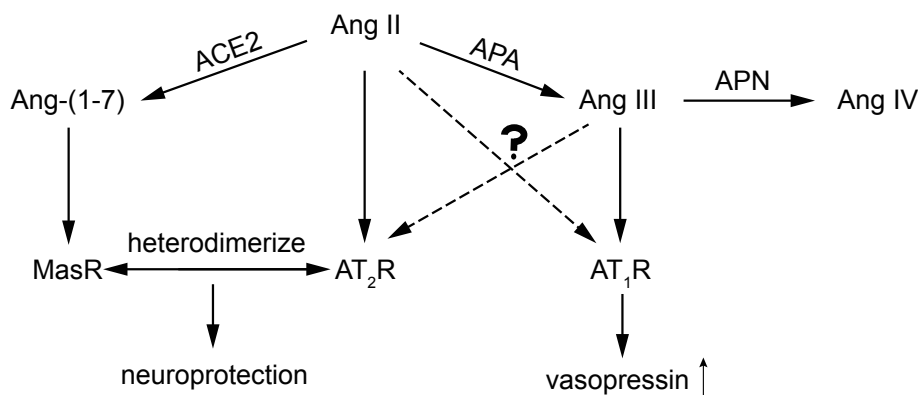


Figure 3. Formation of angiotensin (Ang) III and Ang-(1-7) from Ang II, and the receptors which are believed to be activated by the various angiotensin metabolites. The application of central aminopeptidase A (APA) inhibitors is based on the concept that Ang III is the endogenous activator of AT₁ receptors, resulting in vasopressin release. Aminopeptidase N (APN) degrades Ang III to the inactive Ang IV. Yet, others argue that Ang II is the preferred agonist of this receptor, while both agonists may also bind to AT₂ receptors. The latter heterodimerize with Mas receptors, potentially explaining the identical neuroprotective effects observed with AT₂ and Mas receptor agonists in stroke models.

of the AT₂ receptor. Assuming that the latter receptor exerts beneficial effects, e.g. coronary vasodilation and diuresis [34-36], blocking APA seems counterintuitive in hypertension. Yet, it has been claimed that in the brain Ang III rather than Ang II is the endogenous AT₁ receptor agonist, and on the basis of this concept centrally acting APA inhibitors are now being tested in hypertensive patients. This claim relates to the observation that central application of Ang II did not affect vasopressin release (a well-known effect of central AT₁ receptor activation) when simultaneously blocking APA with EC33, while simultaneous inhibition of aminopeptidase N (APN, the enzyme that degrades Ang III) with PC18 enhanced the effects of Ang II on vasopressin release [37]. Since the Ang II effects were blocked by an AT₁ receptor antagonist, it was concluded that they involved AT₁ receptor stimulation by Ang III rather than by Ang II. However, the authors did not quantify brain Ang III *in vivo* during these procedures, and thus the underlying biochemical evidence for this concept is still lacking. Confusingly, when employing LC-MS/MS we were unable to demonstrate Ang III in the brain [1], while others observed identical responses to Ang II and Ang III following intracerebroventricular application, even when making use of APA-resis-

Chapter 2

tant analogues [38]. An alternative explanation of the findings on APA and APN inhibition during Ang II application should therefore be considered, i.e., the possibility that such inhibition interferes with pathways beyond the RAS. This is not unlikely since these aminopeptidases not only act on multiple substrates, but are also ubiquitously present in- and outside the brain. Nevertheless, an EC33 prodrug, RB150, has now been synthesized which is capable of passing the blood-brain barrier. This drug decreased blood pressure in DOCA-salt rats [39], but also attenuated cardiac dysfunction after myocardial infarction [40]. As expected it reduced vasopressin and increased diuresis. A Phase IIa study assessed the blood pressure-lowering effect of a 4-week oral application of RB150 (also known as QGC001 or firibastat) in 34 patients with grade I or II essential hypertension (EudraCT Number: 2014-003071-37, unpublished results). Although there were no significant effects on blood pressure versus placebo, the drug was found to be safe and did not affect renin. At the recent American Heart Association meeting in Chicago (November 2018), a follow-up trial (NEW-HOPE, NCT03198793, unpublished results) in a much larger hypertensive, overweight subject population of multiple ethnic origin (n=250) reported antihypertensive effects of the drug (250 mg, 500 mg or 500 mg + 25 mg hydrochlorothiazide) over an 8-week treatment period. A detailed analysis of its dose-dependency and the effect of adding hydrochlorothiazide was not provided, and the trial did not include a placebo arm. Taken together, APA inhibition may well be a promising novel treatment strategy in patients displaying low systemic RAS activity (like in DOCA-salt-treated rats) but whether this truly involves suppression of brain Ang III remains to be proven(Figure.3).

AT₂ and Mas receptor agonism in the brain

AT₁ receptor blockers have often been suggested to offer cerebrovascular protection, in contrast to ACE inhibitors, although clinical evidence for this concept is still missing [41]. The underlying mechanism of this concept would be that only AT₁ receptor blockers allow central AT₂ receptor agonism. Possibly, AT₂ receptor stimulation by endogenous Ang II might already exert protective effects. Indeed, the neurological deficit after middle cerebral artery occlusion was greater in AT₂ receptor knock-out mice, and without AT₂ receptors the beneficial effects of AT₁ receptor blockade were diminished [42]. Now that AT₂ receptor agonists like C21 are available, the next step is to evaluate these drugs in stroke models, like the middle cerebral artery occlusion model and the endothelin-1-in-

Brain RAS and novel therapies

duced ischemic stroke model. Indeed, in both models, C21 exerted cerebroprotection, not only when applied introcerebroventricularly, but also when applied systemically [43, 44]. To explain the efficacy of the latter approach, considering that C21 cannot pass the blood-brain barrier, it has to be assumed that C21 enters the brain under conditions where this barrier has been disturbed, like in the above models. An exciting novel approach is to administer C21 via the nose-to-brain route to bypass the blood-brain barrier [45]. When applying C21 via this route at 1.5 hours after stroke, it reduced infarct size and improved neurological scores. Furthermore, angiotensin-(1-7) (Ang-(1-7)), generated from Ang II by ACE2, also offers neuroprotection, both when applied centrally and orally, as did the putative ACE2 activator diminazene [46]. Ang-(1-7) is believed to act via Mas receptors. One possible explanation for the identical beneficial effects of AT_2 and Mas receptor stimulation is that both receptors co-localize and are functionally interdependent [47]. Importantly, none of these approaches supports actual angiotensin synthesis in the brain allowing AT_2 /Mas receptor activation by endogenous angiotensins. A further complicating factor is that both C21 and diminazene exert AT_2 receptor- and ACE2-independent effects, respectively [48, 49], while Ang-(1-7) was recently reported not to act as Mas agonist at all [50]. Clearly, these observations remain controversial, and even if they can be taken as evidence for AT_2 /Mas receptor activation, they do not automatically imply that these receptors are normally seen by brain-derived endogenous agonists. In fact, their stimulation may depend on breakdown of the blood-brain barrier (Figure 1), allowing circulating angiotensins access to brain receptors [42].

Conclusion

Convincing evidence that angiotensin synthesis occurs independently at brain tissue sites is lacking. Renin is absent, and brain angiotensin levels are exceptionally low as compared to other organs. In fact, they may well represent binding of circulating Ang II to brain AT_1 receptors in brain nuclei outside the blood-brain barrier. To investigate whether brain-originating angiotensinogen, if existing, contributes to brain angiotensin synthesis, experiments need to be performed under conditions where hepatic angiotensinogen synthesis is silenced, preferably in a model where brain angiotensin is assumed to play an important role, like the DOCA-salt

Chapter 2

rat. Before concluding that novel therapies aimed at APA, APN, ACE2, AT₂ receptors and Mas receptors interfere with the brain RAS, we not only need to exclude non-specific effects of the applied drugs, but also show that they truly affect brain angiotensin levels, and that this explains their effects. In other words, it would help to demonstrate brain-selective Ang III suppression during RB150 treatment, and Ang-(1-7) upregulation after diminazene. Here, the application of a highly sensitive method with little or no background noise like LC-MS/MS is essential. Yet, given the fact that APA, APN and ACE2 have multiple other substrates, one simultaneously needs to rule out that effects are seen due to interference with these alternative substrates.

References

1. van Thiel BS, Martini AG, te Riet L, Severs D, Uijl E, Garrelds IM et al. The brain renin-angiotensin system: does it exist? *Hypertension*. 2017;69:1136-40.
2. Matsusaka T, Niimura F, Pastan I, Shintani A, Nishiyama A, Ichikawa I. Podocyte injury enhances filtration of liver-derived angiotensinogen and renal angiotensin II generation. *Kidney Int*. 2014;85:1068-77.
3. Matsusaka T, Niimura F, Shimizu A, Pastan I, Saito A, Kobori H et al. Liver angiotensinogen is the primary source of renal angiotensin II. *J Am Soc Nephrol*. 2012;23:1181-9.
4. Thomas WG, Sernia C. Immunocytochemical localization of angiotensinogen in the rat brain. *Neuroscience*. 1988;25:319-41.
5. Ito T, Eggena P, Barrett JD, Katz D, Metter J, Sambhi MP. Studies on angiotensinogen of plasma and cerebrospinal fluid in normal and hypertensive human subjects. *Hypertension*. 1980;2:432-6.
6. Davisson RL, Yang G, Beltz TG, Cassell MD, Johnson AK, Sigmund CD. The brain renin-angiotensin system contributes to the hypertension in mice containing both the human renin and human angiotensinogen transgenes. *Circ Res*. 1998;83:1047-58.
7. Koizumi M, Niimura F, Fukagawa M, Matsusaka T. Adipocytes do not significantly contribute to plasma angiotensinogen. *J Renin Angiotensin Aldosterone Syst*. 2016;17:1470320316672348.
8. Krop M, Danser AHJ. Circulating versus tissue renin-angiotensin system: on the origin of (pro)renin. *Curr Hyp Rep*. 2008;10:112-8.
9. Danser AH. The Role of the (Pro)renin Receptor in Hypertensive Disease. *Am J Hypertens*. 2015;28:1187-96.
10. Batenburg WW, Lu X, Leijten F, Maschke U, Müller DN, Danser AHJ. Renin- and prorenin-induced effects in rat vascular smooth muscle cells overexpressing the human (pro)renin receptor: does (pro)renin-(pro)renin receptor interaction actually occur? *Hypertension*. 2011;58:1111-9.
11. Sun Y, Danser AHJ, Lu X. (Pro)renin receptor as a therapeutic target for the treatment of cardiovascular diseases? *Pharmacol Res*. 2017;125:48-56.

12. Ren L, Sun Y, Lu H, Ye D, Han L, Wang N et al. (Pro)renin receptor inhibition reprograms hepatic lipid metabolism and protects mice from diet-induced obesity and hepatosteatosis. *Circ Res.* 2018;122:730-41.
13. Lu X, Meima ME, Nelson JK, Sorrentino V, Loregger A, Scheij S et al. Identification of the (pro)renin receptor as a novel regulator of low-density lipoprotein metabolism. *Circ Res.* 2016;118:222-9.
14. Kinouchi K, Ichihara A, Sano M, Sun-Wada GH, Wada Y, Kurauchi-Mito A et al. The (pro)renin receptor/ATP6AP2 is essential for vacuolar H⁺-ATPase assembly in murine cardiomyocytes. *Circ Res.* 2010;107:30-4.
15. Trepiccione F, Gerber SD, Grahammer F, Lopez-Cayuqueo KI, Baudrie V, Pautescu TG et al. Renal ATP6ap2/(pro)renin receptor is required for normal vacuolar H⁺-ATPase function but not for the renin-angiotensin system. *J Am Soc Nephrol.* 2016;27:3320-30.
16. Ganten D, Minnich JL, Granger P, Hayduk K, Brecht HM, Barbeau A et al. Angiotensin-forming enzyme in brain tissue. *Science.* 1971;173:64-5.
17. Li W, Sullivan MN, Zhang S, Worker CJ, Xiong Z, Speth RC et al. Intracerebroventricular infusion of the (pro)renin receptor antagonist PRO20 attenuates deoxycorticosterone acetate-salt-induced hypertension. *Hypertension.* 2015;65:352-61.
18. Li W, Peng H, Mehaffey EP, Kimball CD, Grobe JL, van Gool JMG et al. Neuron-specific (pro)renin receptor knockout prevents the development of salt-sensitive hypertension. *Hypertension.* 2014;63:316-23.
19. Shinohara K, Liu X, Morgan DA, Davis DR, Sequeira-Lopez ML, Cassell MD et al. Selective deletion of the brain-specific isoform of renin causes neurogenic hypertension. *Hypertension.* 2016;68:1385-92.
20. Lee-Kirsch MA, Gaudet F, Cardoso MC, Lindpaintner K. Distinct renin isoforms generated by tissue-specific transcription initiation and alternative splicing. *Circ Res.* 1999;84:240-6.
21. van Esch JHM, Gembardt F, Sterner-Kock A, Heringer-Walther S, Le T, Lassner D et al. Cardiac phenotype and angiotensin II levels in AT1a, AT1b and AT2 receptor single, double and triple knockouts *Cardiovasc Res.* 2010;86:401-9.
22. van Esch JHM, Moltzer E, van Veghel R, Garrelds IM, Leijten F, Bouhuizen AM et al. Beneficial cardiac effects of the renin inhibitor aliskiren in spontaneously hypertensive rats. *J Hypertens.* 2010;28:2145-55.
23. van Kats JP, van Meegen JR, Verdouw PD, Duncker DJ, Schalekamp MADH, Danser AHJ. Subcellular localization of angiotensin II in kidney and adrenal. *J Hypertens.* 2001;19:583-9.
24. Biancardi VC, Son SJ, Ahmadi S, Filosa JA, Stern JE. Circulating angiotensin II gains access to the hypothalamus and brain stem during hypertension via breakdown of the blood-brain barrier. *Hypertension.* 2014;63:572-9.
25. Biancardi VC, Stern JE. Compromised blood-brain barrier permeability: novel mechanism by which circulating angiotensin II signals to sympathoexcitatory centres during hypertension. *J Physiol.* 2016;594:1591-600.
26. Cao W, Li A, Wang L, Zhou Z, Su Z, Bin W et al. A Salt-Induced Reno-Cerebral Reflex Activates Renin-Angiotensin Systems and Promotes CKD Progression. *J Am Soc Nephrol.* 2015;26:1619-33.
27. Cao W, Li A, Li J, Wu C, Cui S, Zhou Z et al. Reno-Cerebral Reflex Activates the

Chapter 2

- Renin-Angiotensin System, Promoting Oxidative Stress and Renal Damage After Ischemia-Reperfusion Injury. *Antioxid Redox Signal*. 2017;27:415-32.
28. Balcarek J, Sev Pessa B, Bryson C, Azizi M, Menard J, Garrelds IM et al. Multiple ascending dose study with the new renin inhibitor VTP-27999: nephrocentric consequences of too much renin inhibition. *Hypertension*. 2014;63:942-50.
 29. Hollenberg NK, Fisher ND, Nussberger J, Moukarbel GV, Barkoudah E, Danser AHJ. Renal responses to three types of renin-angiotensin system blockers in patients with diabetes mellitus on a high-salt diet: a need for higher doses in diabetic patients? *J Hypertens*. 2011;29:2454-61.
 30. Herrera M, Sparks MA, Alfonso-Pecchio AR, Harrison-Bernard LM, Coffman TM. Lack of specificity of commercial antibodies leads to misidentification of angiotensin type 1 receptor protein. *Hypertension*. 2013;61:253-8.
 31. Wang HW, Huang BS, White RA, Chen A, Ahmad M, Leenen FH. Mineralocorticoid and angiotensin II type 1 receptors in the subfornical organ mediate angiotensin II - induced hypothalamic reactive oxygen species and hypertension. *Neuroscience*. 2016;329:112-21.
 32. Lu J, Wang HW, Ahmad M, Keshtkar-Jahromi M, Blaustein MP, Hamlyn JM et al. Central and peripheral slow-pressor mechanisms contributing to Angiotensin II-salt hypertension in rats. *Cardiovasc Res*. 2018;114:233-46.
 33. Stern JE, Son S, Biancardi VC, Zheng H, Sharma N, Patel KP. Astrocytes contribute to angiotensin II stimulation of hypothalamic neuronal activity and sympathetic outflow. *Hypertension*. 2016;68:1483-93.
 34. van Esch JHM, Oosterveer CR, Batenburg WW, van Veghel R, Danser AHJ. Effects of angiotensin II and its metabolites in the rat coronary vascular bed: is angiotensin III the preferred ligand of the angiotensin AT2 receptor? *Eur J Pharmacol*. 2008;588:286-93.
 35. van Esch JHM, Schuijt MP, Sayed J, Choudry Y, Walther T, Danser AHJ. AT2 receptor-mediated vasodilation in the mouse heart depends on AT1A receptor activation. *Br J Pharmacol*. 2006;148:452-8.
 36. Padia SH, Kemp BA, Howell NL, Gildea JJ, Keller SR, Carey RM. Intrarenal angiotensin III infusion induces natriuresis and angiotensin type 2 receptor translocation in Wistar-Kyoto but not in spontaneously hypertensive rats. *Hypertension*. 2009;53:338-43.
 37. Reaux A, Fournie-Zaluski MC, David C, Zini S, Roques BP, Corvol P et al. Aminopeptidase A inhibitors as potential central antihypertensive agents. *Proc Natl Acad Sci U S A*. 1999;96:13415-20.
 38. Kokje RJ, Wilson WL, Brown TE, Karamyan VT, Wright JW, Speth RC. Central pressor actions of aminopeptidase-resistant angiotensin II analogs: challenging the angiotensin III hypothesis. *Hypertension*. 2007;49:1328-35.
 39. Marc Y, Hmazzou R, Balavoine F, Flahault A, Llorens-Cortes C. Central antihypertensive effects of chronic treatment with RB150: an orally active aminopeptidase A inhibitor in deoxycorticosterone acetate-salt rats. *J Hypertens*. 2018;36:641-50.
 40. Boitard SE, Marc Y, Keck M, Mougenot N, Agbulut O, Balavoine F et al. Brain renin-angiotensin system blockade with orally active aminopeptidase A inhibitor prevents cardiac dysfunction after myocardial infarction in mice. *J Mol Cell Cardiol*. 2018;127:215-22.

Brain RAS and novel therapies

41. Hackam DG. Angiotensin receptor blockers should be regarded as first-line drugs for stroke prevention in both primary and secondary prevention settings: yes. *Stroke*. 2009;40:3159-60.
42. Iwai M, Liu HW, Chen R, Ide A, Okamoto S, Hata R et al. Possible inhibition of focal cerebral ischemia by angiotensin II type 2 receptor stimulation. *Circulation*. 2004;110:843-8.
43. Joseph JP, Mecca AP, Regenhardt RW, Bennion DM, Rodriguez V, Desland F et al. The angiotensin type 2 receptor agonist Compound 21 elicits cerebroprotection in endothelin-1 induced ischemic stroke. *Neuropharmacology*. 2014;81:134-41.
44. Min LJ, Mogi M, Tsukuda K, Jing F, Ohshima K, Nakaoka H et al. Direct stimulation of angiotensin II type 2 receptor initiated after stroke ameliorates ischemic brain damage. *Am J Hypertens*. 2014;27:1036-44.
45. Bennion DM, Jones CH, Dang AN, Isenberg J, Graham JT, Lindblad L et al. Protective effects of the angiotensin II AT2 receptor agonist compound 21 in ischemic stroke: a nose-to-brain delivery approach. *Clin Sci (Lond)*. 2018;132:581-93.
46. Bennion DM, Haltigan EA, Irwin AJ, Donnangelo LL, Regenhardt RW, Pioquin to DJ et al. Activation of the neuroprotective angiotensin-converting enzyme 2 in rat ischemic stroke. *Hypertension*. 2015;66:141-8.
47. Patel SN, Ali Q, Samuel P, Steckelings UM, Hussain T. Angiotensin II Type 2 Receptor and Receptor Mas Are Colocalized and Functionally Interdependent in Obese Zucker Rat Kidney. *Hypertension*. 2017;70:831-8.
48. Haber PK, Ye M, Wysocki J, Maier C, Haque SK, Batlle D. Angiotensin-converting enzyme 2-independent action of presumed angiotensin-converting enzyme 2 activators: studies in vivo, ex vivo, and in vitro. *Hypertension*. 2014;63:774-82.
49. Verdonk K, Durik M, Abd-Alla N, Batenburg WW, van den Bogaardt AJ, van Veghel R et al. Compound 21 induces vasorelaxation via an endothelium- and angiotensin II type 2 receptor-independent mechanism. *Hypertension*. 2012;60:722-9.
50. Gaidarov I, Adams J, Frazer J, Anthony T, Chen X, Gatlin J et al. Angiotensin (1-7) does not interact directly with MAS1, but can potently antagonize signaling from the AT1 receptor. *Cell Signal*. 2018;50:9-24.

Important (•) recent references:

- Ref. 1: • First paper that critically addresses the origin of brain renin
- Ref. 26: • This paper introduces the reno-cerebral reflex concept
- Ref. 32: • This paper demonstrates that centrally applied RAS blockers also block the effects of systemic Ang II and aldosterone
- Ref. 39: • Central aminopeptidase A inhibition lowers blood pressure in a model with low systemic RAS activity
- Ref. 45: • Nose-to-brain delivery enhances brain accumulation of the putative AT₂ receptor agonist C21

Chapter 3

No evidence for brain renin-angiotensin system activation during DOCA-salt hypertension

Estrellita Uijl[#], Liwei Ren[#], Katrina M. Mirabito Colafella, Richard van Veghel, Ingrid M. Garrelds, Oliver Domenig, Marko Poglitsch, Ivan Zlatev, Jae B. Kim, Stephen Huang, Lauren Melton, Ewout J. Hoorn, Don Foster, A.H. Jan Danser

Clin Sci (Lond). 2021;135:259–274

[#]Contributed equally

Abstract

Brain renin-angiotensin system (RAS) activation is thought to mediate deoxycorticosterone acetate (DOCA)-salt hypertension, an animal model for human primary hyperaldosteronism. Here, we determined whether brainstem angiotensin II is generated from locally synthesized angiotensinogen and mediates DOCA-salt hypertension. To this end, chronic DOCA-salt-hypertensive rats were treated with liver-directed siRNA targeted to angiotensinogen, the angiotensin II type 1 receptor antagonist valsartan, or the mineralocorticoid receptor antagonist spironolactone (n=6-8/group). We quantified circulating angiotensinogen and renin by enzyme-kinetic assay, tissue angiotensinogen by western blotting, and angiotensin metabolites by LC-MS/MS. In rats without DOCA-salt, circulating angiotensin II was detected in all rats, whereas brainstem angiotensin II was detected in 5 out of 7 rats. DOCA-salt increased mean arterial pressure by 19 ± 1 mmHg and suppressed circulating renin and angiotensin II by $>90\%$, while brainstem angiotensin II became undetectable in 5 out of 7 rats (<6 fmol/g). Gene silencing of liver angiotensinogen using siRNA lowered circulating angiotensinogen by $97 \pm 0.3\%$, and made brainstem angiotensin II undetectable in all rats ($P < 0.05$ vs. non-DOCA-salt), although brainstem angiotensinogen remained intact. As expected for this model, neither siRNA nor valsartan attenuated the hypertensive response to DOCA-salt, whereas spironolactone normalized blood pressure and restored brain angiotensin II together with circulating renin and angiotensin II. In conclusion, despite local synthesis of angiotensinogen in the brain, brain angiotensin II depended on circulating angiotensinogen. That DOCA-salt suppressed circulating and brain angiotensin II in parallel, while spironolactone simultaneously increased brain angiotensin II and lowered blood pressure, indicates that DOCA-salt hypertension is not mediated by brain RAS activation.

Keywords: brain; angiotensinogen; angiotensin II; salt-sensitive hypertension; RNA, small interfering; RNAi therapeutics; mineralocorticoid receptor antagonism

Introduction

Hypertension is the leading risk factor for death and disability worldwide.¹ End-organ damage caused by hypertension can be effectively prevented by blocking the renin-angiotensin system (RAS), even when circulating RAS activity is low.²⁻⁴ The underlying concept is that in these organs angiotensin (Ang) II generation relies on the local synthesis of angiotensinogen (AGT), i.e., occurs independently of AGT synthesis in the liver.⁵ Indeed, even though liver-derived AGT is the main – if not the only – source of circulating Ang II⁶, gene expression of *Agt* also occurs in brain, kidney and adipose tissue.^{7,8} Yet when the *Agt* gene was deleted selectively in hepatocytes, it was found that Ang II generation in kidney and adipose tissue did depend on the uptake of liver-derived AGT from the circulation.^{6,9,10} To what degree this is also true for the brain is unknown.

The brain RAS is thought to be activated by the combination of deoxycorticosterone acetate and excess dietary salt (DOCA-salt). The DOCA-salt rat represents a model for human primary hyperaldosteronism in which the circulating RAS is suppressed by volume-dependent hypertension. That intracerebroventricular, but not intravenous, administration of RAS blockers partially reversed the hypertensive response to DOCA-salt has supported the concept of selective brain RAS activation.¹¹⁻¹³ The underlying assumption is that the blood-brain barrier prevents the diffusion of circulating AGT and Ang II into the brain, so that any Ang II in the brain must be derived from locally synthesized AGT. However, it is widely accepted that high blood pressure disrupts the blood-brain barrier, thereby allowing circulating Ang II access to the brain.^{14,15} This perspective offers an alternative explanation as to why intracerebroventricular administration of an Ang II type 1 (AT₁) receptor blocker (ARB) attenuated hypertension better than its intravenous application.¹⁶

An additional argument against selective brain RAS activation by DOCA-salt is that the brain lacks renin. Originally, it was proposed that intracellular renin – the isoform of renin expressed in the brain¹⁷ – cleaves brain AGT. Yet, surprisingly, its deletion increased blood pressure and made mice more susceptible to Ang II-induced organ damage.¹⁸ Consequently, intracellular renin is now believed to play a protective, RAS-suppressing role, without acting on AGT.¹⁸ Furthermore, brain renin levels

Chapter 3

in DOCA-salt-hypertensive mice decreased in parallel with circulating renin.¹⁹ In fact, brain renin levels were so low that they likely represented renin in trapped blood.¹⁹ The same is true for prorenin¹⁹, which opposes the concept that prorenin's interaction with the (pro)renin receptor underlies brain RAS activation in DOCA-salt treated animals.

In the current study, we set out to determine the contribution of liver-derived AGT to brain RAS activation in chronic DOCA-salt-hypertensive rats, making use of liver-targeted small interfering RNA (siRNA) to selectively silence hepatic Agt.²⁰ We focused on the brainstem as a proxy for brain RAS activation, because this region is fully sequestered from the circulation by the blood brain barrier and it contains the highest levels of renin in the brain.¹⁹ To simultaneously delineate the role of blood pressure and AT₁ receptor-mediated uptake of circulating Ang II into the brain, we also evaluated DOCA-salt rats treated with the mineralocorticoid receptor antagonist spironolactone (which normalizes blood pressure in this model), the ARB valsartan, or their combination. We found that, in contrast to AGT in the kidney or adipose tissue, AGT in the brain did not depend on uptake of liver-derived AGT from the circulation. Yet, DOCA-salt suppressed levels of brain Ang II in parallel with those in blood, kidney and adipose tissue. Thus, selective brain RAS activation by DOCA-salt did not occur, while a role for brain-derived AGT still needs to be demonstrated.

Methods

Animal studies

All studies were performed at the Erasmus MC (Rotterdam, The Netherlands) under the regulation and permission of the Animal Care Committee of the Erasmus MC (protocol number 17-870-01). Male, 14-week old Sprague Dawley rats (Janvier Labs, France) were housed in individual cages and maintained on a 12-h light-dark cycle with access to standard rat chow and tap water ad libitum. Radiotelemetry transmitters (HD-S10, Data Sciences International, St. Paul, USA) were implanted to continuously measure blood pressure, heart rate and activity.²¹ Peri-operative analgesia consisted of buprenorphine (0.5 mg/kg s.c.) given 1h prior to surgery and 6 hours after surgery, followed by twice daily injections up until 2 days after surgery. After a two-week recovery period, hypertension was induced by subcutaneous implantation of a DOCA-pellet (200 mg; 60-

day release; Innovative Research of America, Sarasota, FL, USA) and by replacing the drinking water with saline (DOCA-salt). Normotensive control rats (non-DOCA; $n=7$) were sham operated and remained on tap water. DOCA-salt-hypertensive rats were studied for 7 weeks; telemetry data was recorded every 10 minutes from 3 days prior to DOCA-pellet implantation onwards. During the final 3 weeks, DOCA-salt was supplemented with vehicle ($n=7$), liver-targeted siRNA directed against AGT (AGT siRNA; $n=7$; 30 mg/kg fortnightly by subcutaneous injection; provided by Alnylam Pharmaceuticals, Cambridge, MA, USA), valsartan ($n=8$; 31 mg/kg/day; Santa Cruz Biotechnology, Heidelberg, Germany), spironolactone ($n=8$; 80 mg/kg/day; Sigma Aldrich, Zwijndrecht, The Netherlands) or the combination of spironolactone and valsartan ($n=6$). The siRNA consisted of a chemically modified antisense strand with sequence UUGAUUUUUGCCCAGGAUAGCUC, hybridized with a chemically modified sense strand of sequence GCUAUCCUG-GGCAAAAUAUCAA. Oligonucleotides were synthesized as previously described.²² To ensure selective and efficient delivery to hepatocytes, a triantennary N-acetylgalactosamine (GalNAc) – a high-affinity ligand for the hepatocyte-specific asialoglycoprotein receptor – was attached to the 3' end of the sense strand.²⁰ Valsartan was dissolved in 1 mol/L sodium hydroxide (Sigma Aldrich; made up in saline). The solution was titrated back to a pH of ~ 7 with 10% hydrochloric acid (Sigma Aldrich) and delivered by an osmotic mini-pump (Alzet, Cupertino, CA, USA). Spironolactone was dissolved in sesame oil (Sigma Aldrich) and delivered by daily subcutaneous injection. To control for effects of these methods of delivery, all rats underwent a sham pump implantation and received daily injections of equivalent volumes of sesame oil. For biochemical measurements, we collected 24-hour urine in metabolic cages and blood plasma by venipuncture from the lateral tail vein at 3 points in time: prior to DOCA-salt, and after 4 and 7 weeks of DOCA-salt. At the end of the 7-week study period, rats were anaesthetized by inhalation of isoflurane and exsanguinated: 1 mL blood was collected in 10 mL of 4 mol/L guanidine thiocyanate (Sigma Aldrich) and used for quantification of angiotensin metabolites; remaining blood was supplemented with EDTA and centrifuged at $16000 \times g$ to obtain plasma. Liver, brainstem, cerebellum, kidneys, heart, epididymal adipose tissue (AT), inguinal AT and brown AT were excised, weighed, and snap frozen in liquid nitrogen for gene expression and protein analysis.

Biochemical measurements

Chapter 3

In plasma, AGT was measured by enzyme-kinetic assay as the maximum quantity of Ang I generated during incubation, at pH 7.4 and 37°C, with rat kidney renin in the presence of a mixture of ACE, angiotensinase, and serine protease inhibitors.^{23, 24} The lower limit of detection (LLOD) of this assay was 0.2 nmol/L. We have previously shown that the results produced by this assays correlate strongly with those obtained from AGT ELISA (Immuno-Biological Laboratories Co. Ltd.).²² Active plasma renin concentration (APRC) was measured by enzyme kinetic assay, by quantifying Ang I generation in the presence of excess porcine AGT (LLOD 0.17 ng Ang I/mL per hour).²³ In the cases that measurements were at or below the LLOD, this limit was applied to allow for statistical analysis. Ang metabolites in plasma, kidney, brainstem, epididymal AT and heart tissue (left ventricle) were measured by LC-MS/MS analysis as described before.^{25, 26} Briefly, tissue samples were homogenized under liquid nitrogen and extracted with a guanidinium based extraction buffer. Stabilized whole blood and tissue extracts were spiked with stable isotope labeled internal standards for each individual target analyte (Sigma Aldrich) before being subjected to C18 based solid phase extraction and subsequent LC-MS/MS analysis. **Table S1** specifies the lower limits of quantification (LLOQ) for each metabolite per tissue. NT-proBNP was measured with a rat ELISA NT-proBNP kit (LLOD 15.6 pg/mL; Aviva Systems Biology, San Diego, USA). Plasma and urinary sodium and urinary potassium (both 24-hour urine) were measured at the clinical chemistry laboratory of the Erasmus MC.

Quantitative polymerase chain reaction (qPCR)

Total RNA was isolated from snap-frozen liver, kidney, brainstem, epididymal AT, inguinal AT and brown AT using TRI Reagent (Sigma Aldrich) and reverse transcribed into cDNA using the QuantiTect Reverse Transcription Kit (Qiagen, Venlo, The Netherlands). cDNA was amplified in triplicate in 40 cycles (denaturation at 95°C for 3 min; thermal cycling at 95°C for 3 sec, annealing/extension at 60°C for 20 sec) followed by a melt curve with a CFX384 (Bio-rad, Veenendaal, The Netherlands) using Kapa SYBR® Fast (Kapa Biosystems). The intron-spanning oligonucleotide primers were designed with NCBI Primer-BLAST (Table S2). The DDCT method was used for relative quantification of mRNA expression levels, using the geometric mean of β_2 -microglobulin (B2M) and β -actin (ActB) for normalization.

siRNA quantification

siRNA quantification was performed as described previously.²⁷ Antisense levels in siRNA standard curve dilutions and homogenized liver, kidney and cerebellum samples were quantified by stem loop reverse transcription followed by qPCR. The primer and probe sequences were GTCGTATCCAGTGCAGGGTCCGAGGTATTCGCACTGGATACGACGAGCTATCCT (RT primer), GCCGCGCTTGATTTTGGCCC (Forward qPCR primer), CTGGATACGACGAGCTATCC (Taqman probe), GTGCAGGGTCCGAGGT (Reverse qPCR primer), using 5' FAM and 3' MGBNFQ for the probe. C_t values derived from samples were interpolated onto the standard curve, adjusted for sample dilution, and expressed as micrograms of antisense strand per gram of tissue.

Western blotting

Snap frozen liver, kidney, brainstem, epididymal AT, inguinal AT and brown AT were homogenized on ice in a buffer containing 0.3 mol/L sucrose, 50 mmol/L Tris-HCl pH 7.5, 1 mmol/L EDTA, 1 mmol/L EGTA, 50 mmol/L sodium fluoride, 1 mmol/L DTT, and 1 mmol/L PMSF supplemented with protease inhibitors. Subsequently, 20-50 μ g of protein (DCTM protein assay kit, Bio-Rad) was separated by electrophoresis on a Criterion TGX precast protein gel (Bio-Rad) and transferred to a membrane using the Trans-Blot Turbo Transfer System (Bio-Rad). Membranes were blocked with 5% bovine serum albumin in Tris-buffered saline containing 0.1% Tween-20, followed by incubation overnight at 4°C with a primary antibody directed against AGT (1:100; polyclonal antibody raised in rabbits against a synthetic peptide modeled after the C-terminal part of mouse AGT and purified by antigen affinity; Immuno-Biological Laboratories Co. Ltd., Japan; lot #1E-711). After washing, blots were incubated with an anti-rabbit horseradish peroxidase-conjugated secondary antibody (1:3000; Bio-Rad). Signals were detected by chemiluminescence (Clarity Western ECL substrate; Bio-Rad) and quantified using ImageQuant LAS 4000 (GE Healthcare, Diegem, Belgium). Glyceraldehyde-3-phosphate dehydrogenase (GAPDH; 1:5000; Gene-Tex, Irvine, CA, USA) was used for normalization of protein levels. Using the method described above, AGT antibody target specificity was validated by demonstrating a single band at ~53 kD in tissues obtained from wild-type but not in tissues from Agt knockout mice²⁸ (tissues were a kind gift from Prof. M. Bader; Figure S1). Specificity was confirmed for rat tissues by demonstrating a single band at ~53 kD in liver homog-

Chapter 3

enates from untreated control rats but not in liver homogenates from AGT siRNA-treated rats (**Figure S1**).

For comparison, brainstem AGT in western blot samples was also measured by AGT ELISA (Immuno-Biological Laboratories Co. Ltd.; LLOD 0.32 ng/mL).

Kidney function

Glomerular filtration rate (GFR) was determined prior to DOCA-salt, and after 4 and 7 weeks of DOCA-salt, by transcutaneous measurement of fluorescein isothiocyanate (FITC)-labeled sinistrin (Mannheim Pharma & Diagnostics GmbH, Mannheim, Germany), administered as a bolus injection (0.3 mg/kg dissolved in saline) via the tail vein. A non-invasive clearance (NIC)-kidney fluorescent detection device together with partner software (Mannheim Pharma & Diagnostics GmbH) were used to generate the elimination kinetics curve of FITC-sinistrin. GFR was derived from the excretion half-life ($t_{1/2}$) of FITC-sinistrin, using a conversion factor and formula validated for rats²⁹:

$$\text{GFR (mL/min per 100g body weight (BW))} = 31.26 \text{ (mL/100g BW)} / t_{1/2} \text{ FITC-sinistrin (minutes)}.$$

Histology

Transverse heart sections fixed in 4% paraformaldehyde were dehydrated and paraffin-embedded. Deparaffinized sections (5 μ m) were stained with Gomori silver to visualize individual cardiomyocytes. Only left-ventricular, transversally cut cardiomyocytes showing a nucleus were analyzed with Qwin (Leica, Cambridge, UK) for surface area quantification.

Myograph studies

Responses of iliac arteries were measured in a Mulvany myograph as changes in isometric force. Iliac arteries were precontracted with U46619 to construct concentration-response curves to the endothelium-dependent vasodilator acetylcholine, in the absence or presence of the NO synthase inhibitor L-NAME, the small conductance Ca^{2+} -activated K^{+} channel inhibitor apamin and the intermediate conductance Ca^{2+} -activated K^{+} channel inhibitor TRAM34.

Statistical analyses

Parametric data are expressed as mean values \pm SEM and were analyzed

using a one-way analysis of variance (ANOVA). Before statistical testing, data on Ang metabolites were log-transformed to conform to normality. Non-parametric data that did not follow a normal distribution after log transformation (APRC) are expressed as median (interquartile range) and were analyzed using a Kruskal-Wallis test. Data obtained at multiple points in time were analyzed using a repeated-measures ANOVA. Post-hoc correction according to Dunnett or Dunn was performed in case of multiple comparisons. Univariate linear associations were assessed by calculation of Pearson's coefficient of correlation. Two-tailed P values <0.05 were considered statistically significant. All analyses were performed using Prism v8.0 (Graphpad Software Inc., La Jolla, USA)

Results

Spironolactone with or without valsartan reverses DOCA-salt hypertension

Upon induction of DOCA-salt, rats developed polydipsia and polyuria, accompanied by an increase in plasma sodium concentration and urinary sodium and potassium excretion (Table S3). Prior to DOCA-salt, mean arterial pressure (MAP) was 103 ± 1 mm Hg. Over a 4-week period, DOCA-salt increased MAP by 19 ± 2 mm Hg and decreased heart rate by 52 ± 3 BPM ($P < 0.0001$ vs. baseline for both; Figure 1A-B). The rise was greater for systolic than for diastolic blood pressure (24 ± 2 vs. 15 ± 2 mm Hg; $P < 0.0001$; data not shown). The hypertensive response to DOCA-salt was not attenuated when DOCA-salt was supplemented with vehicle, AGT siRNA or valsartan for the final 3 weeks (Figure 1A). In contrast, spironolactone with or without valsartan fully normalized MAP ($P < 0.01$ and $P < 0.05$ vs. vehicle, respectively; Figure 1A). When combined with valsartan, the antihypertensive effect of spironolactone occurred faster and tended to be stronger ($P = 0.12$ vs. spironolactone). Reductions in MAP were matched by increases in heart rate (Figure 1B). Although AGT siRNA did not lower MAP, heart rate also rose in these rats ($P < 0.05$ vs. vehicle; Figure 1B). None of the treatments, nor DOCA-salt on its own, affected locomotor activity or physiological weight gain (Figure 1C; Table S3).

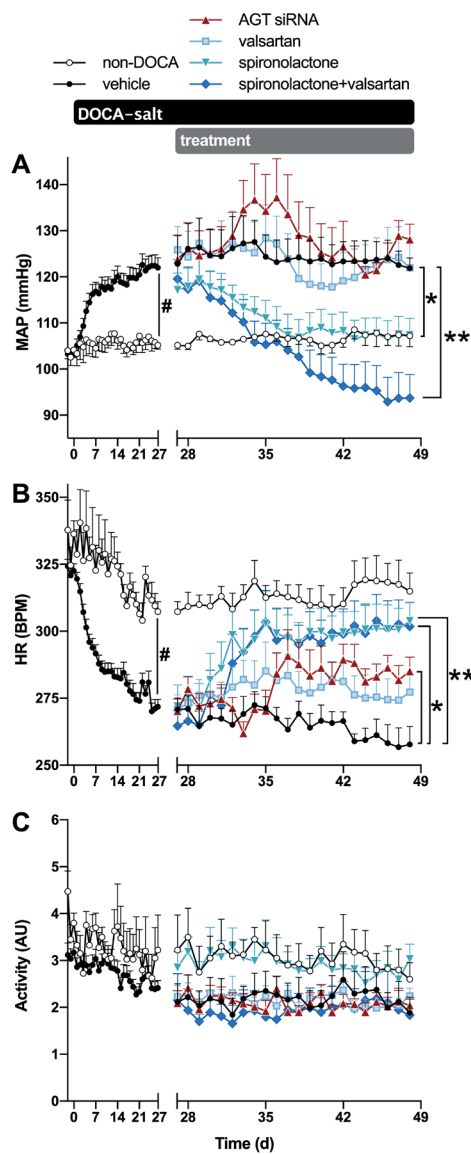


Figure 1: Mean arterial pressure, heart rate and locomotor activity.

Rats were sham operated (non-DOCA normotensive controls; open circles) or received DOCA-salt for 7 weeks and were treated with vehicle (solid circle), AGT siRNA (triangle), valsartan (square), spironolactone (upside-down triangle) or valsartan+spironolactone (diamond) during the final 3 weeks (n=6-8 per group). A) Mean arterial pressure (MAP), B) heart rate (HR) and C) locomotor activity were recorded via radiotelemetry. Data, represented as means \pm SEM, were analyzed using two-way ANOVA and post-hoc Dunnett (# $P \leq 0.0001$ vs baseline; * $P \leq 0.05$, ** $P \leq 0.01$ vs. vehicle). Abbreviations: BPM, beats per minute; AU, arbitrary units.

Spironolactone with or without valsartan reverses the suppressive effect of DOCA-salt on circulating RAS activity

Prior to DOCA-salt, circulating AGT levels were 698 ± 29 nmol/L and active plasma renin concentrations (APRC) were 11.8 ± 0.8 ng Ang I/mL per hour. Although DOCA-salt suppressed APRC by $98 \pm 0.5\%$ ($P < 0.0001$ vs. baseline), circulating AGT remained unaffected (Figure 2A-B),

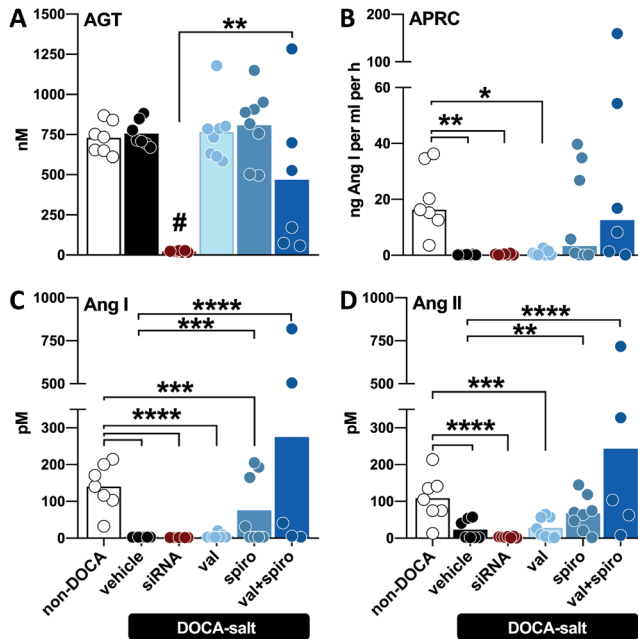


Figure 2: Circulating RAS parameters. Plasma levels of A) angiotensinogen (AGT), B) active plasma renin concentration (APRC), C) angiotensin (Ang) I, and D) Ang II of rats not given DOCA-salt (non-DOCA) or given DOCA-salt for 7 weeks and treated with vehicle, AGT siRNA, valsartan (val), spironolactone (spiro) or valsartan+spironolactone (val+spiro) during the final 3 weeks (n=6-8 per group). Data are represented as means (AGT and Ang) or medians (APRC). AGT and log-transformed Ang data were analyzed using one-way ANOVA and post-hoc Dunnett, APRC was analyzed using Kruskal-Wallis test and post-hoc Dunn (# $P \leq 0.0001$ vs all other groups; * $P \leq 0.05$, ** $P \leq 0.01$, **** $P \leq 0.0001$ vs. non-DOCA or otherwise indicated in graph).

most likely because rat AGT levels approximate the Michaelis-Menten constant for renin. Addition of AGT siRNA lowered circulating AGT by $97 \pm 0.3\%$ (Figure 2A). APRC remained suppressed by $96 \pm 1\%$ and $95 \pm 2\%$ when DOCA-salt was supplemented with AGT siRNA or valsartan, respectively (Figure 2B). As APRC determined circulating Ang I ($r=0.95$; $P<0.0001$) and Ang II ($r=0.72$; $P<0.0001$; Figure S2A-B), levels of Ang I and II were downregulated together with APRC in DOCA-salt-treated rats given vehicle, AGT siRNA or valsartan (Figure 2C-D). However, consistent with the restoration of a strong inverse relationship between MAP and APRC ($r=-0.80$; $P<0.001$; Figure S2C-D), spironolactone with or without valsartan reversed the suppressive effect of DOCA-salt on circulating APRC, Ang I, and Ang II in parallel with its antihypertensive efficacy (Figure 2C-D).

Extrahepatic *Agt* gene expression is not affected by liver-targeted AGT siRNA

Agt gene expression in control rats that had not received DOCA-salt was lowest in inguinal adipose tissue ($3\pm1\%$ of liver *Agt* expression), followed by kidney ($7\pm1\%$), brown adipose tissue ($15\pm3\%$), epididymal adipose tissue ($27\pm5\%$) and brainstem ($55\pm8\%$; $P<0.001$ vs liver; Figure 3A). DOCA-salt increased *Agt* mRNA expression by 1.5-fold in liver and by 2-fold in brown adipose tissue (both $P<0.05$; Figure 3A). Treatment with liver-directed siRNA for 3 weeks resulted in siRNA levels of 87 ± 17 mg/g in the liver and 4 ± 0.4 mg/g in the kidney, whereas none could be detected in the brain. Accordingly, liver *Agt* mRNA was silenced by $98\pm1\%$, while expression remained intact in kidney, adipose and brainstem tissue of siRNA-treated rats (Figure 3A). In fact, in the brainstems of DOCA-salt-hypertensive rats given siRNA, *Agt* mRNA was doubled when compared to rats that had not received DOCA-salt ($P<0.05$) or only DOCA-salt ($P<0.001$; Figure 3A).

In contrast to kidney and adipose AGT, brain AGT is liver-independent

We quantified tissue AGT protein to determine whether locally transcribed *Agt* mRNA was also translated. In rats not given DOCA-salt, the lowest amount of AGT protein was detected in liver, followed by kidney (1.3-fold higher), brainstem (2.1-fold higher), brown adipose tissue (2.2-fold higher), epididymal adipose tissue (3.2-fold higher) and inguinal adipose tissue (5-fold higher; Figure 3B). DOCA-salt on its own doubled AGT protein in brown adipose tissue ($P<0.0001$; Figure 3C). In DOCA-salt-treated rats given siRNA, hepatic *Agt* silencing eliminated AGT protein levels in liver and plasma concomitantly (Figure 3C, Figure 2A). Absence of AGT from the circulation also eliminated AGT protein in kidney and epididymal adipose tissue ($P<0.0001$ for both), whereas levels were reduced by three-quarters in brown adipose tissue and halved in inguinal adipose tissue ($P<0.0001$ and $P<0.01$ vs. vehicle, respectively; Figure 3C). Depletion of AGT protein despite retention of mRNA expression indicates that AGT levels in these tissues are fully or partially dependent on circulating/liver AGT, consistent with previous observations.^{6, 10} In contrast to kidney and adipose tissue, hepatic *Agt* silencing did not affect brainstem AGT protein (Figure 3C). Equal brainstem

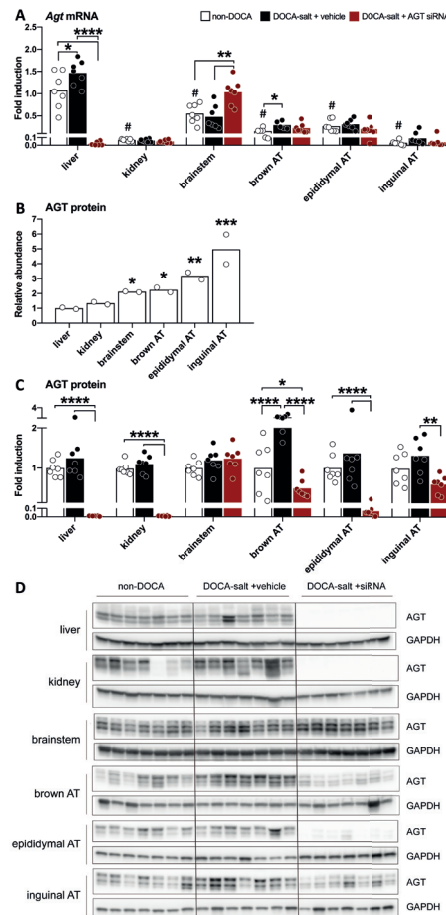


Figure 3: *Agt* gene expression and AGT protein abundance in tissues of rats not given DOCA-salt (non-DOCA) or given DOCA-salt for 7 weeks and treated with vehicle or AGT siRNA during the final 3 weeks (n=7 per group). A) Gene expression of *Agt*, represented as mean fold induction relative to *Agt* expression in the livers of non-DOCA controls, was analyzed using one-way ANOVA and post-hoc Bonferroni. Protein abundance of AGT in B) tissues of non-DOCA controls, normalized to liver AGT, and in C) tissues of non-DOCA and DOCA-salt-treated rats given vehicle or siRNA, represented as mean fold induction relative to AGT abundance in the non-DOCA controls of each tissue, was analyzed using one-way ANOVA and post-hoc Dunnett or Bonferroni. D) Representative immunoblots. (# $P \leq 0.001$ vs. non-DOCA liver; * $P \leq 0.05$, ** $P \leq 0.01$, *** $P \leq 0.001$, **** $P \leq 0.0001$). Abbreviations: AT, adipose tissue.

AGT content was confirmed with an ELISA, which detected 7.1 ± 1.1 ng AGT per mg protein in DOCA-salt-treated rats given siRNA versus 9.1 ± 1.6 ng AGT per mg protein in rats that had not received DOCA-salt (n=7 for both, $P=0.42$).

DOCA-salt suppresses brain Ang II in parallel with circulating, kidney and adipose Ang II

In DOCA-salt-treated rats, suppression of circulating RAS activity was mirrored in the kidney, where renin expression was $88\pm6\%$ lower ($P<0.001$; Figure S3), Ang I was $98\pm0.5\%$ lower ($P<0.001$; Table S4) and Ang II was $99\pm0.3\%$ lower than in rats not given DOCA-salt ($P<0.05$; Figure 4A). Except for Ang (3-8), all Ang metabolites could be detected in the kidneys of rats not given DOCA-salt (Table S4). In contrast, only renal Ang I and II were detectable in the majority of DOCA-salt-treated rats given vehicle, and none of the Ang metabolites could be detected in any DOCA-salt-treated rat given AGT siRNA (Table S4). Kidney Ang I became detectable again in $\sim 85\%$ of the DOCA-salt-treated rats given valsartan, spironolactone or their combination, while renal Ang II was detected again in 25% of the rats given valsartan, and in $\sim 85\%$ of the rats given spironolactone with or without valsartan (Figure 4A). In the

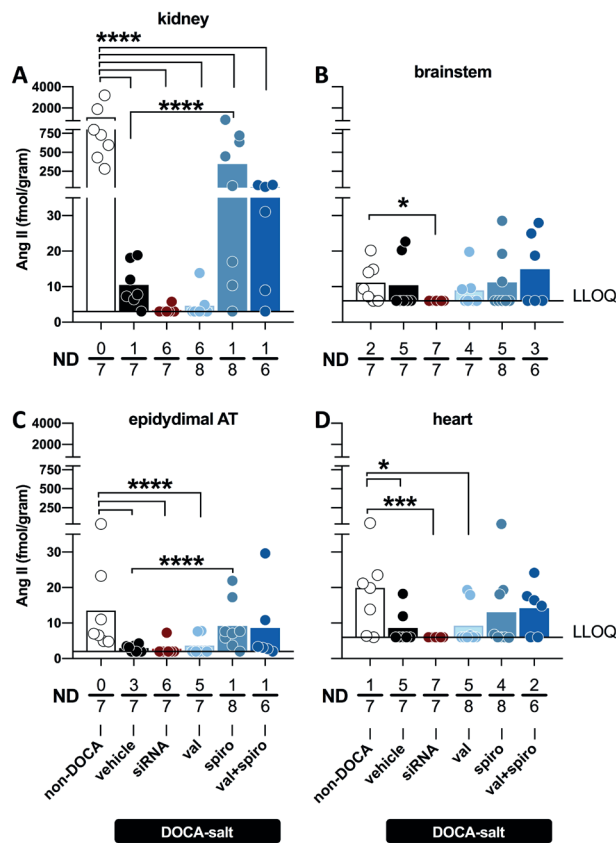


Figure 4: Tissue levels of angiotensin (Ang) II were measured by LC-MS/MS in A) kidneys, B) brainstems, C) epididymal adipose tissue (AT), and D) hearts of rats not given DOCA-salt (non-DOCA) or given DOCA-salt for 7 weeks and treated with vehicle, AGT siRNA, valsartan (val), spironolactone (spiro) or valsartan+spironolactone (val+spiro) during the final 3 weeks (n=6-8 per group). Data, represented as medians, were analyzed after log transformation using ANOVA and post-hoc Dunnett (* $P \leq 0.05$, ** $P \leq 0.01$, *** $P \leq 0.001$, **** $P \leq 0.0001$). Abbreviations: ND, not detectable; LLOQ, lower limit of quantification.

brainstem, only Ang II could be detected, and none of the other metabolites (Table S4). Brainstem Ang II was detected in 71% of the rats not given DOCA-salt, but only in 29% of the DOCA-salt-treated rats given vehicle, and in none of the DOCA-salt-treated rats given siRNA ($P < 0.05$; Figure 4B). In contrast, treatment with valsartan, spironolactone or their combination reconstituted brainstem Ang II in 40-50% of the rats (Figure 4B). Ang II levels in epididymal adipose and heart tissue followed the exact same pattern of elimination and reconstitution as was observed for kidney and brainstem (Figure 4C-D).

DOCA-salt on its own halved the expression of Ang II type 1A receptors ($P < 0.05$) in the brainstem, whereas the expression of Ang II type 1B and Ang II type 2 receptors remained comparable to that of rats that were not given DOCA-salt (Figure S3).

Effects on kidney function, endothelial function and cardiac hypertrophy

Glomerular filtration rate was 1.0 ± 0.04 mL/min per 100 g body weight at baseline, and was not affected by DOCA-salt ($P = 0.34$) or any other treatment (Table S3). Acetylcholine relaxed precontracted iliac arteries of rats not given DOCA-salt by $87 \pm 5\%$, and by $79 \pm 5\%$ after seven weeks of DOCA-salt ($P = 0.31$; Figure S4). This indicates that endothelial function was also left intact by DOCA-salt. The development of cardiac hypertrophy in DOCA-salt-treated rats was indicated by greater heart weights (normalized to tibia length; $P < 0.05$) and surface areas of individual cardiomyocytes ($P < 0.001$) than those measured in rats that had not been given DOCA-salt (Figure 5A-B). Cardiac hypertrophy could be prevented by spironolactone combined with valsartan, which lowered heart weight, cardiomyocyte surface area and plasma levels of NT-proBNP – a marker for cardiac dysfunction ($P < 0.05$ vs. vehicle for all; Figure 5A-C). Unexpectedly, AGT siRNA normalized the heart weights ($P < 0.01$

Chapter 3

vs. vehicle; Figure 5A), even though MAP had remained high throughout the treatment period (Figure 1A). However, cardiomyocyte surface area and NT-proBNP were unaffected by AGT siRNA (Figure 5B-C).

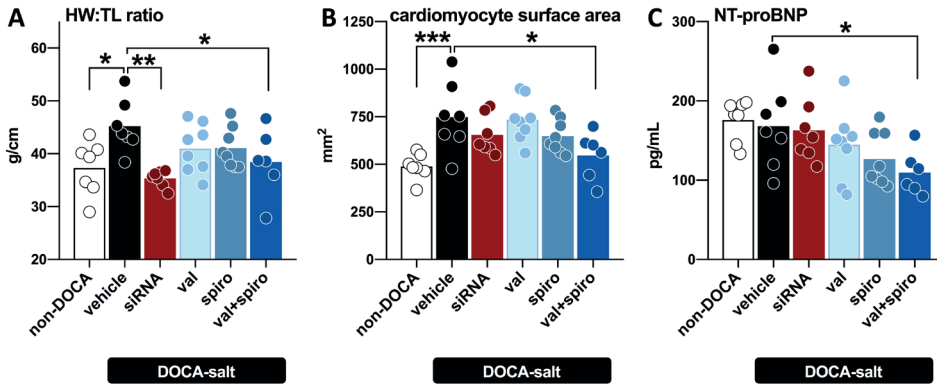


Figure 5: Indices of cardiac hypertrophy. A) Heart weight relative to tibia length (HW:TL ratio), B) cardiomyocyte surface area and C) plasma NT-proBNP levels of rats not given DOCA-salt (non-DOCA) or given DOCA-salt for 7 weeks and treated with vehicle, AGT siRNA, valsartan (val), spironolactone (spiro) or valsartan+spironolactone (val+spiro) during the final 3 weeks (n=6-8 per group). Data, represented as means, were analyzed using a one-way ANOVA and post-hoc Dunnett (* $P \leq 0.05$, ** $P \leq 0.01$, *** $P \leq 0.001$ vs. vehicle).

Discussion

This study evaluated the concept that DOCA-salt selectively upregulates the brain RAS via locally synthesized AGT. Controversy has existed for decades regarding brain renin. Recently not only intracellular renin and secreted renin (i.e., the regular form of renin as it is released from the kidney), but also prorenin were ruled out as potential contributors to brain angiotensin generation.^{18, 19} This leaves increased brain AGT production, combined with its cleavage by an as of yet unidentified enzyme, as a potential mechanism for brain RAS upregulation. Making use of siRNA targeting liver Agt, our current data fully confirm the independent existence of AGT in the brain: decreasing circulating (i.e. liver-derived) AGT by 97% did not affect brain AGT levels. In fact, brain AGT levels (expressed per gram protein) were higher than liver AGT levels. However, DOCA-salt did not upregulate brain AGT. Moreover, DO-

Brain RAS and DOCA-salt

CA-salt did not increase brain Ang II. Instead, brain Ang II was lowered to values below the detection limit in 70% of the rats given only DOCA-salt, and in 100% of the rats given the combination of DOCA-salt and AGT siRNA. Yet suppression of brain Ang II by siRNA did not attenuate DOCA-salt hypertension (Figure 6). Surprisingly, upregulating circulating RAS activity in DOCA-salt rats using spironolactone, particularly in combination with valsartan, restored brain Ang II levels, despite the fact that these treatments fully reversed the hypertensive response to DOCA-salt. In other words, brain Ang II levels related neither to blood pressure, nor to brain AGT levels, but did parallel the levels of circulating Ang II. The latter was also true for kidney, cardiac and adipose tissue levels of Ang II, and suggests that at all these sites angiotensin genera-

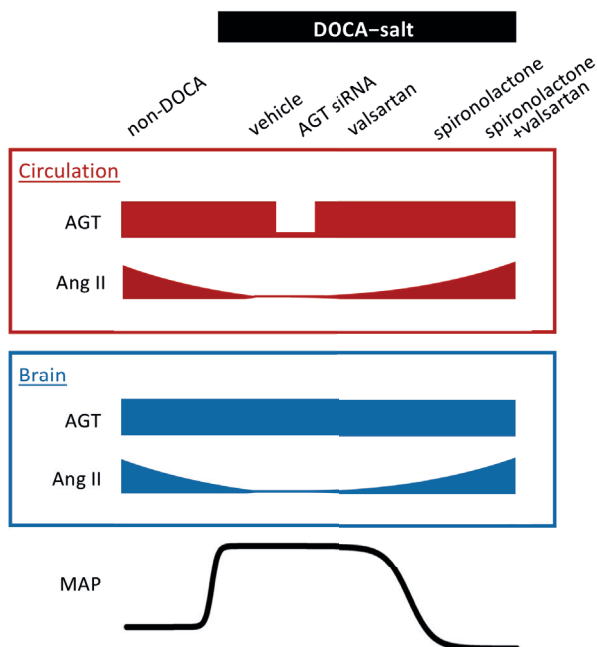


Figure 6: Schematic overview of changes induced by DOCA-salt in mean arterial pressure (MAP) and circulating and brain renin-angiotensin system (RAS) parameters. DOCA-salt increased MAP, while suppressing circulating and brainstem angiotensin (Ang) II in parallel. Liver-targeted angiotensinogen (AGT) siRNA eliminated circulating AGT in DOCA-salt-hypertensive rats and lowered brainstem Ang II to undetectable levels in all rats, even though brainstem AGT was intact. Yet blood pressure remained high. In contrast, brainstem Ang II was detectable in normotensive control rats and in DOCA-salt-treated rats after blood pressure normalization by spironolactone. This indicates that DOCA-salt hypertension is not mediated by brain RAS activation, and that Ang II in the brain is not generated from locally synthesized AGT, but instead must be derived from the circulation.

Chapter 3

tion depends on AGT of hepatic origin.

This raises the question what the function, if any, of locally synthesized AGT is in the brain. Previous studies demonstrated that deleting kidney Agt does not affect kidney angiotensin levels, both under normal and pathological conditions, while deleting hepatic AGT entirely abolishes kidney angiotensin generation.^{6, 30} Apparently, therefore, kidney angiotensin generation relies on hepatic AGT, and the function of kidney AGT is unknown. The same now appears to be true for brain AGT, at least in the DOCA-salt model. Yet, brain AGT levels (expressed per gram tissue) were much higher than renal AGT levels. We confirmed that brain AGT truly is AGT by using both an immunoblot approach and a direct ELISA. Previous immunohistochemical studies have localized brain AGT intracellularly.³¹ This is remarkable, as AGT is not typically retained but secreted, consistent with our observation that hepatic AGT levels are low. Taken together, a unifying concept might be that brain AGT cannot be converted to yield Ang I, either because there is neither renin, nor prorenin, nor any other enzyme capable of reacting with this substrate in the brain, or because AGT is located at an (intracellular) site where it cannot meet with any of these enzymes. Under either circumstance, the only possible source of Ang II in the brain is circulating Ang II. It may either diffuse into the brain at sites where the blood-brain barrier is disturbed^{14, 15}, or bind to AT₁ receptors.³² In support of the latter, ARB treatment greatly diminished the brain/plasma Ang II concentration ratio in spontaneously hypertensive rats.¹⁹ In the current study, DOCA-salt decreased circulating Ang II levels by >90%, and reduced brainstem Ang II levels in 5 out of 7 rats to undetectable levels, making the calculation of a tissue/plasma ratio impossible. Hence, a further reduction after valsartan could not be demonstrated. Brainstem tissue was chosen for this purpose, since renin levels are highest here,¹⁹ while the rostral ventrolateral medulla is an important cardiovascular control center that is fully sequestered from the circulation by the blood-brain barrier.³³ Additionally, the brainstem has often been used as an indicator of brain RAS activation in the DOCA-salt model.^{34, 35} Although the paraventricular nucleus has also been studied extensively and is similarly sequestered, it was less suited for our studies because it is known to respond to signals transmitted by binding of circulating Ang II to the subfornical organ³⁶ – an area that is not shielded by the blood brain barrier. Importantly, none of the other angiotensin metabolites could be demonstrated in brainstem

tissue, in contrast with tissues like the heart and kidney, where Ang I is easily detectable. Indirectly, this argues against local Ang II formation from locally generated Ang I. It also argues against a role for angiotensin metabolites other than Ang II, like Ang-(1-7) and Ang III, in the brain.

Partial reversal of DOCA-salt hypertension has been demonstrated when administering RAS blockers intracerebroventricularly instead of intravenously.¹¹⁻¹³ Yet in these studies, circulating and brainstem Ang II levels were not reported and there was severe hypertension, due to the combination of DOCA-salt with uninephrectomy. Such high blood pressures are likely to have disturbed the blood-brain barrier, thus allowing access of multiple RAS components from the circulation. Therefore, it cannot be excluded that the intracerebroventricularly administered RAS blockers were actually interfering with Ang I or Ang II taken up from the circulation. Secondly, several decades ago both AGT and AT₁ receptor antisense oligonucleotides were injected intracerebroventricularly in various hypertension rat models other than the DOCA-salt rat.³⁷⁻⁴¹ Although these approaches lowered blood pressure, intracardiac administration was equally effective,⁴⁰ while direct injection into the paraventricular nucleus (PVN) did not affect blood pressure.³⁹ Effects were short-lasting and could not be linked to consistent lowering of brain Ang II levels, while AGT suppression was not verified. Taken together, convincing evidence that suppression of brain AGT selectively reduces brain Ang II and thereby lowers blood pressure is still missing.

It has been suggested that brain angiotensin generation occurs in select nuclei only, e.g., the PVN or rostral ventrolateral medulla. If true, brain angiotensin levels would be severely diluted when highly localized angiotensin production sites are evaluated as part of a broader region, thereby reducing interpretability or utility of data. Lombard-Banek et al. recently applied a novel micro-analytical capillary electrophoresis-coupled mass spectrometry approach to determine Ang II in the PVN.⁴² Making use of 0.2 mg tissue, they reported levels of approximately 65 pmol Ang II/g.⁴³ At such levels, even if “diluting” our samples 10,000-fold with non-Ang II-containing brain tissue, we should still have detected brain Ang II given our detection limits (Table S1). In reality, Ang II levels of 65 pmol/g are many orders of magnitude above the levels measured in tissues with an abundance of the peptide, like the adrenal and kidney, and equivalent to the amount of AGT we observed in brain tissue (

Chapter 3

≈ 10 ng/mg protein, which corresponds to ≈ 20 pmol AGT/g, given that 1 gram of tissue contains ≈ 100 mg protein). Hence, before concluding that such high regional levels exist, ex-vivo AGT degradation needs to be excluded. Brainstem Ang II levels in the current study were detectable in 5 out of 7 normotensive SD rats, and this decreased to 0 out of 7 DOCA-salt-treated rats given siRNA. Had Ang II been independently upregulated in a regional manner after DOCA-salt, the opposite should have been observed. A final argument for brain RAS activation might be AT receptor upregulation independent of changes in Ang II levels. However, the opposite was observed for Ang II type 1A receptors, while no changes occurred in Ang II type 1B or type 2 receptors.

DOCA-salt suppressed the renal RAS by $>95\%$. The RAS is essential to preserve renal function and glomerular filtration.⁴⁴ AGT siRNA on top of DOCA-salt lowered but not fully annihilated renal Ang II. This may explain why GFR remained intact. Alternatively, GFR in this model may be less dependent on renal RAS activity.

Spironolactone reversed the blood pressure rise observed after DOCA-salt, implying that this rise is mineralocorticoid receptor-mediated. It also restored RAS activity. Although valsartan (31 mg/kg/day) tended to reduce blood pressure even further on top of spironolactone, this effect was not significantly different from that of spironolactone alone. Neither valsartan monotherapy nor AGT siRNA attenuated DOCA-salt hypertension, while applying the same or lower dosages robustly lowered blood pressure in spontaneously hypertensive rats.²² Hence, as has been shown before^{11, 13}, systemic RAS blockade is of limited or no use in the DOCA-salt model. This comes to no surprise when considering that DOCA-salt suppressed circulating RAS activity by at least 95%. Nevertheless, AGT siRNA did fully reverse cardiac hypertrophy, to the same degree as spironolactone combined with valsartan. Since this occurred independently of a change in blood pressure or NT-proBNP, these data imply that it was due to a reduction of cardiac Ang II. Indeed, like in the brain, siRNA reduced cardiac Ang II to undetectable levels in 7 out of 7 DOCA-salt-treated rats. Such observations were not made with valsartan, possibly because it did not fully suppress cardiac Ang II, unlike siRNA. Taken together, these findings confirm that cardiac angiotensin generation relies on hepatic AGT, and that liver-targeted AGT siRNA is therefore capable of exerting cardiac-specific effects in a blood pres-

sure-independent manner.

Determining the functional significance of local, tissue-based AGT production may guide the development of tissue-targeted antihypertensive drugs. However, our data indicate that liver-derived AGT is the sole determinant of tissue angiotensin generation in blood, kidney, heart, adipose tissue and brain. We did not find selective brain RAS upregulation in DOCA-salt-hypertensive rats, and eliminating brain Ang II through hepatic Agt silencing did not lower blood pressure in this animal model for human primary hyperaldosteronism. To the best of our knowledge, brain-targeting of AGT siRNA (other than via intracerebroventricular injection) is not yet feasible. Yet this approach might help to identify a role of brain AGT, if any, in the various hypertension models that currently exist. Ideally, these studies will combine detailed measurements of both AGT and Ang II in the brain, and include a comparison with hepatic AGT siRNA.

Clinical perspectives

Background as to why the study was undertaken

DOCA-salt hypertension - an animal model for human primary hyperaldosteronism - is thought to be mediated by independent generation of angiotensin II in the brain. If so, the development of brain-targeted antihypertensive drugs may help to treat this condition.

Brief summary of the results

In DOCA-salt-hypertensive rats, elimination of circulating angiotensinogen by liver-specific RNA silencing lowered brain angiotensin II to undetectable levels, even though brain angiotensinogen remained intact. Nonetheless, blood pressure remained high. In contrast, brain angiotensin II could be detected in normotensive control rats and after blood pressure normalization by spironolactone.

Potential significance to human health and disease

These results indicate that angiotensin II in the brain is derived from the circulation, and is not independently generated from locally synthesized angiotensinogen. These results argue against selective brain renin-angiotensin system activation during DOCA-salt hypertension or its human

Chapter 3

equivalent, primary hyperaldosteronism. Yet a role for brain angiotensinogen might still be identified if it becomes possible to target siRNA to the brain.

Data availability statement

All supporting data are included within the main article and its supplementary files.

Sources of funding

This work was partially supported by Alnylam Pharmaceuticals. K.M.MC. was supported by a National Health and Medical Research Council of Australia CJ Martin Fellowship #1112125. L.R. was supported by a National Natural Science Foundation of China grant #81900668.

Disclosures

J.B.K.; I.Z.; L.M.; S.H. and D.F. are employees of Alnylam Pharmaceuticals. A.H.J.D. received a grant from Alnylam Pharmaceuticals which has partially supported this work. O.D. and M.P. are employees of Attoquant Diagnostics.

References

1. Stanaway JD, Afshin A, Gakidou E, Lim SS, Abate D, Abate KH, Abbafati C, Abbasi N, Abbastabar H, Abd-Allah F, et al. Global, regional, and national comparative risk assessment of 84 behavioural, environmental and occupational, and metabolic risks or clusters of risks for 195 countries and territories, 1990-2017: A systematic analysis for the global burden of disease study 2017. *Lancet* (London, England). 2018;392:1923-1994
2. Hayakawa H, Coffee K, Raij L. Endothelial dysfunction and cardiorenal injury in experimental salt-sensitive hypertension: Effects of antihypertensive therapy. *Circulation*. 1997;96:2407-2413
3. Agodoa LY, Appel L, Bakris GL, Beck G, Bourgoignie J, Briggs JP, Charleston J, Cheek D, Cleveland W, Douglas JG, et al. Effect of ramipril vs amlodipine on renal outcomes in hypertensive nephrosclerosis: A randomized controlled trial. *Jama*. 2001;285:2719-2728
4. Sagnella GA. Why is plasma renin activity lower in populations of african origin? *Journal of human hypertension*. 2001;15:17-25
5. Kobori H, Nangaku M, Navar LG, Nishiyama A. The intrarenal renin-angiotensin system: From physiology to the pathobiology of hypertension and kidney disease. *Pharmacological reviews*. 2007;59:251-287

6. Matsusaka T, Niimura F, Shimizu A, Pastan I, Saito A, Kobori H, Nishiyama A, Ichikawa I. Liver angiotensinogen is the primary source of renal angiotensin ii. *Journal of the American Society of Nephrology : JASN*. 2012;23:1181-1189
7. Campbell DJ, Habener JF. Angiotensinogen gene is expressed and differentially regulated in multiple tissues of the rat. *The Journal of clinical investigation*. 1986;78:31-39
8. Campbell DJ, Habener JF. Cellular localization of angiotensinogen gene expression in brown adipose tissue and mesentery: Quantification of messenger ribonucleic acid abundance using hybridization in situ. *Endocrinology*. 1987;121:1616-1626
9. Yiannikouris F, Wang Y, Shoemaker R, Larian N, Thompson J, English VL, Charnigo R, Su W, Gong M, Cassis LA. Deficiency of angiotensinogen in hepatocytes markedly decreases blood pressure in lean and obese male mice. *Hypertension (Dallas, Tex. : 1979)*. 2015;66:836-842
10. Koizumi M, Niimura F, Fukagawa M, Matsusaka T. Adipocytes do not significantly contribute to plasma angiotensinogen. *Journal of the renin-angiotensin-aldosterone system : JRAAS*. 2016;17:1470320316672348
11. Pochiero M, Nicoletta P, Losi E, Bianchi A, Caputi AP. Cardiovascular responses of conscious doca-salt hypertensive rats to acute intracerebroventricular and intravenous administration of captopril. *Pharmacological research communications*. 1983;15:173-182
12. Itaya Y, Suzuki H, Matsukawa S, Kondo K, Saruta T. Central renin-angiotensin system and the pathogenesis of doca-salt hypertension in rats. *The American journal of physiology*. 1986;251:H261-268
13. Kubo T, Yamaguchi H, Tsujimura M, Hagiwara Y, Fukumori R. Blockade of angiotensin receptors in the anterior hypothalamic preoptic area lowers blood pressure in doca-salt hypertensive rats. *Hypertension research : official journal of the Japanese Society of Hypertension*. 2000;23:109-118
14. Biancardi VC, Son SJ, Ahmadi S, Filosa JA, Stern JE. Circulating angiotensin ii gains access to the hypothalamus and brain stem during hypertension via breakdown of the blood-brain barrier. *Hypertension (Dallas, Tex. : 1979)*. 2014;63:572-579
15. Pelisch N, Hosomi N, Ueno M, Nakano D, Hitomi H, Mogi M, Shimada K, Kobori H, Horiuchi M, Sakamoto H, Matsumoto M, Kohno M, Nishiyama A. Blockade of at1 receptors protects the blood-brain barrier and improves cognition in dahl salt-sensitive hypertensive rats. *American journal of hypertension*. 2011;24:362-368
16. Lu J, Wang HW, Ahmad M, Keshtkar-Jahromi M, Blaustein MP, Hamlyn JM, Leenen FHH. Central and peripheral slow-pressor mechanisms contributing to angiotensin ii-salt hypertension in rats. *Cardiovascular research*. 2018;114:233-246
17. Lee-Kirsch MA, Gaudet F, Cardoso MC, Lindpaintner K. Distinct renin isoforms generated by tissue-specific transcription initiation and alternative splicing. *Circulation research*. 1999;84:240-246
18. Shinohara K, Liu X, Morgan DA, Davis DR, Sequeira-Lopez ML, Cassell MD, Grobe JL, Rahmouni K, Sigmund CD. Selective deletion of the brain-specific isoform of renin causes neurogenic hypertension. *Hypertension (Dallas, Tex. : 1979)*.

Chapter 3

- 2016;68:1385-1392
19. van Thiel BS, Góes Martini A, Te Riet L, Severs D, Uijl E, Garrelds IM, Leijten FPJ, van der Pluijm I, Essers J, Qadri F, et al. Brain renin-angiotensin system: Does it exist? *Hypertension* (Dallas, Tex. : 1979). 2017;69:1136-1144
 20. Nair JK, Willoughby JL, Chan A, Charisse K, Alam MR, Wang Q, Hoekstra M, Kandasamy P, Kel'in AV, Milstein S, et al. Multivalent n-acetylgalactosamine-conjugated sirna localizes in hepatocytes and elicits robust rna-mediated gene silencing. *J Am Chem Soc.* 2014;136:16958-16961
 21. van Esch JH, Moltzer E, van Veghel R, Garrelds IM, Leijten F, Bouhuizen AM, Danser AH. Beneficial cardiac effects of the renin inhibitor aliskiren in spontaneously hypertensive rats. *J Hypertens.* 2010;28:2145-2155
 22. Uijl E, Mirabito Colafella KM, Sun Y, Ren L, van Veghel R, Garrelds IM, de Vries R, Poglitsch M, Zlatev I, Kim JB, Hoorn EJ, Foster D, Danser AHJ. Strong and sustained antihypertensive effect of small interfering rna targeting liver angiotensinogen. *Hypertension* (Dallas, Tex. : 1979). 2019;73:1249-1257
 23. de Lannoy LM, Danser AH, van Kats JP, Schoemaker RG, Saxena PR, Schalekamp MA. Renin-angiotensin system components in the interstitial fluid of the isolated perfused rat heart. Local production of angiotensin i. *Hypertension.* 1997;29:1240-1251
 24. van den Heuvel M, Batenburg WW, Jainandunsing S, Garrelds IM, van Gool JM, Feelders RA, van den Meiracker AH, Danser AH. Urinary renin, but not angiotensinogen or aldosterone, reflects the renal renin-angiotensin-aldosterone system activity and the efficacy of renin-angiotensin-aldosterone system blockade in the kidney. *J Hypertens.* 2011;29:2147-2155
 25. Domenig O, Manzel A, Grobe N, Konigshausen E, Kaltenecker CC, Kovarik JJ, Stegbauer J, Gurley SB, van Oyen D, Antlanger M, et al. Neprilysin is a mediator of alternative renin-angiotensin-system activation in the murine and human kidney. *Sci Rep.* 2016;6:33678
 26. Basu R, Poglitsch M, Yogasundaram H, Thomas J, Rowe BH, Oudit GY. Roles of angiotensin peptides and recombinant human ace2 in heart failure. *J Am Coll Cardiol.* 2017;69:805-819
 27. Parmar RG, Brown CR, Matsuda S, Willoughby JLS, Theile CS, Charisse K, Foster DJ, Zlatev I, Jadhav V, Maier MA, Egli M, Manoharan M, Rajeev KG. Facile synthesis, geometry, and 2'-substituent-dependent in vivo activity of 5'-(e)- and 5'-(z)-vinylphosphonate-modified sirna conjugates. *Journal of medicinal chemistry.* 2018;61:734-744
 28. Tanimoto K, Sugiyama F, Goto Y, Ishida J, Takimoto E, Yagami K, Fukamizu A, Murakami K. Angiotensinogen-deficient mice with hypotension. *The Journal of biological chemistry.* 1994;269:31334-31337
 29. Schock-Kusch D, Sadick M, Henninger N, Kraenzlin B, Claus G, Kloetzer HM, Weiss C, Pill J, Gretz N. Transcutaneous measurement of glomerular filtration rate using fite-sinistrin in rats. *Nephrology, dialysis, transplantation : official publication of the European Dialysis and Transplant Association - European Renal Association.* 2009;24:2997-3001
 30. Matsusaka T, Niimura F, Pastan I, Shintani A, Nishiyama A, Ichikawa I. Podocyte injury enhances filtration of liver-derived angiotensinogen and renal angiotensin ii generation. *Kidney international.* 2014;85:1068-1077

31. Sherrod M, Liu X, Zhang X, Sigmund CD. Nuclear localization of angiotensinogen in astrocytes. *American journal of physiology. Regulatory, integrative and comparative physiology.* 2005;288:R539-546
32. Rose JM, Audus KL. Receptor-mediated angiotensin ii transcytosis by brain microvessel endothelial cells. *Peptides.* 1998;19:1023-1030
33. Lavoie JL, Cassell MD, Gross KW, Sigmund CD. Adjacent expression of renin and angiotensinogen in the rostral ventrolateral medulla using a dual-reporter transgenic model. *Hypertension (Dallas, Tex. : 1979).* 2004;43:1116-1119
34. Weyhenmeyer JA, Meyer JM. Angiotensin ii in the brain and brainstem of the doca salt hypertensive rat. *Clinical and experimental hypertension. Part A, Theory and practice.* 1985;7:73-92
35. Li W, Sullivan MN, Zhang S, Worker CJ, Xiong Z, Speth RC, Feng Y. Intracerebroventricular infusion of the (pro)renin receptor antagonist pro20 attenuates deoxycorticosterone acetate-salt-induced hypertension. *Hypertension (Dallas, Tex. : 1979).* 2015;65:352-361
36. Ferguson AV. Angiotensinergic regulation of autonomic and neuroendocrine outputs: Critical roles for the subfornical organ and paraventricular nucleus. *Neuroendocrinology.* 2009;89:370-376
37. Gyurko R, Wielbo D, Phillips MI. Antisense inhibition of at1 receptor mrna and angiotensinogen mrna in the brain of spontaneously hypertensive rats reduces hypertension of neurogenic origin. *Regulatory peptides.* 1993;49:167-174
38. Wielbo D, Sernia C, Gyurko R, Phillips MI. Antisense inhibition of hypertension in the spontaneously hypertensive rat. *Hypertension (Dallas, Tex. : 1979).* 1995;25:314-319
39. Kagiya S, Tsuchihashi T, Abe I, Matsumura K, Fujishima M. Antisense inhibition of angiotensinogen attenuates vasopressin release in the paraventricular hypothalamic nucleus of spontaneously hypertensive rats. *Brain research.* 1999;829:120-124
40. Peng JF, Kimura B, Fregly MJ, Phillips MI. Reduction of cold-induced hypertension by antisense oligodeoxynucleotides to angiotensinogen mrna and at1-receptor mrna in brain and blood. *Hypertension (Dallas, Tex. : 1979).* 1998;31:1317-1323
41. Kagiya S, Varela A, Phillips MI, Galli SM. Antisense inhibition of brain renin-angiotensin system decreased blood pressure in chronic 2-kidney, 1 clip hypertensive rats. *Hypertension (Dallas, Tex. : 1979).* 2001;37:371-375
42. Lombard-Banek C, Yu Z, Swiercz AP, Marvar PJ, Nemes P. A microanalytical capillary electrophoresis mass spectrometry assay for quantifying angiotensin peptides in the brain. *Analytical and bioanalytical chemistry.* 2019;411:4661-4671
43. Danser AHJ, Poglitsch M. Letter to the editor regarding "a microanalytical capillary electrophoresis mass spectrometry assay for quantifying angiotensin peptides in the brain". *Analytical and bioanalytical chemistry.* 2019;411:8163
44. Balcarek J, Sevá Pessôa B, Bryson C, Azizi M, Ménard J, Garrelts IM, McGeehan G, Reeves RA, Griffith SG, Danser AH, Gregg R. Multiple ascending dose study with the new renin inhibitor vtp-27999: Nephrocentric consequences of too much renin inhibition. *Hypertension (Dallas, Tex. : 1979).* 2014;63:942-950

Supplemental data

Supplemental Table S1. Lower limit of quantification (LLOQ; pM or fmol/g) for angiotensin (Ang) metabolites specified per tissue. Abbreviations: AT, adipose tissue.

	Ang(1-10) = Ang I	Ang(1-8) = Ang II	Ang(1-7)	Ang(1-5)	Ang(2-8)	Ang(3-8)
Blood	3	2	8	2	2,5	1
Brainstem	6	6	10	8	6	5
Kidney	6	3	19	13	6	10
Epididymal AT	3	2	6	3	3	2
Heart	8	6	12	8	5	5

Supplemental Table S2. Sequences of primers used for qPCR. Abbreviations: Agt, angiotensinogen; Ren, renin; AT1aR, angiotensin II type 1a receptor; AT1bR, angiotensin II type 1b receptor; AT2R, angiotensin II type 2 receptor; B2M, β_2 -microglobulin; Actb, β -actin.

Gene		Sequences (5' to 3')
Agt	Forward primer	CCAGCACGACTTCCTGACTT
	Reverse primer	GCAGGTTGTAGGATCCCCGA
Ren	Forward primer	TGTGGTAACTGTGGGTGGAAT
	Reverse primer	GCATGAAGGGTATCAGGGGC
AT1aR	Forward primer	ATCACCAGGTCAAGTGGATTTCG
	Reverse primer	TTCCCACCACAAAGATGATGC
AT1bR	Forward primer	CTGAATCTTGCCCTGGCTGA
	Reverse primer	ACATAGGTGGTTGCCGAAGG
AT2R	Forward primer	AAGGAATCCCTGGCAAGCATC
	Reverse primer	TGGCAATGAGGACAGACAAGC
B2M	Forward primer	ATGGCTCGCTCGGTGACCG
	Reverse primer	TGGGGAGTTTCTGAATGGCAAGCA
Actb	Forward primer	GGGAAATCGTGCGTGACATT
	Reverse primer	GCGGCAGTGGCCATCTC

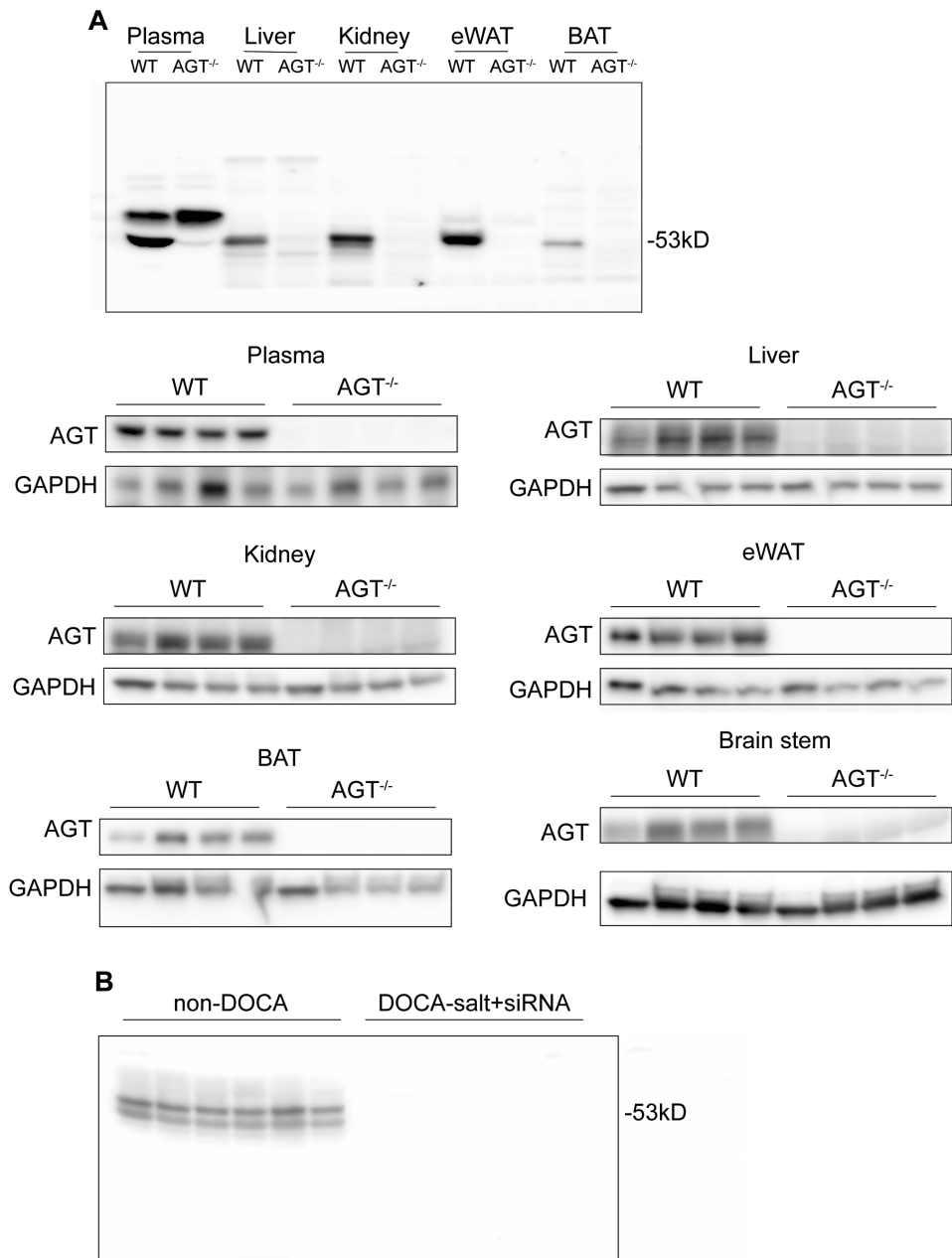
Supplemental Table S3. Growth, intake, 24h-urine parameters and glomerular filtration rate (GFR) of rats placed in metabolic cages prior to DOCA-salt (0 weeks), and after 4 and 7 weeks of DOCA-salt. During the final 3 weeks (i.e. week 5-7), rats were given vehicle, AGT siRNA, valsartan, spironolactone or valsartan+spironolactone (n=6-8 per group). Control rats not given DOCA-salt are denoted by 'non-DOCA'. Data, represented as means \pm SD, were analyzed using a paired t-test (0 vs 4 weeks; \$P<0.001, #P<0.0001) or using a one-way ANOVA and post-hoc Dunnett (*P<0.05, +P<0.01, †P<0.0001 vs. non-DOCA; aP<0.05, bP<0.01, vs. vehicle). Abbreviations: Na⁺, sodium; K⁺, potassium; BW, body weight.

	0 weeks		4 weeks	7 weeks					
				non-DOCA	vehicle	AGT siRNA	valsartan	spironolactone	valsartan+spironolactone
Body weight (g)	554±53		571±59\$	634±82	617±73	578±44	647±93	636±76	671±78
Δ treatment			18±26	43±14	45±30	39±22	70±39	56±23	70±31
Food intake (mg/day)	17±6		20±7	20±2	20±7	24±3	18±6	18±6	15±6
Water intake (mL/day)	23±7		118±64#	19±2	88±68†	54±31*	83±88*	24±8b	29±7a
Urine production (mL/day)	11±4		107±57#	13±4	76±59‡	40±24*	68±71†	22±9b	25±9a
Na+ excretion (mmol/day)	1.5±0.5		16±7#	1.5±0.6	16±13§	9±4§	12±10§	5±2§a	6±3§
K+ excretion (mmol/day)	2.2±0.5		3.6±1#	3.0±0.5	3.2±0.7	3.7±0.8	3.0±0.6	2.8±1	2.6±0.5
Plasma Na+ (mmol/L)	136±2		139±2#	138±2	144±2‡	142±2*	145±4§	141±2	142±3*
GFR (ml/min/100g BW)	1.0±0.04		1.1±0.1	0.9±0.1	1.2±0.2	1.1±0.2	1.0±0.1	0.9±0.1	0.9±0.1

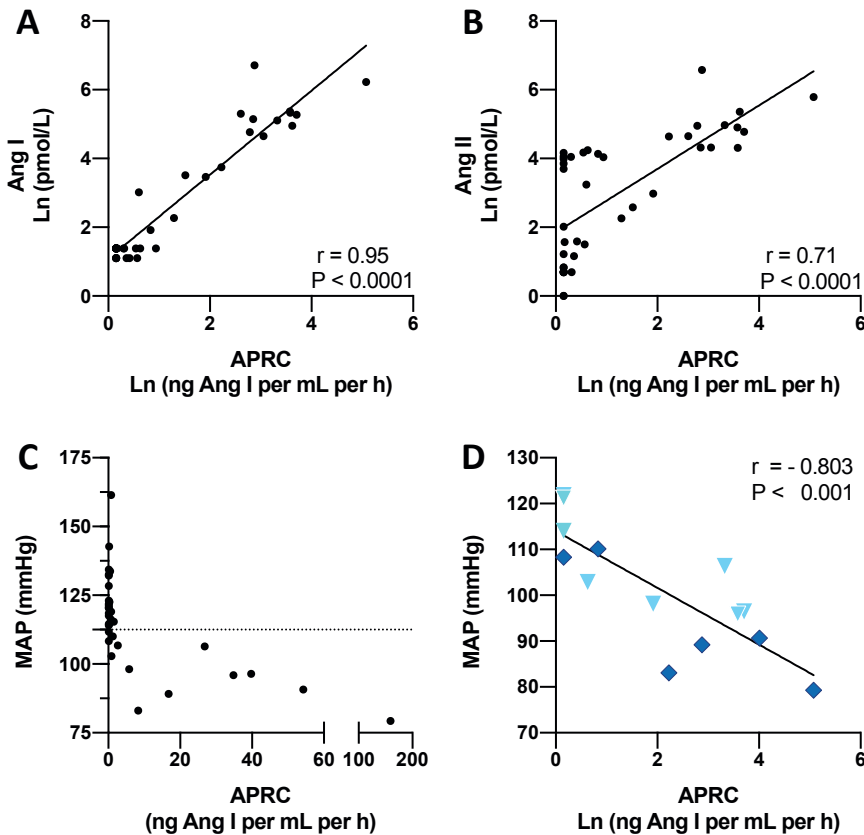
Supplemental Table S4. Angiotensin (Ang) metabolites measured by LC-MS/MS in blood, brainstem, kidney, epididymal adipose tissue (AT) and left ventricle of the hearts of rats that were sham operated (non-DOCA) or rats treated with DOCA-salt for 7 weeks and vehicle, AGT siRNA, valsartan, spironolactone or valsartan+spironolactone during the final 3 weeks (n=6-8 per group). Data, represented as medians (interquartile range), were analyzed after log transformation using ANOVA and post-hoc Dunnett (*P≤0.05, †P≤0.001, ‡P≤0.0001, §P≤0.0001 vs. non-DOCA; aP≤0.05, bP≤0.01, cP≤0.0001, vs. vehicle).

Parameter	non-DOCA	vehicle	AGT siRNA	valsartan	spironolactone	valsartan+spironolactone
Blood fmol/mL						
Ang(1-10) = Ang I	141 (103-200)	<3§	<3§	<3§ (<3-7)	17†c (<3-186)	41c (4-663)
Ang(1-8) = Ang II	105 (75-141)	2§ (<2-54)	3§ (<2-4)	18† (3-58)	67b (27-108)	104c (35-522)
Ang(1-7)	<8	<8	<8	<8	<8	<8
Ang(1-5)	5 (3-6)	<2	<2	<2	<2 (<2-3)	<2 (<2-24)
Ang(2-8)	4 (<2.5-6)	<2.5	<2.5	<2.5	<2.5	<2.5
Ang(3-8)	4 (3-6)	<1*	<1*	<1*	<1 (<1-4)	5b (<2.5-44)
Brainstem fmol/g						
Ang(1-10) = Ang I	<6	<6	<6	<6	8†c (<6-28)	<6a (<6-25)
Ang(1-8) = Ang II	9 (<6-15)	<6 (<6-20)	<6*	<6 (<6-10)	<6 (<6-17)	12 (<6-26)
Ang(1-7)	<10	<10	<10	<10	<10	<10
Ang(1-5)	<8	<8	<8	<8	<8	<8
Ang(2-8)	<6	<6	<6	<6	<6	<6
Ang(3-8)	<5	<5	<5	<5	<5	<5
Kidney fmol/g						

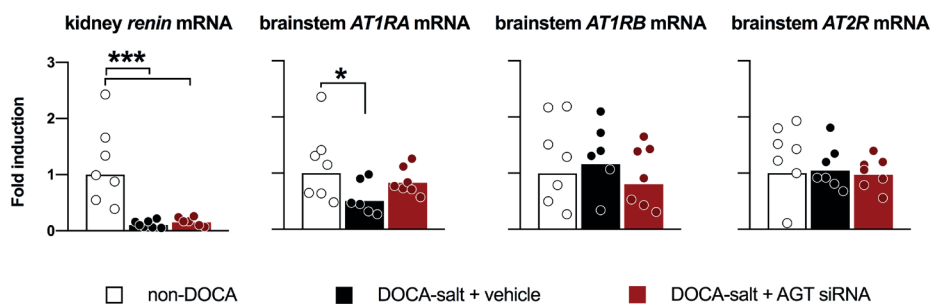
Ang(1-10) = Ang I	564 (313-907)	10§ (<6-15)	<6§	12§ (10-28)	169*c (15-791)	131*c (34-320)
Ang(1-8) = Ang II	729 (431-1892)	8§ (6-18)	<3§	<3§ (<3-4)	252§c (12-700)	38§ (8-70)
Ang(1-7)	173 (65-279)	<19§	<19§	<19§	33* (<19-148)	<19† (<19-47)
Ang(1-5)	17 (<13-40)	<13	<13	<13	<13b (<13-29)	<13 (<13-15)
Ang(2-8)	75 (44-121)	<6§	<6§	<6§	25* (<6-111)	<6§
Ang(3-8)	<10	<10	<10	<10	<10	<10
Epididymal AT fmol/g						
Ang(1-10) = Ang I	<3	<3	<3	<3	<3	<3
Ang(1-8) = Ang II	7 (5-23)	3§ (<2-4)	<2§	<2§ (<2-8)	7c (4-15)	3†b (3-16)
Ang(1-7)	<6	<6	<6	<6	<6	<6
Ang(1-5)	<3	<3	<3	<3	<3	<3
Ang(2-8)	<3	<3	<3	<3	<3	<3
Ang(3-8)	<2	<2	<2	<2	<2	<2
Heart fmol/g						
Ang(1-10) = Ang I	43 (14-117)	<8§	<8§	<8§	<8§ (<8-20)	13† (<8-53)
Ang(1-8) = Ang II	20 (6-24)	<6* (<6-12)	<6†	<6* (<6-15)	6 (<6-19)	16 (<6-19)
Ang(1-7)	<12 (<12-41)	<12	<12	<12	<12	<12
Ang(1-5)	<8	<8	<8	<8	<8	<8
Ang(2-8)	<5	<5	<5	<5	<5	<5
Ang(3-8)	<5	<5	<5	<5	<5	<5



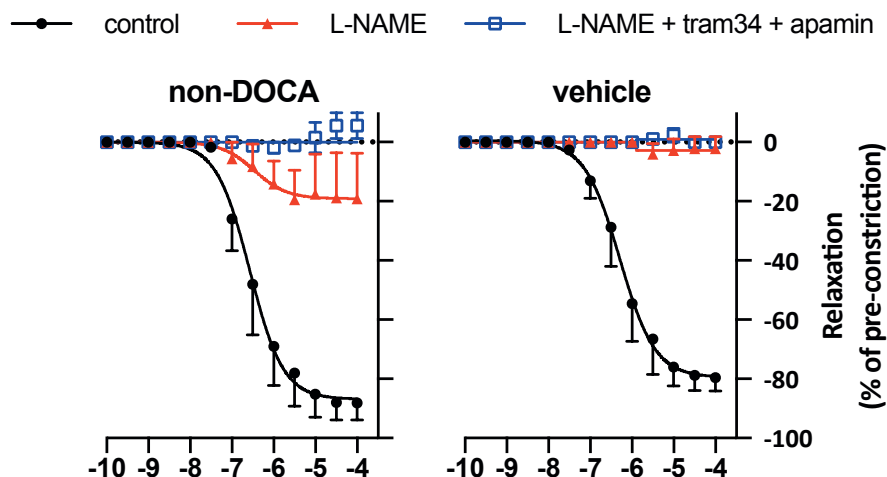
Supplemental Figure S1: Validation of angiotensinogen (AGT) antibody target specificity.
A) Immunoblots showing protein abundance of AGT in tissues from wild-type and Agt knockout mice (tissues were a kind gift of Prof. M. Bader, Berlin, Germany; n=4 per group).
B) Complete immunoblot of liver homogenates from untreated (non-DOCA) control rats and AGT-siRNA-treated rats.



Supplemental Figure S2: Relationship between circulating RAS parameters and antihypertensive effect. Rats were sham operated (non-DOCA normotensive controls; open circles) or given DOCA-salt for 7 weeks and treated with vehicle, AGT siRNA, valsartan, spironolactone or spironolactone+valsartan during the final 3 weeks ($n=6-8$ per group). Correlation between A) angiotensin (Ang) I and active plasma renin concentration (APRC), B) Ang II and APRC, C) mean arterial pressure (MAP) and APRC for all treatment groups or for D) spironolactone (upside-down triangle) and valsartan+spironolactone-treated rats (diamond). r denotes Pearson's correlation coefficient.



Supplemental Figure S3: Kidney renin and brain angiotensin receptor expression. Gene expression of kidney renin and brainstem angiotensin II receptor type IA (AT_1RA); angiotensin II receptor type IB (AT_1RB) and angiotensin II receptor type 2 (AT_2R) of rats that were sham operated (non-DOCA) or rats that had received DOCA-salt for 7 weeks and were treated with vehicle or AGT siRNA during the final 3 weeks (n=7 per group). Data, represented as mean fold induction relative to the non-DOCA controls, were analyzed using one-way ANOVA and post-hoc Dunnett (* $P \leq 0.05$, *** $P \leq 0.001$).



Supplemental Figure S4: Vascular responses to acetylcholine. Relaxations to acetylcholine (% reduction of pre-constriction with U46619) in the absence (control; black circles) or presence of N ω -nitro-L-arginine methyl ester hydrochloride (L-NAME; red triangles) or L-NAME+TRAM34+apamin (blue squares) in iliac arteries of rats not given DOCA-salt or after seven weeks of DOCA-salt (n=7 for both). Emax (maximal effect) and pEC₅₀ (the negative logarithm of the half-maximal effective concentration) were analyzed using one-way ANOVA and post-hoc Bonferroni.

Chapter 4

Renoprotective effects of small interfering RNA targeting liver angiotensinogen in experimental chronic kidney disease

Dominique M. Bovée[#], Liwei Ren[#], Estrellita Uijl,
Marian C. Clahsen-van Groningen, Richard van Veghel,
Ingrid M. Garrelds, Oliver Domenig, Marko Poglitsch, Ivan
Zlatev, Jae B. Kim, Stephen Huang, Lauren Melton, Xifeng Lu,
Ewout J. Hoorn, Don Foster, A.H. Jan Danser

Hypertension. 2021;77:1600-1612

[#]Contributed equally

Abstract

Small interfering RNA targeting liver angiotensinogen (AGT siRNA) lowers blood pressure, but its effectiveness in hypertensive chronic kidney disease (CKD) is unknown. Considering that the kidney may generate its own AGT, we assessed the effectiveness of liver-targeted AGT siRNA in the 5/6th nephrectomy (5/6Nx) rat, a hypertensive CKD model. Five weeks after 5/6Nx (baseline), rats were subjected to vehicle, AGT siRNA, AGT siRNA + losartan, losartan, or losartan + captopril. Baseline MAP was 160 ± 6 mm Hg. Over the course of 4 weeks, MAP increased further by ≈ 15 mm Hg during vehicle treatment. This rise was prevented by AGT siRNA. Losartan reduced MAP by 37 ± 6 mm Hg, and increased plasma angiotensin II. Both AGT siRNA and captopril suppressed these effects of losartan, suggesting that its blood pressure-lowering effect relied on stimulation of vasodilator angiotensin II type 2 receptors by high angiotensin II levels. Proteinuria and cardiac hypertrophy increased with vehicle and these increases were comparably abrogated by all treatments. No intervention improved GFR, while siRNA and losartan equally diminished glomerulosclerosis. AGT siRNA \pm losartan reduced plasma AGT by $>95\%$, and this was accompanied by almost complete elimination of angiotensin II in kidney and heart, without decreasing renal AGT mRNA. Multiple linear regression confirmed both MAP and renal angiotensin II as independent determinants of proteinuria. In conclusion, AGT siRNA exerts renoprotection in the 5/6Nx model in a blood pressure-independent manner. This relies on the suppression of renal angiotensin II formation from liver-derived AGT. Consequently, AGT siRNA may prove beneficial in human chronic kidney disease.

Keywords: chronic kidney disease – novel therapeutics – small interfering RNA – renin-angiotensin system – hypertension – cardiac hypertrophy

Introduction

Treatment of chronic kidney disease (CKD) often involves the use of renin-angiotensin system (RAS) blockers to treat hypertension and confer renoprotection. The latter is believed to be due to interference with either the generation or effects of angiotensin (Ang) II at renal tissue sites. Here it has often been argued that apart from renin synthesis in the kidney, angiotensinogen (AGT) is also synthesized at renal tissue sites, for instance in the proximal tubule.¹ Given the broad expression of ACE in the kidney,² this implies that all components required to synthesize Ang II are present in the kidney,³ thereby allowing locally synthesized Ang II to exert its effects fully independently from circulating Ang II, i.e., by stimulating angiotensin II type 1 and 2 (AT₁, AT₂) receptors at renal tissue sites.

RAS blockade is hampered by counterbalancing mechanisms, the most important of which is renin upregulation.⁴ As a consequence, the degree of RAS suppression may be less than anticipated, even more so if organs express their own AGT. Furthermore, particularly during AT₁ receptor blocker (ARB) treatment, the elevated Ang II levels might stimulate vasodilator AT₂ receptors, thereby lowering blood pressure.⁵

A novel approach of interfering with the RAS is the use of small interfering RNAs (siRNAs) targeting AGT.⁶ Currently siRNA designs exist with hepatocyte-directed, N-acetylgalactosamine (GalNAc)-conjugated molecules which allow stable suppression of hepatic proteins like proprotein convertase subtilisin/kexin type 9, requiring only biannual dosing in humans.⁷ Given the hepatic origin of circulating AGT, this approach could allow a similar suppression of AGT. Importantly, under such circumstances counterbalancing renin rises should no longer be able to restore Ang II in blood, simply because AGT is lacking. Indeed, a GalNAc-conjugated siRNA targeting AGT was highly effective in suppressing circulating AGT in spontaneously hypertensive rats (SHR),⁶ thereby reducing blood pressure to the same degree as ACE inhibitors (ACEi) and ARB. Moreover, combining this AGTsiRNA with an ARB virtually eliminated Ang II, because the accompanying further renin rise now cleaved any remaining AGT and thus exhausted the source of angiotensin peptides.

A remaining question is to what degree this approach also exerts beneficial effects at tissue sites, in particular in the kidney, given its own AGT synthesis. Here, it should be noted that RAS blockade has a limit, and that too much RAS blockade (e.g., by combining multiple RAS blockers at the same time) may result in hypotension, acute kidney injury and hyperkalemia. Disappointingly, a two-week treatment of the 5/6th nephrectomy (Nx) rat, a CKD model which is responsive to RAS blockade,⁸⁻¹⁰ with AGT antisense oligonucleotides (liver-specific or non-specific) revealed no beneficial effect on proteinuria or renal histology.¹¹ Non-specific AGT suppression even impaired renal function (evidenced by a reduced creatinine clearance) and worsened histology, while hepatic-specific suppression was indistinguishable from vehicle treatment. Based on this, the authors argued that non-specific AGT suppression is potentially deleterious, because it lowers renal Ang II too much. Yet, they did not report renal angiotensin levels. Moreover, their results were obtained while exposing the 5/6th Nx rats to a very low-salt diet (0.015 % NaCl). Since this will greatly upregulate the dependency of renal function on the RAS, it may explain why no beneficial effects of AGT suppression were observed.

Therefore, in the present study we set out to investigate the effects of liver-targeted AGT siRNA in the same CKD model (the 5/6th Nx rat) under normal salt conditions, applying treatment for a longer time period (4 weeks) and making a comparison versus the ARB losartan or dual RAS blockade (AGT siRNA + losartan or captopril + losartan). Our hypothesis was, firstly, that AGT siRNA alone would exert renoprotection to the same degree as maximal RAS blockade, and secondly that this would rely on both blood pressure lowering and suppression of renal Ang II. Here it is important to note that the 5/6th Nx procedure results in significant blood pressure elevation when using a 2-step approach (removal of the right kidney, followed by subsequent removal of 2/3 of the remaining kidney 7-10 days later),^{8,12} or when combining right uninephrectomy with immediate infarction of 2/3 of the left kidney.^{9,10,13-15} This is not the case when performing right uninephrectomy at the same time as excision of both poles of the left kidney (1-step approach).¹³⁻¹⁵ In the present study we used the 2-step approach, allowing us to evaluate the contribution of blood pressure to both the development of proteinuria and the deterioration of

glomerular filtration rate (GFR) and renal histology. Furthermore, by simultaneously measuring angiotensin levels in kidney, heart and blood we were able to distinguish the contribution of non-hepatic AGT to their synthesis.

Methods

All supporting data are available within the article and in the Data Supplement.

Animal studies

All animal experiments were approved by the Animal Welfare Committee of the Erasmus MC (protocol number 16-790-06). Male 6-weeks old Sprague-Dawley (SD) rats were obtained from Envigo (Huntingdon, United Kingdom) and maintained on a standard sodium diet (containing 0.27% Na⁺, translating to ≈ 57 mg Na⁺/day per rat). 5/6th Nx was performed in a two-step procedure as previously described.¹² Briefly, right uninephrectomy was performed under isoflurane anesthesia, followed by resection of the poles of the left kidney 10 days later. Right uninephrectomy was combined with telemetry device (HD-S10, Data Sciences International, St. Paul, USA) implantation as previously described.^{16,17} Animals were allowed to recover for 5 weeks, as this period is necessary for the remnant kidney to attain a new steady-state condition.¹⁸ Subsequently, animals were treated for 4 weeks with vehicle (15% dimethylsulfoxide/75% polyethylene glycol-400/10% ethanol; n=10), AGT siRNA (10-30 mg/kg fortnightly by subcutaneous injection, n=12; Alnylam Pharmaceuticals, Cambridge, MA, USA), AGT siRNA + losartan (30 mg/kg per day; n=7; SigmaAldrich, Zwijndrecht, The Netherlands), losartan (n=8), or losartan + captopril (6 mg/kg per day, n=8; Sigma Aldrich). Losartan and captopril doses were chosen on the basis of maximum effectiveness.^{16,19} The siRNA consisted of a chemically modified antisense strand with sequence UUGAUUUUUGCCCAGGAUAGCUC, hybridized with a chemically modified sense strand of sequence GCUAUCCUGGGCAAAAUAUCAA. Oligonucleotides were synthesized as previously described.⁶ To ensure selective and efficient

Chapter 4

delivery to hepatocytes, a triantennary N-acetylgalactosamine (GalNAc) – a high-affinity ligand for the hepatocyte-specific asialoglycoprotein receptor – was attached to the 3' end of the sense strand.²⁰ Two doses of AGT siRNA were tested (10 and 30 mg/kg), but since the degree of AGT depletion was identical with both doses ($97.3 \pm 1.4\%$ versus $95.9 \pm 1.1\%$; Figure S1) data for both doses were combined. Losartan and captopril were administered subcutaneously by osmotic minipump (model 2ML4, Alzet, Cupertino, CA, USA). Four additional 5/6th Nx animals were sacrificed after the recovery period, to establish plasma hormone levels, proteinuria, renal histology and cardiac hypertrophy before the start of treatment ('baseline'). Eight Sprague-Dawley rats (18 weeks old, weight 407 ± 24 g) were sacrificed to establish renal histology in healthy controls. Animals were allocated to treatment groups by stratification based on the 3-day average of mean arterial pressure (MAP) and the glomerular filtration rate (GFR) measured at baseline. For biochemical measurements, we collected 24-hour urine in metabolic cages and blood plasma by venipuncture from the lateral tail vein before treatment (baseline), after 2 weeks and after 4 weeks of treatment. Blood pressure, heart rate and animal activity were recorded continuously via radiotelemetry. At the end of the treatment period, rats were anaesthetized by inhalation of isoflurane and exsanguinated: 1 mL blood was collected in 10 mL of 4 mol/L guanidine thiocyanate²¹ (Sigma Aldrich) and used for quantification of angiotensin metabolites; remaining blood was supplemented with EDTA and centrifuged at $16000 \times g$ to obtain plasma. Kidneys and heart were harvested, weighed, divided into transverse segments, and fixated in 4% paraformaldehyde for histological analysis, or snap frozen in liquid nitrogen for gene - and protein expression analysis. Mesenteric arteries were isolated and used directly in myograph studies.

Biochemical measurements

In plasma, AGT was measured by enzyme- kinetic assay as the maximum quantity of Ang I generated during incubation, at pH 7.4 and 37°C, with rat kidney renin in the presence of a mixture of ACE, angiotensinase, and serine protease inhibitors.²² The lower limit of detection of this assay was 0.2 nmol/L. In renal tissue, AGT was quantified by Western blotting and normalized vs. glyceraldehyde-3-phosphate dehydrogenase (GAPDH) as described before.²³ Plasma renin

concentration (PRC) was measured by quantifying Ang I generation in the presence of excess porcine AGT (detection limit 0.17 ng Ang I/mL per hour).²⁴ Ang I was measured by radioimmunoassay. In the cases that measurements were at or below the detection limit, this limit was applied to allow for statistical analysis. Ang metabolites in plasma, kidney, and heart tissue (left ventricle) were measured by LC-MS/MS analysis as described before.²⁵ Briefly, tissue samples were homogenized under liquid nitrogen and extracted with a guanidinium-based extraction buffer. Stabilized whole blood and tissue extracts were spiked with stable isotope labeled internal standards for each individual target analyte (Sigma Aldrich) before being subjected to C18 based solid phase extraction and subsequent LC-MS/MS analysis. Table S1 specifies the lower limit of quantification for each metabolite. Plasma NT-proBNP was measured with a rat NT-proBNP ELISA kit (detection limit 15.6 pg/mL; Aviva Systems Biology, San Diego, USA). Urine total protein was measured by the clinical chemistry laboratory of the Erasmus MC. Urinary neutrophil gelatinase-associated lipocalin (NGAL) was measured with a rat NGAL ELISA kit (detection limit 0.1 pg/mL; Abcam, Cambridge, UK).

Quantitative polymerase chain reaction (qPCR)

Total RNA was isolated from snap-frozen kidney using TRI Reagent (Sigma Aldrich) and reverse transcribed into cDNA using the QuantiTect Reverse Transcription Kit (Qiagen, Venlo, The Netherlands). cDNA was amplified in triplicate in 40 cycles (denaturation at 95°C for 3 min; thermal cycling at 95°C for 3 sec, annealing/extension at 60°C for 20 sec) followed by a melt curve with a CFX384 (Bio-Rad, Veenendaal, The Netherlands) using Kapa SYBR® Fast (Kapa Biosystems). Intron-spanning oligonucleotide primers were designed with NCBI Primer-BLAST for AGT (forward CCAGCACGACTTCCTGACT, reverse GCAGGTTGTAGGATCCCCGA), renin (forward TGTGGTAACTGTGGGTGGAAT, reverse GCATGAAGGGTATCAGGGGC) and β_2 -microglobulin (B2M; forward ATGGCTCGCTCGGTGACCG, reverse TGGGGAGTTTTCTGAATGGCAAGCA). The DDcT method was used for relative quantification of mRNA expression levels, using the housekeeping gene B2M for normalization.

Kidney function

Glomerular filtration rate (GFR) was determined at baseline and at the end of treatment, by transcutaneous measurement of fluorescein isothiocyanate (FITC)-labeled sinistrin (Mannheim Pharma & Diagnostics GmbH, Mannheim, Germany), administered as a bolus injection (0.24 mg/kg dissolved in saline) via the tail vein. A non-invasive clearance (NIC)-kidney fluorescent detection device together with partner software (Mannheim Pharma & Diagnostics GmbH) were used to generate the elimination kinetics curve of FITC-sinistrin. GFR was derived from the excretion half-life ($t_{1/2}$) of FITC-sinistrin, using a conversion factor and formula validated for rats²⁶: $\text{GFR (mL/min per 100g body weight (BW))} = 31.26 \text{ (mL/100g BW)} / t_{1/2} \text{ FITC-sinistrin (minutes)}$.

Histology

Kidney segments, fixed in 4% paraformaldehyde, were dehydrated and paraffin-embedded. Transversely sliced and deparaffinized kidney sections (2 mm) were stained with periodic acid–Schiff (PAS) and scored semiquantitatively in a blinded fashion by a renal pathologist (M.C.C.v.G.) as previously described.²⁷ Focal segmental glomerulosclerosis (FSGS) was assessed and graded in all glomeruli of one kidney section per rat, basing on an arbitrary scale wherein 0%, <25%, 25-50%, 50-75%, and >75% of glomerular sclerosis were represented by grade zero (n_0), 1 (n_1), 2 (n_2), 3 (n_3), and 4 (n_4), respectively. The glomerulosclerosis index (GSI) was calculated with the formula: $[(1 \times n_1) + (2 \times n_2) + (3 \times n_3) + (4 \times n_4)] / (n_0 + n_1 + n_2 + n_3 + n_4)$. Tubular atrophy, interstitial fibrosis, and tubulointerstitial inflammation were scored in the same kidney section and summed to obtain the tubulointerstitial score (TIS). A score of 0-3 indicated that <25% of tubulointerstitial tissue was affected, a score of 4-6 indicated 25-50% and a score of 7-9 indicated >50%. Finally, observing dilated tubules and acute thrombotic microangiopathy was used as an indication of hypertensive kidney injury.

Myograph studies

Mesenteric arteries were carefully dissected and placed in a cold, Krebs bicarbonate solution (composed as follows [in mmol/L]: NaCl, 118; KCl, 4.7; CaCl₂, 2.5; MgSO₄, 1.2; KH₂PO₄, 1.2; NaHCO₃, 25 and glucose, 8.3; pH = 7.4), aerated with 5% CO₂ in O₂ (carbogen). Arteries were cut into 2 mm segments and mounted in Mulvany myographs (Danish Myo Technology, Aarhus, Denmark) with 6-mL organ baths containing oxygenated Krebs buffer and maintained at 37°C. Changes in tissue tension were measured using a LabChart data acquisition system (AD Instruments Ltd, Oxford, UK). After equilibration for at least 30 min and a wash, the vessel segments were stretched to a tension normalized to 90% of 100 mm Hg. After reaching equilibrium, the contractile capacity of the mesenteric arteries were examined by adding 30 mmol/L KCl. After washout, the tissue was exposed to 100 mmol/L KCl to determine the maximal contraction. Endothelial function was checked by verifying relaxation to 10 mmol/L acetylcholine after preconstriction with the thromboxane A₂ analogue U46619 (10 nmol/L) to >70% of the maximal contraction. Next, segments were equilibrated in fresh Krebs buffer for 30 min, and preincubated for 30 min with the NO synthase inhibitor L-NAME (N^ω-nitro-L-arginine methyl ester hydrochloride; 100 μmol/L), the small- and intermediate-conductance Ca²⁺-activated K⁺-channel (SK_{Ca}, IK_{Ca}) inhibitors apamin (100 nmol/L) and TRAM34 (10 μmol/L), the endothelin type A (ET_A) receptor antagonist BQ123 (1 μmol/L), or the ET_B receptor antagonist BQ788 (1 μmol/L). Thereafter, concentration-response curves (CRCs) were constructed to ET-1. To construct CRCs to the endothelium-dependent dilator acetylcholine (ACh) arteries were precontracted with U46619. All drugs were obtained from Sigma-Aldrich.

Statistics

Data are expressed as mean values ± SEM in case of normal distribution and median with interquartile range in case of non-normal distribution. Non-normally distributed data were log-transformed before statistical analysis. The minimum number of animals per group was calculated to be 7 (4-week treatment, 5 treatment groups, α=0.05, power 80%, standard deviation 10 mm Hg, difference in means 15 mm Hg). Data were analyzed by one-way analysis of variance (ANOVA) and mixed linear models, using treatment and time as fixed effects, if

appropriate. If significant, selected post-hoc analyses were performed between individual groups by controlling for a false-discovery rate of 5%.²⁸ Relaxant responses to either ACh or SNAP are expressed as a percentage of the contraction to U46619. Contractile responses to ET-1 are expressed as a percentage of the contraction to 100 mmol/L KCl. CRCs were analyzed as described before²⁹ to obtain pEC₅₀ ($-\log EC_{50}$) and E_{max} values. Data obtained at multiple points in time were analyzed using a repeated-measures two-way ANOVA, followed by post-hoc correction according to Dunnett or Dunn in case of multiple comparisons, if appropriate. Univariate linear associations were assessed by calculation of Pearson's coefficient of correlation. Two-tailed P values <0.05 were considered statistically significant. Multiple linear regression analysis was performed to identify variables correlating independently with proteinuria. All analyses were performed using Prism version 9.0.0 (GraphPad Software Inc., La Jolla, USA)

Results

AGT siRNA halts the blood pressure rise in the 5/6th Nx model

We have reported earlier that MAP in healthy SD rats is 103±1 mm Hg (n=7).²³ At 5 weeks after 5/6th Nx ('baseline') MAP had increased to 160±6 mm Hg (n=47; Figure 1A). Systolic and diastolic blood pressure (SBP, DBP) were 187±6 and 126±8 mm Hg, respectively. MAP increased further to 174±5 mm Hg during the subsequent 4 weeks of vehicle treatment. AGT siRNA treatment prevented this increase (P<0.05 versus vehicle; Figures 1A and 1B). Losartan lowered MAP by 37±6mmHg, P<0.001 versus vehicle). Adding either AGT siRNA or captopril on top of losartan diminished (P<0.05 versus losartan) the effect of losartan, yielding MAP decreases of 22±7 and 21±6 mm Hg, respectively (both P<0.001 versus vehicle). As a consequence, MAP was identical during treatment with AGT siRNA alone, AGT siRNA + losartan and losartan + captopril, while it was lower in the losartan alone group versus the AGT siRNA alone group (P<0.05). No treatment affected heart rate (Figure 1C), activity (Figure 1D), body weight, or food intake (Table S2). Evaluating the drug effects on the basis of analyses with SBP instead of MAP yielded the same outcome (Figure S2). Figure S2 additionally

provides scatter plots of SBP, DBP and pulse pressure in the various groups at the end of the 4-week treatment.

AGT siRNA suppresses the circulating RAS

PRC in healthy SD rats amounted to 11.8 ± 0.8 ng Ang I/mL per hour.²³ At 5 weeks after 5/6th Nx, PRC had decreased to 2.6 (range 0.8-3.9) ng Ang I/mL per hour (Figure 2A). All treatments modestly increased PRC, although significance ($P < 0.05$ versus baseline) was reached for losartan only (at 2 weeks). PRC correlated negatively with MAP ($P = 0.008$; Figure 2B) and SBP ($P = 0.006$; Figure S3A). As expected, AGT siRNA, either alone or with losartan, diminished plasma AGT by $>95\%$ (Figure 2C). No other treatment affected circulating AGT. Losartan increased plasma Ang I ($P < 0.001$ versus vehicle) and II ($P < 0.01$) (Figures 2D and 2E), while in combination with captopril only plasma Ang I increased ($P < 0.001$). AGT siRNA reduced plasma Ang I ($P = 0.07$) and II ($P < 0.05$) in parallel, with the plasma Ang I levels becoming undetectable in most animals. Combining AGT siRNA with losartan yielded virtually

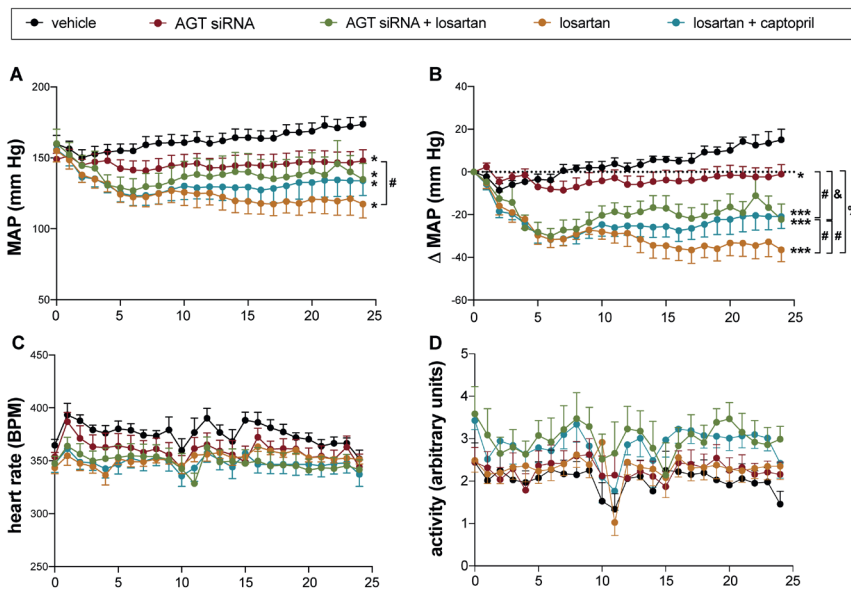


Figure 1. Effects on hemodynamics and activity. Mean arterial pressure (MAP; A), Δ MAP (B), heart rate (bpm; C), and locomotor activity (D) in Sprague-Dawley rats subjected to 5/6th nephrectomy and treated with either vehicle, angiotensinogen (AGT) small interfering RNA (siRNA), AGT siRNA+losartan, losartan, or losartan+captopril for 28 d. Treatment was started after 5 wk of recovery. Data are mean \pm SEM of $n = 7$ to 12. * $P < 0.05$, *** $P < 0.001$ vs vehicle; # $P < 0.05$, & $P < 0.01$, % $P < 0.001$ vs indicated group.

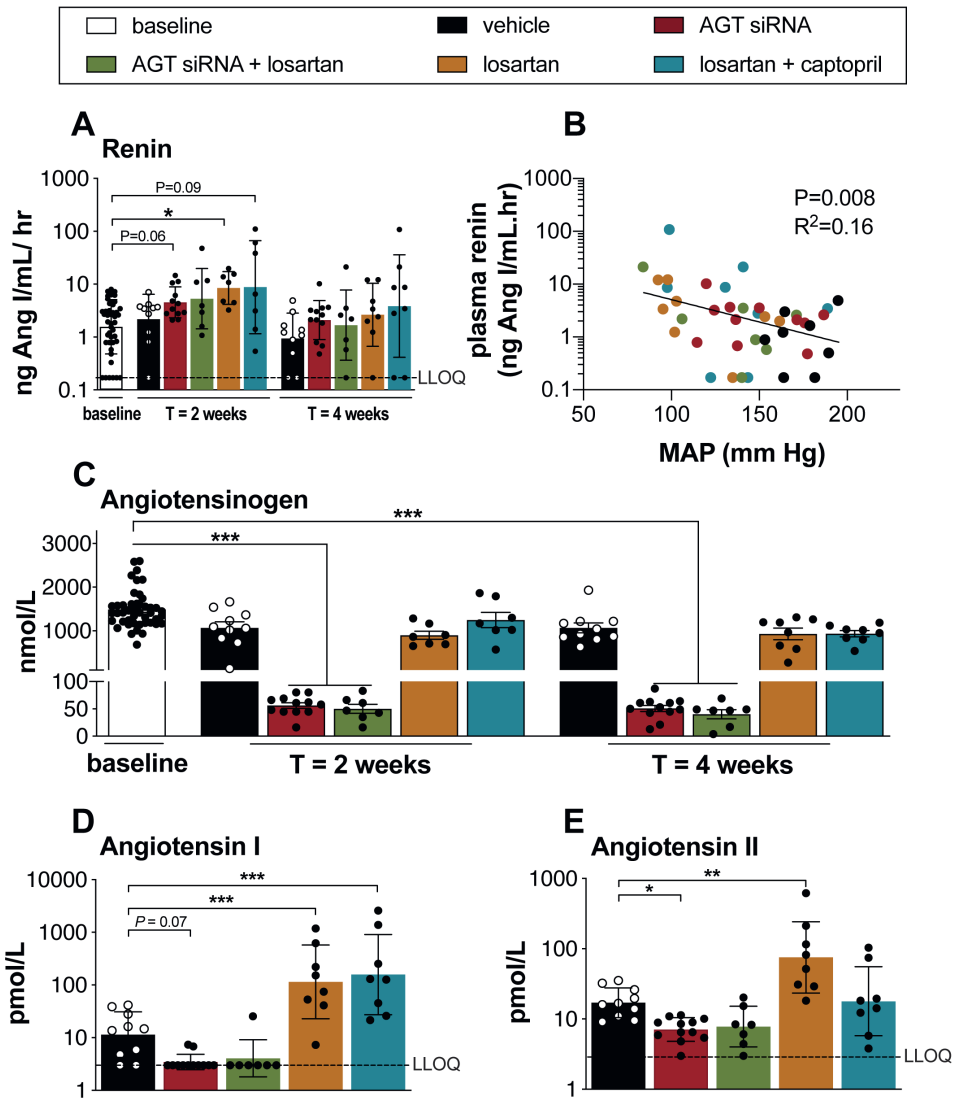


Figure 2. Effects on the circulating renin-angiotensin system. Renin (A), angiotensinogen (AGT; C), Ang (angiotensin) I (D), and Ang II (E) in blood plasma of Sprague-Dawley rats subjected to 5/6th nephrectomy and treated with either vehicle, AGT small interfering RNA (siRNA), AGT siRNA+losartan, losartan, or losartan+captopril for 28d. Treatment was started after 5 wk of recovery (=baseline). Data are mean±SEM of n=7 to 12. B, The relationship between plasma renin and mean arterial pressure (MAP) during the last 3 treatment days. LLOQ indicates lower limit of quantification. *P<0.05, **P<0.01, ***P<0.001, ****P<0.0001 vs indicated group.

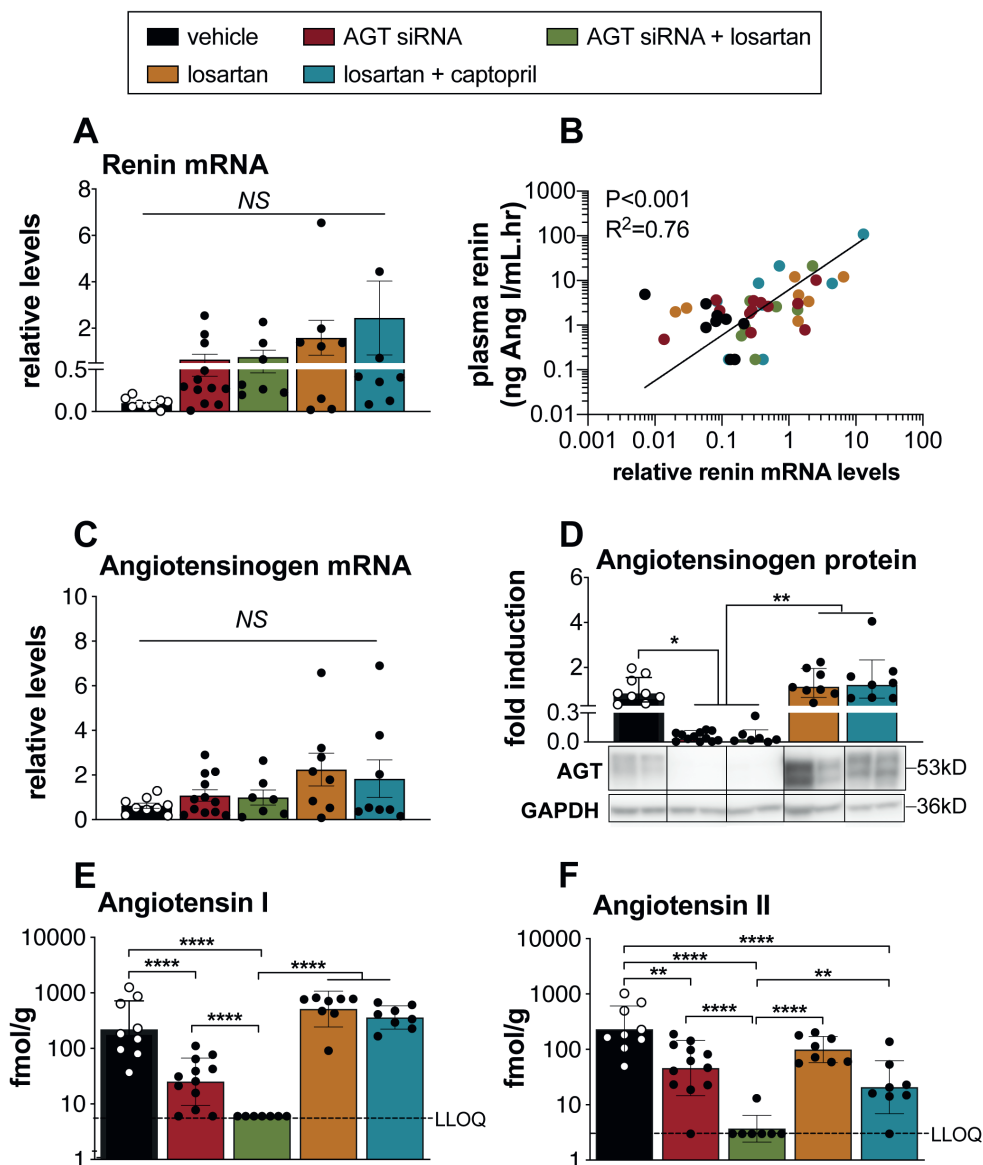


Figure 3. Effects on the renal reninangiotensin system. *Renin* expression (normalized versus $\beta 2$ -microglobulin; A), angiotensinogen (AGT) mRNA (normalized versus $\beta 2$ -microglobulin; C), AGT protein (fold induction versus GAPDH; D), Ang (angiotensin) I (E), and Ang II (F) in kidneys of Sprague-Dawley rats subjected to 5/6th nephrectomy and treated with either vehicle, AGT small interfering RNA (siRNA), AGT siRNA+losartan, losartan, or losartan+captopril for 28d. Treatment was started after 5 wk of recovery. Data are mean \pm SEM of n=7 to 12. B, The relationship between plasma renin and renal *renin* expression. D, Representative blots. LLOQ indicates lower limit of quantification; and NS, not significant. * $P < 0.05$, ** $P < 0.01$, *** $P < 0.001$, **** $P < 0.0001$ vs indicated group.

Chapter 4

identical Ang I and II levels as AGT siRNA alone. Only captopril reduced the Ang II/I ratio (Table S1). Neither Ang-(1-7), nor Ang III or IV were detectable in blood of 5/6th Nx rats (Table S1), and only after losartan (with or without captopril) did these metabolites become detectable.

AGT siRNA and the renal RAS

AGT siRNA, as well as the other treatments, tended to upregulate renal *renin* expression (Figure 3A), but no significance was reached. Renal *renin* expression correlated closely ($P<0.001$) with PRC (Figure 3B). AGT siRNA did not affect renal *AGT* expression (Figure 3C), in agreement with its liver-specificity, nor did any of the other treatments affect this expression. Yet, AGT siRNA greatly suppressed the renal AGT, Ang I, and Ang II levels (Figures 3D-F), while in combination with losartan, renal Ang I and II were virtually eliminated ($P<0.0001$ versus AGT siRNA alone). Losartan, with or without captopril, did not affect renal Ang I. Losartan when given alone, modestly reduced renal Ang II ($P<0.05$ versus vehicle), while in combination with captopril, it reduced renal Ang II more strongly ($P<0.01$). As a consequence, the renal Ang II/I ratio decreased during both losartan alone and losartan + captopril ($P<0.001$ versus vehicle; Table S1), but not during the other treatments. Renal Ang III and Ang IV levels were low in the 5/6th Nx model, and rapidly became undetectable after most treatments (Table S1). In contrast, renal Ang-(1-7) levels were of identical magnitude as the renal Ang II levels, and decreased in parallel with Ang I and II after siRNA (with or without losartan), but not after losartan alone or losartan + captopril.

AGT siRNA is renoprotective

GFR in healthy SD rats is 1.0 ± 0.04 mL/min per 100 g body weight.²³ At 5 weeks after the 5/6th Nx procedure, GFR had decreased to 0.38 ± 0.10 mL/min per 100 g body weight. Neither vehicle, nor any treatment affected GFR over the next 4 weeks (Figure 4A). None of the treatments altered water intake (Table S2), urinary volume (Table S2) or urinary NGAL excretion (Figure 4B), although losartan, with or without AGT siRNA, did tend to reduce the latter ($P=NS$). Proteinuria

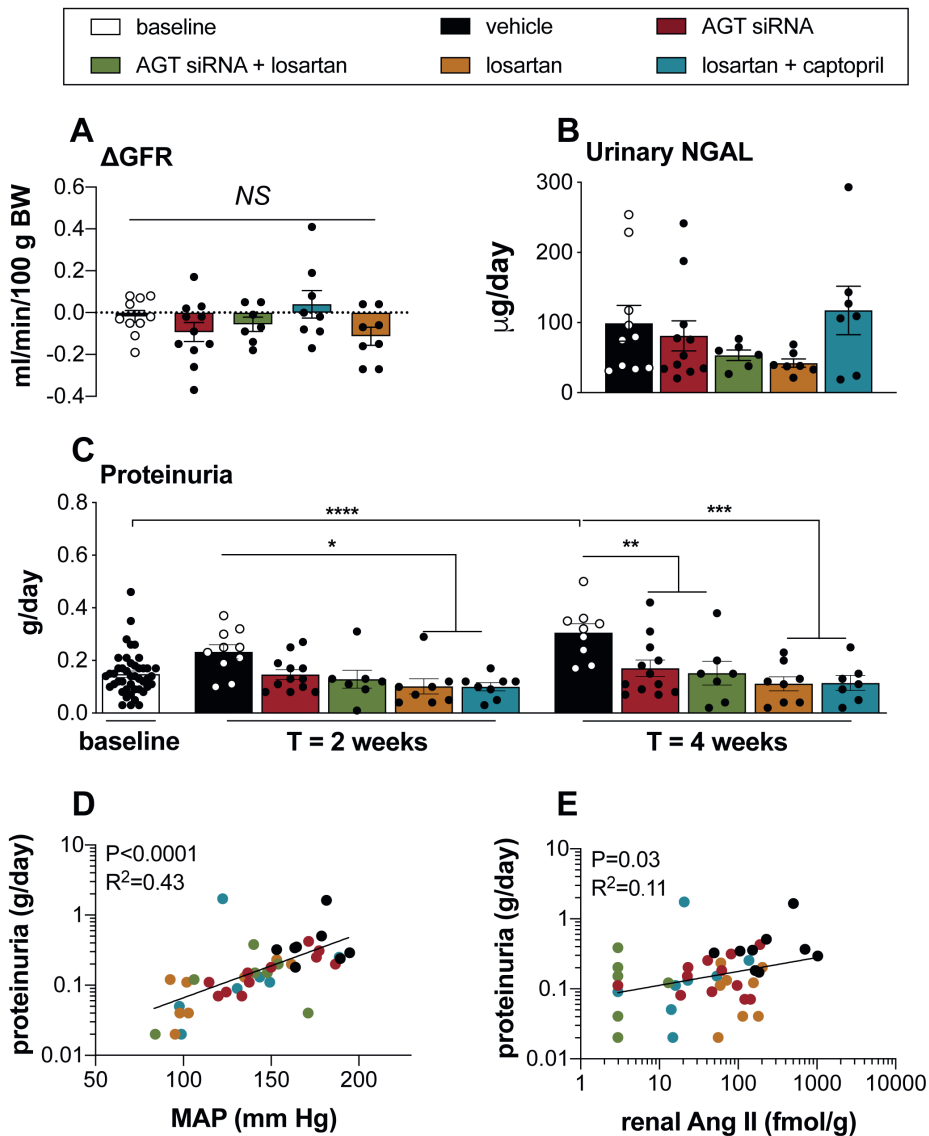


Figure 4. Effects on renal function. Glomerular filtration rate (GFR; expressed as change versus baseline; A), urinary NGAL (neutrophil gelatinase-associated lipocalin) excretion (B), and proteinuria (C) in kidneys of Sprague-Dawley rats subjected to 5/6th nephrectomy and treated with either vehicle, angiotensinogen (AGT) small interfering RNA (siRNA), AGT siRNA+losartan, losartan, or losartan+captopril for 28 d. Treatment was started after 5 wk of recovery (=baseline). Data are mean±SEM of n=7 to 12. D and E, The relationship between proteinuria at 4 wk and mean arterial pressure (MAP) during the last 3 treatment days and the renal Ang (angiotensin) II levels, respectively. BW indicates body weight; and NS, not significant. * $P < 0.05$, ** $P < 0.01$, *** $P < 0.001$ vs indicated group.

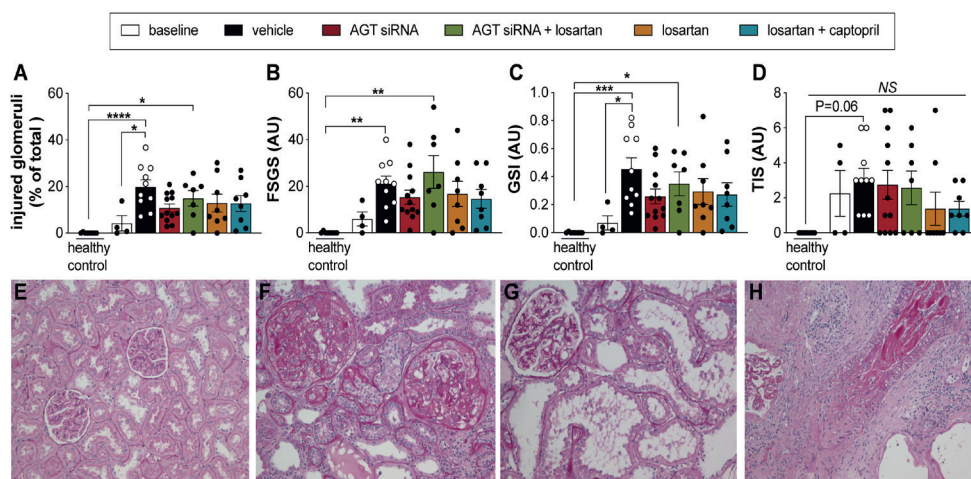


Figure 5. Effects on renal histology. Percentage of glomeruli having any degree of glomerular injury (A), focal segmental glomerulosclerosis (FSGS; B), glomerulosclerosis index (GSI; C), and tubulointerstitial score (TIS; D) in kidneys of Sprague-Dawley rats subjected to 5/6th nephrectomy and treated with either vehicle, angiotensinogen (AGT) small interfering RNA (siRNA), AGT siRNA+losartan, losartan, or losartan+captopril for 28 d. Treatment was started after 5 wk of recovery (=baseline), and data in healthy rats have been added for comparison. Data are mean±SEM of n=7 to 12. E–H, Representative, periodic acid–Schiff-stained renal histological images of different types of damage illustrating a normal kidney (E), thrombotic microangiopathy of glomeruli and arteriole (F), dilated tubules (G), and a thrombus in a main large vessel (H). NS indicates not significant. * $P<0.05$, ** $P<0.01$, *** $P<0.001$ vs indicated group.

(13 (range 8.5–16) mg/day in healthy SD rats (n=73, unpublished results) was 140 (range 92–170) mg/day at 5 weeks after 5/6th Nx. It rapidly increased further during vehicle treatment, and all treatments, whether given alone or in combination, fully prevented this rise (Figure 4C). Proteinuria correlated significantly with MAP ($P<0.001$; Figure 4D), SBP ($P<0.0001$; Figure S3B) and renal Ang II ($P=0.03$; Figure 4E). Incorporating MAP and renal Ang II in a multiple linear regression model confirmed that both MAP (standardized coefficient 0.69, $P<0.0001$) and renal Ang II (standardized coefficient 0.26, $P=0.023$) were independent determinants of proteinuria (adjusted $R^2=0.60$). Results were identical if replacing MAP by SBP (data not shown). The percentage of glomeruli having any degree of glomerular injury, FSGS, GSI and TIS all increased over the 8 weeks period after 5/6th Nx (Figure 5), although statistical significance for the latter was not reached ($P=0.06$). The significant increases in kidney injury scores versus healthy control disappeared after all treatments, except after

the treatment with losartan + AGT siRNA. The number of rats with dilated tubules increased from 0 out of 8 (0/8) in the healthy control group, to 2/4 at baseline and 7/10 after 4 weeks of vehicle exposure. Acute thrombotic microangiopathy featured in these groups in 0/8, 2/4, and 5/10 rats, respectively, with arterial involvement in 1/10 of vehicle-treated rats. AGT siRNA, AGT siRNA + losartan, losartan, and losartan + captopril reduced the number of rats with dilated tubules to 5/12, 2/7, 2/8 and 4/8, and acute thrombotic microangiopathy to 4/12, 2/7, 1/8, and 2/8 rats (with arterial involvement in 2/12 AGT siRNA-treated rats and 1/8 losartan + captopril-treated rats) respectively. These data therefore fully agree with the histology scores.

AGT siRNA is cardioprotective

Cardiac Ang I and II levels in vehicle-treated 5/6th Nx rats were close to or below detection limit (Figures 6A and 6B). siRNA, with or without losartan, lowered these levels even further ($P < 0.05$ vs. vehicle), while losartan alone and losartan + captopril upregulated cardiac Ang I ($P < 0.05$). Losartan did not alter cardiac Ang II, while losartan + captopril lowered cardiac Ang II ($P < 0.05$). As a consequence, the Ang II/I ratio decreased after both losartan and losartan + captopril ($P < 0.05$; Table S1). All other angiotensin metabolites were undetectable in cardiac tissue of 5/6th Nx rats, and only after losartan and losartan + captopril did Ang-(1-7) occasionally rise above lower limit of quantification ($P = \text{NS}$). No treatment lowered NT-proBNP (Figure 6C). Yet, all treatments equally prevented the rise in HW/TL ratio that occurred over the 4 week period after starting therapy (Figure 6D). The HW/TL ratio correlated strongly with MAP ($P < 0.001$; Figure 6E) and SBP ($P < 0.0001$; Figure S3C), but not with cardiac Ang II (data not shown).

5/6th Nx does not alter vascular function

Acetylcholine fully relaxed U46619-precontracted mesenteric arteries of 5/6th Nx rats (Figure S4 and Table S3). Blocking NO (with L-NAME) or EDHF (with TRAM34+apamin) marginally prevented this relaxation, and only when combining L-NAME with TRAM34+ apamin, did the blockade become significant. This indicates that the ACH response depends on both NO and EDHF, and that the two pathways are

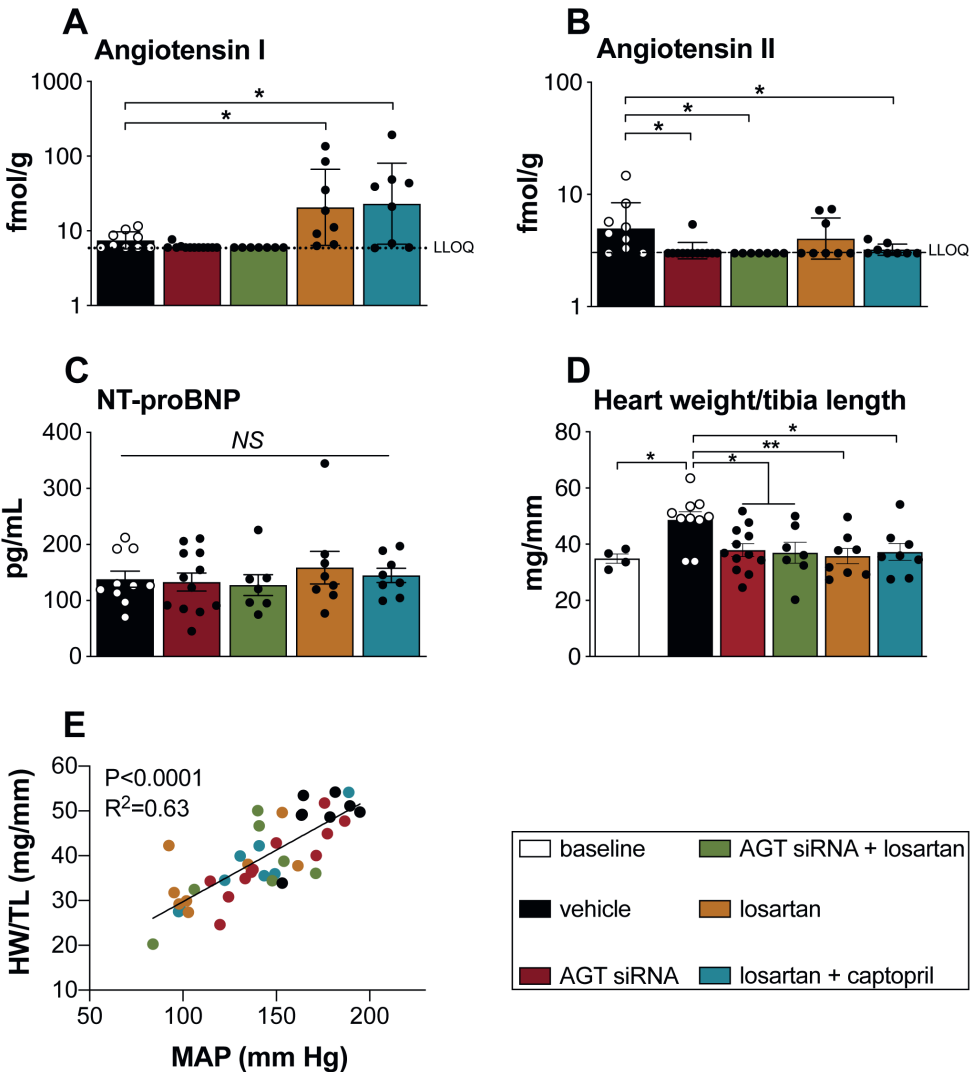


Figure 6. Effects on the cardiac renin-angiotensin system and cardiac hypertrophy. Cardiac angiotensin I (A), cardiac angiotensin II (B), plasma NT-proBNP (N-terminal pro-B-type natriuretic peptide; C), and heart weight/tibia length (HW/TL) ratio (D) in Sprague-Dawley rats subjected to 5/6th nephrectomy and treated with either vehicle, angiotensinogen (AGT) small interfering RNA (siRNA), AGT siRNA+losartan, losartan, or losartan+captopril for 28 d. Treatment was started after 5 wk of recovery (=baseline). Data are mean±SEM of n=7 to 12. E, The relationship between cardiac hypertrophy (HW/TL) and mean arterial pressure (MAP) during the last 3 treatment days. LLOQ indicates lower limit of quantification; and NS, not significant. *P<0.05, **P<0.01 vs indicated group.

interchangeable. No treatment altered this outcome. ET-1 strongly constricted mesenteric arteries of 5/6th Nx rats, and the ET_A receptor antagonist BQ123, but not the ET_B receptor antagonist BQ788, blocked this constriction, indicating that it depended entirely on ET_A receptor stimulation. No treatment altered this outcome.

Discussion

This study is the first to demonstrate reno- and cardioprotection in the rat 5/6th Nx model after a 4-week treatment with liver-directed AGT siRNA. The model is characterized by hypertension, cardiac hypertrophy, proteinuria, reduced GFR, glomerulosclerosis and tubulointerstitial fibrosis, and therefore recapitulates important characteristics of CKD.³⁰ Although it is known to be responsive to RAS blockade,⁸⁻¹⁰ we found circulating RAS activity in the 5/6th Nx rat to be greatly reduced, while renin upregulation during RAS blockade was barely detectable. This may simply reflect the fact that 5/6th of the kidneys was removed, reducing the capacity of the kidneys to release renin and/or to respond appropriately to RAS blockade.³¹ In contrast, renin rises during RAS blockade (including angiotensinogen suppression) in salt-depleted humans⁴ and spontaneously hypertensive rats⁶ can easily be >100-fold, thereby allowing Ang II levels to stay in the normal range, even when blocking the system by >99%.

We compared the effect of AGT siRNA in the 5/6th Nx model to the ARB losartan or combined treatment with losartan and the ACEi captopril, two drugs that are commonly used separately but not together in patients with CKD. Treatment was started at 5 weeks after 5/6th Nx, when blood pressure had already increased by ≈60 mm Hg. Despite the >75% reduction in circulating RAS activity at that time, the Ang II-AT₁ receptor axis may still have contributed to this blood pressure rise. Indeed, losartan did lower blood pressure by 37 mm Hg. This was accompanied by renin and Ang II rises. Remarkably, when combining losartan with either AGT siRNA or captopril, its blood pressure-lowering effect was diminished, while AGT siRNA alone did not lower blood pressure, although it did prevent a further rise in blood pressure after the initial 5-week period. As a consequence, after 4 weeks of treatment MAP was lower in the losartan group than in the AGT

Chapter 4

siRNA group, while MAP in the losartan + AGT siRNA and losartan + captopril groups was identical to that in the AGT siRNA alone group (i.e., ≈ 40 mm Hg above that in healthy SD rats²³). The most likely explanation for these observations is that losartan, by upregulating Ang II, allowed concomitant AT₂ receptor stimulation, which would result in more substantial blood pressure lowering (given that AT₂ receptors cause vasodilation³²⁻³⁴) than might be expected from blockade of the Ang II-AT₁ receptor axis alone. This is not possible in combination with either siRNA or captopril, since these drugs prevented such a rise in circulating Ang II. Although studies with the AT₂ receptor antagonist PD123319 in the 5/6th Nx model confirm this concept,³⁵ the relevance of AT₂ receptor signaling in humans is unclear. Despite the difference in blood pressure reduction, losartan, AGT siRNA and losartan + captopril reduced cardiac hypertrophy, proteinuria and glomerulosclerosis comparably, and a favorable trend was observed for the tubulointerstitial score and urinary NGAL. These protective effects in kidney and heart therefore must reflect the consequence of local RAS blockade. Indeed, AGT siRNA lowered the cardiac and renal Ang I and II levels more strongly than the circulating Ang I and II levels. Taken together, these data illustrate that cardiac and renal angiotensin generation depend on liver-derived AGT, accumulating at tissue sites either via diffusion or by active uptake mechanisms. Our data do not support the concept¹¹ that renal Ang II production in the 5/6th Nx rat depends on locally produced AGT and that liver-targeting of AGT siRNA would keep renal Ang II formation intact. We stress that AGT mRNA expression did occur in renal tissue of the 5/6th Nx rat. In agreement with the liver-specificity of our GalNAc-labeled siRNA, this expression was unaltered after AGT siRNA, nor was it altered by any of the other treatments. Yet, when treating the rats with AGT siRNA + losartan, renal Ang II entirely disappeared. The strong suppression of renal Ang II after AGT siRNA + losartan lowered proteinuria and cardiac hypertrophy to the same degree as single treatment, but no longer improved glomerulosclerosis. This observation supports the concept that complete elimination of the renal RAS is undesirable, and may underlie the renal side-effects of conventional dual and triple RAS blockade.^{36,37} However, the latter particularly concerns a reduction in GFR, and this was not observed in the present study. In fact, no treatment affected the $\approx 60\%$ GFR reduction in our model, although GFR improvement has been observed previously in 5/6th Nx rats after RAS blockade.¹⁰ This may relate to the

larger (>75%) GFR reduction in those earlier studies.

Proteinuria correlated with MAP and the renal Ang II levels. A unifying concept to explain our data is therefore that both a decrease in blood pressure and a decrease in renal Ang II improve proteinuria, most likely in an additive manner, and involving a reduction in glomerulosclerosis. Multiple linear regression confirmed this view. Hence, losartan predominantly exerts its effects via blood pressure lowering (likely depending on AT₂ receptor stimulation), while siRNA rather acts by suppressing renal Ang II. Whether a similar mechanism (blood pressure lowering and suppression of tissue Ang II generation³⁸) underlies the improvement of cardiac hypertrophy remains to be proven. Heart weight/tibia length ratio correlated with MAP only, and not with cardiac Ang II, possibly because cardiac Ang II levels after treatment were often below the detection limit. No effect of any treatment on NT-proBNP was observed, possibly because the blood pressure-lowering effects (with the exception of that of losartan alone) were modest, so that atrial stretch (a major stimulant of BNP synthesis) would be reduced only mildly.

Both captopril and losartan suppressed the Ang II/I ratio in kidney and heart. In the case of captopril, this simply reflects the degree of ACE inhibition. In the case of losartan, like during ACE inhibition, there will be renin upregulation, resulting in enhanced Ang I generation. Ang II generation should increase in parallel. However, tissue Ang II reflects Ang II that has been internalized via AT₁ receptors,^{38,39} and consequently, given the fact that losartan inhibits this process, ARB treatment may indeed lower the tissue Ang II/I ratio, albeit without affecting the Ang II/I ratio in the circulation. Ang-(1-7) has been suggested to be responsible for the beneficial effects of RAS blockade in both kidney and heart, as it counteracts the Ang II-AT₁ receptor axis.⁴⁰ In the present study Ang-(1-7) was not detectable in either blood or cardiac tissue of 5/6th Nx rats, although it was present in the kidney. Nevertheless, AGT siRNA eliminated renal Ang-(1-7), thereby implying that its beneficial effects are unrelated to this peptide.

Perspectives

In summary, liver-targeted AGT siRNA exerts beneficial renal and cardiac effects in the 2-step 5/6th Nx rat despite the fact that this is a low-renin CKD model. Its tissue effects are likely to represent the maximum effect of RAS blockade, since adding losartan on top of AGT siRNA (or combining losartan with captopril) yielded an identical degree of reno- and cardioprotection. These effects reflect the dependency of both renal and cardiac Ang II on liver-derived AGT. In view of the potential long-lasting effects of siRNA treatment (as with inclisiran, which is dosed every six months⁷) targeting hepatic AGT offers new possibilities for the treatment of CKD in humans, especially in non-adherent patients. Future studies will be needed to understand both the long-term risks and benefits of such long-term tissue RAS suppression, considering that too much renal Ang II suppression may not be desirable.

Sources of funding

This work was partially supported by Alnylam Pharmaceuticals. D.M.B. and E.J.H. were supported by the Dutch Kidney Foundation (KSP-14OK19). L.R. was supported by a National Natural Science Foundation of China grant #81900668. X.L. was supported by the National Natural Science Foundation of China (grant #81870605), the Shenzhen Key Laboratory of Metabolism and Cardiovascular Homeostasis (grant #ZDSYS20190902092903237), and the Shenzhen Municipal Science and Technology Innovation Council (grant #JCYJ20190808170401660).

Disclosures

J.B.K.; I.Z.; L.M.; S.H. and D.F. are employees of Alnylam Pharmaceuticals. A.H.J.D. received a grant from Alnylam Pharmaceuticals which has partially supported this work. O.D. and M.P. are employees of Attoquant Diagnostics.

References

1. Kobori H, Nangaku M, Navar LG, Nishiyama A. The intrarenal renin-angiotensin system: from physiology to the pathobiology of hypertension and kidney disease. *Pharmacol Rev.* 2007;59:251-287.
2. Metzger R, Bohle RM, Pauls K, Eichner G, Alhenc-Gelas F, Danilov SM, Franke FE. Angiotensin-converting enzyme in non-neoplastic kidney diseases. *Kidney Int.* 1999;56:1442-1454.
3. van Kats JP, Schalekamp MADH, Verdouw PD, Duncker DJ, Danser AHJ. Intrarenal angiotensin II: interstitial and cellular levels and site of production. *Kidney Int.* 2001;60:2311-2317.
4. Balcarek J, Sevá Pessôa B, Bryson C, Azizi M, Ménard J, Garrelds IM, McGeehan G, Reeves RA, Griffith SG, Danser AHJ, Gregg R. Multiple ascending dose study with the new renin inhibitor VTP-27999: nephrocentric consequences of too much renin inhibition. *Hypertension.* 2014;63:942-950.
5. Schalekamp MA, Danser AH. How does the angiotensin II type 1 receptor 'trump' the type 2 receptor in blood pressure control? *J Hypertens.* 2013;31:705-712.
6. Uijl E, Mirabito Colafella KM, Sun Y, Ren L, van Veghel R, Garrelds IM, de Vries R, Poglitsch M, Zlatev I, Kim JB, Hoorn EJ, Foster D, Danser AHJ. Strong and sustained antihypertensive effect of small interfering RNA targeting liver angiotensinogen. *Hypertension.* 2019;73:1249-1257.
7. Ray KK, Landmesser U, Leiter LA, Kallend D, Dufour R, Karakas M, Hall T, Troquay RP, Turner T, Visseren FL, Wijngaard P, Wright RS, Kastelein JJ. Inclisiran in patients at high cardiovascular risk with elevated LDL cholesterol. *N Engl J Med.* 2017;376:1430-1440.
8. Piecha G, Koleganova N, Gross ML, Geldyyev A, Adamczak M, Ritz E. Regression of glomerulosclerosis in subtotaly nephrectomized rats: effects of monotherapy with losartan, spironolactone, and their combination. *Am J Physiol Renal Physiol.* 2008;295:F137-144.
9. Ma LJ, Nakamura S, Aldigier JC, Rossini M, Yang H, Liang X, Nakamura I, Marcantoni C, Fogo AB. Regression of glomerulosclerosis with high-dose angiotensin inhibition is linked to decreased plasminogen activator inhibitor-1. *J Am Soc Nephrol.* 2005;16:966-976.
10. Cao Z, Cooper ME, Wu LL, Cox AJ, Jandeleit-Dahm K, Kelly DJ, Gilbert RE. Blockade of the renin-angiotensin and endothelin systems on progressive renal injury. *Hypertension.* 2000;36:561-568.
11. Mullick AE, Yeh ST, Graham MJ, Engelhardt JA, Prakash TP, Crooke RM. Blood pressure lowering and safety improvements with liver angiotensinogen inhibition in models of hypertension and kidney injury. *Hypertension.* 2017;70:566-576.
12. van Koppen A, Verhaar MC, Bongartz LG, Joles JA. 5/6th nephrectomy in combination with high salt diet and nitric oxide synthase inhibition to induce chronic kidney disease in the Lewis rat. *J Vis Exp.* 2013:e50398.
13. Griffin KA, Picken M, Bidani AK. Method of renal mass reduction is a critical modulator of subsequent hypertension and glomerular injury. *J Am Soc Nephrol.*

Chapter 4

- 1994;4:2023-2031.
14. Griffin KA, Picken M, Bidani AK. Radiotelemetric BP monitoring, antihypertensives and glomeruloprotection in remnant kidney model. *Kidney Int.* 1994;46:1010-1018.
 15. Griffin KA, Picken MM, Bakris G, Bidani AK. Relative antihypertensive and glomeruloprotective efficacies of enalapril and candesartan cilexetil in the remnant kidney model. *J Renin Angiotensin Aldosterone Syst.* 2001;2:S191-S195.
 16. van Esch JHM, Moltzer E, van Veghel R, Garrelds IM, Leijten F, Bouhuizen AM, Danser AHJ. Beneficial cardiac effects of the renin inhibitor aliskiren in spontaneously hypertensive rats. *J Hypertens.* 2010;28:2145-2155.
 17. van der Lubbe N, Lim CH, Fenton RA, Meima ME, Danser AHJ, Zietse R, Hoorn EJ. Angiotensin II induces phosphorylation of the thiazide-sensitive sodium chloride cotransporter independent of aldosterone. *Kidney Int.* 2011;79:66-76.
 18. Gretz N, Meisinger E, Waldherr R, Strauch M. Acute renal failure after 5/6 nephrectomy: histological and functional changes. *Contrib Nephrol.* 1988;60:56-63.
 19. Zou LX, Imig JD, Hymel A, Navar LG. Renal uptake of circulating angiotensin II in Val5-angiotensin II infused rats is mediated by AT1 receptor. *Am J Hypertens.* 1998;11:570-578.
 20. Nair JK, Willoughby JL, Chan A, Charisse K, Alam MR, Wang Q, Hoekstra M, Kandasamy P, Kel'in AV, Milstein S, Taneja N, O'Shea J, Shaikh S, Zhang L, van der Sluis RJ, Jung ME, Akinc A, Hutabarat R, Kuchimanchi S, Fitzgerald K, Zimmermann T, van Berkel TJ, Maier MA, Rajeev KG, Manoharan M. Multivalent N-acetylgalactosamine-conjugated siRNA localizes in hepatocytes and elicits robust RNAi-mediated gene silencing. *J Am Chem Soc.* 2014;136:16958-16961.
 21. Campbell DJ, Duncan AM, Kladis A. Angiotensin-converting enzyme inhibition modifies angiotensin but not kinin peptide levels in human atrial tissue. *Hypertension.* 1999;34:171-175.
 22. van den Heuvel M, Batenburg WW, Jainandunsing S, Garrelds IM, van Gool JM, Feelders RA, van den Meiracker AH, Danser AHJ. Urinary renin, but not angiotensinogen or aldosterone, reflects the renal renin-angiotensin-aldosterone system activity and the efficacy of renin-angiotensin-aldosterone system blockade in the kidney. *J Hypertens.* 2011;29:2147-2155.
 23. Uijl E, Ren L, Mirabito Colafella KM, van Veghel R, Garrelds IM, Domenig O, Poglitsch M, Zlatev I, Kim JB, Huang S, Melton L, Hoorn EJ, Foster D, Danser AHJ. No evidence for brain renin-angiotensin system activation during DOCA-salt hypertension. *Clin Sci.* 2021;in press.
 24. de Lannoy LM, Danser AHJ, van Kats JP, Schoemaker RG, Saxena PR, Schalekamp MADH. Renin-angiotensin system components in the interstitial fluid of the isolated perfused rat heart. Local production of angiotensin I. *Hypertension.* 1997;29:1240-1251.
 25. Roksnoer LCW, van Veghel R, de Vries R, Garrelds IM, Bhaggoe UM, Friesema ECH, Leijten FPJ, Poglitsch M, Domenig O, Clahsen-van Groningen MC, Hoorn EJ, Danser AHJ, Batenburg WW. Optimum AT1 receptor-neprilysin inhibition has superior cardioprotective effects compared with AT1 receptor receptor blockade alone in hypertensive rats. *Kidney Int.* 2015;88:109-120.
 26. Schock-Kusch D, Sadick M, Henninger N, Kraenzlin B, Claus G, Kloetzer HM, Weiss C, Pill J, Gretz N. Transcutaneous measurement of glomerular filtration

- rate using FITC-sinistrin in rats. *Nephrol Dial Transplant*. 2009;24:2997-3001.
27. Uijl E, 't Hart DC, Roksnoer LCW, Claassen-van Groningen MC, van Veghel R, Garrelds IM, de Vries R, van der Vlag J, Zietse R, Nijenhuis T, Joles JA, Hoorn EJ, Danser AHJ. Angiotensin-neprilysin inhibition confers renoprotection in rats with diabetes and hypertension by limiting podocyte injury. *J Hypertens*. 2020;38:755-764.
28. Benjamini Y, Krieger AM, Yekutieli J. Adaptive linear step-up procedures that control the false discovery rate. *Biometrika*. 2006;93:491-507.
29. MaassenVanDenBrink A, de Vries R, Saxena PR, Schalekamp MADH, Danser AHJ. Vasoconstriction by in situ formed angiotensin II: role of ACE and chymase. *Cardiovasc Res*. 1999;44:407-415.
30. Bovée DM, Cuevas CA, Zietse R, Danser AHJ, Mirabito Colafella KM, Hoorn EJ. Salt-sensitive hypertension in chronic kidney disease: distal tubular mechanisms. *Am J Physiol Renal Physiol*. 2020;319:F729-F745.
31. Pupilli C, Chevalier RL, Carey RM, Gomez RA. Distribution and content of renin and renin mRNA in remnant kidney of adult rat. *Am J Physiol*. 1992;263:F731-738.
32. Kemp BA, Howell NL, Gildea JJ, Keller SR, Padia SH, Carey RM. AT(2) receptor activation induces natriuresis and lowers blood pressure. *Circ Res*. 2014;115:388-399.
33. Li XC, Widdop RE. AT2 receptor-mediated vasodilatation is unmasked by AT1 receptor blockade in conscious SHR. *Br J Pharmacol*. 2004;142:821-830.
34. Sevã Pessõa B, Slump DE, Ibrahimi K, Grefhorst A, van Veghel R, Garrelds IM, Roks AJM, Kushner SA, Danser AHJ, van Esch JHM. Angiotensin II type 2 receptor- and acetylcholine-23 mediated relaxation: essential contribution of female sex hormones and chromosomes. *Hypertension*. 2015;66:396-402.
35. Vázquez E, Coronel I, Bautista R, Romo E, Villalón CM, Avila-Casado MC, Soto V, Escalante B. Angiotensin II-dependent induction of AT₂ receptor expression after renal ablation. *Am J Physiol Renal Physiol*. 2005;288:F207-213.
36. Parving HH, Brenner BM, McMurray JJ, de Zeeuw D, Haffner SM, Solomon SD, Chaturvedi N, Persson F, Desai AS, Nicolaidis M, Richard A, Xiang Z, Brunel P, Pfeffer MA, Investigators A. Cardiorenal end points in a trial of aliskiren for type 2 diabetes. *N Engl J Med*. 2012;367:2204-2213.
37. Danser AHJ, van den Meiracker AH. Heart failure: New data do not SUPPORT triple RAAS blockade. *Nat Rev Nephrol*. 2015;11:260-262.
38. Mazzolai L, Pedrazzini T, Nicoud F, Gabbiani G, Brunner HR, Nussberger J. Increased cardiac angiotensin II levels induce right and left ventricular hypertrophy in normotensive mice. *Hypertension*. 2000;35:985-991.
39. van Kats JP, van Meegen JR, Verdouw PD, Duncker DJ, Schalekamp MADH, Danser AHJ. Subcellular localization of angiotensin II in kidney and adrenal. *J Hypertens*. 2001;19:583-589.
40. Santos RAS, Sampaio WO, Alzamora AC, Motta-Santos D, Alenina N, Bader M, Campagnole-Santos MJ. The ACE2/angiotensin-(1-7)/Mas axis of the renin-angiotensin system: focus on angiotensin-(1-7). *Physiol Rev*. 2018;98:505-553.24

Novelty and significance

What is new?

- Small interfering RNA targeting liver angiotensinogen (AGT) provide cardio- and renoprotection in a blood pressure-independent manner in the 5/6th nephrectomy rat, a hypertensive chronic kidney disease model.
- Multiple linear regression confirmed both blood pressure and renal angiotensin II as independent determinants of proteinuria.
- Renal angiotensin II formation in this model depends entirely on angiotensinogen of hepatic origin.

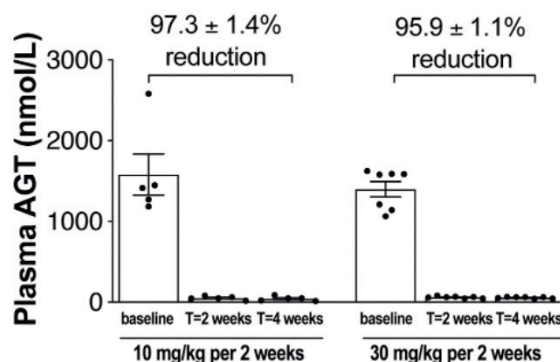
What is relevant?

- Given its stable and sustained efficacy, lasting weeks, RNA interference may prove beneficial in human chronic kidney disease.

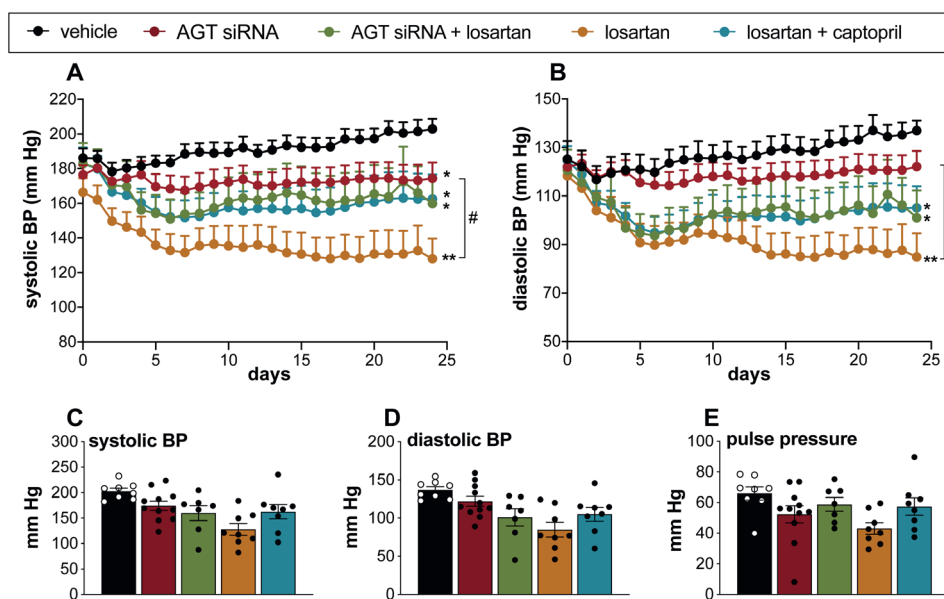
Summary

Small interfering RNA (siRNA) targeting liver angiotensinogen abrogated proteinuria, glomerulosclerosis and cardiac hypertrophy in the 5/6th nephrectomy rat, a hypertensive chronic kidney disease model, to the same degree as the angiotensin II type 1 receptor blocker losartan. Angiotensinogen siRNA reduced plasma angiotensinogen by >95%, and this was accompanied by almost complete elimination of angiotensin II in kidney and heart. Multiple linear regression confirmed both blood pressure and renal angiotensin II as independent determinants of proteinuria. Given its stable and sustained efficacy, lasting weeks, angiotensinogen siRNA may prove beneficial in human chronic kidney disease.

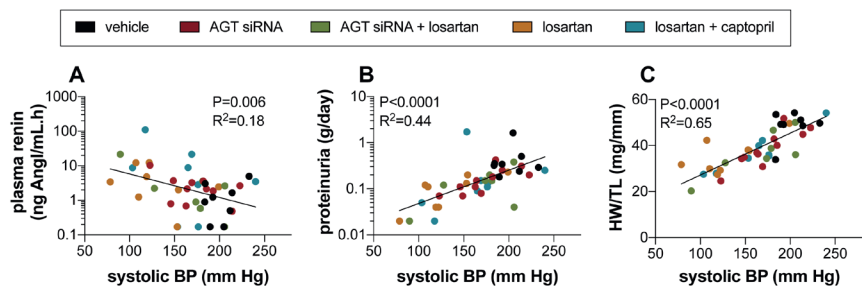
Online Supplement



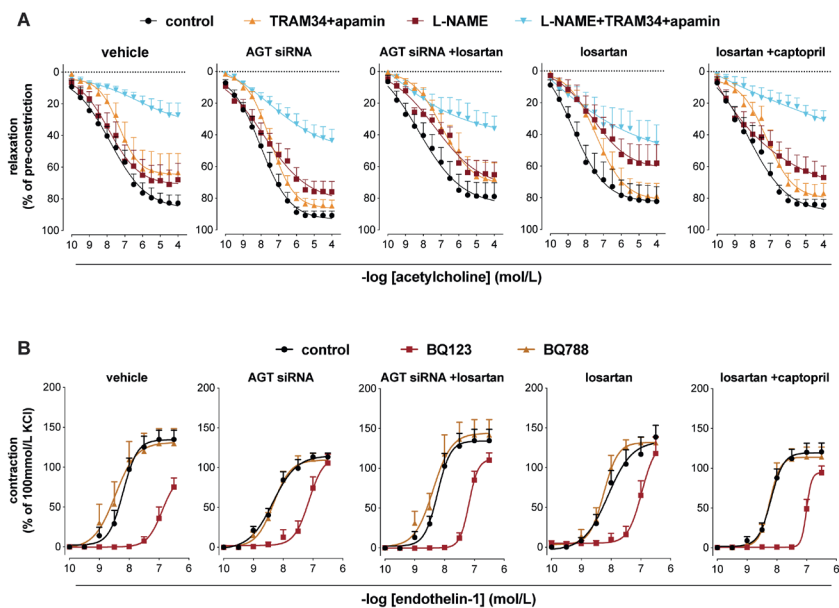
Supplemental Figure S1. Plasma angiotensinogen (AGT) in Sprague-Dawley rats subjected to 5/6th nephrectomy, and treated with AGT siRNA 10 or 30 mg/kg biweekly. Treatment was started 5 weeks after 5/6th Nx (=baseline), and measurements were performed at baseline, after 2 weeks, and after 4 weeks of treatment. Data are mean \pm SEM of $n=5-7$.



Supplemental Figure S2. Systolic blood pressure (systolic BP; panel A), diastolic BP (panel B) in Sprague-Dawley rats subjected to 5/6th nephrectomy, and treated with either vehicle, angiotensinogen (AGT) siRNA, AGT siRNA + losartan, losartan, or losartan + captopril for 28 days. Treatment was started after 5 weeks of recovery. Data are mean \pm SEM of $n=7-12$. Panel C, D and E display the systolic BP, diastolic BP and pulse pressure at the 24th day after those treatments. * $P<0.05$, ** $P<0.005$ versus vehicle; # $P<0.05$ versus indicated group.



Supplemental Figure S3. The relationship between plasma renin and systolic blood pressure (systolic BP) during the last 3 treatment days (panel A), relationship between proteinuria and systolic BP (panel B), and relationship between heart weight/tibia length (HW/TL) and systolic BP (panel C) in Sprague-Dawley rats subjected to 5/6th nephrectomy, and treated with either vehicle, angiotensinogen (AGT) siRNA, AGT siRNA + losartan, losartan, or losartan + captopril for 28 days. Treatment was started after 5 weeks of recovery.



Supplemental Figure S4. Vascular response to acetylcholine and endothelin-1 in mesenteric arteries of Sprague-Dawley rats subjected to 5/6th nephrectomy, and treated with either vehicle, angiotensinogen (AGT) siRNA, AGT siRNA + losartan, losartan, or losartan + captopril for 28 days. Treatment was started 5 weeks after 5/6th Nx. Panel A shows the relaxant responses to acetylcholine, expressed as a percentage of the U46619-induced precontraction, in the absence (control) or absence the inhibitors TRAM34+apamin, L-NAME, and L-NAME+TRAM34+apamin. Panel B shows the responses to endothelin-1, expressed as a percentage of the response to 100 mmol/L KCl in the absence (control) or presence of the endothelin receptor blockers BQ123 and BQ788. Data are mean \pm SEM of $n=5-11$, and the accompanying statistics are shown in supplemental Table S3.

Supplemental Table S1. Angiotensin (Ang) metabolites measured by LC-MS/MS in blood, kidney, and heart in Sprague-Dawley rats subjected to 5/6th nephrectomy, and treated with either vehicle, angiotensinogen (AGT) siRNA, AGT siRNA + losartan, losartan, or losartan + captopril for 28 days. Treatment was started 5 weeks after 5/6th Nx. Data are mean and interquartile range of n=7-12. All data were log-transformed to perform one-way ANOVA, followed by post-hoc correction according to Bonferroni (*P<0.05, #P<0.01, &P<0.001, \$P<0.0001 vs. vehicle). Numbers in combination with the symbol < denote the lower limit of quantification.

Angiotensin metabolite or ratio	vehicle	AGT siRNA	AGT siRNA + losartan	losartan	losartan + captopril
Blood (pmol/L)					
Ang-(1-10) = Ang I	17 (4, 31)	4 (<3, 3)	6 (<3, 3)	295 (44, 522) &	572 (31, 1098) &
Ang-(1-8) = Ang II	19 (10, 27)	8 (5, 10) *	9 (4, 15)	145 (30, 189) #	32 (7, 61)
Ang-(1-7)	<8	<8	<8	9 (8, 8)	16 (8, 25) *
Ang-(2-8) = Ang III	<3	<3	<3	11 (<3, 14) #	3 (<3, 3)
Ang-(3-8) = Ang IV	<1	<1	<1	9 (<1, 14) #	2 (<1, 3)
Ang II/I ratio	2.31 (0.73, 2.77)	2.27 (1.43, 2.99)	2.48 (1.00, 2.80)	0.80 (0.52, 0.73)	0.22 (0.04, 0.49) \$
Kidney (fmol/g)					
Ang-(1-10) = Ang I	394 (88, 755)	37 (10, 59) #	<6 #	604 (437, 777)	399 (243, 576)
Ang-(1-8) = Ang II	345 (129, 602)	71 (23, 115) #	4 (3, 3) &	113 (60, 174) *	35 (14, 46) &
Ang-(1-7)	261 (58, 486)	25 (<19, 19) \$	<19\$	235 (173, 273)	164 (107, 251)
Ang-(2-8) = Ang III	14 (<6, 23)	6 (<6, 14) #	<6 #	<6 #	<6 #
Ang-(3-8) = Ang IV	11 (<10, 10)	<10	<10	<10	<10
Ang II/I ratio	1.19 (0.7, 1.42)	2.36 (1.02, 3.59) *	0.74 (0.50, 0.50)	0.23 (0.13, 0.25) &	0.10 (0.02, 0.17) &
Heart (fmol/g)					
Ang-(1-10) = Ang I	8 (6, 10)	<6	<6	39 (7, 73) *	46 (6, 47) *
Ang-(1-8) = Ang II	5 (<3, 7)	3 (<3, 3) *	<3*	4 (<3, 7)	3 (<3, 4) *
Ang-(1-7)	<19	<19	<19	28 (<19, 31)	30 (<19, 31)
Ang-(2-8) = Ang III	<6	<6	<6	<6	<6
Ang-(3-8) = Ang IV	<10	<10	<10	<10	<10
Ang II/I ratio	0.80 (0.44, 0.87)	0.52(0.50, 0.50)	0.50(0.50, 0.50)	0.26 (0.08, 0.44) #	0.24 (0.07, 0.50) #

Supplemental Table 2. Growth, food and water intake, and 24 hour-urine parameters of Sprague-Dawley rats subjected to 5/6th nephrectomy, and treated with either vehicle, angiotensinogen (AGT) siRNA, AGT siRNA + losartan, losartan, or losartan + captopril for 28 days. Treatment was started 5 weeks after 5/6th Nx (=baseline), and measurements were performed at baseline, after 2 weeks and after 4 weeks of treatment. Data (mean \pm SEM of n=7-12) were analyzed by paired t-test (baseline vs. 4 weeks) or one-way ANOVA followed by post-hoc correction according to Bonferroni.

parameter		vehicle	AGT siRNA	AGT siRNA + losartan	losartan	losartan + captopril
body weight (g)		379 \pm 11	378 \pm 8	388 \pm 18	390 \pm 14	411 \pm 9
Δ treatment		38 \pm 8	38 \pm 7	46 \pm 9	49 \pm 8	57 \pm 5
food intake (g/day)	baseline	21 \pm 1	21 \pm 1	21 \pm 1	22 \pm 1	23 \pm 1
	T=2 weeks	19 \pm 1	21 \pm 1	21 \pm 1	21 \pm 2	21 \pm 1
	T=4 weeks	17 \pm 2	22 \pm 4	20 \pm 1	21 \pm 2	21 \pm 1
water intake (mL/day)	baseline	52 \pm 3	50 \pm 3	50 \pm 4	51 \pm 5	52 \pm 2
	T=2 weeks	55 \pm 3	62 \pm 3	56 \pm 4	51 \pm 6	56 \pm 4
	T=4 weeks	56 \pm 7	48 \pm 6	59 \pm 6	54 \pm 6	60 \pm 4
urine (mL/day)	baseline	39 \pm 3	34 \pm 3	36 \pm 4	37 \pm 4	37 \pm 3
	T=2 weeks	44 \pm 4	41 \pm 3	38 \pm 4	37 \pm 4	40 \pm 5
	T=4 weeks	40 \pm 3	39 \pm 2	39 \pm 6	37 \pm 4	41 \pm 3

Supplemental Table 3. Emax (maximum effect) and pEC50 (the negative logarithm of the half-Emax concentration) for vascular response to acetylcholine (ACh) and endothelin-1 (ET-1) in mesenteric arteries of Sprague-Dawley rats subjected to 5/6th nephrectomy, and treated with either vehicle, angiotensinogen (AGT) siRNA, AGT siRNA + losartan, losartan, or losartan + captopril for 28 days. Treatment was started 5 weeks after 5/6th Nx. ACh responses were studied in the absence (control) or presence of the inhibitors L-NAME, TRAM34+apamin (T+A), or L-NAME+T+A. ET-1 responses were studied in the absence (control) or presence of the endothelin receptor blockers BQ123 and BQ788. Data (mean \pm SEM of n=5-11) were analyzed by one-way ANOVA followed by post-hoc correction according to Bonferroni. *P<0.05, #P<0.01, &P<0.001, \$P<0.0001 vs. no inhibitor.

pEC50	control	AGT siRNA	siRNA+ losartan	losartan	losartan+ captopril
ACh	8.0 \pm 0.3	8.0 \pm 0.2	7.9 \pm 0.3	8.5 \pm 0.5	8.2 \pm 0.3
ACh+ L-NAME	7.9 \pm 0.4	8.0 \pm 0.2	7.6 \pm 0.2	7.6 \pm 0.3	8.2 \pm 0.4
ACh+T+A	7.2 \pm 0.2	7.5 \pm 0.1	7.2 \pm 0.3	7.4 \pm 0.2	7.4 \pm 0.2
ACh+L-NAME +T+A	7.5 \pm 0.4	7.3 \pm 0.3	7.4 \pm 0.5	7.4 \pm 0.6	7.2 \pm 0.5
ET-1	8.2 \pm 0.1	8.3 \pm 0.1	8.3 \pm 0.1	8.1 \pm 0.2	8.2 \pm 0.1
ET-1+BQ123	7.0 \pm 0.1*	7.2 \pm 0.1 #	7.1 \pm 0.04 #	7.2 \pm 0.1*	7.0 \pm 0.03 &
ET-1+BQ788	8.3 \pm 0.5	8.3 \pm 0.3	8.4 \pm 0.4	8.3 \pm 0.3	8.2 \pm 0.1
Emax	control	AGT siRNA	siRNA +losartan	losartan	losartan+ captopril
ACh	82.6 \pm 5.1	90.9 \pm 2.7	78.9 \pm 8.6	82.3 \pm 9.2	84.2 \pm 3.4
ACh+ L-NAME	70.9 \pm 9.0	76.0 \pm 6.	65.1 \pm 7.9	58.1 \pm 11.6	66.9 \pm 7.2
ACh+T+A	63.8 \pm 11.7	84.8 \pm 3.7	68.0 \pm 10.3	79.0 \pm 7.9	77.0 \pm 6.2
ACh+L-NAME +T+A	29.0 \pm 6.9 &	43.6 \pm 7.0 &	36 \pm 7.8 #	45.7 \pm 11.7	30.2 \pm 5.4 &
ET-1	134.8 \pm 11.6	113.4 \pm 5.0	134.7 \pm 14.4	138.5 \pm 14.6	120.6 \pm 11.1
ET-1+BQ123	75.0 \pm 11.5*	105.6 \pm 11.1	110.1 \pm 9.2	117.7 \pm 20.9	94.4 \pm 8.3
ET-1+BQ788	129.7 \pm 18.4	107.1 \pm 9.6	141.8 \pm 19.3	131.1 \pm 7.1	114.1 \pm 12.4

Chapter 5

(Pro)renin Receptor Inhibition Reprograms Hepatic Metabolism and Attenuates Diet- induced Obesity and Liver Steatosis

Liwei Ren[#], Yuan Sun^{1#}, Hong Lu, Dien Ye, Lijuan Han,
Na Wang, Alan Daugherty, Furong Li, Miaomiao Wang,
Fengting Su, Wenjun Tao, Jie Sun, Noam Zelcer,
Adam E. Mullick, A.H. Jan Danser, Yizhou Jiang,
Xiongzong Ruan*, Xifeng Lu*

Circ Res. 2018;122:730-741

[#]Contributed equally

* corresponding author

Abstract

Rationale: An elevated level of plasma LDL (low-density lipoprotein) is an established risk factor for cardiovascular disease. Recently, we reported that the (pro)renin receptor ([P]RR) regulates LDL metabolism in vitro via the LDLR (LDL receptor) and SORT1 (sortilin-1), independently of the renin–angiotensin system.

Objectives: To investigate the physiological role of (P)RR in lipid metabolism in vivo.

Methods and Results: We used N-acetylgalactosamine modified anti-sense oligonucleotides to specifically inhibit hepatic (*P*)RR expression in C57BL/6 mice and studied the consequences this has on lipid metabolism. In line with our earlier report, hepatic (P)RR silencing increased plasma LDL-C (LDL cholesterol). Unexpectedly, this also resulted in markedly reduced plasma triglycerides in a SORT1-independent manner in C57BL/6 mice fed a normal- or high-fat diet. In LDLR-deficient mice, hepatic (P)RR inhibition reduced both plasma cholesterol and triglycerides, in a diet-independent manner. Mechanistically, we found that (P)RR inhibition decreased protein abundance of ACC (acetyl-CoA carboxylase) and PDH (pyruvate dehydrogenase). This alteration reprograms hepatic metabolism, leading to reduced lipid synthesis and increased fatty acid oxidation. As a result, hepatic (P)RR inhibition attenuated diet-induced obesity and hepatosteatosis.

Conclusions: Collectively, our study suggests that (P)RR plays a key role in energy homeostasis and regulation of plasma lipids by integrating hepatic glucose and lipid metabolism.

Keywords: dyslipidemia; hypercholesterolemia; hypertriglyceridemia; liver; renin–angiotensin system; vacuolar H⁺-ATPase

Introduction

Elevated plasma low-density lipoprotein (LDL) levels are a major risk factor for developing atherosclerosis and ensuing ischemic cardiovascular disease (CVD), a leading cause of world-wide death. LDL, which is derived by peripheral lipolysis of very low-density lipoprotein (VLDL), is primarily cleared from the circulation in the liver via the LDL receptor (LDLR) pathway.^{1, 2} Hence, plasma LDL levels are determined by the dynamic balance between hepatic VLDL secretion and LDL clearance.

VLDL particles are formed by lipidation of apo (apolipoprotein) B100, the core protein of VLDL, in the endoplasmic reticulum and Golgi apparatus.³ The assembly of VLDL particles depends on apo B100 production and cellular availability of triglycerides. Accordingly, genetic mutations in apo B100 are associated with altered VLDL secretion and plasma LDL levels.⁴⁻⁶ Overexpression of apo B100 results in increased VLDL secretion and plasma LDL levels in rabbits.⁷ Similarly, the activity of enzymes involved in de novo lipid biosynthesis also affects VLDL assembly and secretion.^{8,9} For example, impaired loading of triglycerides into nascent VLDL particles, caused by mutations in the MTP (microsomal triglyceride carrier protein), results in defective VLDL secretion.¹⁰

Disturbed LDL clearance can increase plasma LDL levels and risk for cardiovascular diseases. In line with this, loss-of-function LDLR mutations are associated with elevated plasma LDL levels and cardiovascular risk.¹¹⁻¹³ Recently, GWAS studies have identified single-nucleotide polymorphisms (SNPs) mapping to 1p13.3 that strongly associated with plasma LDL levels and coronary heart disease.¹⁴⁻¹⁹ Subsequent mechanistic studies revealed that sortilin-1 (SORT1), located within the 1p13.3 region, is a novel regulator of LDL metabolism.²⁰⁻²² Overexpression of SORT1 increases LDL clearance and decreases plasma LDL levels,^{16, 21, 22} while SORT1 deficiency reduces cellular LDL uptake in vitro and LDL clearance in vivo.^{22, 23} In addition, SORT1 also plays a role in VLDL secretion. Overexpressing SORT1 promotes ApoB degradation via an endolysosome-dependent route, and hence reduces VLDL secretion and plasma triglyceride levels.²² Controversially, mice deficient for SORT1 also display reduced VLDL secretion and triglyceride levels.^{20, 22} These opposing results highlight the complex, and not yet fully elucidated, role of SORT1 in lipoprotein metabolism.

The (pro)renin receptor ([P]RR) interacts with renin/prorenin (denoted as [pro]renin) at supra- physiological concentrations that are even several orders of magnitude higher than (patho)physiological concentrations, questioning the physiological relevance of the (P)RR-(pro)renin interaction.^{24, 25} Recently, the (P)RR was reported to play a role in Wnt/ β -catenin signaling pathway, vacuolar H⁺-ATPase (V-ATPase) integrity and T-cell development, independently of (pro)renin.²⁶⁻³⁰ Moreover, we have recently identified the (P)RR as a SORT1-interacting protein,³¹ and demonstrated that silencing (*P*)RR expression in hepatocytes in vitro reduces protein abundance of SORT1 and LDLR post-transcriptionally, and consequently cellular LDL uptake. To understand the role of the (P)RR in lipoprotein metabolism in vivo, we studied here the consequence of hepatic (P)RR silencing on lipoprotein metabolism. We report that hepatic loss of (P)RR in mice results in a SORT1- dependent increase in plasma LDL levels, but unexpectedly also in a reduction in plasma triglycerides that was SORT1-independent that resulted from altered metabolic reprogramming of hepatocytes. Our study thus highlights hepatic (P)RR as a crucial regulator of energy and lipid metabolism.

Methods:

The authors declare that all supporting data are available within the article [and its online supplementary files]. A detailed description of methods used in this study is available in the Online Supplemental Materials.

Results

Inhibiting hepatic (P)RR reduced both hepatic LDL clearance and VLDL secretion

We have previously reported that (P)RR inhibition attenuates cellular LDL uptake by reducing LDLR and SORT1 protein abundance in hepatocytes.³¹ To understand the role of hepatic (P)RR in lipoprotein metabolism in vivo, we used N-Acetylgalactosamine (GalNAc) modified antisense oligos (ASOs) to inhibit hepatic (P)RR expression. At a dose of 3.0 mg/kg/week, GalNAc (P)RR ASO [G- (P)RR] potently reduced

(*P*)RR expression in liver, but had no effects on its expression in other major organs, including heart, kidney, intestine, spleen, and different adipose tissues (Online Figure IA, IC- F). In line with our previous report, inhibiting the (P)RR specifically reduced hepatic LDLR and SORT1 protein levels without affecting their transcript levels (Online Figure I B). As a result of reduced hepatic LDLR and SORT1 protein abundance, (P)RR inhibition elevated plasma cholesterol levels in normal diet (ND) fed mice, primarily by increasing cholesterol content in IDL/LDL fractions (Figure 1 A&B). Since plasma LDL-c concentrations reflect the balance between hepatic LDL clearance and VLDL secretion, we then investigated the effects of (P)RR inhibition on LDL clearance and hepatic VLDL output. In line with decreased LDLR and SORT1, inhibiting hepatic (P)RR led to attenuated clearance of injected Dil-labeled human LDL (Figure 1C). Unexpectedly, (P)RR inhibition also significantly decreased plasma triglyceride concentrations (Figure 1D), a finding could be attributed to reduced hepatic VLDL secretion (Figure 1E).

We then asked if silencing (*P*)RR in hepatocytes could aggravate hypercholesterolemia in C57BL/6J mice fed a high-fat diet (HFD). Like in ND-fed mice, 1 week after (P)RR inhibition, plasma cholesterol levels were 3~4 fold higher than those measured in GalNAc control ASO (G-control) injected mice (Figure 2A). This elevation was primarily attributed to a marked increase in cholesterol content in the IDL/LDL fraction (Figure 2B). Notably, (P)RR inhibition also increased cholesterol contents in the VLDL fraction and reduced cholesterol contents in the HDL fraction. Unexpectedly, within two weeks, plasma cholesterol levels of G-(P)RR injected mice normalized and were similar to those in the saline or G-control injected mice (Figure 2 A&C, Online Figure IG). This contrasts with the sustained increase in plasma cholesterol levels in C57BL/6J mice fed with ND (Online Figure IH). Nevertheless, (P)RR inhibition in HFD-fed mice reduced hepatic LDL clearance and VLDL secretion (Figure 2 D&E). Plasma triglycerides and VLDL triglycerides were both lower in G-(P)RR injected mice as compared to saline or G-control injected mice (Figure 2 F&G), thus mimicking the pattern seen under ND feeding. Importantly, plasma lipoprotein lipase (LPL) activity was not affected by hepatic (P)RR inhibition (Figure 2H). This excludes the possibility that increased triglyceride hydrolysis underpins reduced levels of plasma triglycerides in (P)RR-silenced mice. Since SORT1 deficiency in vivo reduces VLDL secretions and plasma

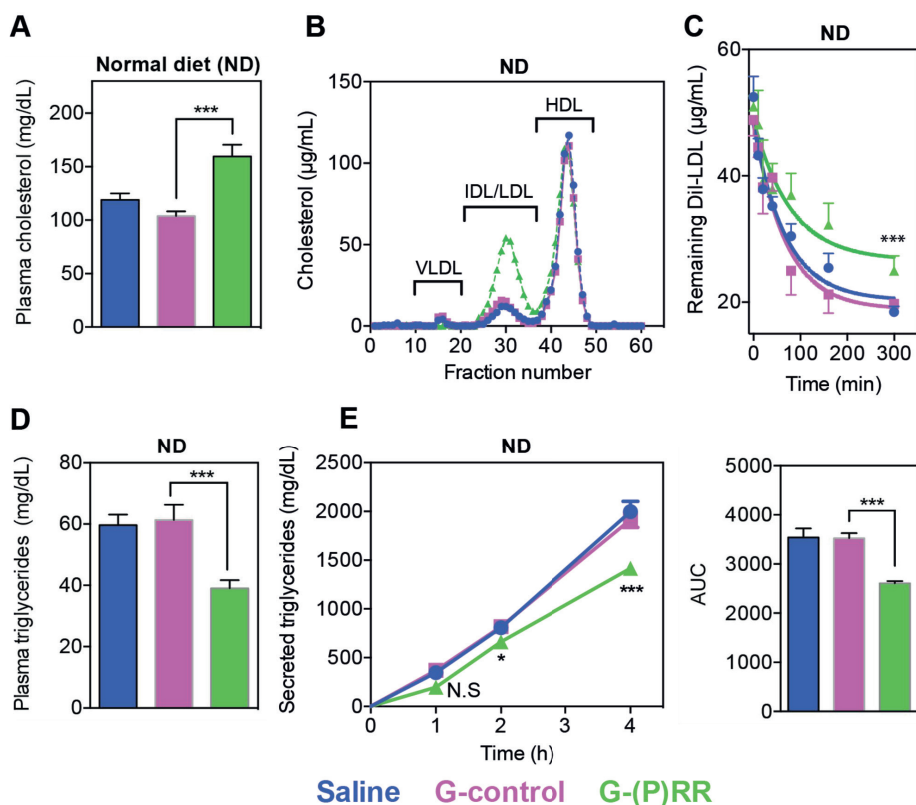


Figure 1. Inhibiting hepatic (P)RR induces hypercholesterolemia by reducing hepatic LDL clearance in normal diet (ND)-fed C57BL/6J mice. Eight-weeks-old male C57BL/6J mice were injected with either saline (blue), G-control (magenta) or G-(P)RR (green) intraperitoneally. Mice were sacrificed after 7 days and blood samples were collected for (A) determining circulating levels of cholesterol (N=12-18 per group). Each bar and error represent the mean \pm SEM; ***: $p < 0.001$, or (B) pooled plasma samples were loaded on FPLC for lipoprotein fractionation analysis, and cholesterol content in each fraction was determined. (C) 7 days after injection, mice (n=6 per group) were injected with 50 μ g Dil-labeled human LDL. Blood samples were drawn retro-orbitally at the indicated time points and the Dil-LDL was determined. Each point represents the mean \pm SEM and the area-under curve (AUC) was constructed for each group and used to compare the difference in LDL clearance. ***: $p < 0.001$. (D) Blood was collected as in (A) and used to determine plasma triglyceride levels. (N=12-18 per group); Each bar and error represent the mean \pm SEM ***: $p < 0.001$. (E) 7 days after injection, mice (n=6 per group) were fasted for 6 hours, and injected with Pluronic F127 to inhibit lipoprotein lipase. Blood samples were drawn retro-orbitally at the indicated time points and the concentration of triglycerides was determined. The mean VLDL secretion for saline-, G-control-, or G-(P)RR-injected mice is 474 ± 16 mg/dL*h, 460 ± 14 mg/dL*h, and 342 ± 10 mg/dL*h, respectively. The AUC was calculated for individual mice and used to compare the differences in the rate of VLDL secretion. ***: $p < 0.001$; G-control vs. G-(P)RR.

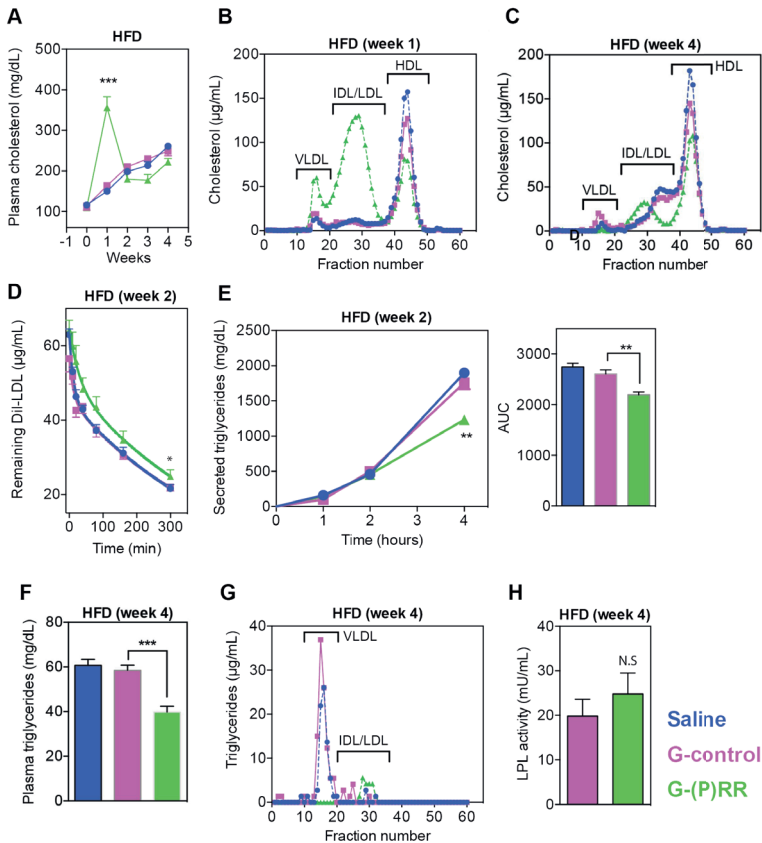


Figure 2. Inhibiting hepatic (P)RR does not result in hypercholesterolemia in HFD-fed C57BL/6J mice. Eight-weeks-old male C57BL/6J mice were injected with either saline (blue), G- control (magenta) or G-(P)RR (green), and fed a HFD for 4 weeks. (A) Plasma cholesterol concentrations were determined weekly and each point represents the mean \pm SEM. N=10 per group; ***: $p<0.001$; G-control vs. G-(P)RR. (B,C) Pooled plasma samples were collected after the (B) 1st week of diet, or (C) following 4 weeks of diet and the lipoprotein distribution was determined. The cholesterol content in each fraction was determined and is plotted. (D) Two weeks after start of HFD diet, mice ($n=6$ per group) were injected with 50 μ g DiI-labeled human LDL, and LDL clearance was assessed. Each point represents the mean \pm SEM and the AUC was constructed for each treatment and used to compare the differences in LDL clearance. *: $p<0.05$. (E) Two weeks after (P)RR inhibition, mice were fasted for 6 hours and VLDL secretion was assessed ($n=6$ per group) by injecting mice with Pluronic F127 to inhibit lipoprotein lipase. Blood samples were drawn retro-orbitally at the indicated time points and the concentration of triglycerides was determined and the AUC was calculated and used to compare the differences in the rate of VLDL secretion. **: $p<0.01$; G-control vs. G-(P)RR. (F,G) Plasma triglyceride levels were analyzed in samples collected following 4 weeks of HFD. Each bar represents the mean \pm SEM, N=10 per group. ***: $p<0.001$, or (G) pooled plasma samples were analyzed by FPLC. (H) Plasma lipoprotein lipase (LPL) activity was determined for mice were injected with G-control or G-(P)RR and fed HFD for 4 weeks. N=9/group

Chapter 5

triglycerides and (P)RR- silencing decreases SORT1,^{20, 22, 31} we wondered if the effect of (P)RR inhibition on hepatic lipid output is SORT1-dependent. To address this possibility, we studied plasma lipid levels in (P)RR - silenced mice in which we overexpressed human SORT1 (hSORT1). Exogenous hSORT1 protein was detected in liver, and hSORT1 partially rescued the (P)RR-inhibition-induced LDLR protein reduction (Online Figure II). Given that SORT1 itself is a clearance receptor for LDL,²⁰⁻²² it is not surprising that hSORT1 overexpression reversed the (P)RR-inhibition-induced increase in plasma cholesterol levels, primarily by decreasing the cholesterol content in the VLDL and IDL/LDL fractions (Figure 3 A&B). However, hSORT1 overexpression did not prevent the reduction in plasma triglycerides caused by (P)RR inhibition (Figure 3C), implying that (P)RR inhibition reduced plasma triglycerides in a SORT1-independent manner.

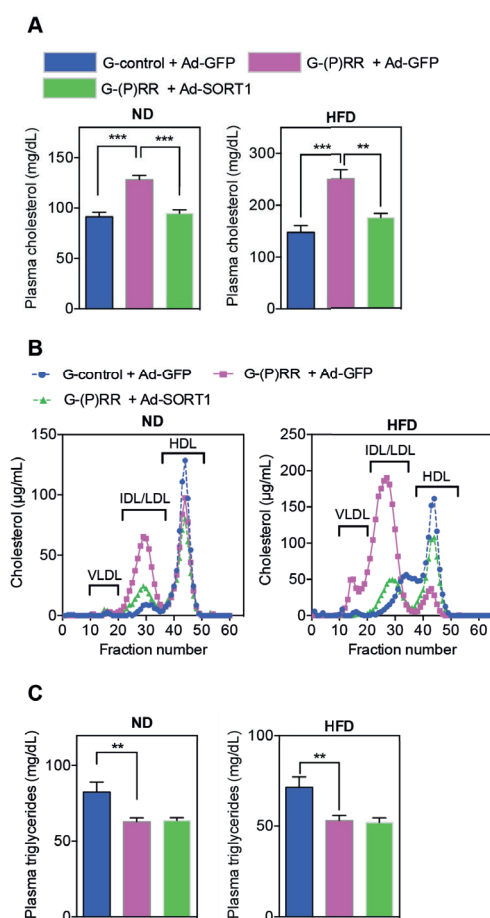


Figure 3. SORT1 overexpression prevents PRR-dependent hypercholesterolemia, but does not affect reduction in plasma triglycerides. Eight-week-old male C57BL/6J mice were injected with G-control or G-(P)RR intraperitoneally, and subsequently injected with either adenovirus carrying GFP (Ad-GFP) or adenovirus carrying human SORT1 (Ad-SORT1) via the tail-vein. Mice were fed with ND or HFD for 1 week and (A) plasma cholesterol levels were determined. Each bar represents the mean \pm SEM (N=6 per group). **: $p < 0.01$; ***: $p < 0.001$. Alternatively, (B) Lipoprotein composition in pooled plasma samples was analyzed by fractionation. (C) Plasma was collected as in (A) and analyzed for triglyceride content. Each bar and error represent the mean \pm SEM (N=6 per group). **: $p < 0.01$.

Hepatic (P)RR inhibition reduced plasma cholesterol levels in LDLR deficient mice

As (P)RR affects both hepatic LDL clearance and VLDL secretion, it is possible that (P)RR has a differential role in governing plasma cholesterol levels under distinct diet conditions. Under ND, LDL clearance may govern plasma cholesterol levels, while under HFD VLDL secretion may become more prominent in determining plasma cholesterol levels. To address this issue, we tested the effects of hepatic (P)RR inhibition on plasma cholesterol levels in mice with impaired LDL clearance by injecting adeno-associated virus (AAVs) expressing the gain-of-function PCSK9 D377Y mutant^{32, 33} and in LDLR^{-/-} mice. As expected, injecting C57BL/6J mice with the PCSK9 D377Y-encoding AAVs led to a marked increase in the circulating levels of LDL cholesterol (from 76.74 ± 1.72 mg/dL to 167.3 ± 2.27 mg/dL, $n=39$). We subsequently injected these mice with either saline, G-control, or G- (P)RR for 4 weeks, and fed either ND or HFD. We found that after this treatment period, (P)RR inhibition reduced plasma cholesterol levels in both ND and HFD fed mice, despite the lack of functional LDLR-mediated clearance (Figure 4 A-D). Similarly, inhibiting hepatic (P)RR in LDLR^{-/-} mice induced a sustained decrease in plasma cholesterol levels independent of diet (Online Figure IIIA&IIIB). These results confirm that LDL clearance is more dominant than VLDL secretion in determining circulating LDL levels in mice fed ND. Similar to the observation in wildtype C57BL/6J mice, plasma triglycerides and VLDL-associated triglycerides were reduced by (P)RR inhibition under ND or HFD feeding (Figure 4 E-H), in PCSK9-induced LDLR deficient mice. Moreover, in LDLR^{-/-} mice, hypertriglyceridemia was prevented by hepatic (P)RR inhibition (Online Figure IIIC&IIID). We reasoned that if (P)RR inhibition primarily affects lipid export pathways, we should observe lipid accumulation in liver, especially under HFD feeding. However, we found that hepatic lipid levels were also reduced by (P)RR inhibition (Figure 4 I-K, Online Figure IV), implying that the reduced plasma lipid levels are not the result of impaired lipid secretion.

Hepatic (P)RR inhibition attenuated diet-induced obesity and improved metabolic disorders

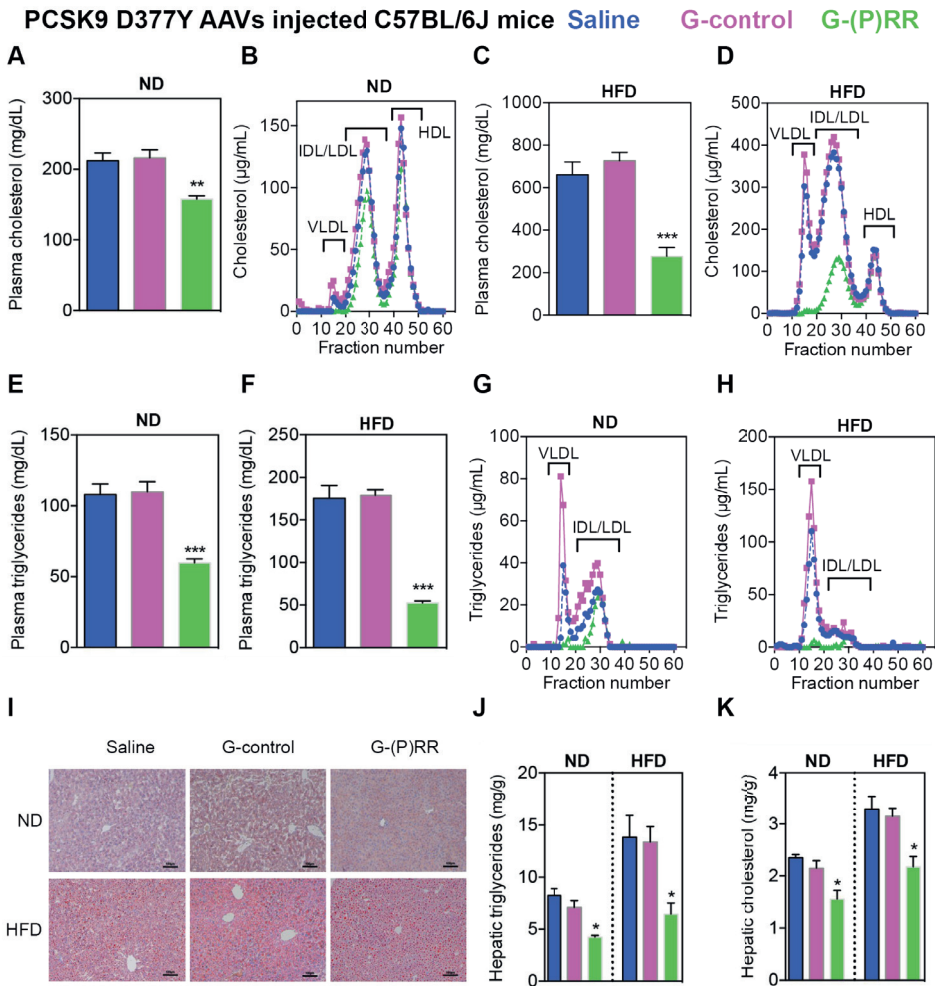


Figure 4. Hepatic (P)RR inhibition in the absence of LDLR reduces plasma lipid levels and hepatic lipid deposition. Eight-week-old male C57BL/6J mice were injected intraperitoneally with 10×10^{10} genomic copies of mouse PCSK9D377Y AAV, and fed with ND for 4 weeks. Subsequently, mice were injected with either saline (blue), G-control (magenta) or G-(P)RR (green) and fed with ND or HFD for an additional 4 weeks. (A-D) Plasma cholesterol levels and lipoprotein profiles at the end of study were determined for ND fed (A,B) and HFD fed (C,D) mice. (E-H) Plasma triglycerides and lipoprotein distribution were determined for ND fed (E,G) and HFD fed (F,H) mice. (N=6 per group). **: $p < 0.01$; ***: $p < 0.001$; G-control vs. G-(P)RR. (I) Representative images of Oil Red O stained liver samples from above-indicated mice fed with ND or HFD for 4 weeks. scale bar = 100μm. (J,K) Lipids were extracted from liver samples and analyzed for triglycerides and cholesterol levels. *: $p < 0.05$; G-control vs G-(P)RR.

(P)RR inhibition resulted in decreased hepatic VLDL secretion without concomitant hepatic lipid accumulation. This could point towards (P)RR regulating hepatic lipid biosynthesis, an important facet of fatty liver disease and obesity.³⁴ We therefore questioned whether hepatic (P)RR inhibition can ameliorate diet-induced fatty liver disease and obesity. To address this, we inhibited hepatic (P)RR expression in C57BL/6J mice fed a HFD for 14 weeks. In line with our hypothesis, loss of hepatic (P)RR attenuated diet-induced obesity in C57BL/6J mice (Figure 5A). Body composition analyses using Echo-MRI revealed that inhibiting hepatic (P)RR lowered fat weight of the mice, but did not affect the weight of lean mass (Figure 5B, Online Figure VA). Furthermore, the size of the livers and white adipose tissues (WATs) of G-(P)RR injected mice were smaller than control mice (Figure 5 C&D). Under HFD, lipid accumulates in liver and increases liver weight. Mean liver weight of saline or G-control injected mice was ~2 gram, which was nearly twice the mean liver weight (1.07 ± 0.02 gram, $n=12$, $p<0.001$) of ND fed C57BL/6J mice at same age (22 weeks old). Hepatic (P)RR inhibition attenuated HFD-induced liver weight gain and prevented abnormal lipid deposition in the liver (Figure 5 E&F). Liver/body weight ratios of G-(P)RR injected mice were also significantly lower than that of G-control injected mice, and resembled the ratio of ND fed C57BL/6J mice at the same age (Online Figure VB). Moreover, mice in which hepatic (P)RR was inhibited had smaller adipocytes in inguinal WATs (Online Figure VC), but normal brown adipose tissues weight (Figure 5D). In agreement with reduced adipose tissues, plasma leptin concentrations were also reduced by hepatic (P)RR inhibition (Online Figure VD). However, plasma adiponectin concentrations were unaltered by (P)RR inhibition despite the marked reduction in adipose tissue weight (Online Figure VE), likely due to increased expression of adiponectin in white adipose tissues (Online Figure VC&VE). This suggests that hepatic (P)RR inhibition can indirectly affect adipokine secretion by adipose tissues, thereby contributing to improved metabolic control.

Accompanied by less body weight gain, fasting blood glucose concentrations were reduced by (P)RR inhibition (Online Figure VF), which also improved glucose tolerance and lowered plasma insulin levels (Online Figure VG&H). Plasma AST, ALT and AST/ALT ratio indicates (P)RR inhibition did not cause liver damage (Online Figure VI). In addition, H&E staining also revealed improved liver morphology by (P)RR inhi-

Chapter 5

bition (Figure 5E). Cumulative food intake of the mice during the 14 weeks experimental period was also recorded. G-(P)RR injected mice consumed slightly less food than saline or G-control injected mice, but when corrected for their body weight, their food consumption was actually higher (Online Figure VJ), suggesting that the reduced body weight gain is not due to reduced food intake. In addition, we did not observe any difference in blood pressure or heart rate between saline, G-control or G-(P)RR injected mice (Online Figure VK&L), suggesting that the activity of the autonomic nervous system was not affected. We then monitored oxygen consumption and physical activity of the mice using

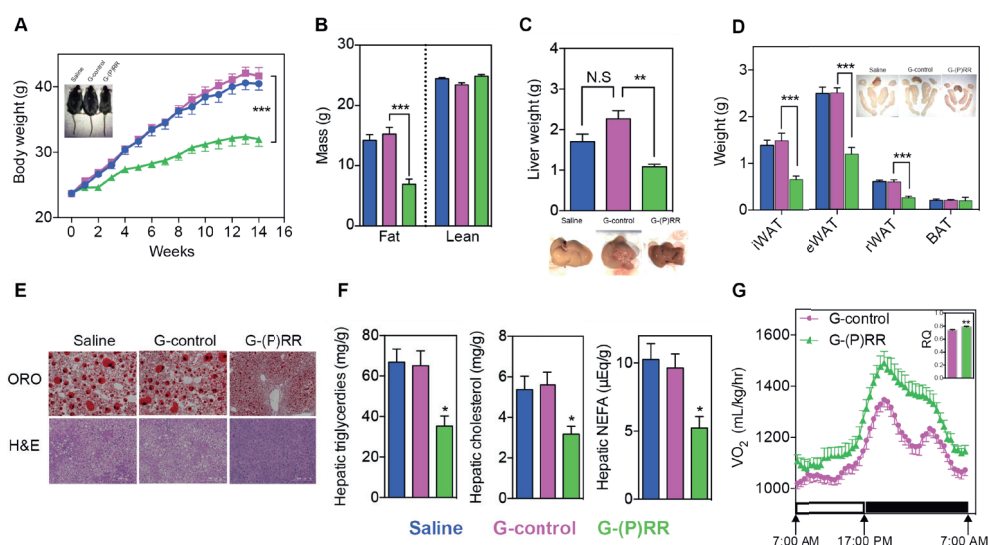


Figure 5. Hepatic (P)RR inhibition attenuates diet-induced obesity and metabolic deregulation. Eight-week-old mice were injected with saline (blue), G-control (magenta) or G-(P)RR (green) and fed a HFD for 14 weeks. (N=10 per group). (A) Body weight was monitored during the study period and each point and error represent the mean \pm SEM. ***: $p < 0.001$. Representative picture showing that G-(P)RR injected mice are leaner than control mice. (B) Fat and lean mass were measured by Echo-MRI. Each bar and error represent the mean \pm SEM. ***: $p < 0.001$. (C) Liver weight, and representative pictures showing G-(P)RR treated mice have less fatty liver. **: $p < 0.01$. (D) Weight and representative picture of different adipose tissue depots. Brown fat tissue of saline and G-control injected mice were surrounded with white fat which was removed to give a correct estimation of the weight of the brown fat. ***: $p < 0.001$. (E) Representative images of Oil Red O and H&E staining of the livers (scale bar = 200 μ m). (F) Hepatic lipids were extracted and measured. *: $p < 0.05$; G-control vs. G-(P)RR. (G) Oxygen consumption and 24h average respiratory quotient (RQ) of G-control injected and G-(P)RR injected mice was monitored with a metabolic monitoring system 4 days prior to sacrifice. N=8 per group.

(Pro)renin receptor regulates lipid metabolism

metabolic cages. Inhibiting hepatic (P)RR increased oxygen consumption and 24h respiratory quotient (RQ) of the mice, implying increased catabolism of energy sources (Figure 5G). Yet, physical activities of the mice were not different (Online Figure VM). Collectively, these results support the beneficial metabolic effects of (P)RR inhibition.

Inhibiting the (P)RR up-regulated genes involved in fatty acid oxidation

Currently recognized functions of the (P)RR are not linked with lipid biosynthesis and energy homeostasis. To understand how (P)RR may regulate these processes, we transcriptionally profiled mice following (P)RR inhibition. Male mice (8-weeks old) were injected either with saline or G- (P)RR for 5 days, and liver samples were collected and extracted for total RNA and RNAseq analysis. We identified that (P)RR inhibition led to up- and down-regulation of 199 genes and 202 genes, respectively (Online Table III). GO enrichment analysis revealed that metabolic pathways, including fatty acid (FA) degradation and elongation, were strongly affected by (P)RR inhibition (Online Figure VIA&B). Among the affected genes, several genes involved in FA β -oxidation, such as *Hadha*, *Acaa2*, *Acadvl*, and *Acadl*, were up-regulated by (P)RR inhibition, as confirmed by qPCR (Online Figure VII). As such, increased FA β -oxidation may contribute to increased oxygen consumption and reduced hepatic lipid content.

Inhibiting (P)RR reduced protein abundance of ACC and PDH

To complement the RNAseq analysis and to better understand the function(s) of the (P)RR, we next performed comparative quantitative proteomics to identify hepatic proteins which are affected by (P)RR inhibition. Through this unbiased approach, we identified 191 and 116 proteins that were down- and up-regulated, respectively, following (P)RR inhibition during feeding of either ND and HFD (Online Table IV). As reported previously, LDLR protein abundance was decreased by (P)RR inhibition (Online Table IV), validating the effectiveness of this approach to identify proteins with altered abundance. GO enrichment analyses revealed that proteins involved in lipid biosynthesis, lipid metabolism, and cholesterol metabolism were markedly affected by (P)RR inhibition (Online Figure VIC and VID). Among the identified proteins, pyruvate de-

Chapter 5

hydrogenase (PDH), acetyl-CoA carboxylase α (ACCA), and acetyl-CoA carboxylase β (ACCB) were markedly decreased. PDH is the enzyme responsible for converting pyruvate to acetyl-CoA, and is a central metabolic node.³⁵ ACC catalyzes the formation of malonyl-CoA, an essential substrate for FA synthesis and a potent inhibitor of FA oxidation.³⁶ ACC is crucial in determining lipid storage and overall energy metabolism.³⁷ Thus, reduced PDH and ACC may contribute to increased FA oxidation and decreased lipid synthesis. To confirm this, we examined ACC α/β and PDH protein abundance in the liver of saline, G-control or G-(P)RR injected C57BL/6J mice fed with HFD for 14 weeks. Corroborating the proteomic-based approach, hepatic ACC α/β , PDHA, and PDHB were reduced by ~40-60% after hepatic (P)RR inhibition (Figure 6A), whereas the transcript abundance of ACC α/β , PDHA, and PDHB remained unaltered (Online Figure VII). Inhibiting the (P)RR in human hepatoma HepG2 cells with siRNAs also reduced protein abundances of ACC α/β , PDHA, and PDHB (Online Figure VIIIA), suggesting that this outcome is conserved in both mouse and humans. The (P)RR knock-down induced reduction in ACC α/β protein abundance was partially reversed by the lysosome inhibitor bafilomycin A1 (BafA1), but was not affected by the autophagy inhibitor 3-methyladenine (3-MA) or the proteasome inhibitor MG-132 (Online Figure VIIIB), suggesting accelerated lysosome-dependent degradation of ACC α/β by (P)RR inhibition. In contrast, BafA1, 3-MA and MG-132 were unable to rescue (P)RR knock-down induced reduction in PDHA and PDHB, implying that a different mechanism underlies the control of these proteins by (P)RR.

(P)RR inhibition reduced cellular acetyl-CoA abundance and FA synthesis in hepatocytes

Collectively, our results suggest that by reducing protein abundance of PDH, (P)RR inhibition reduces pyruvate to acetyl-CoA conversion, and therefore reduces cellular acetyl-CoA production from glucose. Lower cellular acetyl-CoA levels will limit cellular FA and cholesterol synthesis. This biosynthetic block will be compounded by reduced ACC abundance, which will further limit FA synthesis. To test this hypothesis, we first measured relevant hepatic metabolites in mice injected with saline, G-control, or G-(P)RR and fed with HFD for 14 weeks. As expected, G-(P)RR injected mice displayed hepatic pyruvate accumulation (Figure 6B), increased plasma pyruvate and lactate concen-

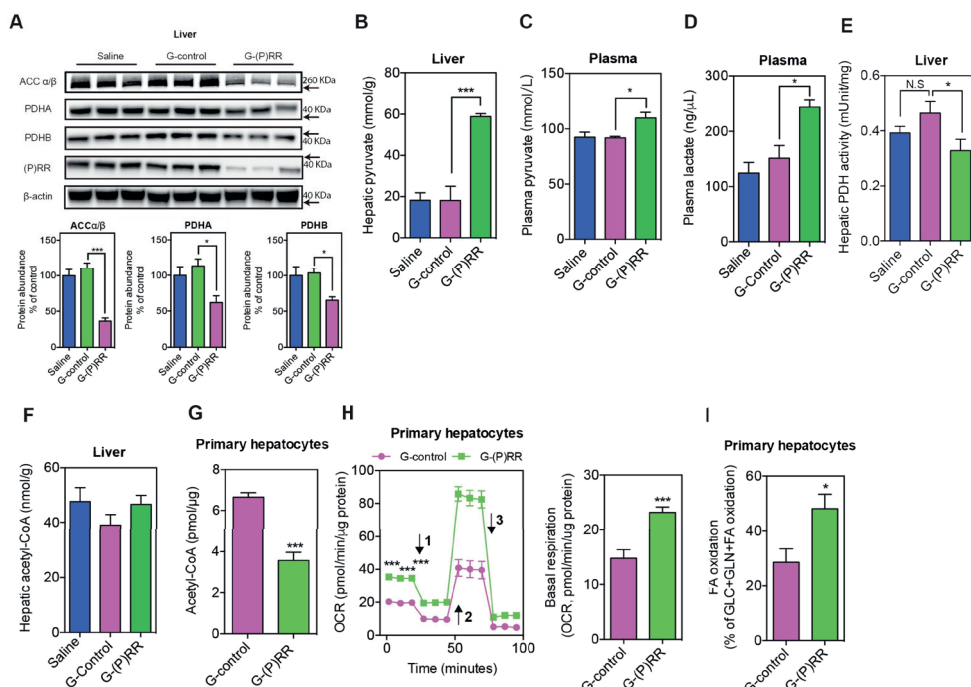


Figure 6. Inhibiting the (P)RR reduces PDH and ACC protein abundance and activity. (A) Representative blot of liver samples from mice injected with saline, G-control, or G-(P)RR, and fed a HFD for 14 weeks. The protein abundance of PDHA, PDHB, and ACCα/β was quantified and normalized to the level of β-actin in the same lysate. (N=6 per group); *: p<0.05; ***: p<0.001. (B) C57BL/6J mice were treated with ASOs and fed with HFD for 14 weeks. Hepatic pyruvate concentrations (B), plasma pyruvate concentrations (C), plasma lactate concentrations (D), hepatic PDH activity (E), and acetyl-CoA concentrations (F) were determined. (G) Mouse primary hepatocytes were treated with G-control or G-(P)RR for 36 hours, and cellular Acetyl-CoA concentrations were determined. Three independent experiments in triplicates were performed. ***: p<0.001. Oxygen consumption rate (OCR) (H) and fuel dependency (I) were measured in mouse primary hepatocytes treated with G-control or G-(P)RR for 36 hours. Arrow 1-3 indicates addition of oligomycin, FCCP and the mixture of rotenone and antimycin, respectively. N=6 per group. *: p<0.05; ***: p<0.001.

trations (Figure 6 C&D), and decreased hepatic PDH activity (Figure 6E). Nevertheless, despite these changes, hepatic acetyl-CoA concentrations were unaltered by (P)RR inhibition (Figure 6F). Yet importantly, cellular acetyl-CoA levels in isolated mouse primary hepatocytes in which (P)RR was inhibited using G-(P)RR ASO, were reduced (Figure 6G). Similarly, acetyl-CoA levels were decreased by (P)RR inhibition in HepG2 cells, combined with a decrease in cellular PDH activity, increased cellular pyruvate concentrations and medium lactate concentrations, and reduced cellular lipid levels (Online Figure VIIC through

Chapter 5

VIII G). These data support our hypothesis, and simultaneously suggest that *in vivo*, alternative sources, especially fatty acids supply, are available to overcome reduced pyruvate to acetyl-CoA conversion. This may also explain why acetyl-CoA levels were not reduced in the liver, as they were in HepG2 cells and primary hepatocytes. It is plausible that increased FA oxidation provides additional acetyl-CoA to compensate the increased energetic demand, which could also explain the increased oxygen consumption observed in G-(P)RR injected mice. Therefore, we examined if (P)RR inhibition affects the oxygen consumption rate (OCR) in mouse primary hepatocytes and HepG2 cells. As expected, inhib-

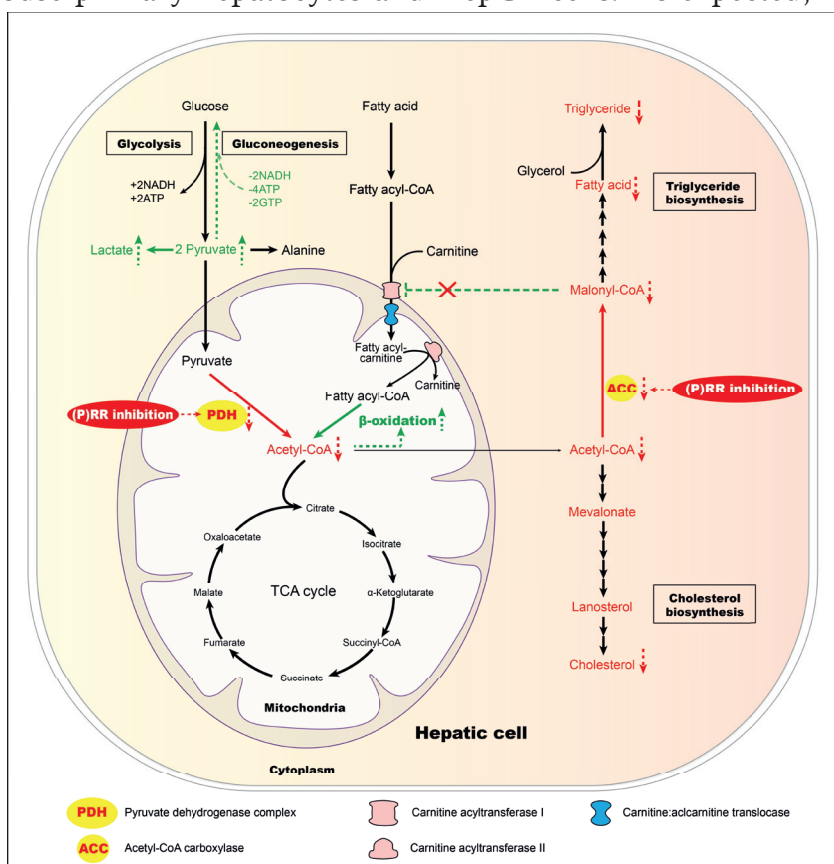


Figure 7. Model for reprogrammed hepatic metabolism by (P)RR inhibition. Inhibiting hepatic (P)RR reduces PDH activity, impairing pyruvate metabolism and reducing acetyl-CoA supply from pyruvate, which limits FA biosynthesis. (P)RR inhibition further limits FA biosynthesis by reducing protein abundance of ACC, the crucial enzyme in FA biosynthesis. Its further signals to increase FA oxidation via reduced malonyl-CoA, an inhibitor of FA oxidation that blocks the transportation of long-chain fatty acyl-carnitine by carnitine acyltransferase I (CAT1).

iting the (P)RR significantly increased basal OCR by ~50% in mouse primary hepatocytes (Figure 6G) and ~30% in HepG2 cells (Online Figure VIIIH) and, implying increased energy expenditure and utilization of high-oxygen- consuming fuels such as FA. To fully understand the mechanism, we further examined cellular fuel dependency on long chain FA (LCFA) in mouse primary hepatocytes and HepG2 cells. In the presence of 50 $\mu\text{mol/L}$ oleic acid, LCFA accounted for ~20-30% oxidized fuels (glucose, glutamine and LCFA together) in control cells, while it accounted for more than 40% oxidized fuels in primary mouse hepatocytes and HepG2 cells with (P)RR inhibited (Figure 6H, Online Figure VIII I). These data suggest that reduced acetyl-CoA supply from pyruvate is compensated by increased FA oxidation, as a mechanism to sustain cellular energy needs.

Discussion

We recently reported that the (P)RR is a novel modulator of LDL metabolism *in vitro*.³¹ In the current study, we demonstrate that also *in vivo*, inhibiting the (P)RR in hepatocytes leads to defective LDL clearance as a result of reduced SORT1 and LDLR protein abundance. SORT1 is a recently identified hepatic clearance receptor for LDL, which also regulates VLDL secretion and plasma triglycerides.^{16, 20-22, 38} SORT1 deficiency reduces VLDL secretion and plasma triglycerides,²⁰ and in line with this, we found that (P)RR inhibition reduced VLDL secretion and plasma triglycerides, likely as a consequence of reduced SORT1. However, hepatic overexpression of hSORT1 in mice with (P)RR silencing was unable to prevent the reduction in plasma triglycerides, despite completely preventing the increase in plasma LDL-c. This implies that the (P)RR regulates plasma triglycerides via a SORT1-independent manner. Furthermore, plasma LPL activity was not affected by (P)RR inhibition, excluding the possibility that increased triglyceride hydrolysis accounts for the reduced plasma triglycerides. In fact, hepatic lipid concentrations, including triglycerides and cholesterol, were both markedly reduced by (P)RR inhibition, indicating that lipid synthesis is diminished. Indeed, we found that the protein abundance of ACC, the crucial enzyme catalyzing the first step in fatty acid synthesis, was markedly reduced by (P)RR inhibition. As a consequence, limited amounts of lipid being available for ApoB lipidation likely caused the reduction in plasma triglycerides. This may also explain why

Chapter 5

(P)RR inhibition even reduced plasma cholesterol levels in LDLR deficient mice, in whom SORT1-dependent LDL clearance is impaired.

Our results raise the question of how the (P)RR regulates cellular lipid levels. Intriguingly, vacuolar H⁺-ATPase (V-ATPase) has recently been identified as a component of the mechanistic target of rapamycin complex 1 (mTORC1) pathway.³⁹ Indeed, acidification of lysosomes by V-ATPase is crucial for mTOR activation and function.⁴⁰ Increased mTORC1 activity is observed in genetic, and HFD-induced obesity, and has been implicated in the regulation of lipogenesis and VLDL secretion.⁴¹⁻⁴³ Knocking down the (P)RR reduces the protein levels of several subunits of the V-ATPase complex.^{28-30, 44} Consequently, (P)RR inhibition may prevent mTORC1 activation. Nevertheless, this seems unlikely as a recent report found that mTORC1 signaling was unaffected by (P)RR.⁴⁵

An alternative explanation for the effect of (P)RR on hepatic lipid metabolism may be related to the renin-angiotensin system, which has been linked with obesity and lipid metabolism.⁴⁶ However, this too seems unlikely, as the affinity of (P)RR to (pro)renin is very low, and in fact their interaction requires supraphysiological concentrations of (pro)renin. Rather, by using a combined unbiased transcriptome and proteomic approach, we now identified PDH and ACC as downstream effectors of (P)RR inhibition. (P)RR inhibition has previously been reported to reduce PDHB protein levels via a tyrosine-phosphorylation dependent manner in mouse retina and human retinal pigment epithelium cells.⁴⁷ We found that both PDHA and PDHB were reduced by (P)RR inhibition. PDH is a ubiquitously expressed enzyme complex that catalyzes the conversion of pyruvate to acetyl-CoA,^{48, 49} acting as a central node that links lipid metabolism, glucose metabolism and the tricarboxylic acid (TCA) cycle. We thus speculated that by reducing PDH protein abundance and activity, (P)RR inhibition would reduce acetyl-CoA production from glucose, and consequently diminish FA synthesis and increase FA oxidation (Figure 7).⁵⁰ Indeed, this is what we observe in the livers of (P)RR- silenced mice. Additionally, (P)RR inhibition also reduced ACC protein abundance. ACC plays an essential role in regulating FA synthesis and degradation.³⁷ Genetic deletion, or inhibition, of ACC reduces body-weight gain and fat mass, suppresses triglycerides synthesis, and increases FA oxidation and energy expenditure,^{51, 52} which resembles the phenotype of hepatic (P)RR inhibition.

Moreover, PPAR γ expression was reduced by (P)RR inhibition by ~50% (Figure VII), and this may also have contributed to the reduced hepatic lipogenesis, as hepatic PPAR γ plays important roles in HFD-induced upregulation of lipogenic genes and de novo lipogenesis.⁵³⁻⁵⁵ Recent studies have reported that genetically deleting adipose (P)RR in mice resulted in resistance to diet-induced obesity⁵⁶ and accelerated oxygen consumption,⁵⁷ yet causing severe hepatosteatosis.⁵⁶ Unaltered (P)RR expression in both white adipose tissues and brown adipose tissues excluded the possibility that adipose (P)RR deficiency also contributed to the observed phenotype in our study. However, it raises the question whether inhibiting the (P)RR in both adipose tissue and liver would provide additional beneficial effects in treating metabolic disorders.

Post-transcriptional regulation of ACC and PDH is not well understood, and thus novel studies are required to fully understand their protein degradational regulation, and the role of the (P)RR in this process. TRB3 has been reported to control ACC degradation under fasting conditions by coupling ACC to the E3 ligase COP1.⁵⁸ Interestingly, (P)RR inhibitions upregulated the expression of several E3 ligases, including HECTD1 (Online Table III), and both ACC α and ACC β have been reported to interact with HECTD1.⁵⁹ It is therefore conceivable that (P)RR inhibition accelerates ACC degradation via lysosomes by upregulating HECTD1. Simultaneously, the (P)RR-inhibition-induced reduction in PDH abundance is more difficult to understand. Inhibiting either autophagy, the lysosome or the proteasome did not rescue this reduction, nor did was inhibiting mitophagy, a special form of autophagy involved in degradation of mitochondrial proteins (data not shown). This may suggest that (P)RR inhibition regulates PDH abundance via an as yet unsolved mechanism, as seems to be the case with SORT1 as well.³¹

In conclusion, we report that hepatic (P)RR is a crucial regulator of lipid metabolism. Inhibiting hepatic (P)RR reduced ACC and PDH protein levels, and consequently increases FA oxidation and reduces lipid synthesis, thus attenuating diet-induced obesity and liver steatosis, as well as improving glycemic controls in C57BL/6J mice. Taken together, our study highlights the potential of inhibiting hepatic (P)RR as a therapeutic treatment for metabolic disorders such as fatty liver diseases, and

familial hypercholesterolemia.

Sources of Funding

X. Lu is supported by National Natural Science Foundation of China (grant no. 81500667), Shenzhen Municipal Science and Technology Innovation Council (grant no. JCYJ20160307160819191), Shenzhen Peacock Plan (start-up fund). Y. Jiang is supported by National Natural Science Foundation of China (grant no. 81500354). X. Ruan is supported by Shenzhen Peacock Plan (grant no. KQTD20140630100746562), and Shenzhen Municipal Science and Technology Innovation Council (grant no. JCYJ20140509172719310, CXZZ20150601140615135). N. Zelcer is supported by a European Research Council Consolidator grant (617376) and is an Established Investigator of the Dutch Heart Foundation (2013T111). A.H. Jan Danser is supported by the Top Institute Pharma (T2- 301).

Disclosures

Adam E. Mullick is an employee and shareholder of Ionis Pharmaceuticals.

Novelty and Significance

What Is Known?

- We recently demonstrated that the (pro)renin receptor [(P)RR] regulates low-density lipoprotein (LDL) metabolism in vitro, independent of the renin-angiotensin system.
- Regulation of cellular LDL uptake by the (P)RR is dependent on SORT1 and the LDLR.

What New Information Does This Article Contribute?

- Inhibiting hepatic (P)RR lowers plasma triglyceride and cholesterol levels in LDL receptor deficient mice.
- Hepatic (P)RR inhibition prevents diet-induced obesity, liver steatosis, and improves glycemic control.

- Hepatic (P)RR controls the protein abundance of pyruvate dehydrogenase (PDH) and acetyl-CoA carboxylase (ACC), thereby promoting fatty acid oxidation and reducing lipid synthesis.

The renin-angiotensin system independent functions of the (P)RR are not yet completely understood. Previously, we observed that hepatic (P)RR regulates LDL metabolism in vitro by controlling protein abundance of the LDL receptor and sortilin-1. In this study, we evaluated the role of (P)RR in vivo and found that inhibiting hepatic (P)RR regulates LDL metabolism, but that unexpectedly this also decreases plasma triglycerides. These actions are, at least in part, a result of decreased lipid synthesis and increases fatty acid oxidation in the liver as a result of decreased protein abundance of PDH and ACC. Thus, our study identifies the (P)RR as a crucial regulator of hepatic lipid metabolism, and suggests hepatic (P)RR inhibition as a potential strategy to treat dyslipidemia and fatty liver diseases.

References

1. Brown MS, Goldstein JL. A receptor-mediated pathway for cholesterol homeostasis. *Science*. 1986;232:34-47
2. Spady DK. Hepatic clearance of plasma low density lipoproteins. *Semin Liver Dis*. 1992;12:373-385
3. Olofsson SO, Stillemark-Billton P, Asp L. Intracellular assembly of vldl: Two major steps in separate cell compartments. *Trends Cardiovasc Med*. 2000;10:338-345
4. Hooper AJ, van Bockxmeer FM, Burnett JR. Monogenic hypocholesterolaemic lipid disorders and apolipoprotein b metabolism. *Crit Rev Clin Lab Sci*. 2005;42:515-545
5. Innerarity TL, Mahley RW, Weisgraber KH, Bersot TP, Krauss RM, Vega GL, Grundy SM, Friedl W, Davignon J, McCarthy BJ. Familial defective apolipoprotein b-100: A mutation of apolipoprotein b that causes hypercholesterolemia. *J Lipid Res*. 1990;31:1337-1349
6. Young SG, Hubl ST, Smith RS, Snyder SM, Terdiman JF. Familial hypobetalipoproteinemia caused by a mutation in the apolipoprotein b gene that results in a truncated species of apolipoprotein b (b-31). A unique mutation that helps to define the portion of the apolipoprotein b molecule required for the formation of buoyant, triglyceride-rich lipoproteins. *J Clin Invest*. 1990;85:933-942
7. Fan J, McCormick SP, Krauss RM, Taylor S, Quan R, Taylor JM, Young SG. Overexpression of human apolipoprotein b-100 in transgenic rabbits results in increased levels of ldl and decreased levels of hdl. *Arterioscler Thromb Vasc Biol*. 1995;15:1889-1899
8. Bou Khalil M, Sundaram M, Zhang HY, Links PH, Raven JF, Manmontri B, Sariahmetoglu M, Tran K, Reue K, Brindley DN, Yao Z. The level and compartmentalization of phosphatidate phosphatase-1 (lipin-1) control the assembly and

Chapter 5

- secretion of hepatic vldl. *J Lipid Res.* 2009;50:47-58
9. Yamazaki T, Sasaki E, Kakinuma C, Yano T, Miura S, Ezaki O. Increased very low density lipoprotein secretion and gonadal fat mass in mice overexpressing liver dgat1. *J Biol Chem.* 2005;280:21506-21514
 10. Sharp D, Blinderman L, Combs KA, Kienzle B, Ricci B, Wager-Smith K, Gil CM, Turck CW, Bouma ME, Rader DJ, et al. Cloning and gene defects in microsomal triglyceride transfer protein associated with abetalipoproteinaemia. *Nature.* 1993;365:65-69
 11. Hobbs HH, Brown MS, Goldstein JL. Molecular genetics of the ldl receptor gene in familial hypercholesterolemia. *Hum Mutat.* 1992;1:445-466
 12. Khachadurian AK, Uthman SM. Experiences with the homozygous cases of familial hypercholesterolemia. A report of 52 patients. *Nutr Metab.* 1973;15:132-140
 13. Soutar AK, Naoumova RP. Mechanisms of disease: Genetic causes of familial hypercholesterolemia. *Nat Clin Pract Cardiovasc Med.* 2007;4:214-225
 14. Kathiresan S, Willer CJ, Peloso GM, et al. Common variants at 30 loci contribute to polygenic dyslipidemia. *Nat Genet.* 2009;41:56-65
 15. Kathiresan S, Melander O, Guiducci C, et al. Six new loci associated with blood low-density lipoprotein cholesterol, high-density lipoprotein cholesterol or triglycerides in humans. *Nat Genet.* 2008;40:189-197
 16. Linsel-Nitschke P, Heeren J, Aherrahrou Z, et al. Genetic variation at chromosome 1p13.3 affects sortilin mrna expression, cellular ldl-uptake and serum ldl levels which translates to the risk of coronary artery disease. *Atherosclerosis.* 2010;208:183-189
 17. Muendlein A, Geller-Rhomberg S, Saely CH, Winder T, Sonderegger G, Rein P, Beer S, Vonbank A, Drexel H. Significant impact of chromosomal locus 1p13.3 on serum ldl cholesterol and on angiographically characterized coronary atherosclerosis. *Atherosclerosis.* 2009;206:494-499
 18. Sandhu MS, Waterworth DM, Debenham SL, et al. Ldl-cholesterol concentrations: A genome-wide association study. *Lancet.* 2008;371:483-491
 19. Willer CJ, Sanna S, Jackson AU, et al. Newly identified loci that influence lipid concentrations and risk of coronary artery disease. *Nat Genet.* 2008;40:161-169
 20. Kjolby M, Andersen OM, Breiderhoff T, Fjorback AW, Pedersen KM, Madsen P, Jansen P, Heeren J, Willnow TE, Nykjaer A. Sort1, encoded by the cardiovascular risk locus 1p13.3, is a regulator of hepatic lipoprotein export. *Cell Metab.* 2010;12:213-223
 21. Musunuru K, Strong A, Frank-Kamenetsky M, et al. From noncoding variant to phenotype via sort1 at the 1p13 cholesterol locus. *Nature.* 2010;466:714-719
 22. Strong A, Ding Q, Edmondson AC, et al. Hepatic sortilin regulates both apolipoprotein b secretion and ldl catabolism. *J Clin Invest.* 2012;122:2807-2816
 23. Tveten K, Strom TB, Cameron J, Berge KE, Leren TP. Mutations in the sort1 gene are unlikely to cause autosomal dominant hypercholesterolemia. *Atherosclerosis.* 2012;225:370- 375
 24. Batenburg WW, Lu X, Leijten F, Maschke U, Muller DN, Danser AH. Renin- and prorenin- induced effects in rat vascular smooth muscle cells overexpressing the human (pro)renin receptor: Does (pro)renin-(pro)renin receptor interaction actually occur? *Hypertension.* 2011;58:1111-1119

25. Batenburg WW, Danser AH. (pro)renin and its receptors: Pathophysiological implications. *Clin Sci (Lond)*. 2012;123:121-133
26. Cruciat CM, Ohkawara B, Acebron SP, Karaulanov E, Reinhard C, Ingelfinger D, Boutros M, Niehrs C. Requirement of prorenin receptor and vacuolar h⁺-atpase-mediated acidification for wnt signaling. *Science*. 2010;327:459-463
27. Geisberger S, Maschke U, Gebhardt M, Kleinewietfeld M, Manzel A, Linker RA, Chidgey A, Dechend R, Nguyen G, Daumke O, Muller DN, Wright MD, Binger KJ. New role for the (pro)renin receptor in t-cell development. *Blood*. 2015;126:504-507
28. Kinouchi K, Ichihara A, Sano M, Sun-Wada GH, Wada Y, Kurauchi-Mito A, Bokuda K, Narita T, Oshima Y, Sakoda M, Tamai Y, Sato H, Fukuda K, Itoh H. The (pro)renin receptor/atp6ap2 is essential for vacuolar h⁺-atpase assembly in murine cardiomyocytes. *Circ Res*. 2010;107:30-34
29. Oshima Y, Kinouchi K, Ichihara A, et al. Prorenin receptor is essential for normal podocyte structure and function. *J Am Soc Nephrol*. 2011;22:2203-2212
30. Riediger F, Quack I, Qadri F, et al. Prorenin receptor is essential for podocyte autophagy and survival. *J Am Soc Nephrol*. 2011;22:2193-2202
31. Lu X, Meima ME, Nelson JK, Sorrentino V, Loregger A, Scheij S, Dekkers DH, Mulder MT, Demmers JA, G MD-T, Zelcer N, Danser AH. Identification of the (pro)renin receptor as a novel regulator of low-density lipoprotein metabolism. *Circ Res*. 2016;118:222-229
32. Lu H, Howatt DA, Balakrishnan A, Graham MJ, Mullick AE, Daugherty A. Hypercholesterolemia induced by a pcsk9 gain-of-function mutation augments angiotensin ii- induced abdominal aortic aneurysms in c57bl/6 mice-brief report. *Arterioscler Thromb Vasc Biol*. 2016;36:1753-1757
33. Goettsch C, Hutcheson JD, Hagita S, Rogers MA, Creager MD, Pham T, Choi J, Mlynarchik AK, Pieper B, Kjolby M, Aikawa M, Aikawa E. A single injection of gain-of-function mutant pcsk9 adeno-associated virus vector induces cardiovascular calcification in mice with no genetic modification. *Atherosclerosis*. 2016;251:109-118
34. Postic C, Girard J. Contribution of de novo fatty acid synthesis to hepatic steatosis and insulin resistance: Lessons from genetically engineered mice. *J Clin Invest*. 2008;118:829-838
35. Sugden MC, Holness MJ. Recent advances in mechanisms regulating glucose oxidation at the level of the pyruvate dehydrogenase complex by pdks. *Am J Physiol Endocrinol Metab*. 2003;284:E855-862
36. Foster DW. Malonyl-coa: The regulator of fatty acid synthesis and oxidation. *J Clin Invest*. 2012;122:1958-1959
37. Tong L. Acetyl-coenzyme a carboxylase: Crucial metabolic enzyme and attractive target for drug discovery. *Cell Mol Life Sci*. 2005;62:1784-1803
38. Teslovich TM, Musunuru K, Smith AV, et al. Biological, clinical and population relevance of 95 loci for blood lipids. *Nature*. 2010;466:707-713
39. Zoncu R, Bar-Peled L, Efeyan A, Wang S, Sancak Y, Sabatini DM. Mtorc1 senses lysosomal amino acids through an inside-out mechanism that requires the vacuolar h⁽⁺⁾-atpase. *Science*. 2011;334:678-683
40. Hu Y, Carraro-Lacroix LR, Wang A, Owen C, Bajenova E, Corey PN, Brumell JH, Voronov I. Lysosomal ph plays a key role in regulation of mtor activity in os-

Chapter 5

- teoclasts. *J Cell Biochem.* 2016;117:413-425
41. Li S, Brown MS, Goldstein JL. Bifurcation of insulin signaling pathway in rat liver: Mtorc1 required for stimulation of lipogenesis, but not inhibition of gluconeogenesis. *Proc Natl Acad Sci U S A.* 2010;107:3441-3446
 42. Peterson TR, Sengupta SS, Harris TE, Carmack AE, Kang SA, Balderas E, Guertin DA, Madden KL, Carpenter AE, Finck BN, Sabatini DM. Mtor complex 1 regulates lipin 1 localization to control the srebp pathway. *Cell.* 2011;146:408-420
 43. Ai D, Baez JM, Jiang H, et al. Activation of er stress and mtorc1 suppresses hepatic sortilin-1 levels in obese mice. *J Clin Invest.* 2012;122:1677-1687
 44. Lu X, Garrelts IM, Wagner CA, Danser AH, Meima ME. (pro)renin receptor is required for prorenin-dependent and -independent regulation of vacuolar h(+)-atpase activity in mdck.C11 collecting duct cells. *Am J Physiol Renal Physiol.* 2013;305:F417-425
 45. Kissing S, Rudnik S, Damme M, Lullmann-Rauch R, Ichihara A, Kornak U, Eskelinen EL, Jabs S, Heeren J, De Brabander JK, Haas A, Saftig P. Disruption of the vacuolar-type h+- atpase complex in liver causes mtorc1-independent accumulation of autophagic vacuoles and lysosomes. *Autophagy.* 2017;13:670-685
 46. Engeli S, Negrel R, Sharma AM. Physiology and pathophysiology of the adipose tissue renin- angiotensin system. *Hypertension.* 2000;35:1270-1277
 47. Kanda A, Noda K, Ishida S. Atp6ap2/(pro)renin receptor contributes to glucose metabolism via stabilizing the pyruvate dehydrogenase e1 beta subunit. *J Biol Chem.* 2015;290:9690- 9700
 48. Patel MS, Nemeria NS, Furey W, Jordan F. The pyruvate dehydrogenase complexes: Structure-based function and regulation. *J Biol Chem.* 2014;289:16615-16623
 49. Harris RA, Bowker-Kinley MM, Huang B, Wu P. Regulation of the activity of the pyruvate dehydrogenase complex. *Adv Enzyme Regul.* 2002;42:249-259
 50. Sun Y, Danser AHJ, Lu X. (pro)renin receptor as a therapeutic target for the treatment of cardiovascular diseases? *Pharmacological Research.* 2017;In press
 51. Choi CS, Savage DB, Abu-Elheiga L, Liu ZX, Kim S, Kulkarni A, Distefano A, Hwang YJ, Reznick RM, Codella R, Zhang D, Cline GW, Wakil SJ, Shulman GI. Continuous fat oxidation in acetyl-coa carboxylase 2 knockout mice increases total energy expenditure, reduces fat mass, and improves insulin sensitivity. *Proc Natl Acad Sci U S A.* 2007;104:16480-16485
 52. Abu-Elheiga L, Matzuk MM, Abo-Hashema KA, Wakil SJ. Continuous fatty acid oxidation and reduced fat storage in mice lacking acetyl-coa carboxylase 2. *Science.* 2001;291:2613- 2616
 53. Inoue M, Ohtake T, Motomura W, Takahashi N, Hosoki Y, Miyoshi S, Suzuki Y, Saito H, Kohgo Y, Okumura T. Increased expression of ppargamma in high fat diet-induced liver steatosis in mice. *Biochem Biophys Res Commun.* 2005;336:215-222
 54. Gavrilova O, Haluzik M, Matsusue K, Cutson JJ, Johnson L, Dietz KR, Nicol CJ, Vinson C, Gonzalez FJ, Reitman ML. Liver peroxisome proliferator-activated receptor gamma contributes to hepatic steatosis, triglyceride clearance, and regulation of body fat mass. *J Biol Chem.* 2003;278:34268-34276
 55. Zhang YL, Hernandez-Ono A, Siri P, Weisberg S, Conlon D, Graham MJ, Crooke RM, Huang LS, Ginsberg HN. Aberrant hepatic expression of ppargam-

- ma2 stimulates hepatic lipogenesis in a mouse model of obesity, insulin resistance, dyslipidemia, and hepatic steatosis. *J Biol Chem.* 2006;281:37603-37615
56. Wu CH, Mohammadmoradi S, Thompson J, Su W, Gong M, Nguyen G, Yian-nikouris F. Adipocyte (pro)renin-receptor deficiency induces lipodystrophy, liver steatosis and increases blood pressure in male mice. *Hypertension.* 2016;68:213-219
 57. Shamansurova Z, Tan P, Ahmed B, Pepin E, Seda O, Lavoie JL. Adipose tissue (p)rr regulates insulin sensitivity, fat mass and body weight. *Mol Metab.* 2016;5:959-969
 58. Qi L, Heredia JE, Altarejos JY, et al. Trb3 links the e3 ubiquitin ligase cop1 to lipid metabolism. *Science.* 2006;312:1763-1766
 59. Rouillard AD, Gundersen GW, Fernandez NF, Wang Z, Monteiro CD, McDermott MG, Ma'ayan A. The harmonizome: A collection of processed datasets gathered to serve and mine knowledge about genes and proteins. *Database (Oxford).* 2016;2016

Online Supplement

Methods

Animals

C57BL/6 mice and LDLR^{-/-} mice were obtained from Model Animal Research Center of Nanjing University (Nanjing, China), and were housed at a 10-hour light/14-hour dark cycle. 8-week old male C57BL/6 mice were injected weekly with saline, GalNAc control ASOs (G-control), or GalNAc (P)RR ASOs [G-(P)RR] subcutaneously. For experiments ≤ 4 weeks, ASOs were dosed at 3 mg/kg/week. For experiments ≥ 4 weeks, ASOs were dosed at 3 mg/kg/week in the first 4 weeks, and were then reduced to 1.5 mg/kg/week until end of the experiment. Mice were either fed with ND (Harlan Teklad) or HFD (42% kcal fat, 0.2% cholesterol, Harlan Teklad). LDLR^{-/-} mice were treated in the same way as C57BL/6 mice. Body weight was monitored weekly. Food consumption of each cage hosting 6 mice was recorded weekly. Blood samples were collected via submandibular bleeding after 6h fasting. Plasma lipid TC and TG levels were monitored bi-weekly, unless indicated elsewhere. Experimental procedures were approved by local animal ethics committee (no. 2014-0140).

Antisense Oligonucleotides (ASOs)

ASOs with 5'-methyl modified cytosine and a phosphorothioate back-

Chapter 5

bone containing 2-O, 4-C-[(S)-ethylidene]-D-ribose (cEt) modified sugars were synthesized as described previously.¹ Chimeric ASOs containing 16mer cEt chemistries were used with the gapmer design of 3-10-3 wherein the terminal 5' and 3' nucleotides contained the cET modified sugars that flanked 10 nucleotides with unmodified sugars. The liver targeting conjugate GalNAc was connected through a trishexylamino-(THA)-C6 linker at the 5' end of the ASO². Extensive in vitro activity screens were performed followed by in vivo tolerability and activity studies to identify the lead (P)RR ASO with the following nucleotide sequence AGATATTGGTCCATTT. A control ASO that did not hybridize to any known rodent mRNA was used and had the following nucleotide sequence, GGCCAATACGCCGTCA.

Intraperitoneal glucose tolerance test (IPGTT)

IPGTT was performed as described elsewhere,³ one week prior to the end of the study. Briefly, following 16h fasting, 2 g/kg glucose was injected intraperitoneally to mice. Blood samples were collected from tail vein at 0, 15, 30, 60 and 120 min after glucose injection, and blood glucose was measured using a glucometer (Roche). Glucose levels at each time point were compared, and overall differences in glycemic control were compared using area under curve (AUC).

In vivo LDL clearance assay

In vivo LDL clearance was measured as described before.⁴ In short, mice were injected with 50 µg human Dil-labeled LDL (AngYuBio, Shanghai) via a tail-vein. Then, blood samples were collected retro-orbitally at 2, 10, 20, 40, 80, 160, and 300 min after injection. A standard curve was constructed by serial dilution of the human Dil-labeled LDL into mice plasma. Dil-LDL concentrations at 2 min after injection were the highest and were thus set as the baseline value for further analysis. Differences in VLDL secretion were compared using area under curve (AUC).

Hepatic VLDL secretion

To determine VLDL-TG secretion rate, mice were fasted for 4 hours and injected intraperitoneally with 1 mg/g Pluronic F127 (Sigma Aldrich), a detergent that inhibits lipolysis. Subsequently, blood samples were collected by retroorbital bleeding at 0, 1, 2 and 4 hours after Pluronic F127 injection. Differences in VLDL secretion were compared using area un-

der curve (AUC).

Fast Protein Liquid Chromatography (FPLC) analysis of plasma lipoproteins

FPLC analysis of plasma lipoproteins was performed as described before.⁵ In short, plasma samples were pooled, and cleared by centrifugation and filtering through a 0.22 μm filter. 200 μL cleared plasma samples were loaded for FPLC analysis using an AKTA purifier (GE) and Superose-6 Increase 10/300 GL (GE). Flow rate was set to 0.5 mL/min, and fractions between 10-16 mL were collected at intervals of 0.25 mL/fraction. Cholesterol and triglycerides content in each fraction was measured.

Oxygen consumption and physical activity measurement

Metabolic and physical activity of the mice were measured using an indirect open-circuit calorimeter (Oxylet, Panlab).⁶ Mice were housed individually in metabolic chambers and oxygen consumption, CO₂ production, and physical activity were recorded at 30 min intervals for consecutive 48 hours. For accuracy, the recorded data from the first 12-14 hours after the mice have been housed in the chamber were not analyzed.

Body composition analysis

Fat and lean mass composition of the mice were evaluated by EchoMRI (Echo Medical Systems, Houston, TX, USA) before sacrifice. Weights of different fat tissues were measured using a scale balance with 0.0001-gram accuracy (Sartorius).

H&E staining and Oil Red O staining

Hematoxylin and eosin (H&E) staining was performed on 5 μm tissue sections which were Bouin's-fixed and paraffin-embedded. Oil Red O staining was used to detected hepatic neutral lipids. Fresh liver and adipose tissues embedded in OCT were cryosectioned for 7 μm . After fixation with 4% paraformaldehyde, sections were stained with 0.3% oil red o following standard procedures⁷ and then counterstained with hematoxylin. Images were scanned using Cytation 5 Cell Imaging Multi-mode reader (Biotek).

Measurement of ALT and AST

Blood samples were pre-cleared by centrifugation at $3,000\times g$ for 5 minutes. Plasma alanine aminotransferase (ALT) and aspartate aminotransferase (AST) activities were measured by commercial kits (Biosino) following the manufacture's protocol.

Adenovirus and Adeno-associated virus

Adeno-associated virus (AAV) expressing the D377Y PCSK9 mutant and their use was previously described.⁸ Eight-week-old mice were intraperitoneally with AAV-PCSK9 at a concentration of 10×10^{10} genomic copies, and fed a chow-diet for 4 weeks to induce LDLR degradation. Afterwards, mice were treated with saline, G-control, or G-(P)RR for 4 weeks, and fed with chow or HFD. Human SORT1 under control of a CMV promotor was cloned and inserted in to pAd-EF1a-GFP vector (Vigenebio, China). Packaging of adenovirus was performed by linearization of the plasmid and transfection of 293A cells. Adenoviral particles were purified by ultracentrifugation, and virus titer was determined by serial dilution and plaque formation. 8-weeks old male mice were injected with 1.5×10^9 pfu Ad-hSORT1 or Ad-GFP (purchased from Vigenebio) via tail-vein. Mice were fed with chow or HFD for 7 days, and sacrificed after 6h fasting.

Transcriptome analysis

To assess whether silencing hepatic (*P*)RR affects gene expression in the liver, we injected mice (3 mice/group) intraperitoneally with saline or G-(P)RR as described above. After 5 days, the mice were sacrificed after 6h fasting, and liver samples were collected immediately and stored in Trizol at $-80\text{ }^{\circ}\text{C}$ until use. Total RNA was extracted and a RNA sequencing library was constructed for each sample using the Illumina mRNA-Seq Prep Kit. Paired-End libraries were prepared following Illumina's protocols and sequenced on the Illumina HiSeq X10 platform. RNA Sequencing reads were analyzed following the reported protocol with HISAT, StringTie and Ballgown.⁹ More specifically, high quality sequencing reads were firstly mapped to the mouse reference genome (version Ensembl GRCm38) using HISAT with default parameters.¹⁰ Transcriptomic expression at gene and transcript level, characterized by FPKM (Fragments Per Kilobase of transcript per Million mapped

reads), was then quantified by StringTie.⁹ The Ballgown package was used to identify differential expressed genes (DEGs) with $P < 0.05$ between G-(P)RR and saline control.¹¹ Functional analysis of all DEGs was preformed using DAVID functional annotation clustering tool.¹² Gene numbers were calculated for each Gene ontology (GO) category, and a hypergeometric test was used to identify significantly enriched GO categories in DEGs.

Comparative proteomics using iTRAQ

To understand how does (P)RR inhibition affects lipid metabolism and energy metabolism, we performed comparative proteomics analysis. Mice (n=3/group) were treated with G-control or G-(P)RR for 4 weeks, and fed with chow or HFD. Mice were sacrificed after 6h fasting. Livers were collected and homogenized in lysis buffer by TissueLyzer. Proteins were precipitated by acetone and resuspended with dissolving buffer containing 6 M guanidine hydrochloride and 300 mM TEAB (triethylammonium bicarbonate). Protein concentrations were determined by BCA, and equal amounts of proteins from individual samples per group were mixed and processed for iTRAQ labeling. Labeled samples were fractionated by high pH separation using Acquity UPLC H-Class Bio system (Waters Corporation, Milford, MA) connected to a reverse phase column (XBridge C18 column, 2.1 mm×150 mm, 3.5 μ m, 300 Å, Waters Corporation, Milford, MA). High pH separation was performed using a linear gradient, starting from 5% B to 35% B in 40 min (B: 5 mM ammonium formate in 90% acetonitrile, pH 10.0, adjusted with ammonium hydroxide). The column flow rate was maintained at 200 μ L/min and column temperature was maintained at room temperature. Ten fractions were collected. Each fraction was dried in a vacuum concentrator for the next step. The peptide samples were resuspended with 30 μ L solvent A respectively (A: water with 0.1% formic acid; B: acetonitrile with 0.1% formic acid), separated by nano-RPLC (EASY-nLC 1000, Thermo Fisher Scientific) and analyzed by on-line electrospray tandem mass spectrometry (Q Exactive mass spectrometer, Thermo Fisher Scientific). 5 μ L peptide sample was loaded onto the trap column (Thermo Scientific Acclaim PepMap C18, 75 μ m × 2 cm), and subsequently separated on the analytical column (Acclaim PepMap C18, 75 μ m × 15 cm) with a linear gradient, from 5% B to 35% B in 70 min, at a flow rate of 300 nL/min. The electrospray voltage of 1.6 kV versus the inlet of the mass spectrometer was used. The Q Exactive mass spectrometer was operated

Chapter 5

in the data-dependent mode to switch automatically between MS and MS/MS acquisition. Survey full-scan MS spectra (m/z 300-1600) were acquired in Orbitrap with a mass resolution of 70,000 at m/z 200. The AGC target was set to 1 000 000, and the maximum injection time was 20 ms. The ten most intense peaks were isolated in the quadrupole with isolation window of 2.0 m/z units. Ions with charge states 2+, 3+, and 4+ were sequentially fragmented by higher energy collisional dissociation (HCD) with a normalized collision energy of 27%, fixed first mass was set at 100, and further analyzed in the Orbitrap mass analyzer with 17,500 resolution. The AGC target was set to 500,000, and the maximum injection time was 200 ms. In all cases, one microscan was recorded using dynamic exclusion of 35 seconds.

The expression ratio [G-(P)RR/G-control] was calculated for each protein, under different diet conditions. Cut-off value was set to 1.2-fold [G-(P)RR/G-control >1.2 or <0.083]. Proteins with altered abundance were compared between HFD and chow, and only proteins that were regulated in the same trend by (P)RR inhibition were identified as differential expressed proteins (DEPs). Functional analysis of all DEGs was preformed using DAVID functional annotation clustering tool. Gene numbers were calculated for each Gene ontology (GO) category, and hypergeometric test was used to identify significantly enriched GO categories in DEGs.

Measurement of pyruvate, acetyl-CoA, lactate and PDH activity

Plasma pyruvate and lactate levels were detected using Pyruvate Assay kit (Sigma Aldrich) and Lactate Assay kit (Sigma Aldrich), following the manufacture's protocols. To measure hepatic pyruvate, acetyl-CoA, and PDH activity, liver samples (~25 mg) were homogenized in the assay buffers provided with the kits, and measurements were performed according to the manufacture's protocol. To measure cellular pyruvate levels, HepG2 cells were transfected with either control siRNA (siNC) or (P)RR siRNA [si(P)RR] for 48 hours. Cells were then detached using TrypLE and collected by centrifugation at 4 °C at 100x g, followed by washing with ice-cold PBS for three times. Measurement of pyruvate levels from an equal number of cells was performed according to manufacturer's protocol, and normalized to cell number. Acetyl-CoA levels were measured using the PicoProbe Activity Microplate Assay kit (Abcam) in a similar approach, except that protein concentration was used

to normalize acetyl-CoA levels. To measure lactate concentration, 24h after transfection, cells were switched to conditional medium (CM) that does not contain phenol red for 24 hours. Lactate levels in CM were then measured using the Lactate Assay kit (Sigma Aldrich). PDH activity was detected by a commercial kit (Sigma Aldrich), following the manufacturer's protocol.

Measurement of lipoprotein lipase (LPL) activity

Mice were treated with saline, G-control, or G-(P)RR and fed an HFD for 4 weeks. To measure LPL activity, mice were injected with 0.2 U/g heparin via tail-vein, and blood were drawn 15 min after heparin injection. Plasma LPL activity were then measured with a commercial kit from Abcam (catalog nr. ab204721).

Measurement of plasma insulin

Mice were treated with saline, G-control, or G-(P)RR and fed an HFD for 14 weeks. After 6-hour-fasting, plasma samples were collected and measured for insulin levels with an ultrasensitive mouse insulin ELISA kit from ALPCO (catalog nr. 80-INSMSU-E01), following the standard manufacturer's protocol.

Isolation and culture of primary hepatocytes

Primary hepatocytes were isolated from C57BL/6J mice using previously described two-step collagenase perfusion method with modifications (Cytotechnology. 2012 Mar; 64(2): 187–195.). Briefly, mice were first perfused with O₂ gassed perfusion buffer (5 mmol/L HEPES, 4 mmol/L KCl, 120 mmol/L NaCl, 1 mmol/L KH₂PO₄, 2.4 mmol/L MgSO₄, 40 mmol/L NaHCO₃, 20 mmol/L glucose) supplemented with 0.1 mmol/L EDTA, for 5-7 minutes at a constant flow rate at 7 mL/min. Perfusion path was set to flow into liver via inferior vena cava and flow out through portal vein. After the first perfusion step, mice were then perfused with O₂ gassed perfusion buffer supplemented with 2.7 mmol/L CaCl₂ and 1.6 mg/mL Type IV collagenase (Sigma Aldrich, catalog nr. C5138), for 3-4 minutes at a constant flow rate at 6 mL/min. Primary hepatocytes were released by removing liver capsule, and filtered through 100 µm filtered. Then, primary hepatocytes were washed with ice-cold DMEM and centrifuged at 50x g for 2 min, which was repeated for three times. Primary hepatocytes were seeded at a density of 600,000 cells/

Chapter 5

well or 8,000 cells/well into collagen coated 6-well plate or Seahorse 24-well plate, respectively, and cultured with DMEM GlutaMax™ high glucose supplemented with 5% FBS. To inhibit (P)RR expression in mouse primary hepatocytes, 0.05 mg/mL G-(P)RR ASO was added to culture medium 3 hours after seeding cells.

Seahorse XFe24 analyzer

HepG2 cells were seeded to Seahorse 24-well plate, and cultured with DMEM GlutaMax™ high glucose with 10% FBS. HepG2 cells were transfected with siNC or si(P)RR for 48 hours. Mouse primary hepatocytes were isolated, seeded to Seahorse 24 well plate, and cultured with DMEM GlutaMax™ high glucose supplemented with 5% FBS. To inhibit (P)RR expression, mouse primary hepatocytes were treated with 0.05 µg/mL final concentration of G-(P)RR ASOs for 36 hours. Mitochondrial function and cellular fuel dependency were then measured using Seahorse XF Cell Mito Stress Test Kit and Seahorse XF Mito Fuel Flex Test Kit, following manufacturer's protocol, with the exception that for FA dependency assay oleic acid was added to a final concentration of 50 µmol/L to the cell culture medium 4 hours prior to the start of the assay.

Immunoblotting

For protein expression and phosphorylation studies, 50 mg mouse liver samples were homogenized in RIPA buffer (50 mM Tris-HCl, 150mM NaCl, 1% Triton X-100, 1% sodium deoxycholate, 0.1% SDS, pH 7.4) with phosphatase inhibitor cocktail (Sigma Aldrich) and protease inhibitors cocktail (Roche) using TissueLyzer (Qiagen). Homogenates were centrifuged at 10,000× g at 4 °C for 10 minutes to clear any cell debris or insoluble proteins. Protein concentrations were then determined using BCA assay (Pierce). Equal amounts of proteins (30-40 mg) were loaded and separated on 4-20% Bis-Tris gels (GenScript), and transferred to PVDF membranes using iBlot® 2 Dry Blotting System (Thermo Fisher Scientific). For high-molecular weight proteins such as acetyl-CoA carboxylase (ACC), samples were loaded and separated on 6% SDS-PAGE gels with ice-cold buffers for 3-5 hours, and transferred to PVDF membranes using traditional wet transferring system at 4 °C for 16 hours. The blots were then probed with the antibodies listed in Online Table I and detected by Clarity™ Western Substrate (Bio-rad). The intensities of bands were analyzed using ImageJ.

Online Table I. Antibodies used in the study

Target	Species originated	Dilution	Source	Catalog number
(P)RR	Rabbit	1:1000	Sigma	HPA003156
SORT1	Mouse	1:1000	BD Bioscience	612100
LDLR	Rabbit	1:1000	Thermo Fisher Scientific	PA5-22976
PDHA	Rabbit	1:1000	Proteintech	18068-1-AP
PDHB	Rabbit	1:1000	Proteintech	14744-1-AP
ACCa/b	Rabbit	1:1000	Cell Signaling Technology	9957
PPAR γ	Rabbit	1:1000	Cell Signaling Technology	2435
Adiponectin	Rabbit	1:1000	Cell Signaling Technology	2789
β -actin	Mouse	1:3000	Proteintech	60008-1

RNA isolation and qPCR analysis

Liver samples were homogenized with Trizol (Thermo Fisher Scientific) and total RNA was extracted using Direct-zol™ RNA MiniPrep kit (ZYMO Research). One microgram of total RNA was reverse transcribed with Prime Script™ RT Master Mix (TaKaRa). SYBR Green real-time quantitative PCR assays were performed on a qTOWER apparatus (Analytic Jena) using SYBR® Premix Ex Taq™ II kit (TaKaRa). Primers used in the study were listed in Online Table II.

Hepatic lipids extraction and measurement

To measure hepatic lipid contents, lipids in the liver were extracted using Folch's method.¹³ In short, 50 mg liver samples were homogenized using Tissue lyzer (60Hz, 30s) in chloroform and methanol mixture (2:1) followed by adding methanol, chloroform and MQ. Extracted lipids were dried with N₂ gas and dissolved with 200 μ l PBS containing 1% Triton X-100. Cholesterol, triglycerides and non-esterified fatty acid (NEFA) were measured using colorimetric kits (Wako).

Statistics

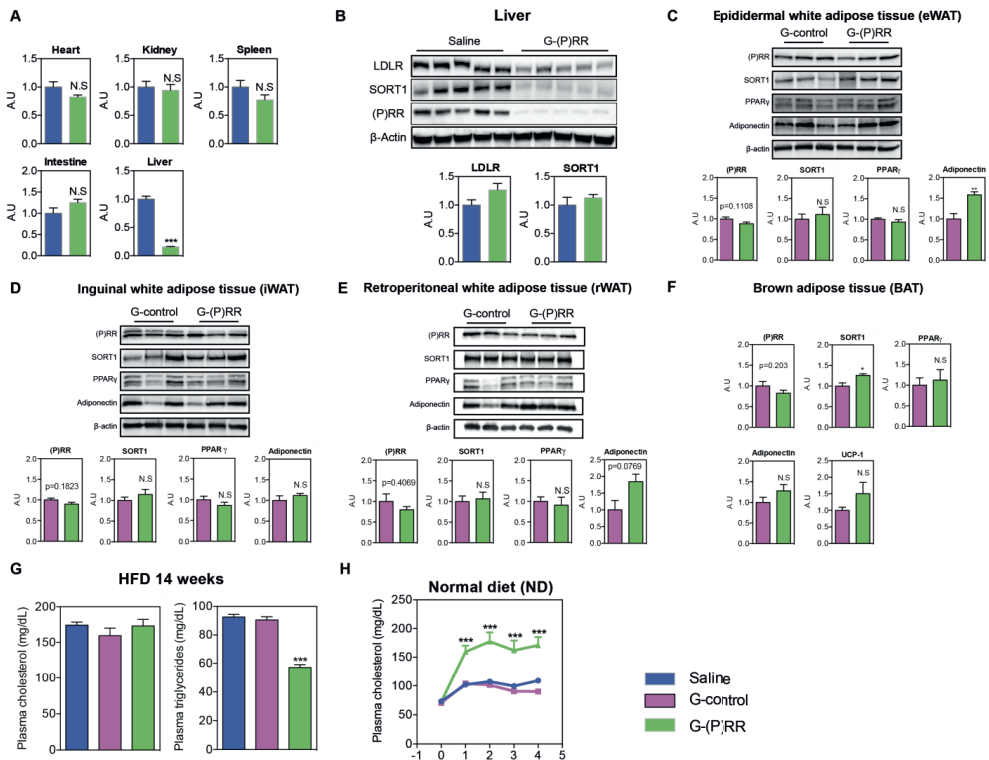
All values were presented as mean \pm SEM. For experiments with n number ≥ 8 /group, D'Agostino-Pearson omnibus test was performed to test normality. For experiments with less n number, Kolmogorov-Smirnov test was performed for normality test. After passing normality test, one-way ANOVA followed by the Bonferroni test was performed for comparison of more than two groups. And student t-test was used to compare the differences between two groups. P values of <0.05 were considered significant.

Online Table II. List of qPCR primer sequences		
Gene		Sequence
(P)RR	Forward	5'-GGGTGGATAAACTGGCACTTC-3'
	Reverse	5'-TGGAATTTGCAACGCTGTC-3'
SORT1	Forward	5'-TGAGGACATGGTCTTCATGC-3'
	Reverse	5'-GGTAAAGATGGTGCCAAACC-3'
LDLR	Forward	5'-GATGGCTATACCTACCCCTCAA-3'
	Reverse	5'-TGCTCATGCCACATCGTC-3'
PDHA	Forward	5'-GGCATCGTTGGAGCTCAG-3'
	Reverse	5'-ACAGACCTCATCTTTTCCATTGT-3'
PDHB	Forward	5'-GAGCTGAGATTTGTGCCAGA-3'
	Reverse	5'-ACATCAGCACCAGTGACACG-3'
ACC α	Forward	5'-GGCTCAAACCTGCAGGTATCC-3'
	Reverse	5'-TTGCCAATCCACTCGAAGA-3'
ACC β	Forward	5'-TGAATCTCACGCGCCTACTA-3'
	Reverse	5'-TTGTGTTCTCGGCCTCTCT-3'
PPAR γ	Forward	5'-GAAAGACAACGGACAAATCACC-3'
	Reverse	5'-GGGGGTGATATGTTTGAACCTTG-3'
Adiponectin	Forward	5'-GGGGGTGATATGTTTGAACCTTG-3'
	Reverse	5'-CTTTCCTGCCAGGGGTTC-3'
UCP-1	Forward	5'-GGCCTCTACGACTCAGTCCA-3'
	Reverse	5'-TAAGCCGGCTGAGATCTTGT-3'
Hadha	Forward	5'-GAAATGGATAATATCTTGGCAAATC-3'
	Reverse	5'-TGGACGTCTTCATCAGAGGAG-3'
Acaa2	Forward	5'-AAATGTGCGCTTCGGAAC-3'
	Reverse	5'-CGTTAATCCTGCCACAAAG-3'
Acadv1	Forward	5'-GGTGGTTTGGGCCTCTCTA-3'
	Reverse	5'-TCCCAGGGTAACGCTAACAC-3'
Acadl	Forward	5'-GCTTATGAATGTGTGCAACTCC-3'
	Reverse	5'-CCGAGCATCCACGTAAGC-3'
β -actin	Forward	5'-CTAAGGCCAACCGTGAAAAG-3'
	Reverse	5'-ACCAGAGGCATACAGGGACA-3'

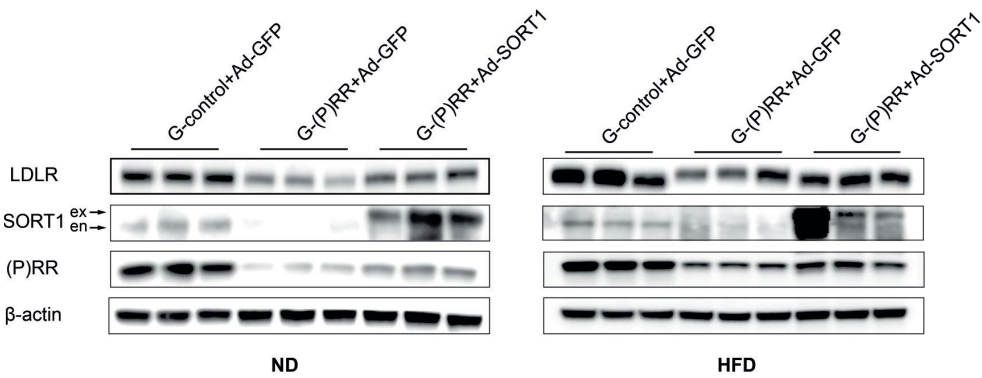
Results

Online table III:

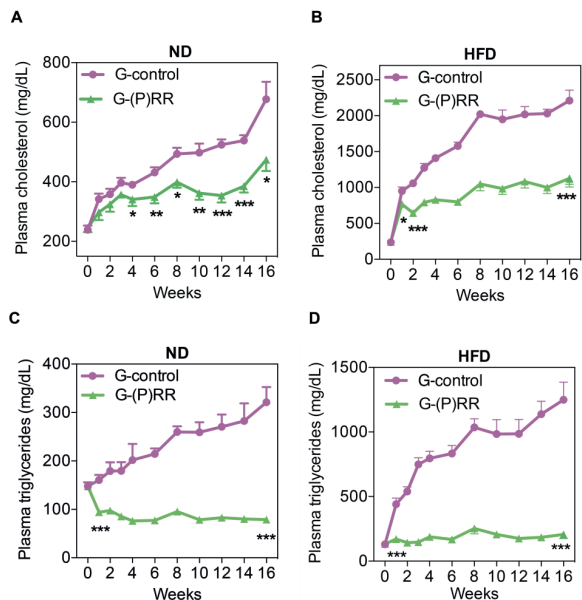
<http://circres.ahajournals.org/lookup/suppl/doi:10.1161/CIRCRESA-HA.117.312422/-/DC1>.



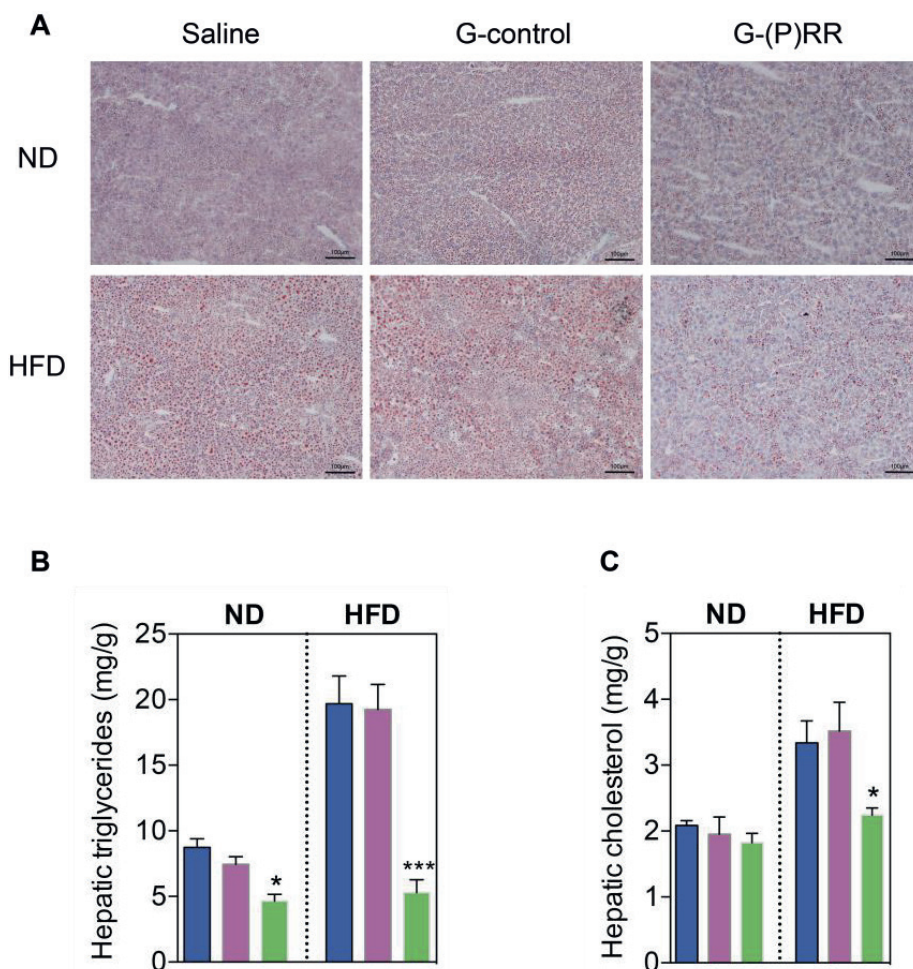
Online Figure I. GalNAc-(P)RR ASO specifically targets hepatic (P)RR and affects plasma lipid concentrations. (A) Eight-weeks-old male C57BL6 mice were injected with saline (blue) or G-(P)RR (green). After 5 days, mice were sacrificed and tissues were collected and analyzed for (P)RR expression. (P)RR expression was normalized by the geometric mean of the expression of actin, 36B4 and GAPDH. N=5/group; ***: p<0.001. (B) Immunoblotting of liver samples from saline or G-(P)RR treated mice. (C-E) (P)RR expression levels and protein abundance in epididymal white adipose tissue (eWAT), inguinal white adipose tissue (iWAT), and retroperitoneal white adipose tissue (rWAT) of mice treated with G-control or G-(P)RR for 14 weeks and fed with HFD. (F) (P)RR expression in brown adipose tissue (BAT) of mice treated with G-control or G-(P)RR for 14 weeks and fed with HFD. (G) G-(P)RR did not affect mRNA levels of LDLR and SORT1. N=6 per group. (D) Plasma triglycerides and cholesterol concentration of C57BL6 mice injected with saline (blue), G-control (magenta) or G-(P)RR (green), and fed HFD for 14 weeks. N=10 per group. ***: p<0.001. G-control v.s G-(P)RR. (H) Plasma cholesterol levels of C57BL6 mice treated as indicated, and fed ND for 4 weeks. N=12 per group. ***: p<0.001. G-control v.s G-(P)RR.



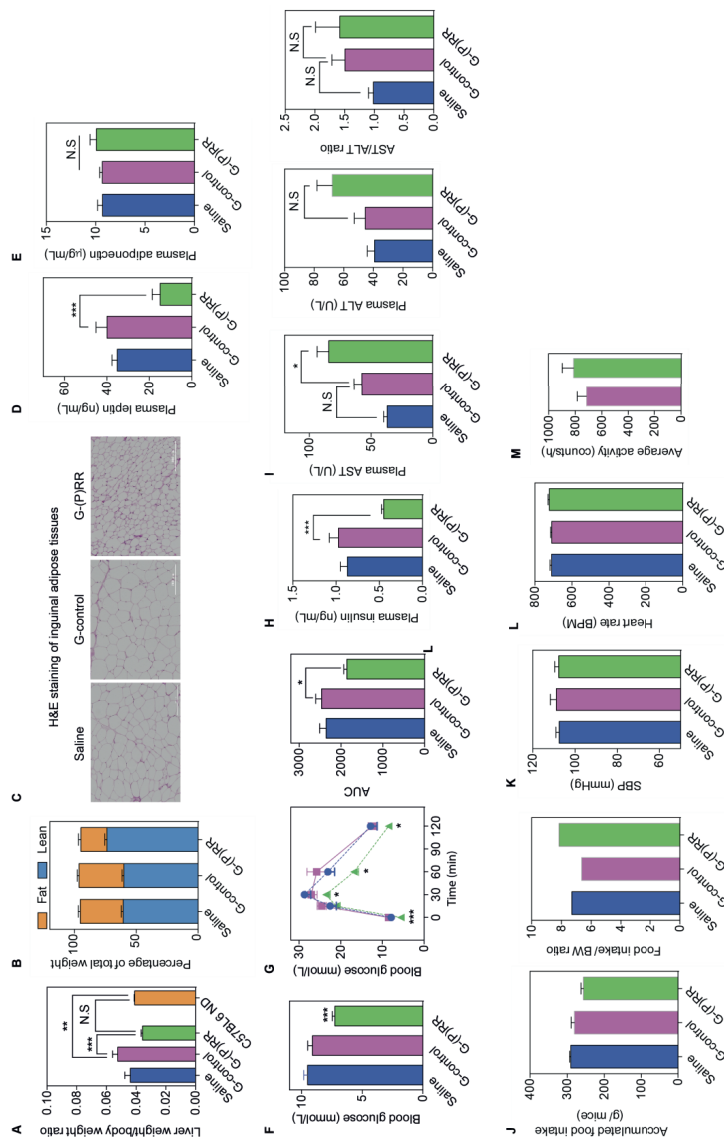
Online Figure II. SORT1 overexpression does not prevent PRR deficiency induced reduction in LDLR protein levels in the liver. Eight-week-old male mice were treated with G-control or G-(P)RR, in combination of control adenovirus (Ad-GFP) or SORT1 expressing adenovirus (Ad-SORT1). N=6 per mice. Representative blot. Ex: exogenously expressed hSORT1. En: endogenously expressed mSORT1.



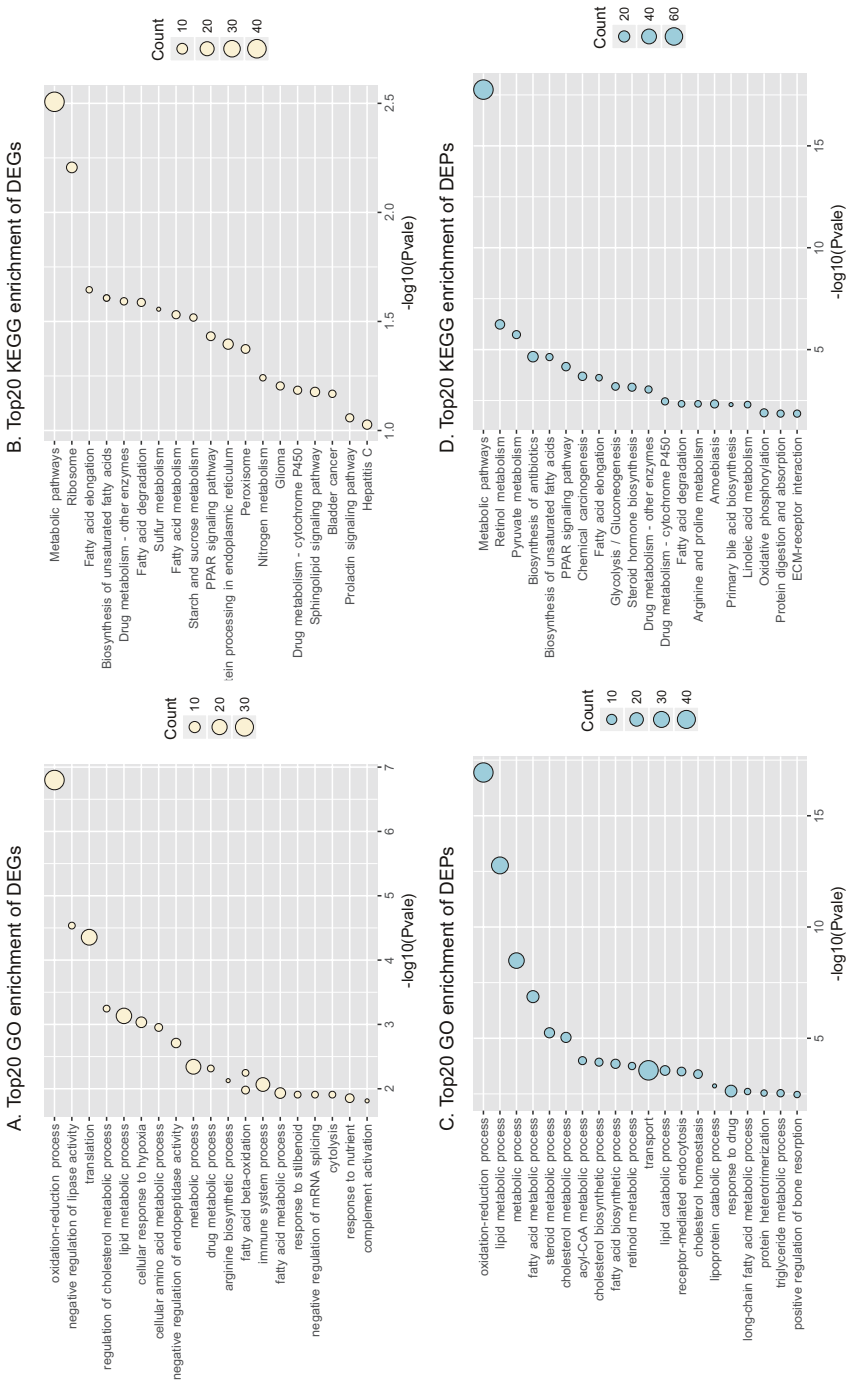
Online Figure III. Inhibiting hepatic (P)RR in LDLR^{-/-} mice reduces plasma cholesterol and triglyceride levels under both chow and HFD conditions. Eight-weeks-old male mice were treated with G-control (magenta) or G-(P)RR (green), and fed with ND or HFD for 16 weeks. Plasma cholesterol levels (A&B) and plasma triglyceride levels (C&D) were monitored weekly in the first 4 weeks, and bi-weekly afterwards. N=8 per group. *: p<0.05; **: p<0.01; ***: p<0.001.



Online Figure IV. Inhibiting the (P)RR reduces hepatic lipid levels under both ND and HFD conditions. Eight-week-old male mice were treated with saline (blue), G-control (magenta) or G-(P)RR (green) for 4 weeks, fed ND or HFD. (A) Representative image of Oil Red O staining of liver samples. (B&C) Lipids were extracted from the liver using Folch's method, and dried with N₂ gas. Resuspended lipids were measured for triglycerides and cholesterol, normalized by the weight of liver samples used for lipid extraction. N=12 per group. *: $p < 0.05$; ***: $p < 0.001$.

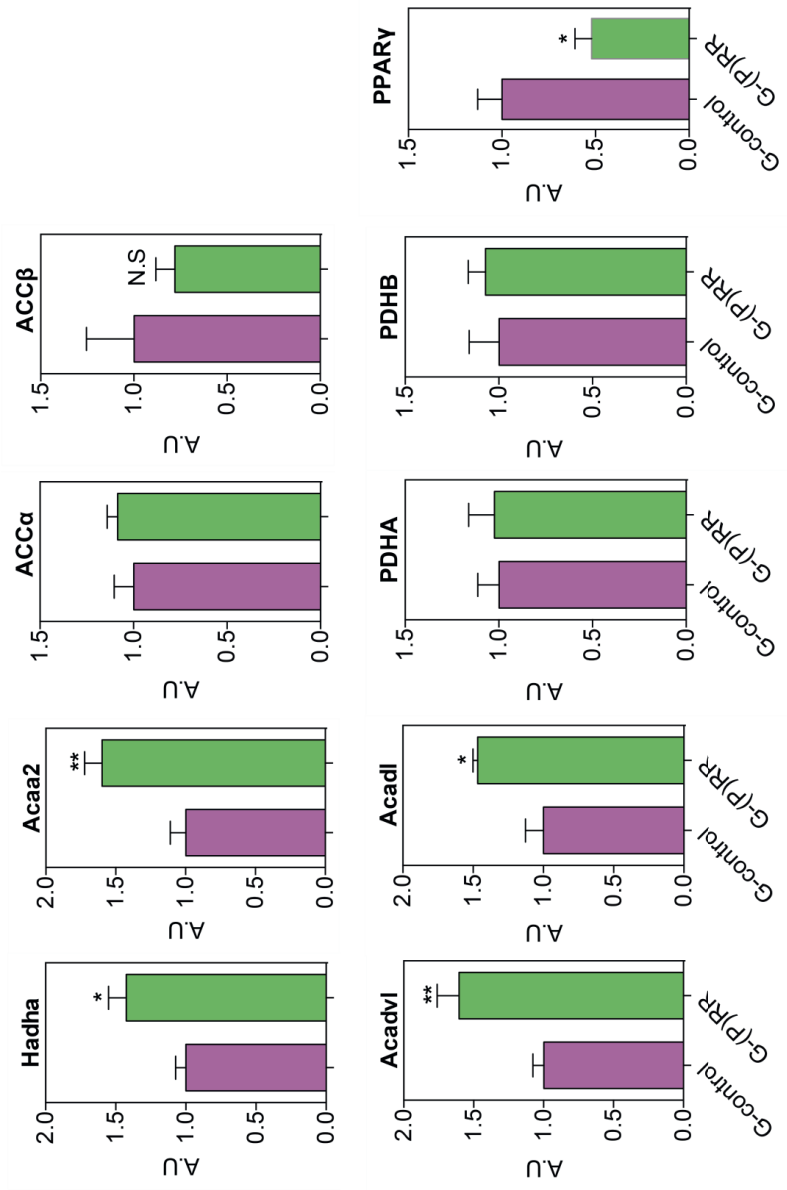


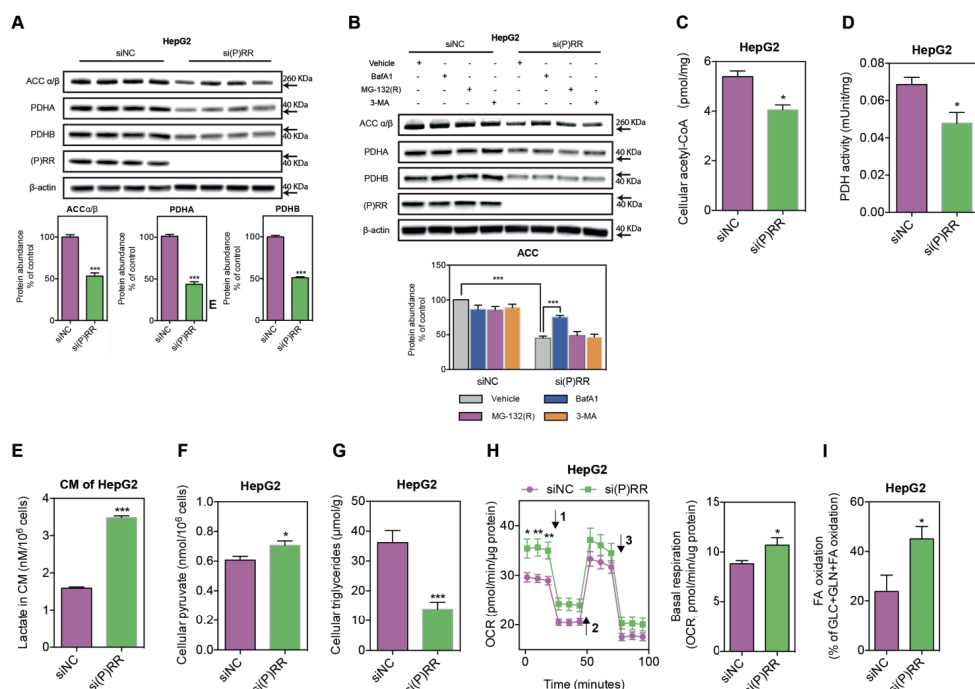
Online Figure V. Relevant information of hepatic (P)RR inhibition in C57BL6 mice fed HFD for 14 weeks. Eight-week-old male mice were treated as indicated, and fed HFD for 14 weeks. (A) LW/BW ratio. LW/BW ratio of C57BL6 mice at similar age, fed ND, was used as a reference value (n=6). N=10 per group. ***: p<0.001. (B) Representative image of H&E staining of inguinal white adipose tissue. (C) Plasma leptin concentrations. (D) Plasma adiponectin concentrations. (E-G) plasma ALT and AST activity, and AST/ALT ratio. N=10 per group; *: p<0.05; (H) accumulated food intake during experimental period. (I) accumulated food intake adjusted by end time body weight. SBP (J) and heart rate (K) measured 7 days prior to sacrifice. N=10 per group. (L) Mice were treated as indicated and fed HFD for 12 weeks. Blood were drawn after 6-hours fasting and plasma insulin levels were measured. N=10 per group.



Online Figure VI. GO enrichment analysis reveals that inhibiting the (P)RR extensively affects genes involved in metabolic processes. Analysis of transcriptome (A&B), or comparative proteomics (C&D). Top 20 enriched biological processes (BP) (A&C). Top 20 enriched KEGG pathways (B&D).

Online Figure VII.
Hepatic gene expression
are affected by (P)RR
inhibition. Eight-week-old
male C57BL6 mice were
treated with G-control
or G-(P)RR, fed HFD for
14 weeks. Hepatic gene
expressions were analyzed,
and normalized by the
expression of β -actin in
the same sample. N=6
per group. *: $p<0.05$; **: $p<0.01$.





Online Figure VIII. Silencing the (P)RR in HepG2 cells reduces ACC and PDH protein abundance resulting in increased oxygen consumption and dependency on fatty acid as fuel source. (A) (P)RR expression was silenced in HepG2 cells and a representative blot of 3 independent experiments in quadruplicate is shown. Total cell lysates were immunoblotted as indicated, and the level of PDHA, PDHB, and ACCα/β protein was quantified and normalized to the level of β-actin in the same lysate. ***: $p < 0.001$. (B) HepG2 cells were transfected with control or (P)RR siRNAs for 48h. Cells were incubated with vehicle control, 100 nmol/L bafilomycin A1 (BafA1), 7.5 mmol/L 3-3-Methyladenine, and 20 μmol/L MG-132(R) for 8 hours. A representative blot of 4 independent experiments and corresponding quantification is shown. (C-G) To measure cellular metabolites, HepG2 cells were transfected with control siRNA (siNC) or siRNA against (P)RR [si(P)RR] for 48 hours. Subsequently, cells or medium were prepared as described to measure intracellular acetyl-CoA levels (C), PDH activity (D), lactate levels in the conditional medium (CM) (E), intracellular pyruvate levels (F), and intracellular triglyceride levels (G). Three independent experiments in triplicate were performed for each measurement and values were corrected with either the amount of protein or number of cells. $N = 9$ per group; *: $p < 0.05$; ***: $p < 0.001$. (H-I) Cellular oxygen consumption rates (OCR) (H) and fuel dependency (I) were measured in HepG2 cells treated with siNC or si(P)RR for 48 hours. Arrow 1-3 indicates addition of oligomycin, FCCP and the mixture of rotenone and antimycin, respectively. $N = 6$ per group. *: $p < 0.05$; **: $p < 0.01$.

References

1. 1. Seth PP, Siwkowski A, Allerson CR, Vasquez G, Lee S, Prakash TP, Kinberger G, Migawa MT, Gaus H, Bhat B, Swayze EE. Design, synthesis and evaluation of constrained methoxyethyl (cmoe) and constrained ethyl (cet) nucleoside analogs. *Nucleic Acids Symp Ser (Oxf)*. 2008;553-554
2. 2. Prakash TP, Yu J, Migawa MT, et al. Comprehensive structure-activity relationship of triantennary n-acetylgalactosamine conjugated antisense oligonucleotides for targeted delivery to hepatocytes. *J Med Chem*. 2016;59:2718-2733
3. 3. Bowe JE, Franklin ZJ, Hauge-Evans AC, King AJ, Persaud SJ, Jones PM. Metabolic phenotyping guidelines: Assessing glucose homeostasis in rodent models. *J Endocrinol*. 2014;222:G13-25
4. 4. Wagschal A, Najafi-Shoushtari SH, Wang L, et al. Genome-wide identification of micrnas regulating cholesterol and triglyceride homeostasis. *Nat Med*. 2015;21:1290-1297
5. 5. Roche-Molina M, Sanz-Rosa D, Cruz FM, Garcia-Prieto J, Lopez S, Abia R, Muriana FJ, Fuster V, Ibanez B, Bernal JA. Induction of sustained hypercholesterolemia by single adeno-associated virus-mediated gene transfer of mutant hpcsk9. *Arterioscler Thromb Vasc Biol*. 2015;35:50-59
6. 6. Franckhauser S, Munoz S, Elias I, Ferre T, Bosch F. Adipose overexpression of phosphoenolpyruvate carboxykinase leads to high susceptibility to diet-induced insulin resistance and obesity. *Diabetes*. 2006;55:273-280
7. 7. Thatcher SE, Zhang X, Howatt DA, Lu H, Gurley SB, Daugherty A, Cassis LA. Angiotensin-converting enzyme 2 deficiency in whole body or bone marrow-derived cells increases atherosclerosis in low-density lipoprotein receptor-/- mice. *Arterioscler Thromb Vasc Biol*. 2011;31:758-765
8. 8. Lu H, Howatt DA, Balakrishnan A, Graham MJ, Mullick AE, Daugherty A. Hypercholesterolemia induced by a pcsk9 gain-of-function mutation augments angiotensin ii-induced abdominal aortic aneurysms in c57bl/6 mice-brief report. *Arterioscler Thromb Vasc Biol*. 2016;36:1753-1757
9. 9. Pertea M, Kim D, Pertea GM, Leek JT, Salzberg SL. Transcript-level expression analysis of rna-seq experiments with hisat, stringtie and ballgown. *Nat Protoc*. 2016;11:1650-1667
10. 10. Kim D, Langmead B, Salzberg SL. Hisat: A fast spliced aligner with low memory requirements. *Nat Methods*. 2015;12:357-360
11. 11. Frazee AC, Pertea G, Jaffe AE, Langmead B, Salzberg SL, Leek JT. Ballgown bridges the gap between transcriptome assembly and expression analysis. *Nat Biotechnol*. 2015;33:243-246
12. 12. Huang DW, Sherman BT, Tan Q, Kir J, Liu D, Bryant D, Guo Y, Stephens R, Baseler MW, Lane HC, Lempicki RA. David bioinformatics resources: Expanded annotation database and novel algorithms to better extract biology from large gene lists. *Nucleic Acids Res*. 2007;35:W169-175
13. 13. Folch J, Lees M, Sloane Stanley GH. A simple method for the isolation and purification of total lipides from animal tissues. *J Biol Chem*. 1957;226:497-509

Chapter 6

(Pro)renin Receptor Inhibition Reduces Plasma Cholesterol and Triglycerides but Does Not Attenuate Atherosclerosis in Atherosclerotic Mice

Dien Ye[#], Xiaofei Yang[#], Liwei Ren, Hong S. Lu, Yuan Sun, Hui Lin, Lunbo Tan, Na Wang, Genevieve Nguyen, Michael Bader, Adam E. Mullick, A.H. Jan Danser, Alan Daugherty, Yizhou Jiang, Furong Li*, Xifeng Lu*

Submitted

[#]Contribute equally

* corresponding author

Abstract

Rationale: Elevated plasma cholesterol concentrations contributes to ischemic CVD. Recently, we showed that inhibiting hepatic (P)RR attenuated diet-induced hypercholesterolemia and hypertriglyceridemia in LDLR deficient mice. The purpose of this study was to determine whether inhibiting hepatic (P)RR could attenuate atherosclerosis.

Methods and Results: Eight weeks-old male LDLR^{-/-} mice were injected with saline or GalNAc-modified antisense oligos (G-ASOs) primarily targeting hepatic (P)RR weekly and fed a western-type diet (WTD) for 16 weeks. (P)RR G-ASOs markedly reduced plasma cholesterol concentrations from 2211±146 mg/dL to 1128±121 mg/dL. FPLC analysis reveals that cholesterol in VLDL and IDL/LDL fraction were potentially reduced by (P)RR ASOs. Moreover, (P)RR G-ASOs reduced plasma triglyceride concentrations by more than 80%. Strikingly, despite drastic reduction in plasma lipids, (P)RR G-ASOs did not attenuate atherosclerosis in these mice. Further testing in ApoE^{-/-} mice confirmed that (P)RR G-ASOs reduced plasma lipids but accelerated atherosclerosis. To understand the reason behind, we compared the transcriptomic changes in aortic arch segment from saline and (P)RR ASOs treated LDLR^{-/-} mice fed with WTD for 4 weeks, and found that (P)RR G-ASOs induced the expression of genes involved in immune response and inflammation. Further investigation reveals that macrophage is an additional target of (P)RR G-ASOs, and inhibiting (P)RR in macrophages enhanced pro-inflammatory response to exogenous stimuli. Moreover, deleting the (P)RR in macrophages did not affect plasma lipids but accelerated atherosclerosis in WTD fed ApoE^{-/-} mice.

Conclusion: (P)RR G-ASOs reduced plasma cholesterol and triglycerides in atherosclerotic mice due to hepatic (P)RR deficiency. However, the beneficial effects of lowered plasma lipids on atherosclerosis were abolished by augmented pro-inflammatory responses in macrophages as a result of unexpected downregulation of (P)RR in macrophages. Our study demonstrates that hepatic (P)RR and macrophagic (P)RR play a counteracting role in atherosclerosis.

Introduction

Atherosclerosis is a major cause of morbidity and mortality. Increased concentrations of plasma cholesterol and triglycerides, increased blood pressure, and impaired blood glucose metabolism are major risk factors for developing atherosclerosis and ischemic cardiovascular diseases (CVD). The (pro)renin receptor [(P)RR] can bind both renin and prorenin, and activate intracellular signaling cascades, including extracellular signal-regulated kinase 1/2 and phosphatidylinositol 3-kinase/Akt.¹ Upon binding, the (P)RR activates prorenin in a non-proteolytic manner, leading to renin-angiotensin system (RAS) activation. However, the interaction of (P)RR with renin/prorenin at supraphysiological concentrations questioned the physiological relevance with RAS. Indeed, recently studies show that the (P)RR is an accessory protein of the vacuolar H⁺-ATPase (V-ATPase) and indispensable for V-ATPase integrity and functions.²⁻⁵ We recently identified that the (P)RR plays an RAS-independent role in regulating lipoprotein and lipid metabolism.^{6, 7} Suppressing the (P)RR in hepatocytes reduced protein abundance of the low-density lipoprotein receptor (LDLR), the major receptor for low-density lipoprotein (LDL), thus reducing cellular LDL uptake.⁶ Inhibiting the hepatic (P)RR on the one hand reduced hepatocyte LDL clearance as a consequence of decreased LDLR protein abundance, but simultaneously decreased hepatic very low density lipoprotein (VLDL) secretion, which overall resulted in decreased plasma cholesterol and triglycerides concentrations in wild type C57BL/6J mice fed a Western-type diet (WTD).⁷ We further discovered that inhibiting the hepatocyte (P)RR in gene deletion induced- or proprotein convertase subtilisin/kexin type 9 overexpression-induced LDLR deficient mice drastically reduces the plasma concentrations of cholesterol and triglycerides, regardless of diet feeding. We thus hypothesized that (P)RR inhibition would be an effective way to lower plasma cholesterol and triglycerides concentrations, and reduce the risk for atherosclerosis, especially in familial hypercholesterolemia patients whose LDLR activity is reduced or diminished and response to statin is less pronounced than in normal patients.⁸

Methods

The data that support the findings reported in this manuscript are available from the corresponding authors upon reasonable request.

Chapter 6

Animals experiments

LDLR^{-/-}, ApoE^{-/-}, and Lyz2-Cre mice were purchased from the Model Animal Research Center of Nanjing University (Nanjing, China), and mice carrying floxed (P)RR allele were kindly provided by Prof. Michael Bader and Prof. Genevieve Nguyen.⁹ Mice were housed on a 10-hour light/14-hour dark cycle. Eight weeks-old male LDLR^{-/-} and ApoE^{-/-} mice were injected weekly with either saline or GalNAc modified ASOs targeting (P)RR [(P)RR G-ASOs] subcutaneously. Only male mice were studied because our previous study focused on male mice. Also, the estrus cycle in female mice may affect atherosclerosis and other parameters.¹⁰ ASOs were synthesized as described before.^{7, 11, 12} G-(P)RR ASOs were injected subcutaneously at 3.0 mg/kg/week at the first 4 weeks and were then reduced to 1.5 mg/kg/week. Mice were fed aWTD (42% kcal/kcal fat, 0.2% wt/wt cholesterol, Envigo) for 16 weeks. Blood samples were collected via submandibular bleeding after 6 h fasting. Systolic blood pressure was measured on conscious mice with a computerized noninvasive tail-cuff system (Softron, BP-2010A). Blood pressure was measured weekly for 4 weeks, prior to the end of the study. The mean of five repeated measurements at the last week (16th week) is reported. To isolate peritoneal macrophages, C57BL/6J mice were first injected with saline or 3.0 mg/kg (P)RR G-ASOs, and 4 days later mice were injected with 6% autoclaved starch broth into intraperitoneal cavity. Three days after starch broth injection, peritoneal macrophages were isolated as described.¹³ To obtain macrophage (P)RR knockout mice on ApoE^{-/-} background, Lyz2-Cre and (P)RR flox mice were first crossed with ApoE^{-/-} mice, and the offsprings were intercrossed to obtain Lyz2-Cre^{+/-} (P)RR^{wt/Y} ApoE^{-/-} mice and Lyz2-Cre^{+/-} (P)RR^{fl/Y} ApoE^{-/-} mice, which were further intercrossed to obtain macrophage (P)RR knockout mice. Genotyping primers were listed in Supplemental Table I. These mice were fed with WTD for 12 weeks to assess the consequences on atherosclerosis. Experimental procedures were approved by the Animal Ethic Committee of Shenzhen Health Science Center (no. 2014-0140).

Isolation of mouse aortas and en face analysis

Aortic segments between the aortic root and the iliac arteries, were dissected and fixed with 4% paraformaldehyde for 24 hours. After fixation, adventitial tissues were carefully removed, and the aortas were cut open. Isolated aortas were quantified with or without Oil Red O (ORO) as described in the AHA statement.¹⁴ En face aortas were imaged with a

microscope (Nikon, SMZ1270), and lesion areas were measured and quantified using Image J. In addition to quantification of plaque sizes in the whole aorta, plaque sizes of the ascending aorta, arch, and from the aortic orifice of left subclavian artery to 3 mm below were also quantified, which was designated as aortic arch in the figures.

Histology analysis of aortic root

Mouse hearts were isolated and fixed with 4% paraformaldehyde for 24 hours, embedded in OCT, and cryosectioned at 7 μ m thickness. Aortic root sections were prepared as recommended with some modifications.¹⁴ In short, serial tissue sections were acquired from the initial appearance of the aortic valves. Three tissue sections were placed on a single slide, and in total 45-48 slides were obtained. The slide showing the largest aortic valves were chosen for hematoxylin and eosin (H&E) and ORO staining. Stained slides were scanned using Cytation 5 Cell Imaging Multi-mode reader (Biotek). Lesion areas of the aortic root were measured for the three sections on the same slide with Image J, and average plaque size was reported.

Biochemical measurements

Plasma total cholesterol and triglycerides concentration were measured by commercial kit (Wako) following the manufacturer's protocol. Plasma renin concentrations were measured by enzyme-kinetic assay in the presence of excess sheep angiotensinogen as described previously.¹⁵ The plasma concentrations of apolipoprotein B (ApoB) were determined by ELISA kit (Signalway Antibody, EK0320). Fractionation of plasma was described earlier,⁷ and cholesterol and triglycerides concentrations in each fraction were determined by commercial kit (Wako).

RNA isolation, quantitative PCR and RNA sequencing

Total RNA was extracted using Direct-zol™ RNA MiniPrep kit (ZYMO Research). One microgram of total RNA was reverse transcribed with Prime Script™ RT Master Mix (TaKaRa). SYBR Green real-time quantitative PCR assays were performed on a qTOWER apparatus (Analytic Jena) using SYBR® Premix Ex Taq™ II kit (TaKaRa). Primers used in the study were listed in Supplemental Table I. Total RNAs extracted from aortic arch region were used to construct RNA sequencing libraries, which were sequenced on Illumina HiSeq X10 platform. DESeq2 was used to identify differently expressed genes (DEGs).

Chapter 6

Gene ontology (GO) and KEGG enrichment analysis were performed using clusterProfiler. Gene set variation analysis (GSVA) was performed as described previously,¹⁶ using described curated datasets (Supplemental Table II) from the literature.^{17, 18}

Cellular experiments

RAW264.7 cells were maintained with DMEM high glucose medium supplemented with 10% fetal bovine serum. To inhibit (P)RR expression, 0.1 mg/mL final concentrations of (P)RR G-ASOs were added to the cells. Twenty-four hours later, cells were stimulated with or without 100 ng/mL liposaccharide (LPS) for 4 hours for measuring gene expression, and 12 hours for measuring cytokine production, respectively. To stimulate cytokine release, cells were treated with 10 μ M nigericin for 30 min before collecting the cell culture medium. Secreted cytokines in the cell culture medium were measured using commercial kits from Thermo Scientific (TNF- α : # 88-7324-88; IL-1b: # 88-5019-88; IL-6: # 88-7064-88; IL-10: 88-7105-88), following the manufacturer's protocol.

Fast Protein Liquid Chromatography (FPLC) analysis of plasma lipoproteins

FPLC analysis was performed as described previously.⁷ In short, plasma samples from 8 mice were pooled, and cleared by centrifugation and further filtered through a 0.22 μ m filter. Two hundred fifty microliters of filtered plasma was loaded for FPLC analysis using Superous-6 Increase 10/300 GL column (GE) on an AKTA purifier (GE). Flow rate was set to 0.5 mL/min, and fractions between 10-16 mL were collected at an interval of 0.25 mL/fraction. Cholesterol and triglycerides concentrations in each fraction was measured.

Statistics

All values are presented as mean \pm SEM. The Kolmogorov-Smirnov test was performed to test normality. When passing the normality test, one-way ANOVA followed by the Bonferroni test was performed for comparison in case of >2 groups. Student T-test was performed when comparison was made between two groups. $P < 0.05$ was considered significant. Statistical analysis was performed using Prism 9 (Graphpad Software).

Results

(P)RR G-ASOs did not ameliorate atherosclerosis in LDLR^{-/-} mice

To evaluate whether hepatic (P)RR inhibition attenuated atherosclerosis, we administered (P)RR G-ASOs to LDLR^{-/-} mice. The efficacy and specificity of G-(P)RR ASOs in reducing hepatic (P)RR was demonstrated in our previous study.⁷ Inhibiting the (P)RR in hepatocytes reduced plasma cholesterol concentrations by ~50% (2211 ± 146 mg/dL versus 1128 ± 121 mg/dL) (Figure 1A). FPLC analysis revealed that the cholesterol content of VLDL and IDL/LDL fractions were reduced (Figure 1B). Plasma triglyceride concentrations were also reduced markedly, mainly by reducing VLDL- and IDL/LDL-triglycerides (Figures 1 C&D). Strikingly, lesion sizes in the aortic arch region and the entire aorta were not reduced by (P)RR inhibition (Figure 1 E-G). Moreover, H&E and ORO staining of the aortic root revealed that lesions sizes were not reduced by (P)RR inhibition (Figure 1 H&I). A previous study reported that systolic blood pressure was elevated in adipose (P)RR knockout mice,¹⁹ suggesting that (P)RR inhibition may affect RAS activity and blood pressure. However, (P)RR inhibition did not alter systolic blood pressure or plasma renin concentrations in LDLR^{-/-} mice (Supplemental Figure J), ruling out altered RAS activity as the counteracting factor for the beneficial effects of lowering lipid concentrations.

(P)RR G-ASOs did not ameliorate atherosclerosis in ApoE^{-/-} mice

We further tested the effects of (P)RR inhibition on atherosclerosis in another atherosclerotic mice model, namely ApoE^{-/-} mice. We found that (P)RR G-ASOs also effectively reduced both plasma cholesterol and triglycerides concentrations in ApoE^{-/-} mice (Supplemental Figure II A&B), to a similar extent as observed in LDLR^{-/-} mice. This suggests that the plasma lipids lowering effect of hepatic (P)RR inhibition is independent of LDLR or ApoE. Yet, plaque size in the whole aorta and aortic arch region remained unaltered by (P)RR inhibition (Supplemental Figure II C-E), despite the strong reduction in plasma lipids. H&E and ORO staining of the aortic root further confirmed that atherosclerosis was not attenuated in ApoE^{-/-} mice treated with (P)RR G-ASOs (Supplemental Figure II F&G).

(P)RR G-ASOs promotes immune responses by stimulating macrophagic pro-inflammatory cytokines

Our observation that (P)RR G-ASOs markedly reduced plasma lipid

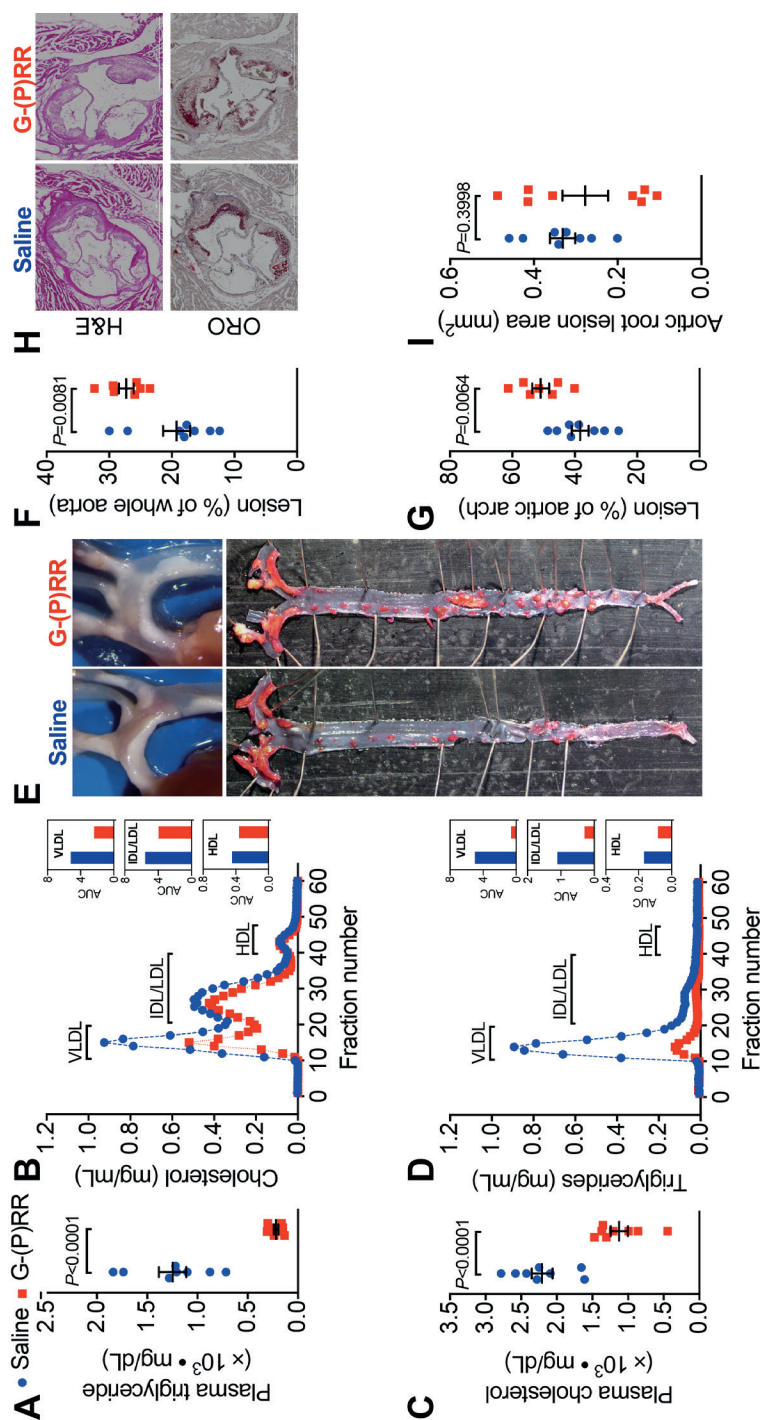
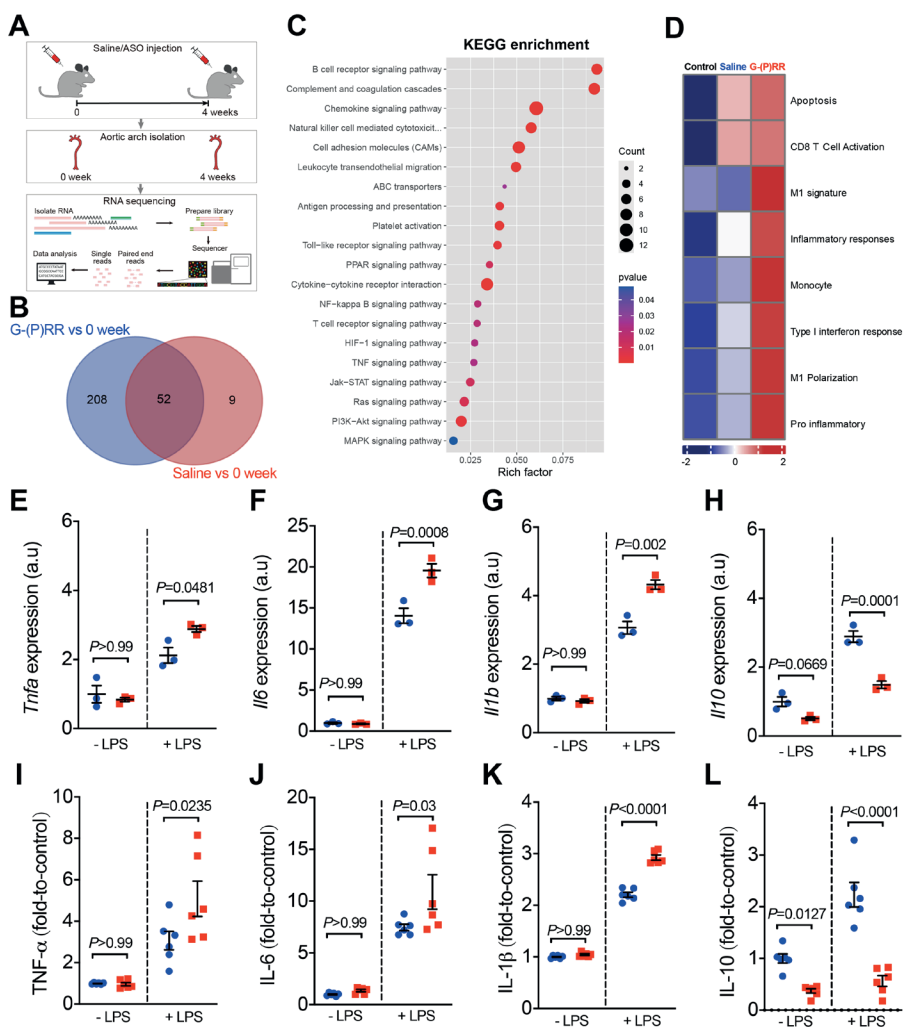


Figure 1. (P)RR G-ASOs reduce plasma cholesterol and triglyceride concentrations but not atherosclerosis in LDLR^{-/-} mice fed a western-type diet (WTD). Eight week-old male LDLR^{-/-} mice were treated with saline (blue) or (P)RR G-ASOs (red) and fed a WTD for 16 weeks. N=8/group. Total plasma cholesterol (A) and triglycerides levels (C). Pooled plasma samples were loaded on FPLC for lipoprotein fractionation analysis, and cholesterol (B) and triglycerides content (D) in each fraction was determined. Representative images of the aorta arch and oil red Oil Red O-stained whole aorta (E). Quantification of lesion areas of the whole aorta (F) and aortic arch region (G). Representative images of cross-sectioned aortic root stained with H&E and ORO (H). Quantification of lesion areas of the aortic root (I).

concentrations, but not atherosclerosis in two different atherosclerotic models, suggested that (P)RR G-ASOs promote other crucial atherogenic factor(s) to counteract the potential benefit of lowered plasma lipids. To clarify this, we mapped the transcriptomic changes in aortic arch region of saline and (P)RR G-ASOs administered treated LDLR^{-/-} mice fed a WTD for 4 weeks (Figure 2A). Using aortic arch region of normal diet-fed control 8-week-old LDLR^{-/-} mice, we identified 58 up-regulated and 3 down-regulated genes in saline administered LDLR^{-/-} mice, and GO enrichment analysis of DEGs revealed that immune response related biological processes were affected mostly (Supplemental Table III & Supplemental Figure III). In comparison, (P)RR G-ASOs upregulated 256 genes and downregulated 4 genes, which are also enriched in immune response related biological processes (Supplemental Table IV & Supplemental Figure IV). We then compared the DEGs and found that 206 genes were specifically altered by (P)RR G-ASOs (Supplemental Table V & Figure 2B). GO enrichment analysis revealed that these genes were related to immune responses (Supplemental Figure V), and KEGG enrichment analysis revealed that inflammation related pathways, such as NF- κ B signaling pathway, chemokine signaling pathway and Toll-like receptor signaling pathway, were mostly affected (Figure 2C). GSVA analysis demonstrated that inflammatory gene set, type I interferon response gene set, and M1 macrophage signature gene set were activated (Figure 2D), suggesting enhanced inflammation in the aortic arch region of (P)RR G-ASOs administered LDLR^{-/-} mice. Despite the relatively high specificity of N-acetylgalactosamine modified ASOs towards hepatocytes,²⁰ macrophages could also be a target as they express asialoglycoprotein receptors which bind N-acetylgalactosamine.²¹ We therefore suspected that (P)RR G-ASOs targeted macrophages and promoted inflammation, thereby counteracting the benefit of lowered plasma lipids concentrations. Indeed, isolated peritoneal macrophages from C57BL/6J mice administered (P)RR G-ASO for 1 week showed marked reduction in (P)RR expression (Supplemental Figure VIA). Moreover, successfully inhibiting (P)RR expression in murine RAW264.7 (Supplemental Figure VIB), a widely used murine macrophage cell line, enhanced LPS-stimulated expression of pro-inflammatory cytokines, including *Tnfa*, *Il6* and *Il1b* (Figure 2 E-G). In RAW264.7 cells, inhibiting the (P)RR reduced abundance of *Il10*, an anti-inflammatory cytokine, with or without LPS stimulation (Figure 2H). In line with the gene abundance findings, (P)RR inhibition in macrophages increased TNF- α , IL-6 and IL-1 β se-



T0

Figure 2. (P)RR G-ASOs promote immune responses in aorta by augmenting macrophagic pro-inflammatory cytokine production. A-D: Eight-week-old LDLR^{-/-} mice were treated with saline or (P)RR G-ASOs and fed a WTD for 4 weeks, and aortas were isolated for transcriptomic analysis. Aortas from 8-week-old LDLR^{-/-} mice (0 week) serve as control. The experimental procedure is illustrated (A). Venn graph showing overlapped and non-overlapped DEGs (B). KEGG enrichment analysis (C) and GSVA analysis (D). E-L: RAW cells were treated with saline (blue) or (P)RR G-ASOs (red), and stimulated with or without LPS. Expression and production of pro-inflammatory and anti-inflammatory cytokines were determined.

cretion (Figure 2 I-K), and decreased IL-10 secretion (Figure 2L). To confirm the effect of macrophage (P)RR downregulation in atherosclerosis, we generated macrophage-specific (P)RR knockout mice on ApoE^{-/-} background (Supplemental Figure VII A-C). We found that deleting the (P)RR in macrophages did not affect plasma cholesterol and triglyceride concentrations (Supplemental Figure VII D-E), further confirming that lowered plasma lipid concentrations were due to hepatic (P)RR deficiency. Yet, macrophage (P)RR-deleted mice did show accelerated atherosclerosis development (Supplemental Figure VII F-I). Collectively, these findings suggest that suppressed (P)RR expression in macrophages enhanced inflammatory responses in lesions, counteracting the benefits of lowered plasma lipid concentrations by hepatic (P)RR inhibition.

Discussion

Increased plasma cholesterol concentrations are thought to initiate atherosclerosis by causing abnormal lipid deposition in the artery wall.²² Reducing plasma cholesterol concentrations, for instance with statins, is an effective way to reduce CVD risk. However, in the current study, we demonstrate that a ~50% reduction in plasma cholesterol concentrations by hepatic (P)RR inhibition failed to attenuate atherosclerosis in either LDLR^{-/-} or ApoE^{-/-} mice. It is worthy to note that reduced plasma cholesterol concentrations were observed as early as 1 week after hepatic (P)RR inhibition.⁷ Thus, reduction of plasma cholesterol concentrations was maintained throughout the experimental period. Moreover, IDL/LDL cholesterol, the most potent atherogenic cholesterol, was reduced ~30% by hepatic (P)RR inhibition. LDL particles are heterogeneous in terms of size, density, and lipid compositions, and LDL particles with smaller size and higher density (more apolipoproteins and less lipids) have higher atherogenic ability.^{23, 24} Thus, it is possible that (P)RR inhibition alters the size and density of LDL. Indeed, we found that plasma ApoB concentrations were increased by inhibiting hepatic (P)RR (Supplemental Figure VIII). This finding, together with reduced cholesterol content in the IDL/LDL fraction, suggested that the densities of LDL particles were likely increased by hepatic (P)RR inhibition. Since small dense LDL enters arterial intima more easily and is more prone to be oxidized,^{25, 26} it may elicit immune responses more easily. This may explain the overactivated immune responses in the aortas of (P)RR inhibited mice.

Chapter 6

Activation of immune responses, characterized by infiltration of macrophages, mast cells, and T lymphocytes, is another hallmark in atherosclerosis development.²⁷ The number of macrophages accumulating in aorta can increase up to 20-fold during atherogenesis.²⁸ These macrophages can internalize accumulated oxidized LDL, leading to foam cell formation and the production of inflammatory cytokines, such as IL-1 β . Oxidized LDL can also directly interact with Toll-like receptors to activate the expression of proinflammatory cytokines and chemokines,²⁷ leading to activation of both innate and adaptive immune responses. Unexpectedly, we found that inhibiting macrophagic (P)RR promoted inflammatory cytokine production in the presence of exogenous stimuli, providing another possibility why (P)RR G-ASOs did not attenuate atherosclerosis although they did reduce plasma lipid concentrations. A recent study demonstrated that WTD feeding increased angiotensinogen and the angiotensin type 1 receptor expression in peritoneal macrophages, and blocking the RAS with the angiotensin type 1 receptor antagonist, valsartan, reduced ox-LDL concentrations and expression of *Il1b* and *Tnfa* in macrophages.²⁹ This highlights that RAS activation plays a role in inflammatory responses of macrophages. However, despite the debate on the role of (P)RR in RAS,³⁰ inhibiting the (P)RR would reduce rather than activate the RAS. Thus, (P)RR depletion is an unlikely cause of macrophage inflammatory responses via RAS activation. In fact, we found no effect on renin concentrations by (P)RR G-ASOs. Thus, the observed effect might be linked with its functions related with V-ATPase. V-ATPase is expressed at the plasma membrane and in lysosomes in macrophages.³¹ Inhibiting V-ATPase using bafilomycin induces TNF- α production in macrophages with and without LPS stimulation, and extends the duration of LPS-stimulated TNF- α production.³¹ Moreover, deleting macrophage *Atp6v0d2*, a subunit of the V-ATPase complex, augmented LPS-stimulated IL-1 β and TNF production *in vivo*.³² Interestingly, this study also showed that LPS stimulation itself reduced *Atp6v0d2* expression, indicating that inhibition of V-ATPase is required for activating inflammatory responses in macrophages. V-ATPase also plays a role in cholesterol efflux in macrophages.³³ Inhibiting V-ATPase using bafilomycin dose-dependently reduced ATP cassette binding protein A1-mediated cholesterol efflux in RAW264.7 cells, and inhibiting the *Atp6v0c* yielded similar effects. In fact, our transcriptomic result shows that the expression of ABC transporters was altered by (P)RR G-ASOs. Thus, it is possible that (P)RR deficiency in macrophages augments inflamma-

tion and impairs cholesterol efflux by impairing V-ATPase activity.

In summary, we showed that (P)RR G-ASOs lowered plasma lipid concentrations in WTD fed LDLR^{-/-} and ApoE^{-/-} mice due to hepatocyte (P)RR inhibition. However unexpectedly, downregulation of (P)RR in macrophages due to (P)RR G-ASOs promotes inflammatory cytokine production and suppressed anti-inflammatory cytokine production, thus counteracting the benefits of lowering plasma lipid concentrations. Overall, (P)RR G-ASOs did not attenuate atherosclerosis in WTD fed LDLR^{-/-} and ApoE^{-/-} mice.

Acknowledgement

We thank Dr. Shaojun Xing and his laboratory members for their technical assistant in measuring macrophage cytokines production. We thank Dr. Ingrid M. Garrelds for her technical assistant in measuring plasma renin concentrations.

Source of Funding

X. Lu is supported by National Natural Science Foundation of China (grant no. 81870605), Shenzhen Municipal Science and Technology Innovation Council (grant no. JCYJ20170817093928508 and JCYJ20160307160819191), and Shenzhen Key Laboratory of Metabolism and Cardiovascular Homeostasis (grant no. ZDSYS20190902092903237). Yuan is supported by National Natural Science Foundation of China (grant no. 81800383). F. Li is supported by National Natural Science Foundation of China (grant no. 81670702), and Shenzhen Municipal Science and Technology Innovation Council (grant no. GJHZ20170310090257380). A.H.J. Danser is supported by the Top Institute Pharma (T2-301). Yidan Sun is supported by Guangdong Natural Science Foundation (Guangdong-Shenzhen Joint Fund, 2019A1515110993). Y. Jiang is supported by Shenzhen Municipal Science and Technology Innovation Council (grant no. JCYJ20180305124812444).

Disclosure

A.E. Mullick is an employee and shareholder of Ionis Pharmaceuticals. The other authors report no conflicts of interest.

References

1. Nguyen G. Renin, (pro)renin and receptor: An update. *Clin Sci (Lond)*. 2011;120:169-178
2. Ludwig J, Kerscher S, Brandt U, Pfeiffer K, Getlawi F, Apps DK, Schagger H. Identification and characterization of a novel 9.2-kda membrane sector-associated protein of vacuolar proton-atpase from chromaffin granules. *J Biol Chem*. 1998;273:10939-10947
3. Kinouchi K, Ichihara A, Sano M, Sun-Wada GH, Wada Y, Kurauchi-Mito A, Bokuda K, Narita T, Oshima Y, Sakoda M, Tamai Y, Sato H, Fukuda K, Itoh H. The (pro)renin receptor/atp6ap2 is essential for vacuolar h⁺-atpase assembly in murine cardiomyocytes. *Circ Res*. 2010;107:30-34
4. Cruciat CM, Ohkawara B, Acebron SP, Karaulanov E, Reinhard C, Ingelfinger D, Boutros M, Niehrs C. Requirement of prorenin receptor and vacuolar h⁺-atpase-mediated acidification for wnt signaling. *Science*. 2010;327:459-463
5. Lu X, Garrelds IM, Wagner CA, Danser AH, Meima ME. (pro)renin receptor is required for prorenin-dependent and -independent regulation of vacuolar h⁽⁺⁾-atpase activity in mdck.C11 collecting duct cells. *Am J Physiol Renal Physiol*. 2013;305:F417-425
6. Lu X, Meima ME, Nelson JK, Sorrentino V, Loregger A, Scheij S, Dekkers DH, Mulder MT, Demmers JA, G MD-T, Zelcer N, Danser AH. Identification of the (pro)renin receptor as a novel regulator of low-density lipoprotein metabolism. *Circ Res*. 2016;118:222-229
7. Ren L, Sun Y, Lu H, Ye D, Han L, Wang N, Daugherty A, Li F, Wang M, Su F, Tao W, Sun J, Zelcer N, Mullick AE, Danser AHJ, Jiang Y, He Y, Ruan X, Lu X. (pro)renin receptor inhibition reprograms hepatic lipid metabolism and protects mice from diet-induced obesity and hepatosteatosis. *Circ Res*. 2018;122:730-741
8. Choumerianou DM, Dedoussis GV. Familial hypercholesterolemia and response to statin therapy according to ldlr genetic background. *Clin Chem Lab Med*. 2005;43:793-801
9. Riediger F, Quack I, Qadri F, Hartleben B, Park JK, Potthoff SA, Sohn D, Sihn G, Rousselle A, Fokuhl V, Maschke U, Purfurst B, Schneider W, Rump LC, Luft FC, Dechend R, Bader M, Huber TB, Nguyen G, Muller DN. Prorenin receptor is essential for podocyte autophagy and survival. *J Am Soc Nephrol*. 2011;22:2193-2202
10. Robinet P, Milewicz DM, Cassis LA, Leeper NJ, Lu HS, Smith JD. Consideration of sex differences in design and reporting of experimental arterial pathology studies-statement from atvb council. *Arterioscler Thromb Vasc Biol*. 2018;38:292-303
11. Prakash TP, Yu J, Migawa MT, Kinberger GA, Wan WB, Ostergaard ME, Carty RL, Vasquez G, Low A, Chappell A, Schmidt K, Aghajan M, Crosby J, Murray HM, Booten SL, Hsiao J, Soriano A, Machemer T, Cauntay P, Burel SA, Murray SF, Gaus H, Graham MJ, Swayze EE, Seth PP. Comprehensive structure-activity relationship of triantennary n-acetylgalactosamine conjugated antisense oligonucleotides for targeted delivery to hepatocytes. *J Med Chem*. 2016;59:2718-2733
12. Seth PP, Siwkowski A, Allerson CR, Vasquez G, Lee S, Prakash TP, Kinberger G, Migawa MT, Gaus H, Bhat B, Swayze EE. Design, synthesis and evaluation of

- constrained methoxyethyl (cmoe) and constrained ethyl (cet) nucleoside analogs. *Nucleic Acids Symp Ser (Oxf)*. 2008;553-554
13. Ray A, Dittel BN. Isolation of mouse peritoneal cavity cells. *J Vis Exp*. 2010
 14. Daugherty A, Tall AR, Daemen M, Falk E, Fisher EA, Garcia-Cardena G, Lusis AJ, Owens AP, 3rd, Rosenfeld ME, Virmani R, American Heart Association Council on Arteriosclerosis T, Vascular B, Council on Basic Cardiovascular S. Recommendation on design, execution, and reporting of animal atherosclerosis studies: A scientific statement from the american heart association. *Arterioscler Thromb Vasc Biol*. 2017;37:e131-e157
 15. de Lannoy LM, Danser AH, van Kats JP, Schoemaker RG, Saxena PR, Schalekamp MA. Renin-angiotensin system components in the interstitial fluid of the isolated perfused rat heart. Local production of angiotensin i. *Hypertension*. 1997;29:1240-1251
 16. Lambrechts D, Wauters E, Boeckx B, Aibar S, Nittner D, Burton O, Bassez A, Decaluwe H, Pircher A, Van den Eynde K, Weynand B, Verbeken E, De Leyn P, Liston A, Vansteenkiste J, Carmeliet P, Aerts S, Thienpont B. Phenotype molding of stromal cells in the lung tumor microenvironment. *Nat Med*. 2018;24:1277-1289
 17. Azizi E, Carr AJ, Plitas G, Cornish AE, Konopacki C, Prabhakaran S, Nainys J, Wu K, Kisieliovas V, Setty M, Choi K, Fromme RM, Dao P, McKenney PT, Wasti RC, Kadaveru K, Mazutis L, Rudensky AY, Pe'er D. Single-cell map of diverse immune phenotypes in the breast tumor microenvironment. *Cell*. 2018;174:1293-1308 e1236
 18. Orecchioni M, Ghosheh Y, Pramod AB, Ley K. Macrophage polarization: Different gene signatures in m1(lps+) vs. Classically and m2(lps-) vs. Alternatively activated macrophages. *Front Immunol*. 2019;10:1084
 19. Wu CH, Mohammadmoradi S, Thompson J, Su W, Gong M, Nguyen G, Yianikouris F. Adipocyte (pro)renin-receptor deficiency induces lipodystrophy, liver steatosis and increases blood pressure in male mice. *Hypertension*. 2016;68:213-219
 20. Springer AD, Dowdy SF. Galnac-sirna conjugates: Leading the way for delivery of rnaï therapeutics. *Nucleic Acid Ther*. 2018;28:109-118
 21. Iobst ST, Drickamer K. Selective sugar binding to the carbohydrate recognition domains of the rat hepatic and macrophage asialoglycoprotein receptors. *J Biol Chem*. 1996;271:6686-6693
 22. Bergheanu SC, Bodde MC, Jukema JW. Pathophysiology and treatment of atherosclerosis : Current view and future perspective on lipoprotein modification treatment. *Neth Heart J*. 2017;25:231-242
 23. Toft-Petersen AP, Tilsted HH, Aaroe J, Rasmussen K, Christensen T, Griffin BA, Aardestrup IV, Andreasen A, Schmidt EB. Small dense ldl particles--a predictor of coronary artery disease evaluated by invasive and ct-based techniques: A case-control study. *Lipids Health Dis*. 2011;10:21
 24. Ikezaki H, Lim E, Cupples LA, Liu CT, Asztalos BF, Schaefer EJ. Small dense low-density lipoprotein cholesterol is the most atherogenic lipoprotein parameter in the prospective framingham offspring study. *J Am Heart Assoc*. 2021:e019140
 25. Nordestgaard BG, Zilversmit DB. Comparison of arterial intimal clearances of ldl from diabetic and nondiabetic cholesterol-fed rabbits. Differences in intimal clear-

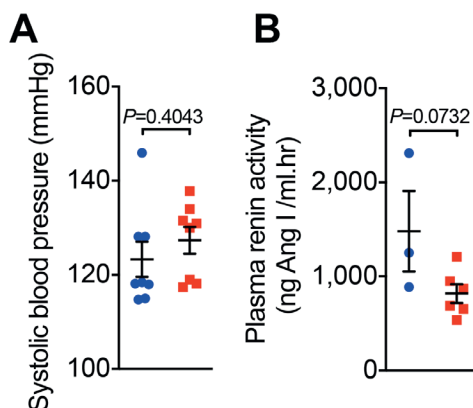
Chapter 6

- ance explained by size differences. *Arteriosclerosis*. 1989;9:176-183
26. de Graaf J, Hak-Lemmers HL, Hectors MP, Demacker PN, Hendriks JC, Stalenhoef AF. Enhanced susceptibility to in vitro oxidation of the dense low density lipoprotein subfraction in healthy subjects. *Arterioscler Thromb*. 1991;11:298-306
 27. Hansson GK, Hermansson A. The immune system in atherosclerosis. *Nat Immunol*. 2011;12:204-212
 28. Barrett TJ. Macrophages in atherosclerosis regression. *Arterioscler Thromb Vasc Biol*. 2020;40:20-33
 29. Nagai N, Kawashima H, Toda E, Homma K, Osada H, Guzman NA, Shibata S, Uchiyama Y, Okano H, Tsubota K, Ozawa Y. Renin-angiotensin system impairs macrophage lipid metabolism to promote age-related macular degeneration in mouse models. *Commun Biol*. 2020;3:767
 30. Sun Y, Danser AHJ, Lu X. (pro)renin receptor as a therapeutic target for the treatment of cardiovascular diseases? *Pharmacol Res*. 2017;125:48-56
 31. Conboy IM, Manoli D, Mhaikar V, Jones PP. Calcineurin and vacuolar-type h⁺-atpase modulate macrophage effector functions. *Proc Natl Acad Sci U S A*. 1999;96:6324-6329
 32. Xia Y, Liu N, Xie X, Bi G, Ba H, Li L, Zhang J, Deng X, Yao Y, Tang Z, Yin B, Wang J, Jiang K, Li Z, Choi Y, Gong F, Cheng X, O'Shea JJ, Chae JJ, Laurence A, Yang XP. The macrophage-specific v-atpase subunit atp6v0d2 restricts inflammasome activation and bacterial infection by facilitating autophagosome-lysosome fusion. *Autophagy*. 2019;15:960-975
 33. Lorkowski SW, Brubaker G, Gulshan K, Smith JD. V-atpase (vacuolar atpase) activity required for abca1 (atp-binding cassette protein a1)-mediated cholesterol efflux. *Arterioscler Thromb Vasc Biol*. 2018;38:2615-2625

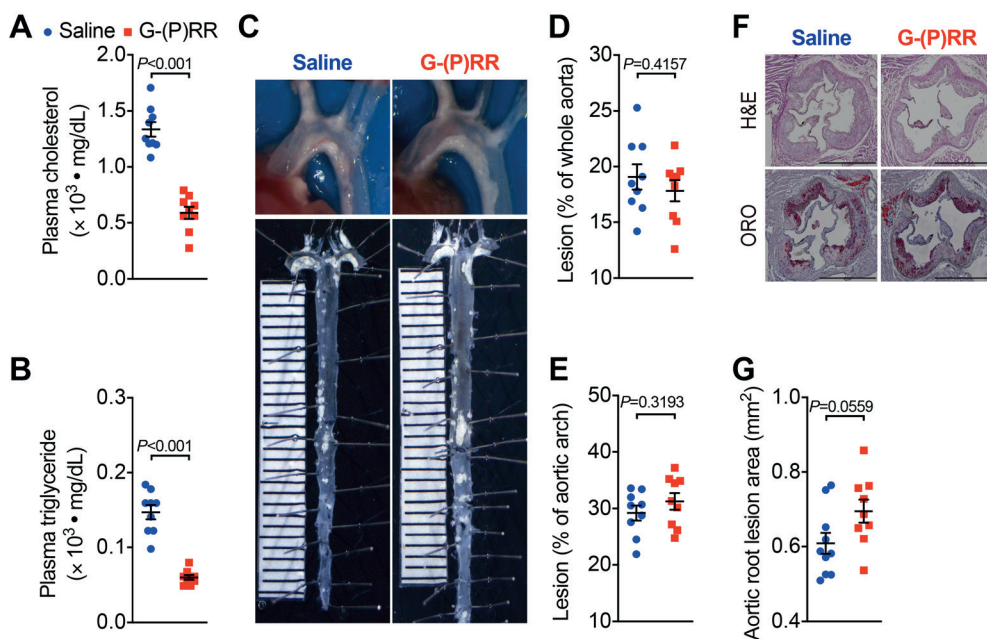
Highlights:

- (P)RR G-ASOs reduce plasma cholesterol and triglycerides concentrations in atherosclerotic mice due to hepatic (P)RR deficiency
- (P)RR G-ASOs also reduces macrophage (P)RR expression and augmented its inflammatory response
- Deletion of macrophage (P)RR accelerates atherosclerosis in ApoE^{-/-} mice

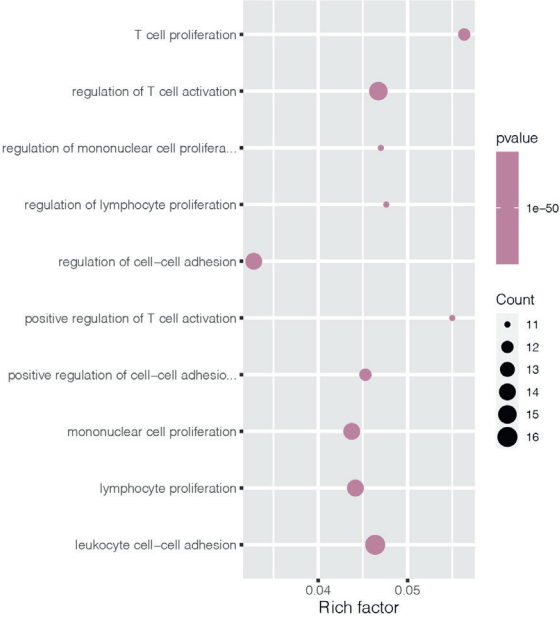
Supplement data



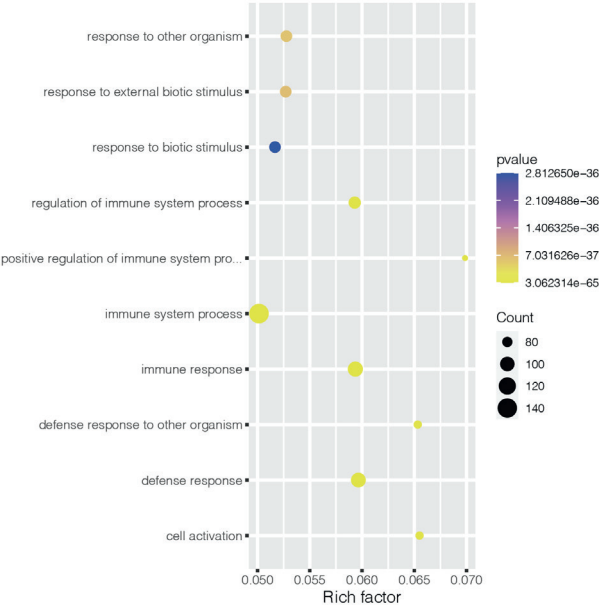
Supplemental Figure I. Systolic blood pressure (A) and plasma renin activity (B) of saline (blue) or (P)RR G-ASOs (red) treated $LDLR^{-/-}$ mice fed with WTD for 16 weeks.



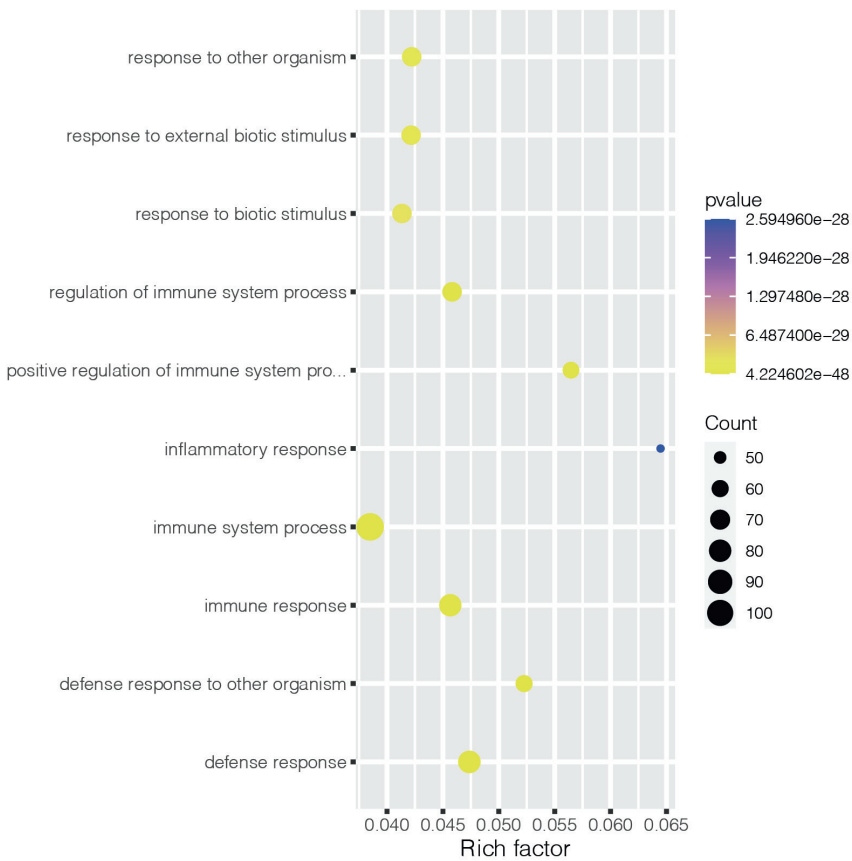
Supplemental Figure II. (P)RR G-ASOs reduces plasma lipids but not atherosclerosis in $ApoE^{-/-}$ mice. Eight-week-old $ApoE^{-/-}$ mice were treated with saline (blue) or (P)RR G-ASO (red) and fed a WTD for 16 weeks. Plasma cholesterol (A) and triglycerides (B). Representative images of aortic arch and en face whole aorta (C). Quantification of lesion are in whole aorta (D) or aortic arch region (E). Representative images showing H&E and ORO stained sectioned aortic root (F), and quantification of lesion size in aortic root (G).



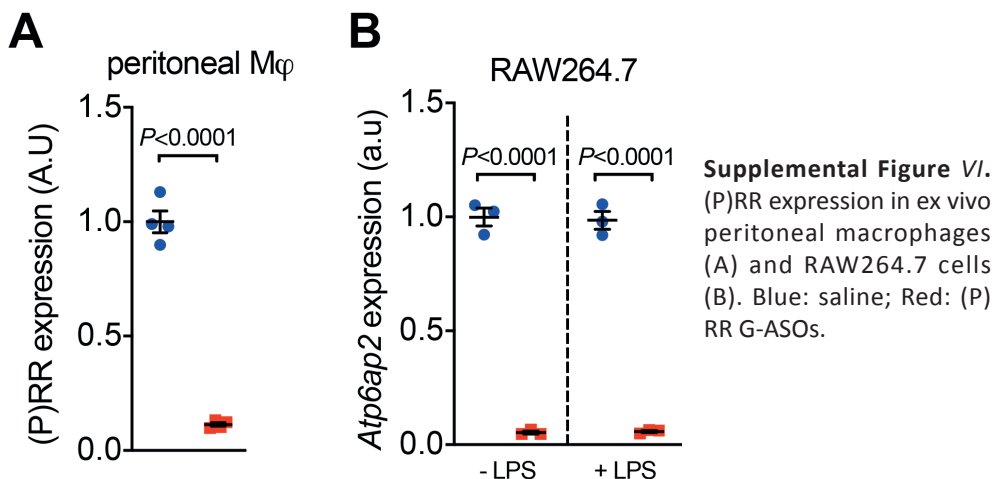
Supplemental Figure III. GO enrichment analysis of biological processes. DEGs (saline treated WTD-fed LDLR^{-/-} mice for 4 weeks vs 0 week control) were used.

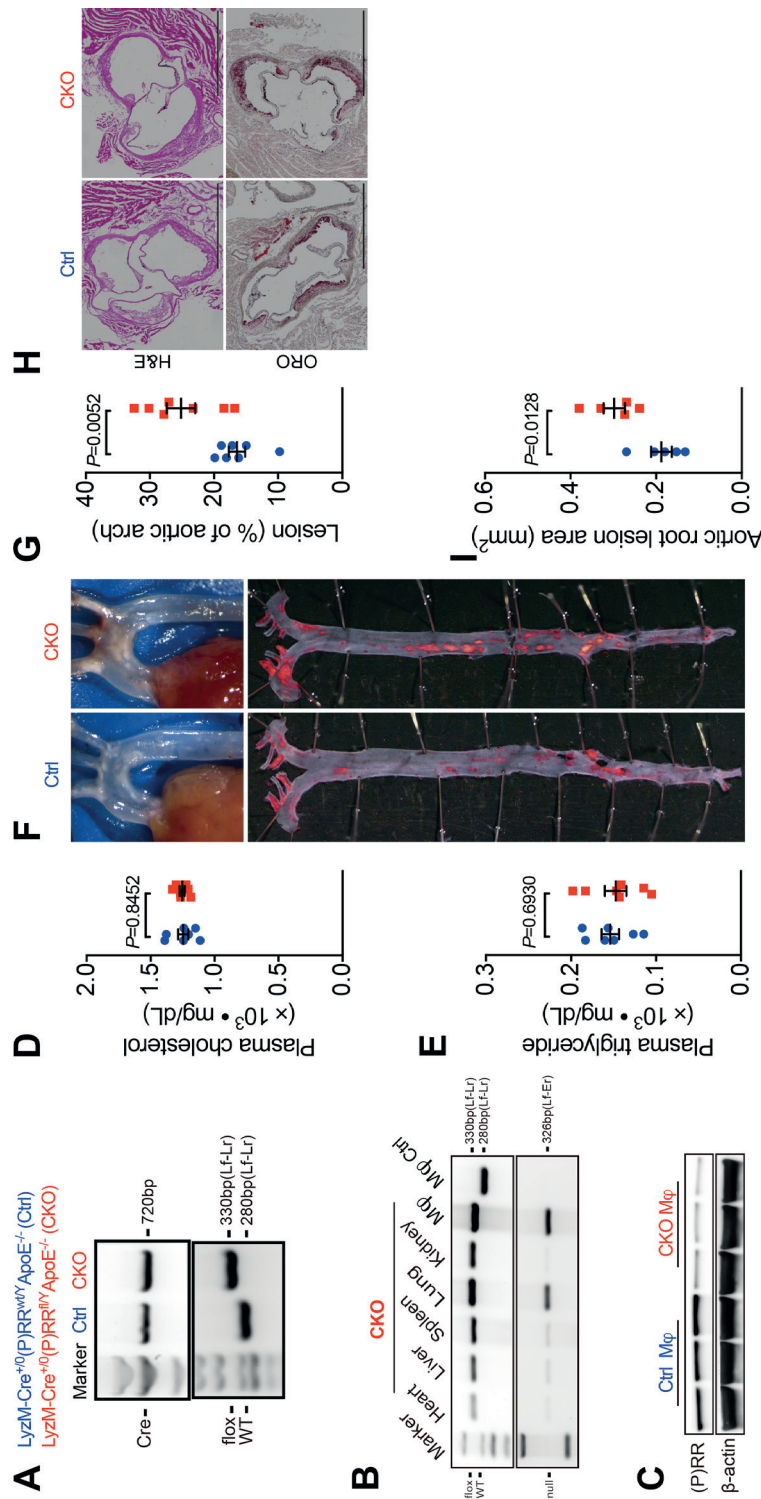


Supplemental Figure IV. GO enrichment analysis of biological processes. DEGs [(P)RR G-ASOs treated WTD-fed LDLR^{-/-} mice for 4 weeks vs 0 week control] were used.

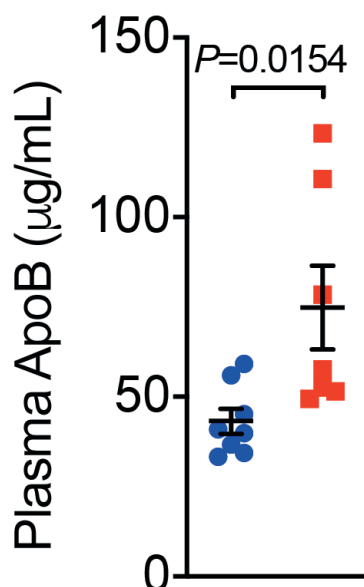


Supplemental Figure V. GO enrichment analysis of biological processes. Non-overlapped DEGs {[(P)RR G-ASOs 4 weeks vs 0 week] vs (saline 4 weeks vs 0 week)} were used.





Supplemental Figure V/I. Deleting (P)RR in macrophages accelerates atherosclerosis in ApoE^{-/-} mice. Eight-week-old *Lyz2-Cre^{re/+0} (P)RR^{wt}/ApoE^{-/-}* mice (Ctrl) and *Lyz2-Cre^{re/+0} (P)RRfl/VApoE^{-/-}* mice (CKO) were fed a WTD for 12 weeks. Genotyping of the mice (A). Deletion of (P)RR in macrophages were confirmed by PCR and western blotting (B&C). Plasma cholesterol and triglycerides (D&E). Representative images showing aortic arch and ORO stained whole aorta (F). Quantification of lesion area in aortic arch region (G). Representative images showing H&E and ORO stained sections of aortic root (H), and quantification of lesion size in aortic root (I).

Saline G-(P)RR

Supplemental Figure VIII. Plasma ApoB concentrations of saline (blue) or (P)RR G-ASOs (red) treated $LDLR^{-/-}$ mice fed a WTD for 16 weeks.

Supplemental Table I. Primers used.

Target		Sequence
(P)RR	Forward	5'-GGGTGGATAAACTGGCACTTC-3'
	Reverse	5'-TGGAATTTGCAACGCTGTC-3'
36b4	Forward	5'-ACTGGTCTAGGACCCGAGAAG-3'
	Reverse	5'-CTCCACCTTGCTCTCCAGTC-3'
Il1b	Forward	5'-AACTGTTCTGAACTCAACTGT-3'
	Reverse	5'-GAGATTTGAAGCTGGATGCTCT-3'
Tnfa	Forward	5'-AAGCCTGTAGCCACGTCGTA-3'
	Reverse	5'-GGCACCAGTAGTTGGTTGTCTTTG-3'
Il6	Forward	5'-TAGTCCTTCCTACCCCAATTTC-3'
	Reverse	5'-TTGGTCCTTAGCCACTCCTTC-3'
Il10	Forward	5'-GCTGCGGACTGCCTTCA-3'
	Reverse	5'-TGCATTAAGGAGTCGGTTAGCA-3'
Lf	Forward	5'-AGCACTCTCTTCCAGGTATGTTGTG-3'
Lr	Forward	5'-CTGGATCCCGGAGCATGGGTAAAGG-3'
Er	Forward	5'-GCCCCTCTCTTACAGTTCTATCAGT-3'
Cre	Forward	5'-GCTGCCACGACCAAGTG-3'
	Reverse	5'-TCGCCATCTTCCAGCAG-3'

Supplemental table II
M1 signature
Irg1, Ccl2, Csf2, Marcks1, Il23a, Cmpk2, Rtp4, Slc7a11, Maff, Gpr85, Pde4b, Trex1, Ier3, Ifi47, Nfkbie, Oasl2, Gdf15, Cdkn1a, Slc7a2, Gem, F10, Oas2, Il15, Rnd3, Gbp2, Lif, Irf1, Fabp3, Src, Slc39a14, Ccl9, Ripk2, Plagl1, Iigp1, Rel, Tap1, Sphk1, Stat5a, Sh3bp5, Lad1, Adm, Lcp2, Zc3h12a, Calcr1, Irgm1, Arid5a, Arrdc4, Cebpd, Junb, Etv6, Stk40, Nfkb1, Daxx, E2f8, Tlr7, Fam129a, Tmem2, Znfx1, Cav1, Mmp13, Plek, Trib3, Herpud1, Asns, Tgm2, Klf7, Ptprj, Ccdc86, Slc1a4, Nmi, Tpst1, Hk2, Osgin2, Slamf9, Egr1, Akna, Atp10a, Phldb1, Sesn2, Rbpj, Mthfd2, Parp12, Aff1, Slc12a4, Tor3a, Ogfr, Kpna3, Plagl2, Casp7, Ugcg, N4bp1, Igsf8, Rasa2, Tank, Rcsd1, Trim13, Marcks, Siah2, Hivep1, Rbbp8, Tnfaip2, Tcof1, Myd88, Apbb1ip, Dab2, Psmb10, Stip1, Sp100, Myo10, Psme2, Mtmr14, Plaur, Il2rg, Aftph, Tars, Appl1, Myo1g, Dck, Sap30, Fcgr2b, Sertad2, Rabgef1, Azi2, Rnf19b, Nck1, Vav3, Trim34, Itgav, Prdm1, Aebp2, Larpl, Eef1e1, Ifitm3, Rela, Aars, Epsti1, Slc4a7, Rps6ka2, Rnf14, Gars, Tor1aip1, Katna1, Ddx21, Eif2s2, Nampt, Zfand3, Wars, Wdr43, Aida, Ube2f, Rps6ka4, Ptpn2, Sbds, Notch2, Nup62, Txnrd1, Top1, Eif6, Klf6, Gtpbp2, Lz-tfl1, Hspa9, Mat2a, Abca1, Ptpn12, Surf4, B3gnt2, Ghitm, Gtf2b, Slc3a2, Bcl10, Srgn, Sqstm1, Atf4, Tapbp, Eif3c, Hspa5
M1 Macrophage Polarization
Tnf, Ccl5, Ccr7, Irf1, Il6, Kynu, Cd86, Marco, Il1a, Cd14, Cd40, Cxcl11, Il1b, Cxcl10, Cxcl9, Cd80, Irf5, Ido1,
Type I Interferon response
Trex1, Rtp4, Oasl1, Ly6e, Il15, Ifi441, Irf1,
Pro-inflammatory
Tnf, Ccl2, Ccl3, Il2, Ccl4, Tlr4, Il17a,
Monocyte
Cd14, Ly6cl1, Ly6c2, Adgre1, Ly6g5b, Sirpa,
Apoptosis
FasL, Jun, Sptan1, Ccnd1, Prf1, Bid, Cdkn1a, Il18, Bax, Tnfsf10, Casp8, Tnfrsf12a, Casp9, Cflar, Mcl1, Il1b, Diablo, Birc3, Bcl2l11, Casp6, Gadd45a, F2r, Bik, Casp3, Cd44, Il1a, Tnf, Sqstm1, Ddit3, Btg3, Satb1, Igfbp6, Bnip3l, Dffa, Gsn, Cdkn1b, Egr3, Casp7, Fas, Pmaip1
CD8 T cell activation
Ctla4, Eomes, Icos, Ccr7, Cd8a, Il2ra, Lag3, Cd69, Cd8b1, H2-Ea-ps, Tnfrsf4, Ifng, Cd40lg, Tnfrsf9, Cd47, Tnfrsf18, Gzma, Cd3e, Prf1, Btla, Gzme, Gzmd, Gzmg, Gzmf, Gzmn, Gzmc, Gzmb, Cd27, Lamp1

Inflammatory Response

H2-M11, Il1rl1, Il2ra, Csf3, Bcl6, Ptpn11, H2-Q5, Crh, Srgn, Atg5, Eno1, Tlr9, H2-M9, FasL, C4b, Met, Defb14, Tslp, Lep, Tnfsf9, H2-M1, H2-Q6, H2-Q7, Cr11, Notch1, Abcg3, Jun, Pla2g4a, Plg, Optn, Nod2, Flt1, Stat5b, H2-M10.5, H2-Q10, H2-M10.6, Idh1, Areg, Cyp2d22, Gstm6, Rtn4, Erap1, Ripk2, Apob, Map3k4, Hoxa10, Trpv1, Brd4, Aqp1, Lyn, Tnfsf14, Grm3, Tpsab1, Il12a, C3, Mgp, Stard5, Il18r1, Cyld, Il-17ra, Prkcb, Fadd, Htt, Nlrp4b, Agtr1a, Gfer, Tlr2, Tbxas1, Irf4, Hrh4, Plaur, Stab1, Map3k8, Alox12, Rorc, Myh9, Cd300a, Bmyc, Camk4, Tnip1, Tlr1, Spn, Il17a, Xrcc1, Gm10031, Mmp2, Camk1d, Adrb3, Ano6, Bad, Gstm2, Cyp2d11, Cyp2d10, Egfr, Pik3ca, Ppargc1a, Prlr, Stat5a, Il11, Map3k14, Fn1, Mas1, Gpr4, Ccdc3, Stat3, Tlr6, Trp63, Nlrp4f, Nlrp4a, Nlrp4c, Nlrp4e, Terf2ip, Abca1, Tax1bp1, Bace1, Prkcz, Ogg1, Ccnd1, Glp2r, Bdkrb1, Itga3, Prf1, Tpsb2, Fgf15, Apc, Lgals1, Casp12, Vcan, Bdkrb2, Map3k7, Bmp6, H2-M5, Mecp2, Ptpa, Pik3cg, Irak1, Sulf1, Ptgs1, Trim28, Pycard, Npsr1, Ager, Fgf2, Ptafr, En1, Ppp1r13l, Hdac3, Jazf1, Ptger4, Dusp10, Ctgf, Ptgs2, Arrb2, P2rx1, Shbg, Rhoa, Pdcd1lg2, Cldn1, Nov, Sod3, Oprm1, Tgfb2, Il21, Cbl, Pim2, Ngf, Mapk14, Orail, Trem2, Havcr2, Ceacam10, Ccl27a, Trp53, Cyp2d9, Park7, Sema3a, Mapk7, Ccl20, Trem1, Gm21973, Itgam, Prkaa1, Il2, Rarres2, Cyp2j13, Cyp2j9, Ptpcr, Esr2, Rxra, Itgal, Irf3, Ptpn6, Crhr1, Nos2, Osm, Iapp, Alox5, Grn, Plce1, Hsp90ab1, Cx3cl1, Prtn3, Ndr1, Mcam, Inhba, Aqp4, Pin1, Bcr, Itgb2, Il7, Il1rap, Itga2b, Hsf1, Cd274, Plau, Cd86, Tnfrsf11b, Gpr68, Scrib, Adcyap1r1, Fcgr2b, Fcgr3, Mvk, Muc16, Cnr1, Cdkn1a, Rit1, Trpv4, Ifnl2, Ifnl3, Rps6ka5, Sigmar1, Fcgr4, Col2a1, Itgb7, Sumo1, Il22ra1, Rock1, Lif, Alox15, Prdx1, Cnr2, Tlr5, Ucp2, Cdh1, Klf6, Rhoc, Ntn1, Pdgfb, Wwox, Jam3, Bach2, Calr, Homer1, Apln, Casr, Dusp4, Pon1, Egfl7, Usp4, Gkn1, Vdr, S100a4, Jak1, Igflr, Polb, Il18, Casp8, Map2k3, Serpine2, Smad7, Sirt1, Trpm7, Map2k2, Ryr1, Npas3, Pthlh, Hmox1, Ahsg, Cd36, Pink1, Tnfsf10, Cga, Ppp5c, Nlrp1a, Nlrp1b, Il6st, Pdpr1, Hfe, Tnfsf12, Cebpg, Tnfrsf12a, Sdc1, Scnn1a, Bap1, Nfe2l2, Il17rc, Prkcd, Igfbp2, Tnfrsf8, Aldh2, Nr3c1, Cd48, Tnfrsf1a, Nr1h2, Flt3l, Sdc2, Il2rg, Gm20489, Ppara, Slc2a1, Nampt, Nfat5, Tlr4, Il7r, Il4ra, Adamts4, Ikbkb, Adora3, Ifngr1, Il1rn, Ifna15, Ifna14, Ifna9, Ifna12, Ifna13, Ifna16, Ifna2, Ifnab, Ifna7, Ifna11, Ifna6, Ifna5, Ifna4, Ifna1, Ppm1d, Syk, Tff1, Wrn, Pag1, Xbp1, Elane, Muc4, Gm10184, Myoc, Hdac4, Fut1, Myc, Foxo1, Ghssr, Egr1, Prdx2, Pdpn, Mal, Arrb1, Il31ra, Vim, Ripk1, Adora2b, Mapk1, Fhit, Esr1, Nr4a2, Has1, Thada, Angptl2, Gclc, Ifnb1, Arid3a, Ccne1, Tab1, P2ry12, Lpar3, Kcnn4, H2-M3, H2-M2, H2-K1, Muc5ac, Dab2, Runx3, Dapk1, Tnfrsf11a, Ly96, Phlpp1, Dst, Ednra, Cflar, Mapt, Pgrmc1, Trib1, Gm13306, Tfrc, Igfbp5, Kit, Bcl3, Gm21541, Gm13304, Gna12, Ptgdr, S100a8, Sgk1, Flg, Cebpa, Pten, Sfrp1, Vgll3, Ret, Pnpla3, Ngfr, Foxp3, Prkci, Pirb, Lila5, Gm14548, Gm15922, Lila6, Gm15448, Pira2, Lila4b, Lila4a, Gm49339, Adamts13, Phb, Cd200, Trap1, Anpep, Adk, Apol7a, Apol9a, Apol7b, Apol10a, Apol11a, Apol7c, Apol10b, Apol11b, Apol7e, Apol9b, Apol8, Il1f6, Psg16, Ceacam3, Psg29, Scnn1b, Apoa2, Cxcl10, Foxp1, Tac1, Ciita, Hspb1, Mitf, Mmp13, Spp1, Csf2, Snx9, Gja1, Apom, Gna11, Braf, Serpinh1, Tollip, Casp9, Adora2a, Cd244a, Tnfsf13, Ido1, Clqtfn3, Scnn1g, Pdcd1, Colla1, Cxcl12, Pdgha, S100a9, Pfkfb4, Oxtr, Abcb11, Ikzf1, Scarb1, Alpl, Tnfrsf1b, Cyp4a32, Cyp4a30b, Cyp4a10, Cyp4a31, Anxa1, Smad2, Adar, Ins2, Smad4, Irf5, Ubd, Atf4, Ier3, Tln1, Itgb3, Bcl10, Tor1a, Il33, Lmna, Jak3, Klf4, Nr4a1, Lgals8, Tmem9, Relb, Hspa4

Chapter 6

Inflammatory Response

Cxcr4, Ptger2, Stk39, Nradd, Ptpkr, Agtr1b, Nlrp3, Prom1, Slamf1, Pld2, Fabp4, Chuk, Il6ra, Ddr1, Fbln5, Rel, Cfr, Hif1a, Cyp19a1, Cav1, Klf5, Creb3l3, Inpp5d, Bax, Prl3a1, Prl6a1, Prl2c2, Prl8a2, Prl2c5, Prl2b1, Prl8a6, Prl8a8, Prl8a9, Prl8a1, Prl7b1, Prl7a1, Prl, Prl7a2, Prl3d1, Prl3d2, Prl7d1, Prl3d3, Prl7c1, Prl2a1, Prl2c1, Prl4a1, Prl5a1, Prl3c1, Prl3b1, Fpr1, Nrg1, Nr3c2, Cyp26b1, Prkg1, Ccr7, Zmiz1, Ywhaq, Mef2c, Ptgir, Nod1, Sod2, Alk, Gm49368, Cyp2d12, Cyp2d34, Cyp2d40, Cyp2d26, Bche, Apoe, Cxcl16, Nfia, Robo1, Selenos, Ltbr, Tnfrsf14, Bcl2, Fgf21, Rnaset2b, Cldn2, Hnmt, Atp11a, Setd7, Foxo3, Cfl1, Smad3, Ccr3, Cd83, Mcl1, Eng, Nos3, Prrc2a, Fstl1, Gba, Socs3, Tacr1, Ifngr2, Fgf10, Vcam1, Inpp4b, Ace2, Ar, Cd44, Nr2f2, Agtr2, Nudc, Nr1h4, Ace, Rarres1, Adgrb1, Sbno2, Lag3, Chil1, Ccl21a, Myd88, Mid1, Prmt5, Cxcr5, Tnf, S1pr2, Crebbp, Slc6a4, Adm, Scn10a, Olr1, Il1a, Smad1, Adcyap1, Pak1, Camp, Tnfaip8l2, Cdk5, Myo9b, Tab2, Hsp90b1, Erbb2, Ets1, Irf7, Egl1, Gnas, Cln3, Tgfb1, Retnla, Retnlg, Cdh11, Siglece, Rgs2, Ikbkg, Csf1r, Hrh1, Ptk2, Cdkn1b, Fndc4, Tnfrsf25, Pomc, Bpifb1, Calca, Map2k4, Pla2g2a, Nfkb1, Dmbt1, Ptgfr, Entpd1, Cd28, Map4k4, Gli1, Sphk1, Tbk1, Pltp, Erg, Il4, Itch, Hnf1a, Ptgis, Hnf4a, Apex1, Psm10, Ghrl, Vwf, Hmmer, Spred2, Ifng, Ctl4, Thbs1, Ada, Hpse, Bdnf, Alb, Rps6kb1, Gpr55, Sp3, Cyba, Dlk1, Kdr, Egf, Ctsd, Gm49369, Oxt, Ranbp2, Cd40, G6pc3, Itga2, Nts, Abcb1a, Abcb1b, Mavs, Map2k5, Duox1, Ctsk, Tshr, Traf2, Ticam1, Cd180, Il34, Elavl1, Prkca, Itga4, Txnrd1, Traf3ip2, Ipmk, Zyx, Bmp4, Adam17, Egr2, Trpc1, Tnfsf15, Slc38a9, Tle1, Prl2c3, Nr0b2, Slc39a11, Ctnnbip1, Plcg1, Trpc5, Pglyrp1, Tnfaip3, Ecm1, Socs2, Wnt5a, Meritk, Gata2, Ceacam5, Ceacam14, Gm5155, Ceacam11, Ceacam13, Ceacam12, Psg18, Psg28, Psg26, Psg25, Psg27, Psg21, Psg23, Psg20, Psg22, Psg19, Ceacam1, Psg17, Ceacam2, Rasgrp1, Klk1b8, Klk1b9, Klk1b1, Klk1b11, Klk1b26, Klk1b27, Klk1b21, Klk1b22, Klk1b16, Klk1b3, Klk1b4, Klk1b24, Klk1b5, Klk1, Edn1, Mpo, Blnk, Map2k1, Angpt2, Crp, Pdyn, Ccr1, Ccr1l1, Yy2, Yy1, Parp1, Map3k5, Cd226, Snail, Aicda, Mthfr, Irf2, Arf6, Il22, Il1fb, Stat1, Traf1, Cd40lg, Rbpj, Adcy3, Ackr1, Psm4, Cisd1, Slit3, Tnfrsf26, Tnfrsf22, Tnfrsf23, Pgf, Chrna7, Igf1, Serpinb2, Clu, Serpine1, Ltb, Pla2g7, Slc22a5, Slc22a21, Eln, Slit2, Traf6, H2-D1, H2-Q1, H2-Q2, H2-Q4, H2-T22, H2-T23, Gm11127, H2-B1, H2-T10, Gm7030, Gm8909, H2-T3, H2-M10.2, H2-M10.1, H2-M10.3, H2-M10.4, Nes, Prkcq, Adipoq, S100b, Casp6, Srebf2, Cbr3, Cltc, Epo, Trpc6, F3, Tmbim6, Ctnnd1, F10, Efnb1, Ahr, Hcar2, Pdgfrb, Birc5, Pik3cb, Nfkb1a, Creg1, Tnfsf13b, Elf3, Tyk2, Grem1, Xdh, Src, Tiam1, Vegfa, Bpi, Icosl, Clec4e, Brd2, Ednrb, Tnfrsf17, Cdc37, Spred1, Bcl2l11, Gper1, Mme, Faah, Timp1, Foxf1, Icam1, Rarb, Nfatc2, Retn, Cd47, Ptx3, H2-Eb2, Mdm2, Tnfrsf21, Irak3, Ffar1, Irf8, Ccl2, F2r, Satb1, Cntf, Il10, Nfatc4, Itgb2l, Tek, Pin1rt1, Il27, Cd19, Ntrk3, Fut2, Ffar2, Tgfa, Il25, Gpc5, Rictor, Ormdl3, Il1r2, Adamts9, Igfbp3, Cd4, Irak4, Shh, Med1, Sqstm1, Clqa, Traf5, Dio2, Nlrc4, Habp2, Pkm, Tymp, Muc1, Litaf, Selp, Akt1, Zap70, Hdac1, Bmp2, Mill1, Mill2, Hnrnpd, Ifi206, Ifi209, Ifi207, Ifi204, Ifi203, Ifi202b, Tbx21, Rac1, Rev3l, Txn1, Il24, Prkd1, Il12b, Ep300, Glul, Il23r, Kat2b, Lin28a, Cybb, Ptpn22, Ntrk1, Ifnar1, Map2k6, Kpna2, Btk, Nusap1, Itga5, F2, Ikzf3, Cdh5, Il13, Htr2a, Ctnnb1, Nox1, Gch1, Enpp2, Diablo, Cdk5r1, Apoa1, Fyn, Casp3, F2r1l, Csf1, Il1b, Fgf23, Cd247, Hsp90aa1, Adam10, Malt1, Bst2, Pik3cd, Acl, Dcn, Ctsb, Tgfb2, Smad6, Il10ra, Vip, Ncstn, Rgs16, S1pr3, Slc9a3, Pgr, Flt4, Acvr1, Prkdc, Gsk3b, Sod1, Mmp9, Has2, Thbd, Rcan1, Lta, Cebpb, Dio3, Eif2ak2, Postn, Tgfb1

Inflammatory Response

Il12rb1, Mmp3, Klrk1, Slc9a1, Ikzf2, Ccl28, Socs5, Serping1, Pappa, Sost, Rb1, F7, Gsto1, Apcs, Aimp1, Eif4g1, E2f1, Pparg, Masp1, Creb1, Kitl, Fli1, Irs1, Ptpn1, Kl, Serpinc1, Socs1, Pkd1, Bcl2l1, Hamp2, Hamp, Trpm8, Tnfrsf4, Plat, Ccr6, Twist1, Dnmt1, Slc7a5, Ddx58, Cxcr2, Csnk2a1, Ccl19, Nedd9, Ccr5, Star, Hpgd, Keap1, Ncf2, Axl, Agt, Jag1, Mtdh, Atf3, Sdc4, Nppc, Lrrk2, Bmp7, Hsh2d, Gdf15, Sp1, Adipor1, Tnc, Il6, Rnaset2a, Il1r1, Erbb4, App, Angpt1, Tab3, Tirap, Gckr, Clock, Cd93, Snca, Mst1, Comt, Ezh2, Cxcr3, Dock2, Il13ra2, Bcl2a1d, Bcl2a1a, Gm29094, Bcl2a1b, Lepr, Cd59b, Cd59a, Ror2, Etv6, Pde4b, Gip, Hspa1b, Hspal1a, Fos, Stk11, Lpar1, Nr4a3, Cirbp, Adipor2, Hc, Pim1, F8, Hyal1, Il20, Epas1, Prok1, Tlr7, P2rx7, Adam15, Snai2, Gab2, Itga1, Sftpb, Cd55b, Cd55, Rapgef3, Kras, Il5, Ptpn2, Pecam1, Ikbke, Mcph1, Ctss, Ccr8, Rnf11, Mc1r, Traf3, Procr, Il9, Zfp831, Dusp16, Cdkal1, Aplnr, Nr1h3, Mtus1, Brca2, Fndc5, Tlr8, Irs2, Gzmc, Gzmb, Stim1, Il15, Gpbar1, Mif, Bmx, Itgav, Tnfsf11, Sirt6, Sele, Npy, Dll4, Ppard, Nr1i2, Prok2, Birc3, Irf1, Lcn2, Gsk3a, Lum, Hgf, Adm2, Nppa, Rela, Lgals3, Rspo3, Clec7a, Nox4, Srebf1, Bmpr2, Icos, Hspa5, Tbx2r, Mst1r, Gstp1, Gstp2, Akt2, Cd209a, Cd209e, Cd209d, Cd209b, Cd209c, Psen1, Birc2, S1pr1, Mapk9, Tgm2, Cebpd, Mtor, Serpinf1, C5ar2, Mmp1b, Mmp1a, Dusp1, Adcy7, Gcg, Apod, Mirlet7a-1, Mir122, Tmem173, Dpp4, Cd74, Gm5849, Mir200b, Mir219a-2, Pdcd4, Ins1, Stat2, Gm28635, Gm6665, Cd46, Il2rb, Serpina1b, Serpina1d, Serpina1a, Serpina1c, Serpina1e, Ndfip1, Mir200c, Mir222, Mir29a, Il23a, Casp1, Mir155, Cd34, Ankrd2, Trib2, Dab2ip, Mapk3, Eno1b, Nfatc1, Fads2, Mir22, Mir143, Stat6, Itgb1, Itga6, Itgb4, Mir101a, Gm10591, Ccl21c, Ccl21b, Ccl27b, Ccl27, Mir29b-1, Sftpc, Nrp1, Isg15, Bsg, Adrb1, Mir200a, Hspg2, Mir24-1, Mir342, Adam28, Mir30a, Lime1, Pbbp, Stc1, Nfkb2, Bcl2a1c, Cd14, Mir23b, Lrp1, Klf9, Igf2, Mmp11, Tlr3, Mir125b-1, Jak2, Gm2564, Ifih1, Mir18, Pdlim2, Mapkbp1, Mir7-1, Mir27b, Mir19b-1, Fas, Hbegf, Fgf7, Mir145a, Adrb2, Sh2d1a, Mapk8, Rbp4, Casp7, Mir142, Mbl2, Mir26a-1, Nkx3-1

Supplemental table III				
Gene ID	log-2FC	PValue	Gene name	Gene description
ENSMUSG000000112449	-2,69	0,0092	Srp54b	signal recognition particle 54B [Source:MGI Symbol;Acc:MGI:3714357]
ENSMUSG000000041771	-2,23	0,0247	Slc24a4	solute carrier family 24 (sodium/potassium/calcium exchanger), member 4 [Source:MGI Symbol;Acc:MGI:2447362]
ENSMUSG000000022066	-2,14	0,0436	Entpd4b	ectonucleoside triphosphate diphosphohydrolase 4B [Source:MGI Symbol;Acc:MGI:5435040]
ENSMUSG000000002985	1,90	0,0499	Apoe	apolipoprotein E [Source:MGI Symbol;Acc:MGI:88057]
ENSMUSG000000021281	2,01	0,0409	Tnfrsf2	tumor necrosis factor, alpha-induced protein 2 [Source:MGI Symbol;Acc:MGI:104960]
ENSMUSG000000025473	2,01	0,0425	Adam8	a disintegrin and metalloproteinase domain 8 [Source:MGI Symbol;Acc:MGI:107825]
ENSMUSG000000049103	2,04	0,0466	Ccr2	chemokine (C-C motif) receptor 2 [Source:MGI Symbol;Acc:MGI:106185]
ENSMUSG000000058818	2,04	0,0401	Pirb	paired Ig-like receptor B [Source:MGI Symbol;Acc:MGI:894311]
ENSMUSG000000024610	2,06	0,0343	Cd74	CD74 antigen (invariant polypeptide of major histocompatibility complex, class II antigen-associated) [Source:MGI Symbol;Acc:MGI:96534]
ENSMUSG000000028581	2,07	0,0351	Laptn5	lysosomal-associated protein transmembrane 5 [Source:MGI Symbol;Acc:MGI:108046]
ENSMUSG000000028327	2,07	0,0451	Stra6l	STRA6-like [Source:MGI Symbol;Acc:MGI:1921402]
ENSMUSG000000030830	2,07	0,0451	Irfal	interferon alpha L [Source:MGI Symbol;Acc:MGI:96606]
ENSMUSG000000055805	2,10	0,0374	Fmn1l	formin-like 1 [Source:MGI Symbol;Acc:MGI:1888994]
ENSMUSG000000021998	2,11	0,0320	Lcp1	lymphocyte cytosolic protein 1 [Source:MGI Symbol;Acc:MGI:104808]
ENSMUSG000000030798	2,11	0,0374	Cd37	CD37 antigen [Source:MGI Symbol;Acc:MGI:88330]
ENSMUSG00000018774	2,12	0,0315	Cd68	CD68 antigen [Source:MGI Symbol;Acc:MGI:88342]
ENSMUSG000000071713	2,14	0,0325	Csf2rb	colony stimulating factor 2 receptor, beta, low-affinity (granulocyte-macrophage) [Source:MGI Symbol;Acc:MGI:1339759]
ENSMUSG000000073421	2,14	0,0291	H2-Ab1	histocompatibility 2, class II antigen A, beta 1 [Source:MGI Symbol;Acc:MGI:103070]

ENSMUSG00000000290	2,15	0,0309	Itgb2	integrin beta 2 [Source:MGI Symbol;Acc:MGI:96611]
ENSMUSG00000026832	2,17	0,0375	Cytip	cytohesin 1 interacting protein [Source:MGI Symbol;Acc:MGI:2183535]
ENSMUSG00000022468	2,17	0,0375	Endou	endonuclease, polyU-specific [Source:MGI Symbol;Acc:MGI:97746]
ENSMUSG00000045312	2,17	0,0318	Lhfp12	lipoma HMGIC fusion partner-like 2 [Source:MGI Symbol;Acc:MGI:2145236]
ENSMUSG00000045763	2,18	0,0342	Basp1	brain abundant, membrane attached signal protein 1 [Source:MGI Symbol;Acc:MGI:1917600]
ENSMUSG00000046805	2,18	0,0261	Mpeg1	macrophage expressed gene 1 [Source:MGI Symbol;Acc:MGI:1333743]
ENSMUSG00000023992	2,20	0,0278	Trem2	triggering receptor expressed on myeloid cells 2 [Source:MGI Symbol;Acc:MGI:1913150]
ENSMUSG00000028859	2,20	0,0322	Csf3r	colony stimulating factor 3 receptor (granulocyte) [Source:MGI Symbol;Acc:MGI:1339755]
ENSMUSG00000022415	2,20	0,0330	Syng1	synaptogyrin 1 [Source:MGI Symbol;Acc:MGI:1328323]
ENSMUSG00000048163	2,22	0,0293	Selp1g	selectin, platelet (p-selectin) ligand [Source:MGI Symbol;Acc:MGI:106689]
ENSMUSG00000030707	2,23	0,0246	Coro1a	coronin, actin binding protein 1A [Source:MGI Symbol;Acc:MGI:1345961]
ENSMUSG00000035004	2,23	0,0328	Igsf6	immunoglobulin superfamily, member 6 [Source:MGI Symbol;Acc:MGI:1891393]
ENSMUSG00000018654	2,24	0,0293	Ikzf1	IKAROS family zinc finger 1 [Source:MGI Symbol;Acc:MGI:1342540]
ENSMUSG00000060586	2,24	0,0228	H2-Eb1	histocompatibility 2, class II antigen E beta [Source:MGI Symbol;Acc:MGI:95901]
ENSMUSG00000020143	2,24	0,0285	Dock2	dedicator of cyto-kinesis 2 [Source:MGI Symbol;Acc:MGI:2149010]
ENSMUSG00000002111	2,24	0,0260	Spi1	spleen focus forming virus (SFFV) proviral integration oncogene [Source:MGI Symbol;Acc:MGI:98282]
ENSMUSG00000029816	2,26	0,0212	Gpmb	glycoprotein (transmembrane) nmb [Source:MGI Symbol;Acc:MGI:1934765]
ENSMUSG00000036594	2,26	0,0216	H2-Aa	histocompatibility 2, class II antigen A, alpha [Source:MGI Symbol;Acc:MGI:95895]
ENSMUSG00000041836	2,29	0,0288	Ptpre	protein tyrosine phosphatase, receptor type, E [Source:MGI Symbol;Acc:MGI:97813]
ENSMUSG00000030789	2,29	0,0231	Itgax	integrin alpha X [Source:MGI Symbol;Acc:MGI:96609]
ENSMUSG00000020911	2,32	0,0268	Krt19	keratin 19 [Source:MGI Symbol;Acc:MGI:96693]

ENSMUSG000000030263	2,32	0,0253	Lrmp	lymphoid-restricted membrane protein [Source:MGI Symbol;Acc:MGI:108424]
ENSMUSG000000026395	2,33	0,0205	Ptpnc	protein tyrosine phosphatase, receptor type, C [Source:MGI Symbol;Acc:MGI:97810]
ENSMUSG000000028238	2,34	0,0207	A t p - 6v0d2	ATPase, H+ transporting, lysosomal V0 subunit D2 [Source:MGI Symbol;Acc:MGI:1924415]
ENSMUSG000000040747	2,35	0,0190	Cd53	CD53 antigen [Source:MGI Symbol;Acc:MGI:88341]
ENSMUSG00000112148	2,37	0,0201	Lilrb4a	leukocyte immunoglobulin-like receptor, subfamily B, member 4A [Source:MGI Symbol;Acc:MGI:102701]
ENSMUSG000000034652	2,39	0,0204	Cd300a	CD300A molecule [Source:MGI Symbol;Acc:MGI:2443411]
ENSMUSG00000112023	2,42	0,0157	Lilr4b	leukocyte immunoglobulin-like receptor, subfamily B, member 4B [Source:MGI Symbol;Acc:MGI:102702]
ENSMUSG000000041515	2,44	0,0166	Irf8	interferon regulatory factor 8 [Source:MGI Symbol;Acc:MGI:96395]
ENSMUSG000000020901	2,46	0,0153	Pik3r5	phosphoinositide-3-kinase regulatory subunit 5 [Source:MGI Symbol;Acc:MGI:2443588]
ENSMUSG000000025877	2,49	0,0151	Hk3	hexokinase 3 [Source:MGI Symbol;Acc:MGI:2670962]
ENSMUSG000000024737	2,52	0,0149	Slc15a3	solute carrier family 15, member 3 [Source:MGI Symbol;Acc:MGI:1929691]
ENSMUSG000000038642	2,53	0,0107	Ctss	cathepsin S [Source:MGI Symbol;Acc:MGI:107341]
ENSMUSG000000029925	2,56	0,0146	Tbxas1	thromboxane A synthase 1, platelet [Source:MGI Symbol;Acc:MGI:98497]
ENSMUSG000000049382	2,63	0,0125	Krt8	keratin 8 [Source:MGI Symbol;Acc:MGI:96705]
ENSMUSG000000071714	2,73	0,0080	Csf2rb2	colony stimulating factor 2 receptor, beta 2, low-affinity (granulocyte-macrophage) [Source:MGI Symbol;Acc:MGI:1339760]
ENSMUSG000000052142	2,82	0,0068	Ras13	RAS protein activator like 3 [Source:MGI Symbol;Acc:MGI:2444128]
ENSMUSG000000033220	2,88	0,0065	Rac2	Rac family small GTPase 2 [Source:MGI Symbol;Acc:MGI:97846]
ENSMUSG000000026822	2,95	0,0049	Lcn2	lipocalin 2 [Source:MGI Symbol;Acc:MGI:96757]
ENSMUSG000000000409	3,08	0,0036	Lck	lymphocyte protein tyrosine kinase [Source:MGI Symbol;Acc:MGI:96756]
ENSMUSG000000049723	3,50	0,0008	Mmp12	matrix metalloproteinase 12 [Source:MGI Symbol;Acc:MGI:97005]
ENSMUSG000000000782	3,96	0,0003	Tcf7	transcription factor 7, T cell specific [Source:MGI Symbol;Acc:MGI:98507]
ENSMUSG000000029304	4,89	0,0000	Spp1	secreted phosphoprotein 1 [Source:MGI Symbol;Acc:MGI:98389]

Supplemental table IV

Gene ID	log2FC	P Value	Gene description
ENSMUSG00000028195	-2,2733	0,0203	cysteine rich protein 61 [Source:MGI Symbol;Acc:MGI:88613]
ENSMUSG00000029675	-2,1512	0,0273	elastin [Source:MGI Symbol;Acc:MGI:95317]
ENSMUSG000000034997	-2,0530	0,0431	5-hydroxytryptamine (serotonin) receptor 2A [Source:MGI Symbol;Acc:MGI:109521]
ENSMUSG000000006538	-2,0330	0,0406	Indian hedgehog [Source:MGI Symbol;Acc:MGI:96533]
ENSMUSG000000026580	1,9216	0,0489	selectin, platelet [Source:MGI Symbol;Acc:MGI:98280]
ENSMUSG000000052688	1,9345	0,0491	RAB7B, member RAS oncogene family [Source:MGI Symbol;Acc:MGI:2442295]
ENSMUSG000000001128	1,9398	0,0458	complement factor properdin [Source:MGI Symbol;Acc:MGI:97545]
ENSMUSG000000004609	1,9676	0,0487	CD33 antigen [Source:MGI Symbol;Acc:MGI:99440]
ENSMUSG000000028832	1,9678	0,0493	stathmin 1 [Source:MGI Symbol;Acc:MGI:96739]
ENSMUSG000000003363	1,9813	0,0415	phospholipase D family, member 3 [Source:MGI Symbol;Acc:MGI:1333782]
ENSMUSG000000054435	1,9820	0,0467	GTPase, IMAP family member 4 [Source:MGI Symbol;Acc:MGI:1349656]
ENSMUSG0000000041378	1,9870	0,0415	claudin 5 [Source:MGI Symbol;Acc:MGI:1276112]
ENSMUSG000000021950	1,9917	0,0459	annexin A8 [Source:MGI Symbol;Acc:MGI:1201374]
ENSMUSG000000050708	1,9942	0,0398	ferritin light polypeptide 1 [Source:MGI Symbol;Acc:MGI:95589]
ENSMUSG000000039062	1,9990	0,0400	alanyl (membrane) aminopeptidase [Source:MGI Symbol;Acc:MGI:5000466]
ENSMUSG000000024349	2,0076	0,0421	transmembrane protein 173 [Source:MGI Symbol;Acc:MGI:1919762]
ENSMUSG000000058624	2,0123	0,0394	guanine deaminase [Source:MGI Symbol;Acc:MGI:95678]
ENSMUSG000000020641	2,0252	0,0470	radical S-adenosyl methionine domain containing 2 [Source:MGI Symbol;Acc:MGI:1929628]
ENSMUSG000000073490	2,0274	0,0381	interferon activated gene 207 [Source:MGI Symbol;Acc:MGI:2138302]
ENSMUSG000000035692	2,0310	0,0431	ISG15 ubiquitin-like modifier [Source:MGI Symbol;Acc:MGI:1855694]
ENSMUSG000000002847	2,0321	0,0422	phospholipase A1 member A [Source:MGI Symbol;Acc:MGI:1934677]
ENSMUSG000000024338	2,0402	0,0395	proteasome (prosome, macropain) subunit, beta type 8 (large multifunctional peptidase 7) [Source:MGI Symbol;Acc:MGI:1346527]
ENSMUSG000000050105	2,0430	0,0466	glycine / arginine rich protein 1 [Source:MGI Symbol;Acc:MGI:1919940]
ENSMUSG000000070427	2,0444	0,0382	interleukin 18 binding protein [Source:MGI Symbol;Acc:MGI:1333800]

ENSMUSG000000024965	2,0531	0,0370	fermitin family member 3 [Source:MGI Symbol;Acc:MGI:2147790]
ENSMUSG000000050022	2,0672	0,0418	archaelysin family metalloproteinase 1 [Source:MGI Symbol;Acc:MGI:2442258]
ENSMUSG000000032122	2,0701	0,0367	solute carrier family 37 (glycerol-3-phosphate transporter), member 2 [Source:MGI Symbol;Acc:MGI:1929693]
ENSMUSG000000030159	2,0783	0,0428	C-type lectin domain family 1, member b [Source:MGI Symbol;Acc:MGI:1913287]
ENSMUSG000000050621	2,0849	0,0325	ribosomal protein S27, retrogene [Source:MGI Symbol;Acc:MGI:3704345]
ENSMUSG000000036553	2,0851	0,0372	SH3 domain and tetratricopeptide repeats 1 [Source:MGI Symbol;Acc:MGI:2678949]
ENSMUSG000000026582	2,0854	0,0421	selectin, endothelial cell [Source:MGI Symbol;Acc:MGI:98278]
ENSMUSG000000053158	2,0858	0,0339	feline sarcoma oncogene [Source:MGI Symbol;Acc:MGI:95514]
ENSMUSG000000035273	2,0947	0,0356	heparanase [Source:MGI Symbol;Acc:MGI:1343124]
ENSMUSG000000073418	2,0970	0,0313	complement component 4B (Chido blood group) [Source:MGI Symbol;Acc:M-GI:88228]
ENSMUSG000000029810	2,0971	0,0320	transmembrane protein 176B [Source:MGI Symbol;Acc:MGI:1916348]
ENSMUSG000000030748	2,0985	0,0322	interleukin 4 receptor, alpha [Source:MGI Symbol;Acc:MGI:105367]
ENSMUSG000000015950	2,1037	0,0339	neutrophil cytosolic factor 1 [Source:MGI Symbol;Acc:MGI:97283]
ENSMUSG000000060063	2,1074	0,0367	arachidonate 5-lipoxygenase activating protein [Source:MGI Symbol;Acc:MGI:107505]
ENSMUSG000000045382	2,1085	0,0361	chemokine (C-X-C motif) receptor 4 [Source:MGI Symbol;Acc:MGI:109563]
ENSMUSG000000015766	2,1273	0,0332	epidermal growth factor receptor pathway substrate 8 [Source:MGI Symbol;Acc:M-GI:104684]
ENSMUSG000000026712	2,1292	0,0295	mannose receptor, C type 1 [Source:MGI Symbol;Acc:MGI:97142]
ENSMUSG000000061068	2,1317	0,0358	mast cell protease 4 [Source:MGI Symbol;Acc:MGI:96940]
ENSMUSG000000001281	2,1358	0,0380	integrin beta 7 [Source:MGI Symbol;Acc:MGI:96616]
ENSMUSG000000027375	2,1489	0,0344	myelin and lymphocyte protein, T cell differentiation protein [Source:MGI Symbol;Acc:MGI:892970]
ENSMUSG000000028459	2,1540	0,0404	CD72 antigen [Source:MGI Symbol;Acc:MGI:88345]
ENSMUSG000000056025	2,1588	0,0308	chloride channel accessory 3A1 [Source:MGI Symbol;Acc:MGI:1316732]
ENSMUSG000000025154	2,1597	0,0293	Rho GTPase activating protein 19 [Source:MGI Symbol;Acc:MGI:1918335]
ENSMUSG000000003644	2,1790	0,0299	ribosomal protein S6 kinase polypeptide 1 [Source:MGI Symbol;Acc:MGI:104558]

ENSMUSG000000027994	2,1863	0,0337	mitochondrial calcium uniporter dominant negative beta subunit [Source:MGI Symbol;Acc:MGI:1914065]
ENSMUSG000000029771	2,1894	0,0275	interferon regulatory factor 5 [Source:MGI Symbol;Acc:MGI:1350924]
ENSMUSG000000024621	2,1909	0,0254	colony stimulating factor 1 receptor [Source:MGI Symbol;Acc:MGI:1339758]
ENSMUSG000000022952	2,1948	0,0323	runt related transcription factor 1 [Source:MGI Symbol;Acc:MGI:99852]
ENSMUSG000000028194	2,1991	0,0349	dimethylarginine dimethylaminohydrolase 1 [Source:MGI Symbol;Acc:MGI:1916469]
ENSMUSG000000023505	2,2035	0,0373	cell division cycle associated 3 [Source:MGI Symbol;Acc:MGI:1315198]
ENSMUSG000000037337	2,2125	0,0339	mitogen-activated protein kinase kinase kinase 1 [Source:MGI Symbol;Acc:MGI:1346882]
ENSMUSG000000024164	2,2205	0,0231	complement component 3 [Source:MGI Symbol;Acc:MGI:88227]
ENSMUSG00000018920	2,2214	0,0247	chemokine (C-X-C motif) ligand 16 [Source:MGI Symbol;Acc:MGI:1932682]
ENSMUSG000000021457	2,2317	0,0238	spleen tyrosine kinase [Source:MGI Symbol;Acc:MGI:99515]
ENSMUSG000000060470	2,2525	0,0287	adhesion G protein-coupled receptor G3 [Source:MGI Symbol;Acc:MGI:1859670]
ENSMUSG000000049130	2,2574	0,0259	complement component 5a receptor 1 [Source:MGI Symbol;Acc:MGI:88232]
ENSMUSG000000022102	2,2576	0,0246	docking protein 2 [Source:MGI Symbol;Acc:MGI:1332623]
ENSMUSG000000073489	2,2601	0,0231	interferon activated gene 204 [Source:MGI Symbol;Acc:MGI:96429]
ENSMUSG000000091649	2,2656	0,0283	PHD finger protein 11B [Source:MGI Symbol;Acc:MGI:3645789]
ENSMUSG000000010651	2,2831	0,0307	acetyl-Coenzyme A acyltransferase 1B [Source:MGI Symbol;Acc:MGI:3605455]
ENSMUSG000000034845	2,2905	0,0198	plasmalemma vesicle associated protein [Source:MGI Symbol;Acc:MGI:1890497]
ENSMUSG000000025743	2,2934	0,0197	syndecan 3 [Source:MGI Symbol;Acc:MGI:1349163]
ENSMUSG000000002668	2,2987	0,0245	DENN/MADD domain containing 1C [Source:MGI Symbol;Acc:MGI:1918035]
ENSMUSG000000001348	2,3003	0,0200	acid phosphatase 5, tartrate resistant [Source:MGI Symbol;Acc:MGI:87883]
ENSMUSG000000037095	2,3016	0,0199	leucine-rich alpha-2-glycoprotein 1 [Source:MGI Symbol;Acc:MGI:1924155]
ENSMUSG000000038811	2,3031	0,0212	guanine nucleotide binding protein (G protein), gamma transducing activity polypeptide 2 [Source:MGI Symbol;Acc:MGI:893584]
ENSMUSG000000022587	2,3056	0,0188	lymphocyte antigen 6 complex, locus E [Source:MGI Symbol;Acc:MGI:106651]
ENSMUSG000000028599	2,3116	0,0198	tumor necrosis factor receptor superfamily, member 1b [Source:MGI Symbol;Acc:MGI:1314883]

ENSMUSG000000006014	2,3177	0,0191	proteoglycan 4 (megakaryocyte stimulating factor, articular superficial zone protein) [Source:MGI Symbol;Acc:MGI:1891344]
ENSMUSG0000000061100	2,3177	0,0193	resistin like alpha [Source:MGI Symbol;Acc:MGI:1888504]
ENSMUSG0000000058099	2,3388	0,0213	Nfat activating molecule with ITAM motif 1 [Source:MGI Symbol;Acc:MGI:1921289]
ENSMUSG0000000034714	2,3402	0,0224	twety family member 2 [Source:MGI Symbol;Acc:MGI:2157091]
ENSMUSG0000000048865	2,3436	0,0191	Rho GTPase activating protein 30 [Source:MGI Symbol;Acc:MGI:2684948]
ENSMUSG0000000030214	2,3457	0,0198	phospholipase B domain containing 1 [Source:MGI Symbol;Acc:MGI:1914107]
ENSMUSG0000000033880	2,3473	0,0172	lectin, galactoside-binding, soluble, 3 binding protein [Source:MGI Symbol;Acc:MGI:99554]
ENSMUSG0000000054196	2,3508	0,0218	collagen triple helix repeat containing 1 [Source:MGI Symbol;Acc:MGI:1915838]
ENSMUSG0000000079419	2,3644	0,0203	membrane-spanning 4-domains, subfamily A, member 6C [Source:MGI Symbol;Acc:MGI:2385644]
ENSMUSG0000000022548	2,3781	0,0165	apolipoprotein D [Source:MGI Symbol;Acc:MGI:88056]
ENSMUSG0000000053835	2,3798	0,0228	histocompatibility 2, T region locus 24 [Source:MGI Symbol;Acc:MGI:95958]
ENSMUSG0000000069917	2,3821	0,0181	hemoglobin alpha, adult chain 2 [Source:MGI Symbol;Acc:MGI:96016]
ENSMUSG0000000042734	2,3849	0,0211	tetratricopeptide repeat domain 9 [Source:MGI Symbol;Acc:MGI:1916730]
ENSMUSG0000000073940	2,3863	0,0179	hemoglobin, beta adult t chain [Source:MGI Symbol;Acc:MGI:5474850]
ENSMUSG0000000037946	2,3915	0,0223	FYVE, RhoGEF and PH domain containing 3 [Source:MGI Symbol;Acc:MGI:1353657]
ENSMUSG0000000038178	2,3924	0,0165	solute carrier family 43, member 2 [Source:MGI Symbol;Acc:MGI:2442746]
ENSMUSG0000000054203	2,3935	0,0185	interferon activated gene 205 [Source:MGI Symbol;Acc:MGI:101847]
ENSMUSG0000000069919	2,3946	0,0151	hemoglobin alpha, adult chain 1 [Source:MGI Symbol;Acc:MGI:96015]
ENSMUSG0000000043004	2,4060	0,0185	guanine nucleotide binding protein (G protein), gamma 2 [Source:MGI Symbol;Acc:MGI:102705]
ENSMUSG0000000024013	2,4083	0,0166	FYVE, RhoGEF and PH domain containing 2 [Source:MGI Symbol;Acc:MGI:1347084]
ENSMUSG000000001865	2,4303	0,0211	carboxypeptidase A3, mast cell [Source:MGI Symbol;Acc:MGI:88479]
ENSMUSG0000000033685	2,4332	0,0137	uncoupling protein 2 (mitochondrial, proton carrier) [Source:MGI Symbol;Acc:MGI:109354]

ENSMUSG00000052142	2,4397	0,0183	RAS protein activator like 3 [Source:MGI Symbol;Acc:MGI:2444128]
ENSMUSG00000037649	2,4422	0,0148	histocompatibility 2, class II, locus DMA [Source:MGI Symbol;Acc:MGI:95921]
ENSMUSG00000074622	2,4483	0,0137	v-naf musculoaponeurotic fibrosarcoma oncogene family, protein B (avian) [Source:MGI Symbol;Acc:MGI:104555]
ENSMUSG00000040613	2,4507	0,0137	apolipoprotein B mRNA editing enzyme, catalytic polypeptide 1 [Source:MGI Symbol;Acc:MGI:103298]
ENSMUSG00000050777	2,4628	0,0178	transmembrane protein 37 [Source:MGI Symbol;Acc:MGI:2157899]
ENSMUSG00000023367	2,4671	0,0133	transmembrane protein 176A [Source:MGI Symbol;Acc:MGI:1913308]
ENSMUSG00000044350	2,4700	0,0171	laccase domain containing 1 [Source:MGI Symbol;Acc:MGI:2445077]
ENSMUSG00000020120	2,4706	0,0132	pleckstrin [Source:MGI Symbol;Acc:MGI:1860485]
ENSMUSG00000015396	2,4716	0,0168	CD83 antigen [Source:MGI Symbol;Acc:MGI:1328316]
ENSMUSG00000030786	2,4772	0,0156	integrin alpha M [Source:MGI Symbol;Acc:MGI:96607]
ENSMUSG00000035697	2,4824	0,0124	Rho GTPase activating protein 45 [Source:MGI Symbol;Acc:MGI:1917969]
ENSMUSG00000079547	2,4879	0,0134	histocompatibility 2, class II, locus Mb1 [Source:MGI Symbol;Acc:MGI:95922]
ENSMUSG00000038910	2,4946	0,0160	phospholipase C-like 2 [Source:MGI Symbol;Acc:MGI:1352756]
ENSMUSG00000006731	2,4946	0,0160	beta-1,4-N-acetyl-galactosaminyl transferase 1 [Source:MGI Symbol;Acc:MGI:1342057]
ENSMUSG00000052305	2,4954	0,0121	hemoglobin, beta adult s chain [Source:MGI Symbol;Acc:MGI:5474852]
ENSMUSG00000013707	2,5086	0,0162	tumor necrosis factor, alpha-induced protein 8-like 2 [Source:MGI Symbol;Acc:MGI:1917019]
ENSMUSG00000056069	2,5128	0,0148	OTU deubiquitinase with linear linkage specificity like [Source:MGI Symbol;Acc:MGI:2687281]
ENSMUSG00000025498	2,5154	0,0119	interferon regulatory factor 7 [Source:MGI Symbol;Acc:MGI:1859212]
ENSMUSG00000025355	2,5226	0,0119	matrix metalloproteinase 19 [Source:MGI Symbol;Acc:MGI:1927899]
ENSMUSG00000074785	2,5339	0,0138	plexin C1 [Source:MGI Symbol;Acc:MGI:1890127]
ENSMUSG00000034947	2,5357	0,0112	transmembrane protein 106A [Source:MGI Symbol;Acc:MGI:1922056]
ENSMUSG00000034641	2,5359	0,0131	CD300 molecule like family member d [Source:MGI Symbol;Acc:MGI:2442358]
ENSMUSG00000031101	2,5548	0,0144	SAM and SH3 domain containing 3 [Source:MGI Symbol;Acc:MGI:1921381]

ENSMUSG000000022372	2,5560	0,0129	src-like adaptor [Source:MGI Symbol;Acc:MGI:104295]
ENSMUSG000000036908	2,5641	0,0100	unc-93 homolog B1, TLR signaling regulator [Source:MGI Symbol;Acc:MGI:1859307]
ENSMUSG000000053175	2,5655	0,0126	B cell leukemia/lymphoma 3 [Source:MGI Symbol;Acc:MGI:88140]
ENSMUSG000000023913	2,5818	0,0100	phospholipase A2, group VII (platelet-activating factor acetylhydrolase, plasma) [Source:MGI Symbol;Acc:MGI:1351327]
ENSMUSG000000026288	2,5880	0,0098	inositol polyphosphate-5-phosphatase D [Source:MGI Symbol;Acc:MGI:107357]
ENSMUSG000000025270	2,5893	0,0108	aminolevulinic acid synthase 2, erythroid [Source:MGI Symbol;Acc:MGI:87990]
ENSMUSG000000026832	2,5952	0,0135	cytohesin 1 interacting protein [Source:MGI Symbol;Acc:MGI:2183535]
ENSMUSG000000017754	2,6000	0,0089	phospholipid transfer protein [Source:MGI Symbol;Acc:MGI:103151]
ENSMUSG000000002699	2,6084	0,0125	lymphocyte cytosolic protein 2 [Source:MGI Symbol;Acc:MGI:1321402]
ENSMUSG0000000030589	2,6202	0,0120	RAS guanyl releasing protein 4 [Source:MGI Symbol;Acc:MGI:2386851]
ENSMUSG000000022014	2,6273	0,0129	epithelial stromal interaction 1 (breast) [Source:MGI Symbol;Acc:MGI:1915168]
ENSMUSG000000000318	2,6329	0,0089	C-type lectin domain family 10, member A [Source:MGI Symbol;Acc:MGI:96975]
ENSMUSG0000000045165	2,6333	0,0119	expressed sequence AI467606 [Source:MGI Symbol;Acc:MGI:2141979]
ENSMUSG000000052974	2,6527	0,0095	cytochrome P450, family 2, subfamily f, polypeptide 2 [Source:MGI Symbol;Acc:MGI:88608]
ENSMUSG000000001131	2,6605	0,0079	tissue inhibitor of metalloproteinase 1 [Source:MGI Symbol;Acc:MGI:98752]
ENSMUSG000000049037	2,6692	0,0099	C-type lectin domain family 4, member a1 [Source:MGI Symbol;Acc:MGI:3036291]
ENSMUSG000000022415	2,6786	0,0102	synaptogyrin 1 [Source:MGI Symbol;Acc:MGI:1328323]
ENSMUSG000000028874	2,6804	0,0093	FGR proto-oncogene, Src family tyrosine kinase [Source:MGI Symbol;Acc:MGI:95527]
ENSMUSG000000050335	2,7014	0,0067	lectin, galactose binding, soluble 3 [Source:MGI Symbol;Acc:MGI:96778]
ENSMUSG000000022504	2,7132	0,0092	class II transactivator [Source:MGI Symbol;Acc:MGI:108445]
ENSMUSG000000055805	2,7134	0,0083	formin-like 1 [Source:MGI Symbol;Acc:MGI:1888994]
ENSMUSG0000000031165	2,7234	0,0098	Wiskott-Aldrich syndrome [Source:MGI Symbol;Acc:MGI:105059]
ENSMUSG000000024300	2,7299	0,0071	myosin IF [Source:MGI Symbol;Acc:MGI:107711]
ENSMUSG000000020911	2,7382	0,0095	keratin 19 [Source:MGI Symbol;Acc:MGI:96693]
ENSMUSG000000042228	2,7424	0,0070	LYN proto-oncogene, Src family tyrosine kinase [Source:MGI Symbol;Acc:MGI:96892]

ENSMUSG00000024180	2,7486	0,0088	transmembrane protein 8 (five membrane-spanning domains) [Source:MGI Symbol;Acc:MGI:1926283]
ENSMUSG00000030047	2,7657	0,0080	Rho GTPase activating protein 25 [Source:MGI Symbol;Acc:MGI:2443687]
ENSMUSG00000015852	2,7867	0,0063	Fc receptor-like 5, scavenger receptor [Source:MGI Symbol;Acc:MGI:1933397]
ENSMUSG00000044583	2,7896	0,0079	toll-like receptor 7 [Source:MGI Symbol;Acc:MGI:2176882]
ENSMUSG00000032690	2,7977	0,0060	2'-5' oligoadenylate synthetase 2 [Source:MGI Symbol;Acc:MGI:2180852]
ENSMUSG000000045312	2,8011	0,0061	lipoma HMGIC fusion partner-like 2 [Source:MGI Symbol;Acc:MGI:2145236]
ENSMUSG000000047810	2,8138	0,0071	coiled-coil domain containing 88B [Source:MGI Symbol;Acc:MGI:1925567]
ENSMUSG000000040751	2,8163	0,0068	linker for activation of T cells family, member 2 [Source:MGI Symbol;Acc:MGI:1926479]
ENSMUSG000000041836	2,8212	0,0078	protein tyrosine phosphatase, receptor type, E [Source:MGI Symbol;Acc:MGI:97813]
ENSMUSG000000024030	2,8382	0,0049	ATP binding cassette subfamily G member 1 [Source:MGI Symbol;Acc:MGI:107704]
ENSMUSG000000029919	2,8404	0,0062	hematopoietic prostaglandin D synthase [Source:MGI Symbol;Acc:MGI:1859384]
ENSMUSG000000026928	2,8412	0,0074	caspase recruitment domain family, member 9 [Source:MGI Symbol;Acc:MGI:2685628]
ENSMUSG000000021319	2,8438	0,0046	secreted frizzled-related protein 4 [Source:MGI Symbol;Acc:MGI:892010]
ENSMUSG000000036887	2,8477	0,0045	complement component 1, q subcomponent, alpha polypeptide [Source:MGI Symbol;Acc:MGI:88223]
ENSMUSG000000034116	2,8552	0,0056	vav 1 oncogene [Source:MGI Symbol;Acc:MGI:98923]
ENSMUSG000000015340	2,8572	0,0047	cytochrome b-245, beta polypeptide [Source:MGI Symbol;Acc:MGI:88574]
ENSMUSG000000070942	2,8764	0,0063	interleukin 1 receptor-like 2 [Source:MGI Symbol;Acc:MGI:1913107]
ENSMUSG000000028327	2,8783	0,0063	STRA6-like [Source:MGI Symbol;Acc:MGI:1921402]
ENSMUSG000000027533	2,8950	0,0041	fatty acid binding protein 5, epidermal [Source:MGI Symbol;Acc:MGI:101790]
ENSMUSG000000047180	2,9070	0,0054	neuralized E3 ubiquitin protein ligase 3 [Source:MGI Symbol;Acc:MGI:2429944]
ENSMUSG000000004266	2,9095	0,0048	protein tyrosine phosphatase, non-receptor type 6 [Source:MGI Symbol;Acc:MGI:96055]
ENSMUSG000000049625	2,9109	0,0057	TRAF-interacting protein with forkhead-associated domain, family member B [Source:MGI Symbol;Acc:MGI:2385852]
ENSMUSG000000055541	2,9124	0,0054	leukocyte-associated Ig-like receptor 1 [Source:MGI Symbol;Acc:MGI:105492]

ENSMUSG000000036896	2,9282	0,0036	complement component 1, q subcomponent, C chain [Source:MGI Symbol;Acc:M-GI:88225]
ENSMUSG000000030263	2,9378	0,0054	lymphoid-restricted membrane protein [Source:MGI Symbol;Acc:MGI:108424]
ENSMUSG000000026177	2,9479	0,0038	solute carrier family 11 (proton-coupled divalent metal ion transporters), member 1 [Source:MGI Symbol;Acc:MGI:1345275]
ENSMUSG000000026395	2,9590	0,0038	protein tyrosine phosphatase, receptor type, C [Source:MGI Symbol;Acc:MGI:97810]
ENSMUSG000000029084	2,9668	0,0037	CD38 antigen [Source:MGI Symbol;Acc:MGI:107474]
ENSMUSG000000018008	2,9697	0,0035	cytohesin 4 [Source:MGI Symbol;Acc:MGI:2441702]
ENSMUSG000000045763	2,9731	0,0045	brain abundant, membrane attached signal protein 1 [Source:MGI Symbol;Acc:M-GI:1917600]
ENSMUSG000000019122	2,9885	0,0032	chemokine (C-C motif) ligand 9 [Source:MGI Symbol;Acc:MGI:104533]
ENSMUSG000000052384	2,9950	0,0034	negative regulator of reactive oxygen species [Source:MGI Symbol;Acc:MGI:2445095]
ENSMUSG0000000031304	2,9952	0,0043	interleukin 2 receptor, gamma chain [Source:MGI Symbol;Acc:MGI:96551]
ENSMUSG000000033777	3,0096	0,0036	toll-like receptor 13 [Source:MGI Symbol;Acc:MGI:3045213]
ENSMUSG000000028931	3,0161	0,0043	potassium voltage-gated channel, shaker-related subfamily, beta member 2 [Source:MGI Symbol;Acc:MGI:109239]
ENSMUSG000000037731	3,0184	0,0036	thymocyte selection associated family member 2 [Source:MGI Symbol;Acc:M-GI:2446213]
ENSMUSG000000027514	3,0230	0,0038	Z-DNA binding protein 1 [Source:MGI Symbol;Acc:MGI:1927449]
ENSMUSG000000002985	3,0233	0,0027	apolipoprotein E [Source:MGI Symbol;Acc:MGI:88057]
ENSMUSG000000032089	3,0242	0,0032	interleukin 10 receptor, alpha [Source:MGI Symbol;Acc:MGI:96538]
ENSMUSG000000024397	3,0377	0,0044	allograft inflammatory factor 1 [Source:MGI Symbol;Acc:MGI:1343098]
ENSMUSG000000028859	3,0456	0,0037	colony stimulating factor 3 receptor (granulocyte) [Source:MGI Symbol;Acc:M-GI:1339755]
ENSMUSG000000003283	3,0473	0,0038	hemopoietic cell kinase [Source:MGI Symbol;Acc:MGI:96052]
ENSMUSG000000005413	3,0700	0,0027	heme oxygenase 1 [Source:MGI Symbol;Acc:MGI:96163]
ENSMUSG000000020865	3,0804	0,0031	ATP-binding cassette, sub-family C (CFTR/MRP), member 3 [Source:MGI Symbol;Acc:MGI:1923658]
ENSMUSG000000025044	3,0823	0,0032	macrophage scavenger receptor 1 [Source:MGI Symbol;Acc:MGI:98257]

ENSMUSG00000016024	3,0908	0,0024	lipopolysaccharide binding protein [Source:MGI Symbol;Acc:MGI:1098776]
ENSMUSG00000022488	3,1039	0,0025	NCK associated protein 1 like [Source:MGI Symbol;Acc:MGI:1926063]
ENSMUSG00000021281	3,1063	0,0023	tumor necrosis factor, alpha-induced protein 2 [Source:MGI Symbol;Acc:MGI:104960]
ENSMUSG00000059498	3,1081	0,0023	Fc receptor, IgG, low affinity III [Source:MGI Symbol;Acc:MGI:95500]
ENSMUSG00000071713	3,1467	0,0023	colony stimulating factor 2 receptor, beta, low-affinity (granulocyte-macrophage) [Source:MGI Symbol;Acc:MGI:1339759]
ENSMUSG00000040345	3,1610	0,0027	Rho GTPase activating protein 9 [Source:MGI Symbol;Acc:MGI:2143764]
ENSMUSG00000052776	3,1670	0,0025	2'-5' oligoadenylate synthetase 1A [Source:MGI Symbol;Acc:MGI:2180860]
ENSMUSG00000052160	3,1713	0,0020	phospholipase D family, member 4 [Source:MGI Symbol;Acc:MGI:2144765]
ENSMUSG00000040552	3,1861	0,0020	complement component 3a receptor 1 [Source:MGI Symbol;Acc:MGI:1097680]
ENSMUSG00000020901	3,1881	0,0022	phosphoinositide-3-kinase regulatory subunit 5 [Source:MGI Symbol;Acc:MGI:2443588]
ENSMUSG00000021322	3,2002	0,0027	acyloxyacyl hydrolase [Source:MGI Symbol;Acc:MGI:1350928]
ENSMUSG00000018927	3,2013	0,0017	chemokine (C-C motif) ligand 6 [Source:MGI Symbol;Acc:MGI:98263]
ENSMUSG00000036905	3,2133	0,0016	complement component 1, q subcomponent, beta polypeptide [Source:MGI Symbol;Acc:MGI:88224]
ENSMUSG00000048163	3,2183	0,0022	selectin, platelet (p-selectin) ligand [Source:MGI Symbol;Acc:MGI:106689]
ENSMUSG00000025993	3,2221	0,0022	solute carrier family 40 (iron-regulated transporter), member 1 [Source:MGI Symbol;Acc:MGI:1315204]
ENSMUSG00000078771	3,2241	0,0024	ecotropic viral integration site 2a [Source:MGI Symbol;Acc:MGI:95458]
ENSMUSG00000049988	3,2472	0,0022	leucine rich repeat containing 25 [Source:MGI Symbol;Acc:MGI:2445284]
ENSMUSG00000029322	3,2491	0,0018	placenta-specific 8 [Source:MGI Symbol;Acc:MGI:2445289]
ENSMUSG00000015355	3,2520	0,0022	CD48 antigen [Source:MGI Symbol;Acc:MGI:88339]
ENSMUSG00000072620	3,2735	0,0016	schlafen 2 [Source:MGI Symbol;Acc:MGI:1313258]
ENSMUSG00000030707	3,2741	0,0015	coronin, actin binding protein 1A [Source:MGI Symbol;Acc:MGI:1345961]
ENSMUSG00000024737	3,2883	0,0019	solute carrier family 15, member 3 [Source:MGI Symbol;Acc:MGI:1929691]
ENSMUSG00000024672	3,3041	0,0016	membrane-spanning 4-domains, subfamily A, member 7 [Source:MGI Symbol;Acc:MGI:1918846]

ENSMUSG00000004730	3,3360	0,0013	adhesion G protein-coupled receptor E1 [Source:MGI Symbol;Acc:MGI:106912]
ENSMUSG000000069516	3,3541	0,0010	lysozyme 2 [Source:MGI Symbol;Acc:MGI:96897]
ENSMUSG00000025473	3,3550	0,0012	a disintegrin and metalloproteinase domain 8 [Source:MGI Symbol;Acc:MGI:107825]
ENSMUSG00000058715	3,3740	0,0011	Fc receptor, IgE, high affinity I, gamma polypeptide [Source:MGI Symbol;Acc:MGI:95496]
ENSMUSG00000020437	3,3816	0,0013	myosin IG [Source:MGI Symbol;Acc:MGI:1927091]
ENSMUSG00000057191	3,3904	0,0015	cDNA sequence AB124611 [Source:MGI Symbol;Acc:MGI:3043001]
ENSMUSG00000030789	3,4013	0,0011	integrin alpha X [Source:MGI Symbol;Acc:MGI:96609]
ENSMUSG00000025877	3,4050	0,0012	hexokinase 3 [Source:MGI Symbol;Acc:MGI:2670962]
ENSMUSG00000112148	3,4082	0,0012	leukocyte immunoglobulin-like receptor, subfamily B, member 4A [Source:MGI Symbol;Acc:MGI:102701]
ENSMUSG00000026656	3,4426	0,0009	Fc receptor, IgG, low affinity IIb [Source:MGI Symbol;Acc:MGI:95499]
ENSMUSG00000020143	3,4599	0,0011	dedicator of cyto-kinesis 2 [Source:MGI Symbol;Acc:MGI:2149010]
ENSMUSG00000069515	3,4599	0,0010	lysozyme 1 [Source:MGI Symbol;Acc:MGI:96902]
ENSMUSG00000056529	3,4611	0,0012	platelet-activating factor receptor [Source:MGI Symbol;Acc:MGI:106066]
ENSMUSG00000028581	3,4639	0,0008	lysosomal-associated protein transmembrane 5 [Source:MGI Symbol;Acc:MGI:108046]
ENSMUSG00000021998	3,4680	0,0008	lymphocyte cytosolic protein 1 [Source:MGI Symbol;Acc:MGI:104808]
ENSMUSG00000021091	3,4742	0,0007	serine (or cysteine) peptidase inhibitor, clade A, member 3N [Source:MGI Symbol;Acc:MGI:105045]
ENSMUSG00000024679	3,4780	0,0009	membrane-spanning 4-domains, subfamily A, member 6D [Source:MGI Symbol;Acc:MGI:1916024]
ENSMUSG00000031827	3,4960	0,0008	coactosin-like 1 (Dictyostelium) [Source:MGI Symbol;Acc:MGI:1919292]
ENSMUSG00000038147	3,5142	0,0008	CD84 antigen [Source:MGI Symbol;Acc:MGI:1336885]
ENSMUSG00000029816	3,5660	0,0006	glycoprotein (transmembrane) nmb [Source:MGI Symbol;Acc:MGI:1934765]
ENSMUSG00000034652	3,5772	0,0008	CD300A molecule [Source:MGI Symbol;Acc:MGI:2443411]
ENSMUSG00000028238	3,5777	0,0007	ATPase, H+ transporting, lysosomal V0 subunit D2 [Source:MGI Symbol;Acc:MGI:1924415]
ENSMUSG00000046805	3,5875	0,0005	macrophage expressed gene 1 [Source:MGI Symbol;Acc:MGI:1333743]

ENSMUSG00000035004	3,5922	0,0007	immunoglobulin superfamily, member 6 [Source:MGI Symbol;Acc:MGI:1891393]
ENSMUSG00000030579	3,6322	0,0005	TYRO protein tyrosine kinase binding protein [Source:MGI Symbol;Acc:MGI:1277211]
ENSMUSG00000024610	3,6503	0,0004	CD74 antigen (invariant polypeptide of major histocompatibility complex, class II antigen-associated) [Source:MGI Symbol;Acc:MGI:96534]
ENSMUSG00000030798	3,6575	0,0006	CD37 antigen [Source:MGI Symbol;Acc:MGI:88330]
ENSMUSG00000073421	3,6601	0,0004	histocompatibility 2, class II antigen A, beta 1 [Source:MGI Symbol;Acc:MGI:103070]
ENSMUSG00000029925	3,6607	0,0007	thromboxane A synthase 1, platelet [Source:MGI Symbol;Acc:MGI:98497]
ENSMUSG000000041515	3,6721	0,0005	interferon regulatory factor 8 [Source:MGI Symbol;Acc:MGI:96395]
ENSMUSG00000021423	3,6754	0,0006	lymphocyte antigen 86 [Source:MGI Symbol;Acc:MGI:1321404]
ENSMUSG00000000290	3,6874	0,0004	integrin beta 2 [Source:MGI Symbol;Acc:MGI:96611]
ENSMUSG000000036594	3,6909	0,0004	histocompatibility 2, class II antigen A, alpha [Source:MGI Symbol;Acc:MGI:95895]
ENSMUSG00000023992	3,7255	0,0004	triggering receptor expressed on myeloid cells 2 [Source:MGI Symbol;Acc:MGI:1913150]
ENSMUSG00000044811	3,7527	0,0005	CD300C molecule 2 [Source:MGI Symbol;Acc:MGI:2153249]
ENSMUSG00000112023	3,7590	0,0004	leukocyte immunoglobulin-like receptor, subfamily B, member 4B [Source:MGI Symbol;Acc:MGI:102702]
ENSMUSG00000071714	3,7732	0,0004	colony stimulating factor 2 receptor, beta 2, low-affinity (granulocyte-macrophage) [Source:MGI Symbol;Acc:MGI:1339760]
ENSMUSG000000002111	3,7956	0,0004	spleen focus forming virus (SFFV) proviral integration oncogene [Source:MGI Symbol;Acc:MGI:98282]
ENSMUSG00000040747	3,8380	0,0003	CD53 antigen [Source:MGI Symbol;Acc:MGI:88341]
ENSMUSG00000018774	3,8417	0,0003	CD68 antigen [Source:MGI Symbol;Acc:MGI:88342]
ENSMUSG00000060586	3,8644	0,0002	histocompatibility 2, class II antigen E beta [Source:MGI Symbol;Acc:MGI:95901]
ENSMUSG00000058818	3,9135	0,0002	paired Ig-like receptor B [Source:MGI Symbol;Acc:MGI:894311]
ENSMUSG00000069792	3,9230	0,0002	WAP four-disulfide core domain 17 [Source:MGI Symbol;Acc:MGI:3649773]
ENSMUSG00000049103	3,9243	0,0003	chemokine (C-C motif) receptor 2 [Source:MGI Symbol;Acc:MGI:106185]
ENSMUSG00000015854	4,0074	0,0001	CD5 antigen-like [Source:MGI Symbol;Acc:MGI:1334419]
ENSMUSG00000038642	4,0314	0,0001	cathepsin S [Source:MGI Symbol;Acc:MGI:107341]

ENSMUSG00000026822	4,0717	0,0002	lipocalin 2 [Source:MGI Symbol;Acc:MGI:96757]
ENSMUSG00000033220	4,0803	0,0002	Rac family small GTPase 2 [Source:MGI Symbol;Acc:MGI:97846]
ENSMUSG00000049723	4,3756	5,56E-5	matrix metalloproteinase 12 [Source:MGI Symbol;Acc:MGI:97005]
ENSMUSG00000029304	6,4297	5,71E-8	secreted phosphoprotein 1 [Source:MGI Symbol;Acc:MGI:98389]

Supplemental table V

Gene name	Gene ID	Gene description
Acaa1b	ENSMUSG00000010651	acetyl-Coenzyme A acyltransferase 1B [Source:MGI Symbol;Acc:MGI:3605455]
Cd38	ENSMUSG00000029084	CD38 antigen [Source:MGI Symbol;Acc:MGI:107474]
Cdca3	ENSMUSG00000023505	cell division cycle associated 3 [Source:MGI Symbol;Acc:MGI:1315198]
Ccl6	ENSMUSG00000018927	chemokine (C-C motif) ligand 6 [Source:MGI Symbol;Acc:MGI:98263]
Ttc9	ENSMUSG00000042734	tetratricopeptide repeat domain 9 [Source:MGI Symbol;Acc:MGI:1916730]
Fcgr3	ENSMUSG00000059498	Fc receptor, IgG, low affinity III [Source:MGI Symbol;Acc:MGI:95500]
Ms4a6c	ENSMUSG00000079419	membrane-spanning 4-domains, subfamily A, member 6C [Source:MGI Symbol;Acc:MGI:2385644]
Alox5ap	ENSMUSG00000060063	arachidonate 5-lipoxygenase activating protein [Source:MGI Symbol;Acc:MGI:107505]
Sdc3	ENSMUSG00000025743	syndecan 3 [Source:MGI Symbol;Acc:MGI:1349163]
Dok2	ENSMUSG00000022102	docking protein 2 [Source:MGI Symbol;Acc:MGI:1332623]
Eln	ENSMUSG00000029675	elastin [Source:MGI Symbol;Acc:MGI:95317]
AB124611	ENSMUSG00000057191	cDNA sequence AB124611 [Source:MGI Symbol;Acc:MGI:3043001]
Aoah	ENSMUSG00000021322	acyloxacyl hydrolase [Source:MGI Symbol;Acc:MGI:1350928]
Gng2	ENSMUSG00000043004	guanine nucleotide binding protein (G protein), gamma 2 [Source:MGI Symbol;Acc:MGI:102705]
Fgr	ENSMUSG00000028874	FGR proto-oncogene, Src family tyrosine kinase [Source:MGI Symbol;Acc:MGI:95527]
Sh3tc1	ENSMUSG00000036553	SH3 domain and tetratricopeptide repeats 1 [Source:MGI Symbol;Acc:MGI:2678949]

Tmem8	ENSMUSG00000024180	transmembrane protein 8 (five membrane-spanning domains) [Source:MGI Symbol;Acc:M-GI:1926283]
Ifi207	ENSMUSG000000073490	interferon activated gene 207 [Source:MGI Symbol;Acc:MGI:2138302]
Itgb7	ENSMUSG00000001281	integrin beta 7 [Source:MGI Symbol;Acc:MGI:96616]
Myo1g	ENSMUSG00000020437	myosin IG [Source:MGI Symbol;Acc:MGI:1927091]
Cybb	ENSMUSG00000015340	cytochrome b-245, beta polypeptide [Source:MGI Symbol;Acc:MGI:88574]
C1qb	ENSMUSG00000036905	complement component 1, q subcomponent, beta polypeptide [Source:MGI Symbol;Acc:M-GI:88224]
Tmem173	ENSMUSG00000024349	transmembrane protein 173 [Source:MGI Symbol;Acc:MGI:1919762]
Retnla	ENSMUSG000000061100	resistin like alpha [Source:MGI Symbol;Acc:MGI:1888504]
Anpep	ENSMUSG00000039062	alanyl (membrane) aminopeptidase [Source:MGI Symbol;Acc:MGI:5000466]
Clec10a	ENSMUSG00000000318	C-type lectin domain family 10, member A [Source:MGI Symbol;Acc:MGI:96975]
Fcrls	ENSMUSG00000015852	Fc receptor-like S, scavenger receptor [Source:MGI Symbol;Acc:MGI:1933397]
Tmem106a	ENSMUSG00000034947	transmembrane protein 106A [Source:MGI Symbol;Acc:MGI:1922056]
Lat2	ENSMUSG00000040751	linker for activation of T cells family, member 2 [Source:MGI Symbol;Acc:MGI:1926479]
Htr2a	ENSMUSG00000034997	5-hydroxytryptamine (serotonin) receptor 2A [Source:MGI Symbol;Acc:MGI:109521]
Runx1	ENSMUSG00000022952	runt related transcription factor 1 [Source:MGI Symbol;Acc:MGI:99852]
Tyrobp	ENSMUSG00000030579	TYRO protein tyrosine kinase binding protein [Source:MGI Symbol;Acc:MGI:1277211]
Irf5	ENSMUSG00000029771	interferon regulatory factor 5 [Source:MGI Symbol;Acc:MGI:1350924]
Slc11a1	ENSMUSG00000026177	solute carrier family 11 (proton-coupled divalent metal ion transporters), member 1 [Source:MGI Symbol;Acc:MGI:1345275]
Ccl19	ENSMUSG00000019122	chemokine (C-C motif) ligand 9 [Source:MGI Symbol;Acc:MGI:104533]
Rsad2	ENSMUSG00000020641	radical S-adenosyl methionine domain containing 2 [Source:MGI Symbol;Acc:M-GI:1929628]
AI467606	ENSMUSG00000045165	expressed sequence AI467606 [Source:MGI Symbol;Acc:MGI:2141979]
Clec1b	ENSMUSG00000030159	C-type lectin domain family 1, member b [Source:MGI Symbol;Acc:MGI:1913287]
Grp1	ENSMUSG00000050105	glycine/arginine rich protein 1 [Source:MGI Symbol;Acc:MGI:1919940]
Ly86	ENSMUSG00000021423	lymphocyte antigen 86 [Source:MGI Symbol;Acc:MGI:1321404]

Oas1a	ENSMUSG00000052776	2'-5' oligoadenylate synthetase 1A [Source:MGI Symbol;Acc:MGI:2180860]
Pid3	ENSMUSG00000003363	phospholipase D family, member 3 [Source:MGI Symbol;Acc:MGI:1333782]
Selp	ENSMUSG00000026580	selectin, platelet [Source:MGI Symbol;Acc:MGI:98280]
Cyr61	ENSMUSG00000028195	cysteine rich protein 61 [Source:MGI Symbol;Acc:MGI:88613]
Mafb	ENSMUSG00000074622	v-maf musculoaponeurotic fibrosarcoma oncogene family, protein B (avian) [Source:MGI Symbol;Acc:MGI:104555]
Myo1f	ENSMUSG00000024300	myosin IF [Source:MGI Symbol;Acc:MGI:107711]
Cd83	ENSMUSG00000015396	CD83 antigen [Source:MGI Symbol;Acc:MGI:1328316]
Cyp2f2	ENSMUSG00000052974	cytochrome P450, family 2, subfamily f, polypeptide 2 [Source:MGI Symbol;Acc:MGI:88608]
Plbd1	ENSMUSG00000030214	phospholipase B domain containing 1 [Source:MGI Symbol;Acc:MGI:1914107]
Hbb-bs	ENSMUSG00000052305	hemoglobin, beta adult s chain [Source:MGI Symbol;Acc:MGI:5474852]
Map4k1	ENSMUSG00000037337	mitogen-activated protein kinase kinase kinase 1 [Source:MGI Symbol;Acc:MGI:1346882]
Ms4a6d	ENSMUSG00000024679	membrane-spanning 4-domains, subfamily A, member 6D [Source:MGI Symbol;Acc:MGI:1916024]
Ihh	ENSMUSG00000006538	Indian hedgehog [Source:MGI Symbol;Acc:MGI:96533]
Cxcr4	ENSMUSG00000045382	chemokine (C-X-C motif) receptor 4 [Source:MGI Symbol;Acc:MGI:109563]
Cd48	ENSMUSG00000015355	CD48 antigen [Source:MGI Symbol;Acc:MGI:88339]
Cl1qa	ENSMUSG00000036887	complement component 1, q subcomponent, alpha polypeptide [Source:MGI Symbol;Acc:MGI:88223]
Card9	ENSMUSG00000026928	caspase recruitment domain family, member 9 [Source:MGI Symbol;Acc:MGI:2685628]
Sfrp4	ENSMUSG00000021319	secreted frizzled-related protein 4 [Source:MGI Symbol;Acc:MGI:892010]
Arhgap30	ENSMUSG00000048865	Rho GTPase activating protein 30 [Source:MGI Symbol;Acc:MGI:2684948]
Sla	ENSMUSG00000022372	src-like adaptor [Source:MGI Symbol;Acc:MGI:104295]
Tlr13	ENSMUSG00000033777	toll-like receptor 13 [Source:MGI Symbol;Acc:MGI:3045213]
Lgals3bp	ENSMUSG00000033880	lectin, galactoside-binding, soluble, 3 binding protein [Source:MGI Symbol;Acc:MGI:99554]
Rps27rt	ENSMUSG00000050621	ribosomal protein S27, retrogene [Source:MGI Symbol;Acc:MGI:3704345]

Phf11b	ENSMUSG00000091649	PHD finger protein 11B [Source:MGI Symbol;Acc:MGI:3645789]
Plxnc1	ENSMUSG00000074785	plexin C1 [Source:MGI Symbol;Acc:MGI:1890127]
Cd300ld	ENSMUSG00000034641	CD300 molecule like family member d [Source:MGI Symbol;Acc:MGI:2442358]
Cd5l	ENSMUSG00000015854	CD5 antigen-like [Source:MGI Symbol;Acc:MGI:1334419]
Il4ra	ENSMUSG00000030748	interleukin 4 receptor, alpha [Source:MGI Symbol;Acc:MGI:105367]
C4b	ENSMUSG00000073418	complement component 4B (Chido blood group) [Source:MGI Symbol;Acc:MGI:88228]
C5ar1	ENSMUSG00000049130	complement component 5a receptor 1 [Source:MGI Symbol;Acc:MGI:88232]
Ly6e	ENSMUSG00000022587	lymphocyte antigen 6 complex, locus E [Source:MGI Symbol;Acc:MGI:106651]
Hmox1	ENSMUSG00000005413	heme oxygenase 1 [Source:MGI Symbol;Acc:MGI:96163]
Vav1	ENSMUSG000000034116	vav 1 oncogene [Source:MGI Symbol;Acc:MGI:98923]
Plac8	ENSMUSG00000029322	placenta-specific 8 [Source:MGI Symbol;Acc:MGI:2445289]
Slc40a1	ENSMUSG00000025993	solute carrier family 40 (iron-regulated transporter), member 1 [Source:MGI Symbol;Acc:MGI:1315204]
Arhgap9	ENSMUSG000000040345	Rho GTPase activating protein 9 [Source:MGI Symbol;Acc:MGI:2143764]
Unc93b1	ENSMUSG000000036908	unc-93 homolog B1, TLR signaling regulator [Source:MGI Symbol;Acc:MGI:1859307]
Cyth4	ENSMUSG000000018008	cytohesin 4 [Source:MGI Symbol;Acc:MGI:2441702]
Hba-a1	ENSMUSG000000069919	hemoglobin alpha, adult chain 1 [Source:MGI Symbol;Acc:MGI:96015]
Evi2a	ENSMUSG00000078771	ecotropic viral integration site 2a [Source:MGI Symbol;Acc:MGI:95458]
Lrrc25	ENSMUSG000000049988	leucine rich repeat containing 25 [Source:MGI Symbol;Acc:MGI:2445284]
Hbb-bt	ENSMUSG000000073940	hemoglobin, beta adult t chain [Source:MGI Symbol;Acc:MGI:5474850]
Inpp5d	ENSMUSG00000026288	inositol polyphosphate-5-phosphatase D [Source:MGI Symbol;Acc:MGI:107357]
Tifab	ENSMUSG000000049625	TRAF-interacting protein with forkhead-associated domain, family member B [Source:MGI Symbol;Acc:MGI:2385852]
Ccdc88b	ENSMUSG000000047810	coiled-coil domain containing 88B [Source:MGI Symbol;Acc:MGI:1925567]
Nfam1	ENSMUSG000000058099	Nfat activating molecule with ITAM motif 1 [Source:MGI Symbol;Acc:MGI:1921289]
Tnem176b	ENSMUSG000000029810	transmembrane protein 176B [Source:MGI Symbol;Acc:MGI:1916348]
Lbp	ENSMUSG000000016024	lipopolysaccharide binding protein [Source:MGI Symbol;Acc:MGI:1098776]

Mcub	ENSMUSG00000027994	mitochondrial calcium uniporter dominant negative beta subunit [Source:MGI Symbol;Acc:MGI:1914065]
Pltp	ENSMUSG00000017754	phospholipid transfer protein [Source:MGI Symbol;Acc:MGI:103151]
Pld4	ENSMUSG00000052160	phospholipase D family, member 4 [Source:MGI Symbol;Acc:MGI:2144765]
Fcgr2b	ENSMUSG00000026656	Fc receptor, IgG, low affinity IIb [Source:MGI Symbol;Acc:MGI:95499]
Neurl3	ENSMUSG00000047180	neutralized E3 ubiquitin protein ligase 3 [Source:MGI Symbol;Acc:MGI:2429944]
Cxcl16	ENSMUSG00000018920	chemokine (C-X-C motif) ligand 16 [Source:MGI Symbol;Acc:MGI:1932682]
Lrg1	ENSMUSG00000037095	leucine-rich alpha-2-glycoprotein 1 [Source:MGI Symbol;Acc:MGI:1924155]
Apobec1	ENSMUSG00000040613	apolipoprotein B mRNA editing enzyme, catalytic polypeptide 1 [Source:MGI Symbol;Acc:MGI:103298]
Cpa3	ENSMUSG00000001865	carboxypeptidase A3, mast cell [Source:MGI Symbol;Acc:MGI:88479]
Timp1	ENSMUSG00000001131	tissue inhibitor of metalloproteinase 1 [Source:MGI Symbol;Acc:MGI:98752]
C3	ENSMUSG00000024164	complement component 3 [Source:MGI Symbol;Acc:MGI:88227]
Sash3	ENSMUSG00000031101	SAM and SH3 domain containing 3 [Source:MGI Symbol;Acc:MGI:1921381]
Nrros	ENSMUSG00000052384	negative regulator of reactive oxygen species [Source:MGI Symbol;Acc:MGI:2445095]
Syk	ENSMUSG00000021457	spleen tyrosine kinase [Source:MGI Symbol;Acc:MGI:99515]
Lyn	ENSMUSG00000042228	LYN proto-oncogene, Src family tyrosine kinase [Source:MGI Symbol;Acc:MGI:96892]
Alas2	ENSMUSG00000025270	aminolevulinic acid synthase 2, erythroid [Source:MGI Symbol;Acc:MGI:87990]
Lacc1	ENSMUSG00000044350	laccase domain containing 1 [Source:MGI Symbol;Acc:MGI:2445077]
Gimap4	ENSMUSG00000054435	GTPase, IMAP family member 4 [Source:MGI Symbol;Acc:MGI:1349656]
Lyz1	ENSMUSG00000069515	lysozyme 1 [Source:MGI Symbol;Acc:MGI:96902]
H2-DMb1	ENSMUSG00000079547	histocompatibility 2, class II, locus Mb1 [Source:MGI Symbol;Acc:MGI:95922]
Ptpn6	ENSMUSG00000004266	protein tyrosine phosphatase, non-receptor type 6 [Source:MGI Symbol;Acc:MGI:96055]
Cla3a1	ENSMUSG00000056025	chloride channel accessory 3A1 [Source:MGI Symbol;Acc:MGI:1316732]
Tmem176a	ENSMUSG00000023367	transmembrane protein 176A [Source:MGI Symbol;Acc:MGI:1913308]
Themis2	ENSMUSG00000037731	thymocyte selection associated family member 2 [Source:MGI Symbol;Acc:MGI:2446213]
Kcnab2	ENSMUSG00000028931	potassium voltage-gated channel, shaker-related subfamily, beta member 2 [Source:MGI Symbol;Acc:MGI:109239]

Ddah1	ENSMUSG00000028194	dimethylarginine dimethylaminohydrolase 1 [Source:MGI Symbol;Acc:MGI:1916469]
Psmb8	ENSMUSG00000024338	proteasome (prosome, macropain) subunit, beta type 8 (large multifunctional peptidase 7) [Source:MGI Symbol;Acc:MGI:1346527]
Dennd1c	ENSMUSG00000002668	DENN/MADD domain containing 1C [Source:MGI Symbol;Acc:MGI:1918035]
H2-T24	ENSMUSG00000053835	histocompatibility 2, T region locus 24 [Source:MGI Symbol;Acc:MGI:95958]
Aif1	ENSMUSG00000024397	allograft inflammatory factor 1 [Source:MGI Symbol;Acc:MGI:1343098]
Ptafr	ENSMUSG00000056529	platelet-activating factor receptor [Source:MGI Symbol;Acc:MGI:106066]
Arhgap25	ENSMUSG00000030047	Rho GTPase activating protein 25 [Source:MGI Symbol;Acc:MGI:2443687]
Cfp	ENSMUSG00000001128	complement factor properdin [Source:MGI Symbol;Acc:MGI:97545]
Stmn1	ENSMUSG00000028832	stathmin 1 [Source:MGI Symbol;Acc:MGI:96739]
Cd33	ENSMUSG00000004609	CD33 antigen [Source:MGI Symbol;Acc:MGI:99440]
Mcpt4	ENSMUSG00000061068	mast cell, protease 4 [Source:MGI Symbol;Acc:MGI:96940]
Tlr7	ENSMUSG00000044583	toll-like receptor 7 [Source:MGI Symbol;Acc:MGI:2176882]
Anxa8	ENSMUSG00000021950	annexin A8 [Source:MGI Symbol;Acc:MGI:1201374]
Fes	ENSMUSG00000053158	feline sarcoma oncogene [Source:MGI Symbol;Acc:MGI:95514]
Plcl2	ENSMUSG00000038910	phospholipase C-like 2 [Source:MGI Symbol;Acc:MGI:1352756]
Hba-a2	ENSMUSG00000069917	hemoglobin alpha, adult chain 2 [Source:MGI Symbol;Acc:MGI:96016]
Fcer1g	ENSMUSG00000058715	Fc receptor, IgE, high affinity I, gamma polypeptide [Source:MGI Symbol;Acc:MGI:95496]
Pla2g7	ENSMUSG00000023913	phospholipase A2, group VII (platelet-activating factor acetylhydrolase, plasma) [Source:MGI Symbol;Acc:MGI:1351327]
Lcp2	ENSMUSG00000002699	lymphocyte cytosolic protein 2 [Source:MGI Symbol;Acc:MGI:1321402]
Slc43a2	ENSMUSG00000038178	solute carrier family 43, member 2 [Source:MGI Symbol;Acc:MGI:2442746]
Irf7	ENSMUSG00000025498	interferon regulatory factor 7 [Source:MGI Symbol;Acc:MGI:1859212]
Sele	ENSMUSG00000026582	selectin, endothelial cell [Source:MGI Symbol;Acc:MGI:98278]
Slc37a2	ENSMUSG00000032122	solute carrier family 37 (glycerol-3-phosphate transporter), member 2 [Source:MGI Symbol;Acc:MGI:1929693]
Hpse	ENSMUSG00000035273	heparanase [Source:MGI Symbol;Acc:MGI:1343124]
Lair1	ENSMUSG00000055541	leukocyte-associated Ig-like receptor 1 [Source:MGI Symbol;Acc:MGI:105492]

Plek	ENSMUSG00000020120	pleckstrin [Source:MGI Symbol;Acc:MGI:1860485]
Arhgap45	ENSMUSG00000035697	Rho GTPase activating protein 45 [Source:MGI Symbol;Acc:MGI:1917969]
Hpgds	ENSMUSG00000029919	hematopoietic prostaglandin D synthase [Source:MGI Symbol;Acc:MGI:1859384]
Fgd2	ENSMUSG00000024013	FYVE, RhoGEF and PH domain containing 2 [Source:MGI Symbol;Acc:MGI:1347084]
Ifi204	ENSMUSG00000073489	interferon activated gene 204 [Source:MGI Symbol;Acc:MGI:96429]
Abcc3	ENSMUSG00000020865	ATP-binding cassette, sub-family C (CFTR/MRP), member 3 [Source:MGI Symbol;Acc:MGI:1923658]
Apod	ENSMUSG00000022548	apolipoprotein D [Source:MGI Symbol;Acc:MGI:88056]
Mmp19	ENSMUSG00000025355	matrix metalloproteinase 19 [Source:MGI Symbol;Acc:MGI:1927899]
Cldn5	ENSMUSG00000041378	claudin 5 [Source:MGI Symbol;Acc:MGI:1276112]
Ciita	ENSMUSG00000022504	class II transactivator [Source:MGI Symbol;Acc:MGI:108445]
Oas2	ENSMUSG00000032690	2'-5' oligoadenylate synthetase 2 [Source:MGI Symbol;Acc:MGI:2180852]
Il10ra	ENSMUSG00000032089	interleukin 10 receptor, alpha [Source:MGI Symbol;Acc:MGI:96538]
Il2rg	ENSMUSG00000031304	interleukin 2 receptor, gamma chain [Source:MGI Symbol;Acc:MGI:96551]
Plala	ENSMUSG00000002847	phospholipase A1 member A [Source:MGI Symbol;Acc:MGI:1934677]
Isg15	ENSMUSG00000035692	ISG15 ubiquitin-like modifier [Source:MGI Symbol;Acc:MGI:1855694]
Lgals3	ENSMUSG00000050335	lectin, galactose binding, soluble 3 [Source:MGI Symbol;Acc:MGI:96778]
Mal	ENSMUSG00000027375	myelin and lymphocyte protein, T cell differentiation protein [Source:MGI Symbol;Acc:MGI:892970]
B4galnt1	ENSMUSG00000006731	beta-1,4-N-acetyl-galactosaminyl transferase 1 [Source:MGI Symbol;Acc:MGI:1342057]
Bcl3	ENSMUSG00000053175	B cell leukemia/lymphoma 3 [Source:MGI Symbol;Acc:MGI:88140]
Fabp5	ENSMUSG00000027533	fatty acid binding protein 5, epidermal [Source:MGI Symbol;Acc:MGI:101790]
Ucp2	ENSMUSG00000033685	uncoupling protein 2 (mitochondrial, proton carrier) [Source:MGI Symbol;Acc:MGI:109354]
Amz1	ENSMUSG00000050022	archaelysin family metalloproteinase 1 [Source:MGI Symbol;Acc:MGI:2442258]
Nckap1l	ENSMUSG00000022488	NCK associated protein 1 like [Source:MGI Symbol;Acc:MGI:1926063]
Prg4	ENSMUSG00000006014	proteoglycan 4 (megakaryocyte stimulating factor, articular superficial zone protein) [Source:MGI Symbol;Acc:MGI:1891344]
Msr1	ENSMUSG00000025044	macrophage scavenger receptor 1 [Source:MGI Symbol;Acc:MGI:98257]

Epsti1	ENSMUSG00000022014	epithelial stromal interaction 1 (breast) [Source:MGI Symbol;Acc:MGI:1915168]
Tnfrsf1b	ENSMUSG00000028599	tumor necrosis factor receptor superfamily, member 1b [Source:MGI Symbol;Acc:MGI:1314883]
Otulinl	ENSMUSG00000056069	OTU deubiquitinase with linear linkage specificity like [Source:MGI Symbol;Acc:MGI:2687281]
Tnfaip8l2	ENSMUSG00000013707	tumor necrosis factor, alpha-induced protein 8-like 2 [Source:MGI Symbol;Acc:MGI:1917019]
Adgre1	ENSMUSG000000004730	adhesion G protein-coupled receptor E1 [Source:MGI Symbol;Acc:MGI:106912]
Ftl1	ENSMUSG00000050708	ferritin light polypeptide 1 [Source:MGI Symbol;Acc:MGI:95589]
Ms4a7	ENSMUSG000000024672	membrane-spanning 4-domains, subfamily A, member 7 [Source:MGI Symbol;Acc:MGI:1918846]
Wfdc17	ENSMUSG000000069792	WAP four-disulfide core domain 17 [Source:MGI Symbol;Acc:MGI:3649773]
Fermt3	ENSMUSG00000024965	fermitin family member 3 [Source:MGI Symbol;Acc:MGI:2147790]
Was	ENSMUSG000000031165	Wiskott-Aldrich syndrome [Source:MGI Symbol;Acc:MGI:105059]
Cthrc1	ENSMUSG00000054196	collagen triple helix repeat containing 1 [Source:MGI Symbol;Acc:MGI:1915838]
Rasgrp4	ENSMUSG00000030589	RAS guanyl releasing protein 4 [Source:MGI Symbol;Acc:MGI:2386851]
Mrc1	ENSMUSG00000026712	mannose receptor, C type 1 [Source:MGI Symbol;Acc:MGI:97142]
Gngt2	ENSMUSG00000038811	guanine nucleotide binding protein (G protein), gamma transducing activity polypeptide 2 [Source:MGI Symbol;Acc:MGI:893584]
Cd72	ENSMUSG00000028459	CD72 antigen [Source:MGI Symbol;Acc:MGI:88345]
Il18bp	ENSMUSG00000070427	interleukin 18 binding protein [Source:MGI Symbol;Acc:MGI:1333800]
Itgam	ENSMUSG00000030786	integrin alpha M [Source:MGI Symbol;Acc:MGI:96607]
Lyz2	ENSMUSG000000069516	lysozyme 2 [Source:MGI Symbol;Acc:MGI:96897]
Cd300c2	ENSMUSG00000044811	CD300C molecule 2 [Source:MGI Symbol;Acc:MGI:2153249]
Clec4a1	ENSMUSG00000049037	C-type lectin domain family 4, member a1 [Source:MGI Symbol;Acc:MGI:3036291]
Eps8	ENSMUSG00000015766	epidermal growth factor receptor pathway substrate 8 [Source:MGI Symbol;Acc:MGI:104684]
Rab7b	ENSMUSG00000052688	RAB7B, member RAS oncogene family [Source:MGI Symbol;Acc:MGI:2442295]
H2-DMa	ENSMUSG00000037649	histocompatibility 2, class II, locus DMa [Source:MGI Symbol;Acc:MGI:95921]

Acp5	ENSMUSG00000001348	acid phosphatase 5, tartrate resistant [Source:MGI Symbol;Acc:MGI:87883]
Cotl1	ENSMUSG000000031827	coactosin-like 1 (Dictyostelium) [Source:MGI Symbol;Acc:MGI:1919292]
C3ar1	ENSMUSG000000040552	complement component 3a receptor 1 [Source:MGI Symbol;Acc:MGI:1097680]
Ttyh2	ENSMUSG000000034714	twenty family member 2 [Source:MGI Symbol;Acc:MGI:2157091]
Arhgap19	ENSMUSG000000025154	Rho GTPase activating protein 19 [Source:MGI Symbol;Acc:MGI:1918335]
Adgrg3	ENSMUSG000000060470	adhesion G protein-coupled receptor G3 [Source:MGI Symbol;Acc:MGI:1859670]
Rps6ka1	ENSMUSG000000003644	ribosomal protein S6 kinase polypeptide 1 [Source:MGI Symbol;Acc:MGI:104558]
Tmem37	ENSMUSG000000050777	transmembrane protein 37 [Source:MGI Symbol;Acc:MGI:2157899]
Fgd3	ENSMUSG000000037946	FYVE, RhoGEF and PH domain containing 3 [Source:MGI Symbol;Acc:MGI:1353657]
Csflr	ENSMUSG000000024621	colony stimulating factor 1 receptor [Source:MGI Symbol;Acc:MGI:1339758]
Plvap	ENSMUSG000000034845	plasmalemma vesicle associated protein [Source:MGI Symbol;Acc:MGI:1890497]
Slnf2	ENSMUSG000000072620	schlafen 2 [Source:MGI Symbol;Acc:MGI:1313258]
Ifi205	ENSMUSG000000054203	interferon activated gene 205 [Source:MGI Symbol;Acc:MGI:101847]
Gda	ENSMUSG000000058624	guanine deaminase [Source:MGI Symbol;Acc:MGI:95678]
Zbp1	ENSMUSG000000027514	Z-DNA binding protein 1 [Source:MGI Symbol;Acc:MGI:1927449]
Hck	ENSMUSG000000003283	hemopoietic cell kinase [Source:MGI Symbol;Acc:MGI:96052]
C1qc	ENSMUSG000000036896	complement component 1, q subcomponent, C chain [Source:MGI Symbol;Acc:MGI:88225]
Cd84	ENSMUSG000000038147	CD84 antigen [Source:MGI Symbol;Acc:MGI:1336885]
Ncf1	ENSMUSG000000015950	neutrophil cytosolic factor 1 [Source:MGI Symbol;Acc:MGI:97283]
Serpina3n	ENSMUSG000000021091	serine (or cysteine) peptidase inhibitor, clade A, member 3N [Source:MGI Symbol;Acc:MGI:105045]
Il1rl2	ENSMUSG000000070942	interleukin 1 receptor-like 2 [Source:MGI Symbol;Acc:MGI:1913107]
Abcg1	ENSMUSG000000024030	ATP binding cassette subfamily G member 1 [Source:MGI Symbol;Acc:MGI:107704]

Chapter //

Summary and Perspectives

Summary

The renin-angiotensin system (RAS) is a major regulator of blood pressure and fluid homeostasis. It is now widely accepted that its active end-product, angiotensin (Ang) II, is produced at tissue sites. Although a wide range of drugs exists to suppress either the formation of Ang II (renin inhibitors, ACE inhibitors [ACEi]) or its effects (Ang II type 1 receptor [AT₁R] antagonists [ARBs]), a substantial proportion of the hypertensive population treated with these drugs remains uncontrolled or suboptimally controlled, due to non-adherence and/or drug ineffectiveness. The latter relates among others to the fact that the body is capable of counteracting the effects of RAS blockade by substantially upregulating renin. A new approach to suppress the RAS might be to delete the substrate, angiotensinogen (AGT), from which all angiotensins are derived. Since the majority of AGT is synthesized in the liver, its suppression might occur with RNA therapeutic approaches, including small interfering RNA (siRNA) and antisense oligonucleotides (ASO), targeted to the liver. This approach is already feasible, given the introduction of inclisiran, targeting the hepatic synthesis of proprotein convertase subtilisin kexin type 9 (PCSK9). Remarkably, this requires only 2 doses per year. **Chapter 1** provides an overview of all RNA therapeutic approaches that are currently in clinical development.

Chapter 2 revisits local Ang II generation in the brain. Although AGT synthesis has been claimed to occur locally in the brain, there is virtually no renin. This raises the question whether angiotensin synthesis occurs in the brain at all. It has been proposed that the brain synthesizes prorenin, the inactive precursor of renin, which would then bind to the (pro)renin receptor [(P)RR], allowing it to display Ang I-generating activity. However, we were unable to demonstrate prorenin in the brain at sufficiently high quantities. Taken together therefore, local angiotensin generation in the brain seems impossible, and a more likely source of Ang II in the brain is circulating Ang II, for instance taken up via AT₁R. Clearly, given the presence of the blood-brain barrier, diffusion of circulation renin, prorenin, or AGT into the brain is impossible. In **Chapter 3**, we have used a N-acetylgalactosamine (GalNAc) modified siRNA targeting liver AGT to finally settle the origin of brain AGT and

Ang II. The siRNA was applied to rats made hypertensive with deoxycorticosterone acetate (DOCA)-salt. This approach will lower the circulating RAS, and is generally believed to upregulate the brain RAS. Yet, in our hands, DOCA-salt turned out to lower brain Ang II in parallel with the circulating Ang II, while after depleting liver-derived AGT, Ang II was entirely absent in the brain. Blood pressure remained high despite the disappearance of brain Ang II. Remarkably, AGT could still be detected in the brain after depleting liver-derived AGT. This confirms that the brain independently synthesizes AGT. However, given the absence of renin and prorenin, this apparently does not result in angiotensin generation in the brain. Moreover, brain Ang II is not responsible for the blood pressure rise in the DOCA-salt model. Whether brain AGT has a role remains to be demonstrated.

Another organ which is believed to synthesize its own AGT is the kidney. Ang II generated in the kidney is known to contribute to renal dysfunction, and thus is a major player in the development of glomerulosclerosis, proteinuria, fibrosis, and glomerular filtration lowering. The 5/6th nephrectomy (5/6th Nx) hypertensive rat is a widely established model for chronic kidney disease. In **Chapter 4**, we have treated 5/6th Nx rats with AGTsiRNA, making a comparison versus the ARB losartan and the ACEi captopril. Unexpectedly, losartan reduced blood pressure most strongly, while this effect was diminished in combination with both captopril and AGT siRNA. Since losartan was the only drug that increased circulating Ang II, the most likely explanation of these data is that this Ang II rise resulted in the stimulation of dilator Ang II type 2 receptors (AT₂R), thereby lowering blood pressure more strongly. Importantly, despite the difference of blood pressure reduction, all treatment groups (AGT siRNA, losartan + AGT siRNA, losartan, losartan + captopril) exerted the same degree of renoprotection, reflected by a reduction in proteinuria and glomerulosclerosis. Multiple linear regression analysis revealed that this was due to the additive effect of lowering blood pressure and renal Ang II. These data support the use of AGT siRNA as a new treatment tool for chronic kidney disease.

The (P)RR has been proposed to act as a receptor for both renin and prorenin, allowing the latter to display Ang I-generating activity due to a binding-induced conformational change. However, the affinity of the receptor for (pro)renin is very low, making the occurrence of an interaction

Chapter 7

between the receptor and (pro)renin in vivo highly unlikely. **Chapters 5 and 6** therefore focus on non-RAS effects of the (P)RR, given that it has been claimed to interact with sortilin-1 (SORT1), thereby affecting LDL metabolism and LDL receptor (LDLR) density. Most likely, this is related to the fact that the (P)RR simultaneously acts as an accessory protein of V-ATPase. Inhibiting the hepatic (P)RR with GalNac ASOs in mice on a normal diet increased LDL cholesterol, as a result of downregulated LDLR and SORT1 protein abundance. Yet, hepatic (P)RR inhibition decreased both plasma cholesterol and triglycerides in LDLR deficient mice, thus preventing the development of obesity and hepatosteatosis. Comparative quantitative proteomics revealed a crucial role for both pyruvate dehydrogenase, which converts pyruvate into acetyl-CoA, and acetyl-CoA carboxylase, which catalyzes the formation of malonyl-CoA, an essential substrate for fatty acid synthesis and a potent inhibitor of fatty acid oxidation. Taken together, this reveals a new function of the (P)RR in lipid metabolism. Despite the reduction in plasma cholesterol and triglycerides in LDLR deficient mice fed a high-fat diet, hepatic (P)RR inhibition did not attenuate atherosclerosis, while the same was true in high fat diet-fed ApoE deficient mice. It turned out that the GalNac ASO approach also downregulated the (P)RR in macrophages, which resulted in augmented pro-inflammatory responses. This therefore annihilated the potential beneficial effects of lipid lowering on atherosclerosis.

Perspectives

Despite hundreds of antihypertensive drugs and their combinations currently being available on the market, there still is a substantial proportion of patients whose blood pressure is not appropriately controlled. This could be due to either non-adherence or drug ineffectiveness. Both siRNA and ASO offer a novel approach to overcome non-adherence, since this approach may require only one dose every few months. Currently, targeting to the liver is possible, and soon approaches may become available that target other organs and cells as well. This has the potential to revolutionize drug therapy, as it may simultaneously result in less side-effects, given it targeting the desired organ/cell only.

In case of suppression of angiotensinogen, a major question is how far its levels should be suppressed. Titrating it down to zero is possible. Yet, it is well-known that too much RAS suppression is not necessarily beneficial, since it may result in too much blood pressure lowering, hyperkalemia and renal dysfunction. Simultaneously, the human body is capable of upregulating renin almost indefinitely¹, and thus even lowering AGT by 90% can still be matched easily by 10-fold rises in renin, as demonstrated in this thesis. Similar matches occur during both ACEi and ARB treatment, and yet these drugs are highly effective. Thus, we should now investigate what the most optimal degree of AGT lowering is, without inducing too severe RAS suppression. Here emphasis may be laid on the lowering of tissue angiotensin levels, as these are possibly more sensitive to AGT suppression than blood angiotensin levels.

Another risk is that under conditions of emergency (e.g., after hemorrhage), when the RAS is needed, the lack of AGT may be acutely deleterious. For this we need approaches that quickly annihilate the effect of the siRNA/ASO, or immediately acting constrictor drugs, like for instance Ang II itself or catecholamines. Animal models should evaluate these possibilities, taking into consideration that the responsiveness to Ang II might be increased due to the lack of receptor stimulation in the absence of Ang II.

An interesting patient population that may profit from AGT suppression are women with preeclampsia, given the beneficial effects of this

Chapter 7

approach in a rodent model of preeclampsia². Here a caveat is that animal models with high RAS activity (like in the aforementioned study by Haase et al².) are not necessarily representative of human preeclampsia, considering that in human preeclampsia, AGT and RAS activity are actually lowered³. Future studies should thus evaluate whether this approach would exert beneficial effects in the hypertensive mother only, quantifying placental AGT levels after such treatment, and studying its passage of the placenta, which if occurring would allow (toxic?) fetal effects.

Our data strongly argue against the existence of local angiotensin generation in the brain, and do not support that the DOCA-salt model is a high brain RAS model. This opposes multiple studies by others, often in transgenic models, which indirectly supported this concept^{4, 5}. However, no study ever measured renin or angiotensin in a reliable manner. Although in our hands brain angiotensin levels were very low as compared to other organs^{6, 7}, they still were detectable, and closely followed the circulating Ang II levels. One possibility that has been proposed is that angiotensins occur at very high levels in specific brain nuclei, which then would result in the detection of “low” levels if “diluting” the sample with sufficient surrounding brain tissue not containing angiotensins. Solving this issue is possible only if one can isolate these nuclei. Although some attempts have been made in rodents⁸, a major issue remained the detection limit in such small samples (often corresponding with micrograms of tissue!). Thus, this might be successful only in larger animal models. Remarkably, angiotensin infusion, or the application of angiotensin receptor agonists (including AT₂R agonists) into the brain does exert effects, confirming the presence of AT receptors in the brain, even at locations that are within the blood-brain barrier⁹. Future studies should solve why we have these receptors, and what angiotensin they eventually see. On the one hand, receptors often do exist without their agonist being released locally (e.g., vascular muscarinic receptors occurring in the absence of parasympathetic nerve endings), while on the other hand, these receptors might also be stimulated with exogenous agonists in pathological conditions (e.g., AT₂R agonism in stroke¹⁰).

The beneficial blood pressure-independent renoprotective effects of hepatic AGT suppression in chronic kidney disease supports that also in the kidney, AGT is liver-derived. Novel insight supports renal AGT up-

take via megalin¹¹, while the same is true for renin and prorenin¹². Thus, future studies should now evaluate how exactly renal Ang II synthesis occurs. Such insight might help to even more selectively interfere with renal angiotensin generation. Since beneficial cardiac effects of AGT siRNA were observed in both the DOCA-salt model and the 5/6th Nx model, we still need to unravel to what degree these effects occurred blood pressure-independently. Ideally, AGT siRNA/ASO should be evaluated in animal models representative for heart failure or post-myocardial infarction, to ascertain its efficacy and safety in these conditions as well.

Finally, we have been able to link the (P)RR to non-RAS effects, focusing on lipids and atherosclerosis. Hepatic (P)RR inhibition prevented high-fat diet-induced obesity, liver steatosis and improved glycemic control. Although this offers new avenues for the treatment for metabolic disorders like fatty liver disease and familial hypercholesterolemia, we also observed that such cholesterol lowering did not improve atherosclerosis. This turned out to be due to off-target effects of liver-targeted (P)RR ASOs in macrophages. Combined with the lethal consequence of (P)RR deletion in heart and kidney^{13, 14} this implies that targeting the (P)RR in humans may still be risky. Given the fact that the (P)RR occurs as an accessory protein of V-ATPase, which exerts crucial functions in virtually every cell of the body, this may not come as a complete surprise. Clearly, we still need to get a better understanding of the (P)RR. Also, the time may have come to change its name, given that a relationship with the RAS after all is unlikely.

References

1. Balcarek J, Seva Pessoa B, Bryson C, Azizi M, Menard J, Garrelds IM, McGeehan G, Reeves RA, Griffith SG, Danser AH and Gregg R. Multiple ascending dose study with the new renin inhibitor VTP-27999: nephrocentric consequences of too much renin inhibition. *Hypertension*. 2014;63:942-50.
2. Haase N, Foster DJ, Cunningham MW, Bercher J, Nguyen T, Shulga-Morskaya S, Milstein S, Shaikh S, Rollins J, Golic M, Herse F, Kräker K, Bendix I, Serdar M, Napieczynska H, Heuser A, Gellhaus A, Thiele K, Wallukat G, Müller DN, Lamarca B and Dechend R. RNA interference therapeutics targeting angiotensinogen ameliorate preeclamptic phenotype in rodent models. *Journal of Clinical Investigation*. 2020;130:2928-2942.
3. Verdonk K, Saleh L, Lankhorst S, Smilde JE, van Ingen MM, Garrelds IM, Friesema EC, Russcher H, van den Meiracker AH, Visser W and Danser AH. Associ-

- ation studies suggest a key role for endothelin-1 in the pathogenesis of preeclampsia and the accompanying renin-angiotensin-aldosterone system suppression. *Hypertension*. 2015;65:1316-23.
4. Feng Y, Xia H, Cai Y, Halabi CM, Becker LK, Santos RA, Speth RC, Sigmund CD and Lazartigues E. Brain-selective overexpression of human Angiotensin-converting enzyme type 2 attenuates neurogenic hypertension. *Circ Res*. 2010;106:373-82.
 5. Littlejohn NK, Siel RB, Jr., Ketsawatsomkron P, Pelham CJ, Pearson NA, Hilzeneder AM, Buehrer BA, Weidemann BJ, Li H, Davis DR, Thompson AP, Liu X, Cassell MD, Sigmund CD and Grobe JL. Hypertension in mice with transgenic activation of the brain renin-angiotensin system is vasopressin dependent. *Am J Physiol Regul Integr Comp Physiol*. 2013;304:R818-28.
 6. Campbell DJ, Kladis A and Duncan AM. Nephrectomy, converting enzyme inhibition, and angiotensin peptides. *Hypertension*. 1993;22:513-22.
 7. Patil J, Schwab A, Nussberger J, Schaffner T, Saavedra JM and Imboden H. Intraneuronal angiotensinergic system in rat and human dorsal root ganglia. *Regul Pept*. 2010;162:90-8.
 8. Lombard-Banek C, Yu Z, Swiercz AP, Marvar PJ and Nemes P. A microanalytical capillary electrophoresis mass spectrometry assay for quantifying angiotensin peptides in the brain. *Anal Bioanal Chem*. 2019;411:4661-4671.
 9. Sumners C, Alleyne A, Rodriguez V, Pioquinto DJ, Ludin JA, Kar S, Winder Z, Ortiz Y, Liu M, Krause EG and de Kloet AD. Brain angiotensin type-1 and type-2 receptors: cellular locations under normal and hypertensive conditions. *Hypertens Res*. 2020;43:281-295.
 10. Bennion Douglas M, Jones Chad H, Dang Alex N, Isenberg J, Graham Justin T, Lindblad L, Domenig O, Waters Michael F, Poglitsch M, Sumners C and Steckelings Ulrike M. Protective effects of the angiotensin II AT2 receptor agonist compound 21 in ischemic stroke: a nose-to-brain delivery approach. *Clinical Science*. 2018;132:581-593.
 11. Koizumi M, Ueda K, Niimura F, Nishiyama A, Yanagita M, Saito A, Pastan I, Fujita T, Fukagawa M and Matsusaka T. Podocyte Injury Augments Intrarenal Angiotensin II Generation and Sodium Retention in a Megalin-Dependent Manner. *Hypertension*. 2019;74:509-517.
 12. Sun Y, Goes Martini A, Janssen MJ, Garrelds IM, Masereeuw R, Lu X and Danser AHJ. Megalin: A Novel Endocytic Receptor for Prorenin and Renin. *Hypertension*. 2020;75:1242-1250.
 13. Riediger F, Quack I, Qadri F, Hartleben B, Park JK, Potthoff SA, Sohn D, Sihn G, Rousselle A, Fokuhl V, Maschke U, Purfurst B, Schneider W, Rump LC, Luft FC, Dechend R, Bader M, Huber TB, Nguyen G and Muller DN. Prorenin receptor is essential for podocyte autophagy and survival. *J Am Soc Nephrol*. 2011;22:2193-202.
 14. Kinouchi K, Ichihara A, Sano M, Sun-Wada GH, Wada Y, Kurauchi-Mito A, Bokuda K, Narita T, Oshima Y, Sakoda M, Tamai Y, Sato H, Fukuda K and Itoh H. The (pro)renin receptor/ATP6AP2 is essential for vacuolar H⁺-ATPase assembly in murine cardiomyocytes. *Circ Res*. 2010;107:30-4.

Nederlandse samenvatting

Het renine-angiotensine systeem (RAS) is een belangrijke regulator van de bloeddruk en de vochthuishouding. Het wordt inmiddels algemeen aangenomen dat het actieve eindproduct, angiotensine (Ang) II, produceerd wordt in weefsels. Alhoewel er een breed assortiment van medicijnen bestaat om de aanmaak van Ang II (renine inhibitors, ACE inhibitors [ACEi]) ofwel de effecten van (Ang II type 1 receptor [AT₁R] blokkers [ARBs]) te remmen, blijft een substantieel deel van de hypertensiepatiënten die met deze medicatie behandeld wordt onbeheersbaar of suboptimaal beheersbaar als het gevolg van therapieontrouw en/of ineffectiviteit van het medicijn. Dit laatste heeft onder andere te maken met het feit dat het lichaam in staat is om de remming van het RAS tegen te werken door de aanmaak van renine aanzienlijk te verhogen.

Een nieuwe aanpak om het RAS te onderdrukken zou kunnen bestaan uit het verwijderen van het substraat, angiotensinogeen (AGT), waaruit alle angiotensines voortkomen. Aangezien het merendeel van AGT gesynthetiseerd wordt in de lever, zou de remming kunnen worden werkstelligd met op RNA aangrijpende methodes, waaronder small interference RNA (siRNA) en antisense oligonucleotiden (ASO) die dan bij voorkeur alleen in de lever werken. Deze aanpak is reeds haalbaar, gezien de introductie van inclisiran dat de hepatische synthese van pro-teïne convertase subtilisine kexine type 9 (PCSK9) remt. Wat opvalt, is dat hiervan slechts 2 doses per jaar nodig zijn. **Hoofdstuk 1** geeft een overzicht van alle therapeutische RNA-gerichte toepassingen die momenteel in klinische ontwikkeling zijn.

Hoofdstuk 2 bekijkt de lokale aanmaak van Ang II in de hersenen. Hoewel beweerd wordt dat AGT synthese lokaal in het brein plaatsvindt, is er vrijwel geen renine. Hierdoor rijst de vraag of er überhaupt angiotensine-synthese in de hersenen plaatsvindt. Er is een theorie dat de hersenen prorenine synthetiseren, de inactieve voorloper van renine, dat dan bindt aan de (pro)renine receptor [(P)RR], waardoor er Ang I-genererende activiteit kan optreden. Wij zijn er echter niet in geslaagd om de aanwezigheid van prorenine in de hersenen in voldoende hoge concentratie aan te tonen. Alles bij elkaar genomen lijkt lokale aanmaak van angiotensine in de hersenen onmogelijk en is het circulerende Ang II, dat bijvoorbeeld via AT₁R binding wordt opgenomen, een meer

Chapter 7

voor de hand liggende bron van Ang II in de hersenen. Gezien de aanwezigheid van de bloed-hersenbarrière, is het sowieso niet mogelijk dat renine, prorenine of AGT vanuit de bloedsomloop naar de hersenen verspreid worden. In **Hoofdstuk 3** hebben we een N-acetylgalactosamine (GalNAc) -gemodificeerd siRNA gebruikt dat alleen aangrijpt op AGT in de lever, om zo eindelijk uitsluitel te verkrijgen over de bron van AGT en Ang II in de hersenen. Dit siRNA werd toegediend aan ratten die hypertensief gemaakt zijn met deoxycorticosteronacetaat (DOCA)-zout.

Deze methode verlaagt het circulerend RAS maar zou het RAS in de hersenen stimuleren. Echter, in onze studie bleek DOCA-zout het Ang II gehalte in de hersenen juist te verlagen, parallel aan Ang II in de bloedsomloop, terwijl na remming van AGT in de lever Ang II in de hersenen volledig verdwenen was. De bloeddruk bleef hoog, ondanks dat Ang II uit de hersenen verdwenen was. Opvallend is dat AGT nog steeds kon worden gedetecteerd in de hersenen na remming van uit de lever afkomstig AGT. Dit bevestigt dat in het brein onafhankelijke AGT synthese plaatsvindt. Gezien de afwezigheid van renine en prorenine, leidt dit klaarblijkelijk niet tot aanmaak van angiotensine in de hersenen. Bovendien is uit het brein afkomstig Ang II niet verantwoordelijk voor de bloeddrukverhoging in het DOCA-zout model. Al met al bewijzen deze data niet dat er een rol voor lokaal gevormd AGT in de hersenen is.

Een ander orgaan dat mogelijk zelf AGT aanmaakt is de nier. Van Ang II dat in de nieren geproduceerd wordt, is bekend dat het bijdraagt aan een verstoorde nierfunctie, en daarmee een belangrijke factor is bij het ontstaan van glomerulosclerose, proteïnurie, fibrose, en een verlaagde glomerulaire filtratiesnelheid. De 5/6th nefrectomie (5/6th Nx) hypertensieve rat is een veelgebruikt model voor de bestudering van chronische nierziekten. In **Hoofdstuk 4** hebben we 5/6th Nx ratten behandeld met AGT siRNA en vergeleken met ratten die behandeld werden met de ARB losartan en/of de ACEi captopril. Tegen de verwachting in, bleek losartan de bloeddruk het sterkst te verlagen, terwijl dit effect afnam wanneer dit middel gecombineerd werd met captopril of AGT siRNA. Aangezien losartan het enige middel was dat de Ang II concentratie in de bloedsomloop verhoogde, is de meest waarschijnlijke verklaring voor deze bevinding dat de Ang II stijging heeft geleid tot stimulatie van bloedvat-verwijdende Ang II type 2 receptoren (AT₂R), zodat de bloeddruk extra daalde. Belangrijker, ondanks de verschillen in bloeddrukverlaging, toonden alle behandelingsgroepen (AGT siRNA,

losartan + AGT siRNA, losartan, losartan + captopril) dezelfde mate van nierbescherming, wat zich uitte als een afgenomen proteinurie en glomerulosclerose. Meervoudige lineaire regressie analyse toonde aan dat dit effect veroorzaakt werd door zowel de verlaagde bloeddruk als de verlaging van Ang II in de nier. Deze bevindingen ondersteunen het gebruik van AGT siRNA als een nieuwe behandelmethode voor chronische nierziekten.

Er is geopperd dat de (P)RR optreedt als een receptor voor zowel renine als prorenine, wat de laatste in staat stelt om Ang I-genererende activiteit te vertonen als gevolg van een binding-geïnduceerde conformatieverandering. De affiniteit van de receptor voor (pro)renine is echter erg laag, wat het plaatsvinden van een interactie tussen de receptor en (pro)renine in vivo onwaarschijnlijk maakt. **Hoofdstuk 5 en 6** richten zich op non-RAS effecten van de (P)RR, op basis van de eerdere bevinding dat de (P)RR een interactie vertoont met sortiline-1 (SORT1), hetgeen het LDL metabolisme en de LDL receptor (LDLR) dichtheid beïnvloedt. Dit laatste heeft waarschijnlijk te maken met het feit dat de (P)RR tegelijkertijd als een hulpeiwit van vasculair H^+ -ATPase (V-ATPase) werkt. Remming van de hepatische (P)RR met GalNac ASOs in muizen met een normaal dieet leidde tot een verhoogd LDL cholesterol, als gevolg van de onderdrukking van de LDLR en SORT1. Onverwacht leidde remming van de hepatische (P)RR tot een verlaging van zowel plasma cholesterol als triglyceriden in muizen met LDLR deficiëntie, als gevolg waarvan de ontwikkeling van obesitas en hepatische steatose voorkomen konden worden. Proteoomanalyse onthulde een cruciale rol voor zowel pyruvaat dehydrogenase, wat pyruvaat omzet in acetyl-CoA, als acetyl-CoA carboxylase, wat de vorming van malonyl-CoA katalyseert, een essentieel substraat voor vetzuursynthese dat de vetzuuroxidatie remt. Alles samen genomen, onthult dit een nieuwe functie van de (P)RR in het vetmetabolisme. Hoewel de plasma concentraties van cholesterol en triglyceriden in muizen met LDLR deficiëntie die tijdens een hoog-vet dieet hepatische (P)RR remming ondergingen dus verlaagd waren, leidde dit niet tot een vermindering van de atherosclerose, en hetzelfde gold voor muizen met een ApoE deficiëntie die een hoog-vet-dieet kregen. Dit bleek te komen doordat de GalNac ASO methode ook leidde tot een daling van de (P)RR in macrofagen, hetgeen resulteerde in een verhoogde pro-inflammatoire respons. Door dit effect werden de mogelijke gunstige effecten van vetvermindering op atherosclerose teniet gedaan.

Abbreviations and Acronyms

5/6 th Nx	5/6 th nephrectomy
ACC	acetyl-CoA carboxylase
AGT	angiotensinogen
Ang	angiotensin
ApoB	apolipoprotein B
APRC	active plasma renin concentration
ARB	Ang II type 1 receptor blocker
AT	adipose tissue
AT ₁ (R)	angiotensin II type 1 (receptor)
AT ₂ (R)	angiotensin II type 2 (receptor)
CKD	chronic kidney disease
DOCA	deoxycorticosterone acetate
ET _A	endothelin type A
ET _B	endothelin type B
FA	fatty acid
G-(P)RR	N-acetylgalactosamine (P)RR antisense oligonucleotide
GFR	glomerular filtration rate
HDL	high-density lipoprotein
HFD	high-fat diet
hSORT1	human SORT1
IDL	intermediate-density lipoprotein
LDL	low-density lipoprotein
LDL-C	low-density lipoprotein cholesterol
LDLR	low-density lipoprotein receptor
LLOQ	lower limit of quantification
L-NAME	N-nitro-L-arginine methyl ester hydrochloride
LPL	lipoprotein lipase
MAP	mean arterial pressure
mTOR	mechanistic target of rapamycin
mTORC1	mechanistic target of rapamycin complex 1
ND (chapter 3)	not detectable
ND (chapter 5)	normal diet
NGAL	neutrophil gelatinase-associated lipocalin
NT-proBNP	N-terminal pro-B-type natriuretic peptide
(P)RR	(pro)renin receptor
PDH	pyruvate dehydrogenase
PRC	plasma renin concentration
PVN	paraventricular nucleus
RAS	renin–angiotensin system.
RAS	renin-angiotensin system
SBP	systolic blood pressure
SD	Sprague-Dawley
SHR	spontaneously hypertensive rat
siRNA	small interfering RNA
SORT1	sortilin 1
VLDL	very low-density lipoprotein

Curriculum Vitae

Liwei Ren was born on March 4th 1989 in Liaocheng, Shandong province, China. She started the clinical medicine of traditional Chinese medicine integrated with the western medicine (5 years program) at medical school, Shandong University of Traditional Chinese Medicine in 2008. After received her medical bachelor degree, she went to the south of China and began her study in Pathology and Pathophysiology in Jinan University, Guangzhou. In 2016, she received her first half PhD



training in Shenzhen University under the supervision of her co-promoter Xifeng Lu. During this period, her research focused on (pro)renin receptor regulating lipid metabolism. In 2018, she came to the Netherland and started the second half of her PhD training at the Division of Vascular Medicine and Pharmacology, of the department of Internal Medicine, Erasmus Medical Center, Rotterdam, under the supervision of her promotor A.H. Jan Danser. Her research focused on Renin-angiotensin System and the effect of angiotensinogen siRNA in anti-hypertension and end-organ damage. Liwei Ren will return to China and continue her research career after her defense ceremony.

PhD Portfolio

Name: Liwei Ren
 Department: Internal Medicine, Division of Vascular Medicine and Pharmacology
 Research School: Molecular Medicine
 Promotor: Prof. dr. A.H.Jan Danser
 Co-promotor: Assoc. Prof. Xifeng Lu

PhD training

Courses	ECTs
Cardiovascular Pharmacology	0.5
New pharmacological targets in age-related cardiovascular disease	0.5
7th course basic and translational endocrinology	2.0
SNP Course XVII: SNPs and Human Diseases	2.0
Basic Human Genetics course: Genetics for Dummies	0.6
Basic and Translational Oncology	1.8
Solving the Mysteries of Atrial Fibrillation- From Basic Science to Clinical Practice	0.3
Course Biomedical Research Techniques XVII	1.5
Laboratory animal science (Article 9 course)	3.0
Advanced flow cytometry	0.5
Basic Introduction Course on SPSS	1.0
The introduction in Graphpad Prism Vs.7	0.3
Workshop on InDesign CC 2019 for PhD-students and other researchers	0.15
The photoshop and illustrator CC 2018 workshop for PhD-students and other researchers	0.3
PowerPoint Tricks you didn't know	0.3
Scientific Integrity	2.0
Academic English writing	2.0
English B2.2 Upper-Intermediate	3.0

Conferences and meetings

ASN Kidney Week (attendance)	1.0
AHA Hypertension 2020 Scientific Sessions (poster + oral)	1.8
Internal Medicine Science Day (poster)	0.9
ATVB/PVD Vascular Discovery (poster)	1.8
Internal Medicine research meeting	1.0
Weekly Pharmacology research meeting	3.0
Weekly Lipid Metabolism research meeting	2.0

Teaching

Automatic nervous system practicum	1.5
------------------------------------	-----

Total	34.75
--------------	--------------

Publication list

L. Ren[#], Y. Sun[#], H. Lu, D. Ye, L. Han, N. Wang, A. Daugherty, F. Li, M. Wang, F. Su, W. Tao, J. Sun, N. Zelcer, A.E. Mullick, A.H.J. Danser, Y. Jiang, Y. He, X. Ruan, X. Lu, (Pro)renin Receptor Inhibition Reprograms Hepatic Lipid Metabolism and Protects Mice From Diet-Induced Obesity and Hepatosteatosis, *Circ Res*, 122 (2018) 730-741.

D.M. Bovee[#], **L. Ren**[#], E. Uijl, M.C. Clahsen-van Groningen, R.V. Veghel, I.M. Garrelds, O. Domenig, M. Poglitsch, I. Zlatev, J.B. Kim, S. Huang, L. Melton, X. Lu, E.J. Hoorn, D. Foster, A.H.J. Danser, Renoprotective Effects of Small Interfering RNA Targeting Liver Angiotensinogen in Experimental Chronic Kidney Disease, *Hypertension*, 77 (2021) 1600-1612.

E. Uijl[#], **L. Ren**[#], K.M. Mirabito Colafella, R. van Veghel, I.M. Garrelds, O. Domenig, M. Poglitsch, I. Zlatev, J.B. Kim, S. Huang, L. Melton, E.J. Hoorn, D. Foster, A.H.J. Danser, No evidence for brain renin-angiotensin system activation during DOCA-salt hypertension, *Clin Sci (Lond)*, (2021).

L. Ren, K.M.M. Colafella, D.M. Bovée, E. Uijl, A.H.J. Danser, Targeting angiotensinogen with RNA-based therapeutics, *Current Opinion in Nephrology and Hypertension*, 29 (2020) 180-189.

E. Uijl[#], K.M. Mirabito Colafella[#], Y. Sun, **L. Ren**, R. van Veghel, I.M. Garrelds, R. de Vries, M. Poglitsch, I. Zlatev, J.B. Kim, E.J. Hoorn, D. Foster, A.H.J. Danser, Strong and Sustained Antihypertensive Effect of Small Interfering RNA Targeting Liver Angiotensinogen, *Hypertension*, 73 (2019) 1249-1257.

L. Ren, X. Lu, A.H.J. Danser, Revisiting the Brain Renin-Angiotensin System-Focus on Novel Therapies, *Curr Hypertens Rep*, 21 (2019) 28.

[7] E. Uijl, L. Ren, A.H.J. Danser, Angiotensin generation in the brain: a re-evaluation, *Clin Sci (Lond)*, 132 (2018) 839-850.

X. Yang[#], **L. Ren**[#], L. Yang, C. Deng, F. Li, In vivo direct reprogramming of liver cells to insulin producing cells by virus-free overexpression of defined factors, *Endocr J*, 64 (2017) 291-302.

[#]Contributed equally

